CBPF
Centro Brasileiro de Pesquisas Físicas
UNIDADE DE PESQUISA DO MCTI

On Effective Field Theories For Disordered Quantum Systems

PhD Thesis

Marcus Marinho

COTEO
Condensed Matter Theory

Advisor:	Prof. Dr. Tobias Micklitz (CBPF)
Internal Reviewer:	Prof. Dr. Mucio Amado Continentino (CBPF)
External Reviewer:	Prof. Dr. Daniel Gustavo Barci (UERJ)
External Reviewer:	Prof. Dr. Fernando Iemini de Rezende (UFF)
External Reviewer:	Prof. Dr. Thiago Rodrigues de Oliveira (UFF)

March 1, 2023

CBPF
Centro Brasileiro de Pesquisas Físicas
SUBORDINADA AO MCTI

MINISTÉRIO DA CIÊNCIA, TECNOLOGIA E INOVAÇÕES

"ON EFFECTIVE FIELD THEORIES FOR DISORDERED QUANTUM SYSTEMS"

MARCUS VINICIUS MARINHO PEREIRA DE MELO

Tese de Doutorado em Física apresentada no Centro Brasileiro de Pesquisas Físicas do Ministério da Ciência Tecnologia e Inovação. Fazendo parte da banca examinadora os seguintes professores:

Tobias Micklitz - Orientador/CBPF

Daniel Gustavo Barci - UERJ

Fernando Iemini de Rezende Aguiar - UFF

Thiago Rodrigues de Oliveira - UFF

Mucio Amado Continentino - CBPF

Rio de Janeiro, 14 de fevereiro de 2023.

Acknowledgments

First of all I would like to thank Professor Tobias Micklitz for giving me the opportunity to write my thesis with his guidance and for suggesting such an enthralling research topic. Throughout these four years, he actively worked to provide a warm and pleasant working atmosphere in his research group. I am also infinitely indebted to Professor Georg Schwiete who with extraordinary patience helped me understand many aspects of the physical content underlying the mathematical machinery of the nonlinear sigma model. I would like to thank Professor Alex Levchenko for his invaluable insights in the discussions involving mesoscopic fluctuations and his amicable personality.

I would like to thank my fellow graduate students who contributed to this research with helpful discussions and support. Furthermore, I am grateful for my undergraduate and graduate professors, whose teachings have certainly helped me throughout my research.

I am thankful for my family for always providing me support when I needed. In special, my aunt, Eunice, her memory will be with me always and I will be ever grateful for her believing in me.

Finally, I would like to express my profound gratitude to my parents José Nilson and Iara for the comprehension, encouragement and financial support throughout my studies. I greatly appreciate the friendship and wisdom that my long-lasting friend Benjamim brought into my life throughout these many years. I am also deeply grateful to my girlfriend Milena for her love and continuous support. Thank you a million times for giving me the extra push when I needed, for hearing my daily grievances about life and, most of all, for being my best friend.

The work reported in here would not be possible without the financial support of the funding agency CNPq, for which I am grateful.

Abstract

In this thesis, we shall explore applications for the famous nonlinear sigma model to describe the spectral and quantum transport properties of low-dimensional disordered systems. In our inaugural application, we use this field theoretical approach to calculate the spectral correlations of Anderson insulating wires for systems with time-reversal symmetry and in the absence of time-reversal symmetry. The calculation of the former observable was a long standing interesting problem within the reach of state-of-the-art experimental measurements.

In the second study, we seek to provide a description of the quantum transport properties of disordered systems consisting of a hybrid structure with two superconductors and a topological insulator layer separating them. Such systems have been drawing a lot of attention since they are potential candidates to host and, consequently, perform manipulations of the elusive Majorana bound states. Since the formation of such elusive states requires the presence of an external magnetic field, this investigation is separated into two parts: we first explore the quantum transport properties of the system in the absence of an external magnetic field, then we switch it on and investigate how it affects the current and the fluctuations of the current in the hybrid structure.

However, before delving into these direct applications, we first discuss the implications of the presence of disorder in an electronic system. Next we introduce the fundamental symmetries that will continuously appear throughout this work, time-reversal being the most present. Having introduce these ideas, we discuss the typical mathematical machinery used in literature to investigate disordered systems via a field theoretical approach. To conclude the theoretical foundations, we discuss the consequences of coherent propagation in disordered systems and the interesting structure it forms in momentum space. The section is closed with an introduction to the key physical concepts involved in hybrid structures with two superconductors spatially separated from each other.

Keywords: Localization Effects, Matter Waves, Wave Propagation in Random Media, Mesoscopic Systems, Josephson junctions, Low-Dimensional Systems

Resumo

Nesta tese, vamos explorar aplicações do famoso modelo sigma não-linear para descrever as propriedades espectrais e de transporte quântico em sistemas de baixas dimensões. Em nossa aplicação inaugural, usaremos essa abordagem envolvendo teoria quântica de campos para calcular as correlações espectrais de fios isolantes de Anderson para sistemas na presença e também na ausência de simetria de reversão temporal. O cálculo dessa observável era uma problema interessante o qual estava em aberto por décadas. Além disso, tal resultado encontra-se dentro do alcance de medidas experimentais no estado da arte em átomos frios.

No segundo estudo, buscaremos um maneira de descrever as propriedades de transporte quântico em sistemas desordenados, os quais são formados por estruturas híbridas com dois supercondutores separados por uma camada de um isolante topológico. Tais sistemas tem recebido bastante atenção, visto que eles são potenciais candidatos para abrigar e, consequentemente, manipular os evasivos estados ligados de Majorana. Esses estados e suas propriedades são famosos pela possibilidade de serem usados para a construção dos tão buscados qbits topológicos. Para que haja a formação desses estados evasivos, precisamos da presença de um campo magnético externo. Sendo assim, separaremos nossa investigação em duas partes: primeiro nós exploraremos as propriedades de transporte quântico do sistema na ausência de um campo magnético externo. Então, na segunda etapa, estudaremos como as propriedades de transporte quântico, a supercorrente e as flutuações da supercorrente, são afetadas pela aplicação de um campo magnético externo.

Entretanto, antes de mergulharmos diretamente nessas aplicações, vamos discutir as implicações da presença da desordem em sistemas eletrônicos. Em particular, apresentaremos as classes de simetrias fundamentais que aparecerão continuamente neste trabalho. Após a introdução desses conceitos essenciais, discutiremos o maquinário matemático usado na literatura para investigar sistemas desordenados por meio de uma abordagem de teoria quântica de campos. Para concluir os fundamentos teóricos, discutiremos as consequências da propagação coerente de ondas matérias em sistemas desordenados e a estrutura peculiar que se manifesta no espaço de momento. A seção é encerrada com uma introdução aos conceitos físicos fundamentais envolvidos no estudo de estruturas híbridas com dois supercondutores espacialmente separados um do outro por um elo fraco suficientemente fino.

Palavras-chave: Efeitos de Localização, Ondas de Matéria, Propagação de Ondas em Sistemas Desordenados, Sistems Mesoscópicos, Junções de Josephson, Sistemas de Baixas Dimensões

Contents

List of Figures

List of Tables

Normal science means research firmly based upon one or more past scientific achievements, achievements that some particular scientific community acknowledges for a time as supplying the foundation for further practice.

Thomas Kuhn, The Structure of Scientific Revolutions

1 Introduction

In this chapter, we shall review the basic background information contained in this work. We start with an introduction to mesoscopic physics and the use of the famous non-linear sigma model to study its transport properties. Later we introduce the fundamental length, energy and time scales which underpin the appearance of mesoscopic phenomena. We provide description of the fate of a wave packet travelling in a disordered environment along with its properties for each particular characteristic time. The chapter is concluded with an introduction to the two applications of the non-linear sigma model we will study in the next chapters.

The manifestations of quantum effects on physical systems are due to the wavelike property of the electrons, an attribute which allows such elements of the nature to be susceptible to interference phenomena. For instance, the interference resulting from electrons propagating in disordered metals and being scattered off by impurities. These phenomena become particularly important for the nature of the transport properties when the system size L is small in comparison to the temperature dependent dephasing length $L_\phi(T)$ [AB02]. The latter scale is of great importance to determine the physics of mesoscopic systems, because this length $L_\phi(T)$ sets the scale above which the mechanisms responsible for the irreversible phase-breaking of the electron's wave function manifest themselves. When the inequality $L < L_\phi(T)$ is satisfied[AM07; Imr08], the quantum phase coherence of the electron can have massive consequences in the nature of the dynamics. Furthermore, in the limit of zero temperature, the dephasing length typically displays an unbounded growth, turning quantum interferences into something that is in theory always important for low enough temperatures. For instance, in reference [Cap+13], considering ring and wire geometries, it was shown that for temperatures $T \sim 1/10K$, the phase coherence length is of the order of micrometers. As a starting point, it is possible to explain many physical phenomena of disordered and mesoscopic physics using a perturbative approach. Unfortunately, this approach cannot capture important details of the physics involved in such systems. In certain limits, the observables may display an unphysical divergence or, since the perturbative approach relies on an expansion in terms of a small parameter, it cannot by any means reproduce nonanalytic contributions. These shortcomings of the perturbation theory indicate that it would helpful to construct a nonperturbative method to investigate the transport properties of disordered and mesoscopic systems. Hence, to analytically study the implications of interference phenomena in the quantum transport of disordered electronic systems, we shall introduce the most powerful field-theoretical technique to perform these calculations: the nonlinear

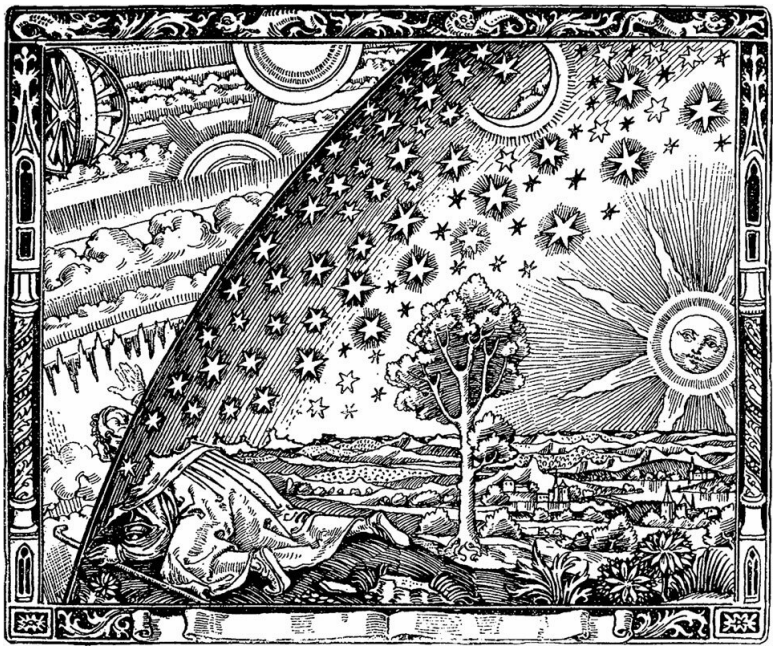

Figure 1.1.: The semiclassical viewpoint can be understood in terms of a system that lives in the classical realm, $\hbar^0$, and yet is allowed to have a glimpse into some features of the quantum realm, $\hbar^n$. For instance, a classical object that carries a phase and ultimately experiences interference phenomena.

sigma model. This model consists of an action which describes the underlying physics in terms of massless modes. Later, in Ch. 2, we shall provide a complete explanation for physical and the involved mathematical machinery required to work with such model. In principle, to calculate physical quantities, we can write down a nonlinear sigma model via the renowned replica trick [EA75], [Eme75], [AS10], where the fields employed in the construction are allowed to be either conventional numbers [Weg79], [SW80], [AI77] or anti-commuting Grassmann variables [EKL80]. Regardless of the nature of the fields, in both approaches the resulting field theory consists of a $n \times n$, n denotes the number of replicas, matrix field Q as our fundamental degree of freedom and at some point the limit of $n \to 0$ is supposed to be taken.

Complementary to the non-linear sigma model based on the replica trick, we have the supersymmetric nonlinear sigma model, where the field-theoretical approach is built on the concept of superspace. The model is described by commuting and anti-commuting variables [PS79]. Notice that in here, the underlying idea behind the concept of a supersymmetric model is the possibility to drastically reduce the number of degrees of freedom in comparison to the replica trick and in this manner circumvent certain combinatorial and averaging problems [Sou85], [VWZ85], [Mir00].

It is known that the nonlinear sigma model based on the replica trick provides a helpful platform to calculate the interaction between diffusion modes and also renormalization group equation [Efe96]. In fact, within this context, both methods have shown to be fully equivalent. However, for some calculations the supersymmetric approach is the only available tool [VZ85]. For instance, in a disordered electronic system, if one wants to explore a nonperturbative region of the parameter space, namely the strong disorder regime $\lambda_F \gg \ell$, where λ_F is the Fermi wavelength and ℓ the mean elastic scattering length, in principle, such endeavour would require a summation over an infinite quantity of diagrams, which is a formidable task. With the aid of the nonlinear sigma model, the summation over the diagrams is replaced by a functional integration over

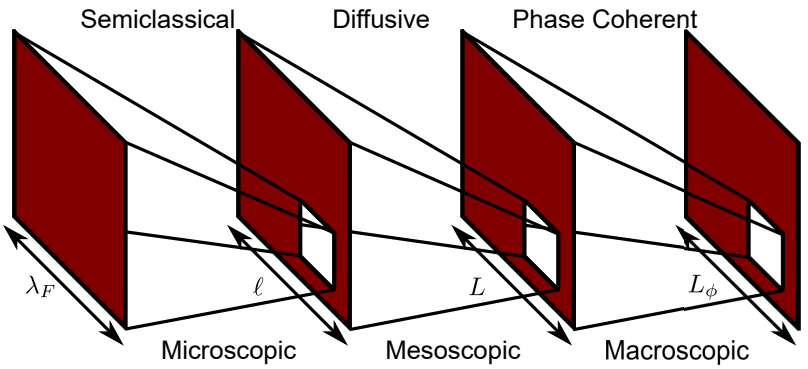

Figure 1.2.: Above we display the hierarchy of length scales: λ_F denotes the Fermi wavelength, ℓ the mean elastic scattering length, L the system size and L_ϕ the dephasing length. For a diffusive and coherent propagation of electrons, the system must satisfy the inequalities $L \gg \ell$ and $L < L_\phi$, respectively.

the superspace where the theory is defined. This construction turns possible to, then, access the striking physical phenomenon of theory of Anderson localization [And58], [Abr+79], [Zir86], [Hik81].

The starting point of any calculation to obtain a nonlinear sigma model representation consists of two steps: average over the disorder and separate out the fast modes from the slow modes. The fast modes are defined as fields carrying energies and momenta of the order of the Fermi energy, E_F, and momentum, p_F, whereas slow modes are associated with fields carrying energies smaller than $1/\tau_{\rm el}$, the inverse of the mean elastic scattering time, and momenta that are small when compared to $1/\ell$. For a system of size $L \gg \ell$, these slow modes describe the diffusive propagation of electrons. In particular, in the weak disorder limit, $\lambda_F \ll \ell$, these slow modes fully reproduce the diagrammatic perturbation theory of the interactions between the diffusion modes, namely, the diffusons and Cooperons. In Fig. 1.2 we display a summary of the involved length scales. In Fig.1.3, we display the summary of the relevant time and energy scales, the region where the study of quantum transport affords a perturbative approach and where the concept of universality holds. In addition to that, with the help of Fig.1.3, assuming that no interactions are present and all collisions are elastic, we discuss the effects of interference phenomena on a wave packet propagating in a weakly disordered environment. Considering first a classical system, we launch particles into a weakly disordered medium. Initially, these particles propagate in a ballistic manner within the disordered medium and their motion is not yet hindered by collisions with the scattering centers. After a sufficient long time, the collisions between particles and the impurities become significant and their motion becomes diffusive. If we give the system even more time for it to evolve, the particles will explore the entire phase space reaching the ergodic regime. In this regime the system can be considered as being structureless and the transport properties can be understood in terms of its symmetries.

Having exposed the characteristics time scales associated with the classical dynamics, we move on to understand the influence of quantum interference processes on the dynamics of a spreading wave packet in a background of weakly scattering random impurities. In contrast with the classical case, in here the ultimate effect of the disordered environment over the wave packet will be determined by dimension d of the system and also the size of the host system, L, in comparison to the localization length, ξ. For a host system with $d \leq 2$ any amount of disorder is capable to drive the system to a localized regime, whereas for $d > 2$ there is a critical amount of disorder separating localized from extended states.

We first investigate the case where $L \ll \xi$ a regime in which localization phenomena is absent. In a first

instance, the wave packet is largely insensitive to the impurity background and the boundary conditions. Analogous to its classical counterpart, for times in excess of the mean elastic scattering time, the dynamics become diffusive. However, in here, such behavior is founded on the manifestations of quantum interference processes due to scattering off the background impurity potential. These processes lead to the appearance of quantum weak localization corrections, which corresponds to trajectories with a single self-intersection. Such effect leads to a renormalization of the diffusion parameter to values smaller than the bare value of the parameter. Furthermore, as we briefly discussed, depending on the dimensionality these quantum corrections can cause the complete absence of quantum transport in the random environment. In the diffusive regime, when the time scale exceeds the diffusive time $\tau_D = L^2/D$, where D is the diffusion parameter, the system enters into what is called the ergodic regime. In such regime, we consider that the wave packet is completely spread over the entire phase space and, in this sense, the only remaining dependences of the system is on its fundamental symmetries and the total number of energetically accessible states. As a consequence of this, the transport properties of the system become universal, they no longer depends on the geometrical or material properties of the system. In this regime, the spectral properties of the system become indistinguishable from those obtained from considering an ensemble of matrices with random entries, whose form satisfies certain symmetry requirements, that is, random matrix theory. When the time scale becomes approximately greater than the Heisenberg time $\tau_H = 1/\delta$, the non-perturbative quantum phenomena become relevant. In this regime, the transport properties of the system are governed by the universal features associated with the resolution of individual levels. In particular, contrary to the classical case, the system displays a dynamical echo, a memory of its initial state that can only be eliminated by inelastic scattering events. Such property manifests itself for times much greater than the Heisenberg time. In this limiting case, the homogeneity of the wave packet is lost as it starts to relax into a form similar to its original state [Pri+94].

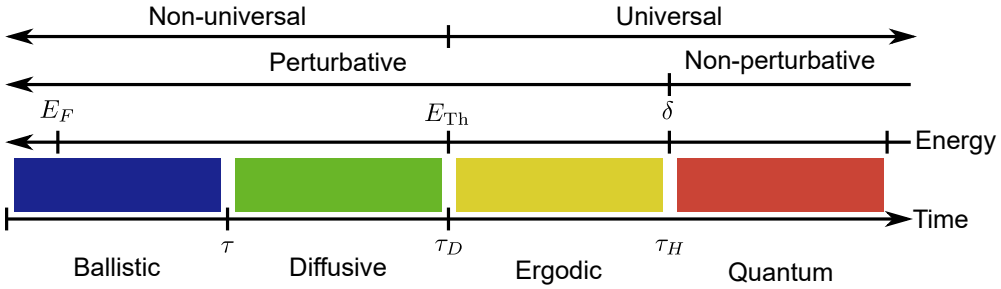

Figure 1.3.: Our complete understanding of the dynamics of a wave packet propagating in a weakly disordered environment. The quantum dynamics is separated into four regimes: ballistic, diffusive, ergodic and quantum. Additionally, we display the regions where universality and perturbation theory holds.

For a system whose size L largely exceeds the localization length, $L \gg \xi$, until the ergodic regime is reached, we adopt the same terminology to describe the dynamics of the electron degrees of freedom. However, for times larger than the diffusive time, it is more appropriate to substitute the ergodic regime by the localized regime. This understanding has to do with the interpretation that the wave packet is still allowed to fully explore only a region limited by the localization length [AF95], [MM18], regions beyond it are not accessible. In the quantum regime, the physical picture is analogous to what we described for the opposite limiting case. In this time scale, we observe the onset of strong localization, there is an unhinged proliferation of trajectories containing infinitely many self-intersecting points, which dramatically hinders the propagation of the wave functions. Moreover, the most striking difference between the two limits is the absence of the

notorious oscillatory behavior present in the level spacing for systems satisfying $L \ll \xi$.

Within the ergodic regime, the random matrix theory, which was initially used to provide an statistical description for the energy levels of highly excited nuclear levels in complex nuclei [Wig51], has been a fruitful tool to investigate low energy regimes of disordered systems. Remarkably, in the ergodic regime, the spectral properties of diffusive systems are indistinguishable from the results obtained via random matrix theory [Mir00], [G5]. In this sense, the random matrix theory provides an innovative framework to study such properties of systems that otherwise would not have been easily investigated. In statistical mechanics, we usually abandon any hope of providing a full analytical description of a given system of particles, not because it is an unfeasible task, the problem lies in the insanely large quantity of degrees of freedom. In random matrix theory, given a complex system, we do not have access to its microscopic Hamiltonian or have it, but it is too cumbersome to extract any meaningful information. Thus, by considering only the fundamental symmetries of a given system, we investigate its properties in terms of an ensemble of random Hamiltonians all sharing the same symmetries as our target system [Meh04]. In addition to that, the statistical description of the spectral properties of a given system via random matrix theory involves introducing a Gaussian distribution with statistical weight given by

$$P(H) = \mathcal{N} \prod_{n,m} \exp\left[-\frac{1}{2}\frac{|H_{mn}|^2}{A_{mn}}\right]. \tag{1.1}$$

This probability distribution function Eq. (1.1) is associated with a non-trivial correlation among the fluctuating matrix entries and $\mathcal{N}$ denotes a normalization constant, H is the system's Hamiltonian in a matrix form with random entries $H_{ij} = H^*_{ji}$ that can take any values with equal probability and all matrix entries fluctuate independently around the zero mean. In addition to that, depending on the form of the variance matrix A, the Gaussian ensemble can be classified as invariant, $A_{mn} = a$ for all possible entries and the matrix entries fluctuates independently and equally around the zero mean. This category of ensemble is well suited to describe the properties of extended systems, as is the case for the ergodic regime. The other alternative is the non-invariant ensemble, where the fluctuations are still independent from each other, but the variance depends on the indices carried by the matrix entry. In contrast with the invariant ensemble, the non-invariant can be explored to investigate the properties of system in the localized regime [RP60; FM91; KS98].

Building on the early work of Wigner [Wig51], Dyson in his seminal paper [Dys62] classified complex many-body systems in accordance with their fundamental symmetries. Such classification comprises three canonical classes of universalities and their categorization fundamentally hinges on the presence or absence of time-reversal symmetry and spin rotational symmetry. For systems with time reversal and spin rotational symmetry, for instance a system without magnetic field or spin-orbit coupling, the Gaussian orthogonal ensemble (GOE) is appropriate to describe the system, this ensemble is defined in the space of real symmetric matrices, $H_{nm} = H^*_{nm}$ and $H_{nm} = H_{mn}$, satisfying two conditions: invariance under rotations $H \to WHW^T$, where W is an orthogonal matrix, and statistical independence of the entries H_{ij}. Both conditions can be conveniently expressed in terms of equations. Let dH be the volume element of the group, the former condition reads

$$P(H)dH = P(H')dH', \tag{1.2}$$

where $H' = WHW^T$ and $WW^T = W^TW = 1$ and the latter condition is simply expressed as

$$P(H) = \prod_{i \leq j} f_{ij}(H_{ij}), \tag{1.3}$$

that is, the probability distribution function can be decomposed into a product over several single variable functions. If we consider a system with time reversal symmetry but the spin rotational symmetry broken, for instance a system with spin-orbit scattering, the Gaussian symplectic ensemble provides the adequate description for the statistical properties of the system. This ensemble is defined in terms of two conditions: the ensemble invariant under rotations $H \to W^R HW$ and the entries of the matrix H are statistically independent. The new notation introduced stands for the self-dual of a given matrix $W^R = (i\sigma_2)W^T(i\sigma_2)^{-1}$, the matrix σ_2 is the Pauli matrix defined as $\sigma_2^{ii} = 0$ and $\sigma_2^{12} = (\sigma_2^{21})^* = -i$, and the matrix H is Hermitian and self-dual. Finally, in the presence of magnetic interactions, the time reversal symmetry is broken and, as a result, the system affords a representation via the Gaussian unitary ensemble (GUE), an ensemble which is defined in the space of Hermitian matrices, $H_{mn} = H^*_{nm}$, satisfying $H' = U^{-1}HU$, where U is a unitary matrix. These are the three celebrated Wigner-Dyson ensembles [Dys62].

In general, the non-linear sigma model is a reliable platform to analytically investigate the properties of disordered systems. In this manuscript, it is our declared goal to employ the non-linear sigma model to study disordered systems with low dimensionality, quantum dot and quasi-one-dimensional geometries. This thesis is made up of three parts, theoretical foundations, applications of the field-theoretical model and the conclusion. The first part will be dedicated to a presentation of the well-established foundations which are required to appreciate the discussions and achievements of this work. We divide this part into two sections, one devoted to review the concept of Anderson localization and its subsequent consequences, the physics of disordered systems and the derivation of the non-linear sigma model. In the second section, we focus on coherent phenomena in the presence of a disorder potential. In particular, we discuss the formation of the coherent backscattering peak, a structure associated with the weak localization effect, and the coherent forward scattering peak, a structure which is a fundamental signature of the Anderson localization. To understand how these two peaks are amenable to an experimental probe in ultra cold atoms setups, we find it helpful to introduce the technical details in a separated appendix A, the quantum kicked rotor and show how it can be mapped onto the tight binding Hamiltonian. In the second part, we will use the tools we presented in the theoretical foundations and mostly focus on two published works: [MM18] and [Mar+22].

In the first work, we shall make good use of the supersymmetric non-linear sigma model to access the physics of Anderson insulating wire, via a non-perturbative method, and calculate the level-level correlation function, allowing then to provide a complete description of the correlation between two neighboring levels. So far, the literature has only contemplated the asymptotics regimes, namely the region far deep within the insulating regime where the dimensionless conductance is much smaller than unity and the metallic regime in which the dimensionless conductance is much larger than unity. In Ref. [MMA14], it was obtained the full analytical expression describing the level-level correlation function for a system under the influence of an external magnetic field. Despite its enormous importance, from the theoretical viewpoint, from the experimental viewpoint realizing such system was a formidable task. Following the necessity of describing the spectral statistics for systems endowed with time-reversal symmetry, we extended their work and calculated the level-level correlation function for such systems. In their calculations, it was mapped the nonlinear sigma model onto the Schrödinger equation [EL83] which lead to a fiendish problem, solving the differential

equation representing the propagation of a quantum mechanical particle in a curved manifold. We will show that by knowing the ground state wave function of the Schrödinger equation on a given manifold [KO17a], whose form is defined by three canonical Wigner-Dyson ensembles; Gaussian orthogonal ensemble (GOE), Gaussian unitary ensemble (GUE) and Gaussian symplectic ensemble (GSE), we can transform this problem into something more feasible via a local generating function.

Then, in the second work, we will construct a nonlinear sigma model based on the replica trick to describe the Josephson effect in a diffusive short junction, whose weak link is a topological insulator in contact with two superconducting leads via its surface states. Since these junctions host the promise of providing a robust platform to perform quantum computations, there is a wealth quantity of data involving this type of junctions and so far none of the results have contemplated the current fluctuations of the supercurrent present in the weak link. Using this setup, we consider the junction in the absence of an external magnetic field, then we switch on an external magnetic field and discuss the changes it generates in the transport properties of the system. Furthermore, it is well known that in such systems the density of states in the metallic region mimics the BCS form, however, with a reduced gap (usually referred to as minigap). We calculate the density of states for the Josephson junction and show that as we increase the external magnetic field, the typical induced energy gap becomes smaller until the Josephson junction becomes gapless. In a next step, we calculate the current-phase relation at the mean field level. Then, we perform an expansion around the metallic saddle point and investigate the properties of the current fluctuations as a function of the difference between the phases of the superconductors, ϕ, the dwell energy, E_t and the magnetic depairing energy, E_Φ.

To conclude the introduction, we find it helpful to present a comprehensive reading guide with only textbooks which provide a solid foundation to navigate among the physics discussed in this thesis. For a complete presentation of the typical framework employed to study condensed matter systems, each one of the following books offer a unique viewpoint on the subject: [Phi12; Col15] and, for an approach using the quantum theory of fields, we recommend [AS10].

For a unified presentation on the topic of quantum interference, the book by Eric Akkermans [AM07] offers a robust set of theoretical tools and methods to explore this important phenomenon present in a wide variety of mesoscopic systems. Within the realm of quantum transport, the book by Yuli Nazarov [NB09] introduces the fundamental physics along with the theoretical background and experimental landmarks that paved the way to success of this developing field of study. For a particular discussion of quantum transport in superconducting systems, we refer the reader to Ref. [Zag14] and, in Josephson junctions, the Ref. [BP82] study many aspects of the Josephson effect, ranging from the physical theory to actual and conceptual engineering applications. For a general guide with a coherent and detailed presentation of the analytical methods employed to study random matrices, we indicate to the reader Ref. [Meh04]. Besides this, Mehta's book offers a complete guide with many results reported in the literature.

Finally, as a initial step to survey the mathematical machinery and underlying physics of the most sophisticated technique to investigate the quantum transport properties of disordered systems, namely, the supersymmetric nonlinear sigma model, we refer the reader to the canonical book by Konstantin Efetov [Efe99]. For a more modern approach with a more mathematically oriented description, the book by Franz Wegner [Weg16] delivers amazing results. This list certainly does cover all the physics and mathematics that has to be known to fully comprehend the thesis, but it offers a starting point from where the readers can start to explore and develop its own understanding of the field.

Mathematics is a part of physics. Physics is an experimental science, a part of natural science. Mathematics is the part of physics where experiments are cheap.

Vladimir Arnold, Mathematical Understanding of Nature

2

Theoretical Foundations

In this chapter we shall discuss the fundamental theoretical foundations used in the works presented in this thesis. We start out with a brief introduction to the phenomenon of Anderson localization and the scaling theory associated with it. Then, we introduce the definitions for the fundamental symmetries in quantum systems. Having established these concepts, we next move on to the effects of the disorder on a quantum system. In particular, we will introduce the Green's function within different contexts, namely, for commuting variables, anti-commuting variables and in a hybrid version containing both types. With the help of these hybrid Green's functions, we will present a detailed derivation of the celebrated non-linear sigma model. In the following part, we move on to a more physical discussion and provide the building blocks to understand the exquisite phenomenon of coherent multiple scattering. We focus on two special cases, the coherent backscattering peak and the coherent forward scattering peak. To conclude this chapter, we study the basics of Josephson junctions along with some important applications.

2.1. Anderson Localization

2.1.1. What is it?

In classical physics, a particle which has a sufficiently small energy can become localized in certain valleys of a disordered potential landscape. In 1957, in his seminal paper [And58], P. W. Anderson demonstrated that a quantum-mechanical particle propagating in a diffusive manner in a random lattice via quantum jumps between sites can become fully localized depending on the disorder concentration and the particle energy. Nowadays, our interpretation of localization phenomena in disordered environment hinges on the interference among trajectories of quantum-mechanical particles. In particular, it is understood that certain types of interferences lead to a phase accumulation, which renormalizes down the diffusion parameter ultimately leading to an absence of quantum transport in the medium, for $d \leq 2$. In higher-dimensional cases, the response to the phase accumulation is sensitive to the impurity concentration, analogous to Anderson's prediction. For systems with $d > 2$, there is a critical value for the disorder such that a mobility edge

Figure 2.1.: Depending on the dimensionality and the strength of the disorder the potential, the states of the host system can be extended or localized.

exists in the density of states, which separates the extended from the exponentially localized states in the spectrum, a fundamental concept in the Anderson localization induced by random disorder.

The most striking feature of this kind of phenomenon is that Anderson localization is a microscopic phenomenon with measurable consequences at a macroscopic level. In the old view of electronic conductivity, the classical Drude theory, the electrons were considered free entities being scattered by positive ions in metal lattice sites. Later on, with the discovery of quantum mechanics, such theory was revised and in the new picture, the electron motion was expected to occur in a zigzag manner between impurities. In this theory, larger impurity concentrations implied a smaller electronic conductivity. The novel idea introduced by Anderson in his seminal work, a tight-binding model of an electron in a disordered lattice, led to the prediction of the appearance of localized states, in the sense that the diffusive zigzag of the electrons was completely ceased for impurity concentrations beyond a certain critical value.

2.1.2. Scaling Theory

Approximately 20 years later, the so called Gang of Four building on a renormalization group scheme, constructed a scaling theory of localization at zero temperature that depends solely on the dimensionless conductance, $g(L)$, where we define g as the ratio between the Thouless energy, E_T, which is inversely proportional to the required time for a particle to travel from one boundary of the system to the other, and the mean level spacing, δ, is defined as the inverse of the time necessary for a particle to distinguish among individual quantum levels. Such scaling function, for a disordered electronic system, defined as

$$\beta(g) = \frac{d \log g}{d \log L}, \tag{2.1}$$

displays the remarkable property of universality [Abr+79], the function does not depend on the system size or the degree of disorder. In this work, it was derived the asymptotic forms for the scaling function in the limiting cases of small and large dimensionless conductances. In Fig. 2.2 we display the plot of a disordered

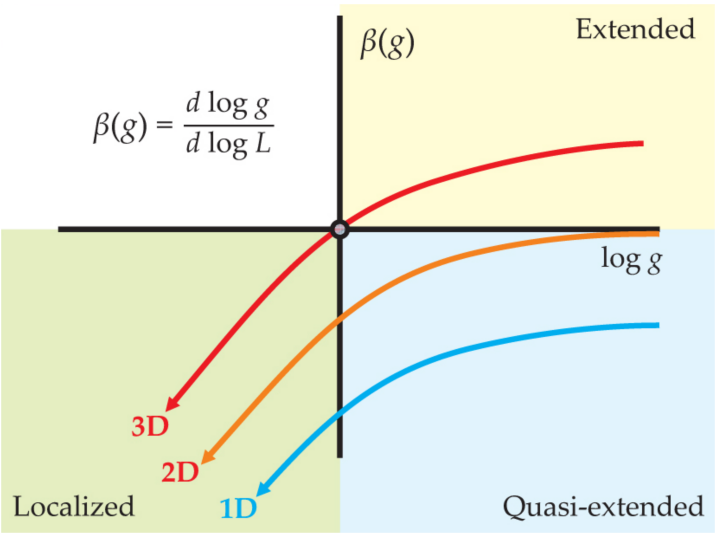

Figure 2.2.: At zero temperature, the scaling function for $d = 1, 2, 3$. For three-dimensional systems, the critical conductance g^* separates extended (metallic) from insulating (localized) behavior. Picture taken from Ref. [LTW09].

electronic system for various dimensions, $d = 1, 2, 3$. In their pioneering article, it was shown that in three dimensional systems, there is a critical conductance which is an unstable fixed point separating insulating from metallic behavior. In two or smaller dimensions, there is no bona fide metallic behavior, no matter how small the disorder is the system is always driven to an insulating phase.

Considering a d-dimensional system, in the limiting case of a small dimensionless conductance, $g < 1$, the system is far deep in the quantum regime and, as a consequence of this, the conductance should decay exponentially in the scale of the localization length, ξ, $g \sim e^{-L/\xi}$. In the opposite limit, $g > 1$, the dimensionless conductance has an Ohmic behavior $g \sim L^{d-2}$. When the dimension, d, of the system is smaller or equal than two, the interpolation between these two asymptotic limits exhibits a behavior that always drives the system into the localized region however small the disorder is. For all values of $\log g$ the scaling function is negative, indicating that as we increase the size of the system, L, there is a reduction of the dimensionless conductance. However, for higher-dimensions, the interpolation now has a critical point signalizing the celebrated Anderson metal-insulator transition. For this case, if $g > g^*$, then the scaling function is positive, as a consequence of that the dimensionless conductance increases as we increase the system size and the system is extended. On the other hand, when $g < g^*$, the scaling function is negative. Hence, if we increase the system size, this results in a decrease of the dimensionless conductance, leading the system to a localized regime.

2.2. Spectral Statistics of Disordered Systems

How does the spectrum of a disordered system respond to these distinct transport regimes, namely, metallic and insulator? The answer to this question depends crucially on the parameter ξ/L. We first study the case where this parameter is a large quantity, $\xi/L \gg 1$.

Considering the limiting case above of a system where electron localization is not important. For a weakly disordered system in the metallic regime, for instance, a good conductor where the electrons can move around the entire sample and also feel the boundaries. This spatial delocalization of the wave functions leads to the

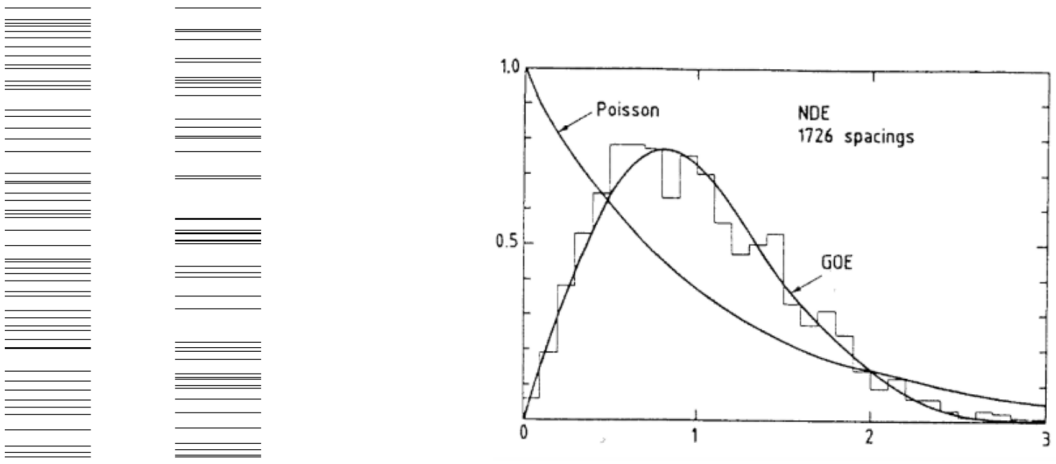

Figure 2.3.: Left panel: good metallic conductor vs Anderson insulator in the thermodynamic limit. Right panel: comparison of the experimental data of heavy nuclei to the theoretical models for the probability distribution of two neighboring levels with no other level in between [Boh91].

appearance of an spatial overlap among the eigenfunctions, which induces spectral correlations. The latter manifests itself in the system via the famous strong level repulsion. The simplest possible case where the phenomenon of level repulsion manifests itself is for a two-level system. Let $\mathcal{H}$ be a real symmetric random matrix

$$\mathcal{H} = \begin{pmatrix} h_{11} & h_{12} \\ h_{12} & h_{22} \end{pmatrix}, \tag{2.2}$$

whose entries are drawn from a Gaussian normalized distribution with zero mean and variance $\sigma^2 = 2/\lambda$:

$$p(h_{ij}) = \sqrt{\frac{\lambda}{\pi}} e^{-\lambda h_{ij}^2}. \tag{2.3}$$

The eigenvalues for such a matrix can be easily obtained

$$2\lambda_{\pm} = h_{11} + h_{22} \pm \sqrt{(h_{11} - h_{22})^2 + 4h_{12}^2} \tag{2.4}$$

and the distance s from each other is

$$s = |\lambda_+ - \lambda_-| = \sqrt{(h_{11} - h_{22})^2 + 4h_{12}^2}. \tag{2.5}$$

Each matrix entry is assumed to be independent from each, this allows us to write down the probability distribution as

$$P(\{h_{ij}\}) = \mathcal{N} e^{-\lambda(h_{11}^2 + h_{22}^2 + 2h_{12}^2)}, \tag{2.6}$$

the symbol $\mathcal{N}$ denotes a normalization factor. The probability of finding two neighboring levels separated by a distance s with no other levels in between is given by the integral

$$P_o(s) = \mathcal{N} \int dh_{11} dh_{22} dh_{12} \delta\left(s - \sqrt{(h_{11} - h_{22})^2 + 4h_{12}^2}\right) e^{-\lambda(h_{11}^2 + h_{22}^2 + 2h_{12}^2)}. \tag{2.7}$$

In this form, the underlying physics we want to access is not immediately obvious. The strong level repulsion is more easily observed if we perform a change of variables: $u = h_{11} - h_{22}$, $v = (h_{11} + h_{22})/2$ and $x =$

$\sqrt{u^2+4h_{12}^2}$. With these new variables, we can identify the physics involved in the calculation and also compute the integral

$$P_o(s) = \frac{1}{\sqrt{2}}\left(\frac{\pi}{\lambda}\right)^{3/2}\int dudvdx\delta(s-x)e^{-\lambda(2v^2+s^2/2)}\frac{2x}{\sqrt{x^2-u^2}} = \frac{\pi}{2}se^{-\frac{\pi}{4}s^2}. \tag{2.8}$$

Now it is clear that for a vanishingly small level separation, the integral linearly goes to vanishingly small values, a result which reflects the phenomenon of the strong level repulsion. At large level separation, the exponential factor causes the probability distribution function to rapidly decrease to zero. It is possible to extend this calculation to the case where $\mathcal{H}$ is an Hermitian matrix, the entries are complex numbers, and also a symplectic matrix, whose entries are given by quaternions. Using that β is a parameter that accounts for the number of degrees of freedom for each type of matrix, we have $\beta = 1, 2, 4$, orthogonal, unitary and symplectic, respectively. For all cases, the probability distribution function display the following form

$$P_\beta(s) = a_\beta s^\beta e^{-b_\beta s^2}, \tag{2.9}$$

where $a_o = \pi/2 = a_u\pi^3/64 = a_s\pi^4 3^6/2^{19}$ and $b_o = \pi/4 = b_u\pi^4/4^2 = b_s 9\pi^2/256$. All these probability distribution function exhibit a degree of level repulsion in the limit of small level separation. In particular, the effect of level repulsion increases with the number degrees of freedom, the strongest case being the symplectic matrix and the weakest the orthogonal matrix. In the opposite region, large level separation, all distributions display the same Gaussian fall-off behavior.

In the opposite limiting case, when the system size L largely exceeds the localization length, $\xi/L \gg 1$, the effects of electron localization become important and previous description fails to describe the spectral statistics of the system. The explanation for this failure lies in the observation that in such systems the electrons are localized around the localization centers. Recalling that we only focus on the weak disorder limit, at an infinitely large system these centers are likely to be well separated from each other, which prevents the overlap among the wave functions, this allows the appearance of energy levels with similar energies. In this sense, the absence of correlations among the wave functions leads to the vanishing of the phenomenon of level repulsion in such systems. As a consequence of that, the probability distribution function $P(s)$ obeys the Poisson law. To understand the origin of this result, consider the following: let N points be distributed along an interval $[0, L]$ and consider two neighboring energy levels ϵ_1 and ϵ_2, whose distance between them $|\epsilon_1 - \epsilon_2|$ is measured in units of the average distance $\Delta = L/N$, that is, $s = |\epsilon_1 - \epsilon_2|/\delta$. Within these conditions, the probability of two neighboring energy levels being distance by a distance s with no levels in between is given by the expression

$$P(s) = \left(1 - \frac{|\epsilon_1 - \epsilon_2|}{L}\right)^{N-2}. \tag{2.10}$$

Then, considering that the quantity of points in the interval N and the system size L can become arbitrarily large, the expression above yields

$$P(s) = e^{-s}, \tag{2.11}$$

which confirms the claim that for an uncorrelated spectrum, the probability distribution function is given by the Poisson law. Furthermore, there is an intimate connection between the probability distribution function

of two neighboring energy levels with the level-level correlation function

$$K(\omega = s\delta) = \delta(s) - 1 + \sum_{n=0}^{\infty} P(n, s), \tag{2.12}$$

where this probability distribution function $P(n, s)$ describes the probability of finding two neighboring levels separated by a distance s with n energy levels distributed inbetween. With the help of the reasoning explored to derive Eq. (2.11), it can be shown that for an Anderson insulator in the thermodynamic limit, this function is given by the expression

$$P(n, s) = \frac{e^{-s} s^n}{n!}. \tag{2.13}$$

Substituting this result , into the Eq. (2.12), it is straightforward to notice that for a system infinitely large, only self-correlations are present $K(s\delta) = \delta(s)$. However, in a finite size Anderson insulator, there are far distant almost degenerate states which display a small region of overlap among the exponentially small tails of the wave functions. The presence of this physics reveals that in such systems correlations are induced in the spectrum, leading to the presence of a residual level repulsion. The contributions coming from this underlying physics are expected to be small

$$K(\omega) = \delta(s) + \frac{\xi}{L} K_{\mathrm{FAI}}(\omega), \tag{2.14}$$

nevertheless, such corrections are within the reach of the state-of-the-art ultracold atoms set-ups. It is certainly worth mentioning the importance of the spectral statistics for quantum chaos. The level-level correlation function displays a striking difference depending whether the system is in the chaotic, metallic, or integrable, insulating, regime. In the former regime, we have the well known Wigner-Dyson statistics, whose form depends sensitively on the fundamental symmetries of the system, we state in here without proof the results for the three Wigner-Dyson ensembles [Efe96]:

$$K_o(\omega) = -\left[\frac{\sin(\pi s)}{\pi s}\right]^2 - \frac{d}{dx}\left[\frac{\sin(\pi s)}{\pi s}\right] \int_1^{\infty} dt \frac{\sin(\pi s t)}{t}, \tag{2.15}$$

$$K_u(\omega) = -\left[\frac{\sin(\pi s)}{\pi s}\right]^2, \tag{2.16}$$

$$K_s(\omega) = -\left[\frac{\sin(\pi s)}{\pi s}\right]^2 + \frac{d}{dx}\left[\frac{\sin(\pi s)}{\pi s}\right] \int_0^{1} dt \frac{\sin(\pi s t)}{t}, \tag{2.17}$$

orthogonal, unitary and symplectic, respectively. In this sense, the spectral statistics can be explored as a form of diagnostic tool to detect the presence of quantum chaos in a given system. Considering a finite size Anderson insulator, later in this work, in Ch. 4, we shall discuss more about the literature, the research gaps in the calculation of the level-level correlation function, the behavior of the spectral correlations in comparison to the metallic regime and how we contributed to expand the boundary of knowledge in the field.

2.3. Symmetries

2.3.1. Time-Reversal

The time reversal operator is represented by an anti-unitary operator

$$T = UK, \tag{2.18}$$

where U is a unitary operator, it satisfies the equalities $U^\dagger U = UU^\dagger = U^{-1}U = U^{-1}U = 1$, where $\dagger$ denotes the conjugated transpose, and K takes the complex conjugate next to it, $K\gamma = \gamma^*$. It can be shown that such operator when squared, can be classified into three distinct categorizations: the system has no time-reversal symmetry or it has time-reversal symmetry and the time-reversal operator squares to 1 or -1. As long as the statistics is required to be invariant under energy shifts, the level statistics of disordered systems in the ergodic limit is bounded to be represented by the Wigner-Dyson statistics. If the stationarity condition is relaxed and additional symmetries are imposed, we can extend the symmetry classifications.

2.3.2. Particle-Hole

In addition to the time-reversal symmetry, there is another important anti-unitary operator, namely, the particle-hole operator

$$P = VK, \tag{2.19}$$

where V is a unitary operator. As we discussed for the time-reversal operator, in here the operator P also may square to two possible values: $-1, 1$ or be absent and in this case we write $P^2 = 0$. Considering these two symmetries, we can already construct 9 distinct symmetry classes. Below we discuss the last possible symmetry class we can construct with these operators.

2.3.3. Chiral

The last symmetry class to be considered is the chiral symmetry. It can be understood in terms of a product between the two symmetries displayed above and it is represented by a unitary operator $C = T * P$. It is easy to see the existence of the 9 possible symmetry, but among all these, one of them is not uniquely fixed. The case where the time-reversal and the particle-hole conjugation are absent can lead to two situations the chiral symmetry is present or absent, $C^2 = 1$ or $C^2 = 0$. Sometimes in the literature, the chiral symmetry is named sublattice symmetry, because this type of symmetry is commonly found in Hamiltonians of systems defined on a bipartite lattice, where the only non-vanishing entries are those describing hopping between two different sublattices.

2.3.4. Tenfold way

Assembling together the ten unique symmetry combinations described above we obtain the renowned tenfold way [AZ97], [Sch+08].

It is instructive to notice that these ten symmetry classes can be grouped into three classes: the Wigner-Dyson class which describes the system in terms of presence or absence of time-reversal symmetry. If the time-reversal symmetry is present in the system, then we have $T^2 = 1$ for system whose $SU(2)$ spin is an

	Class	T^2	P^2	$(PT)^2$	Hamiltonian
Wigner-Dyson	A	0	0	0	$\mathrm{U}(n)$
	AI	1	0	0	$\mathrm{U}(n)/\mathrm{O}(n)$
	AII	-1	0	0	$\mathrm{U}(2n)/\mathrm{Sp}(2n)$
Chiral	AIII	0	0	1	$\mathrm{U}(n+m)/[\mathrm{U}(n)\times\mathrm{U}(m)]$
	BDI	1	1	1	$\mathrm{SO}(n+m)/[\mathrm{SO}(n)\times\mathrm{SO}(m)]$
	CII	-1	-1	1	$\mathrm{Sp}(2n+2m)/[\mathrm{Sp}(2n)\times\mathrm{Sp}(2m)]$
Bogoliubov-De Gennes	D	0	1	0	$\mathrm{SO}(2n)$
	C	0	-1	0	$\mathrm{Sp}(2n)$
	DIII	-1	1	1	$\mathrm{SO}(2n)/\mathrm{U}(n)$
	CI	1	-1	1	$\mathrm{Sp}(2n)/\mathrm{U}(n)$

Table 2.1.: The ten universality classes of single particle Hamiltonians. The first column concerns the classification according to Cartan's nomenclature. The second, third and fourth columns represents the squared time-reversal, particle-hole and chiral operators. The presence of the symmetry is denoted by 1 or -1 and the absence by 0. The first six lines of the table are directed towards the symmetries of non-superconducting systems. The remaining lines are realizable in superconducting systems. The last column categorizes to which class the time-evolution operator associated with a given Hamiltonian belongs to.

integer and $T^2 = -1$ for the half-integer case. The chiral class, which can be thought of as the result of imposing the chiral symmetry on the Wigner-Dyson class. The most standard example of a system belonging to this class is a disordered tight-binding model on a bipartite lattice. Finally, the Bogoliubov-De Gennes class, which corresponds to a system displaying superconducting behavior. The particle-hole operator P squares to 1 when the system does not preserve the $SU(2)$ spin rotation symmetry and to -1 when this symmetry is preserved.

2.4. Effect of Disorder

2.4.1. Green's Function

In the context of single particle physics, below we will construct a convenient integral representation for the Green's function. First, we will consider the case where the integration variables are classical numbers, also named Bosonic variables, in the sense that $ab = ba$. Next, we perform an analogous construction for the case of quantum variables, the famous Fermionic variables, in this scenario we cannot take for granted the property of commutativity among the variables. Finally, we use the information acquired from the previous cases to construct a hybrid theory, which involves both types of variables. It may appear that this mixture of variables can introduce more complications, but we will see that, in fact, this formalism turns out to provide an excellent platform to perform several interesting calculations.

2.4.1.1. Bosonic Integrals

We start out from the most fundamental element of our field theory, namely, the Green's functions

$$G^{\pm}(\epsilon) = (\epsilon \pm i\delta - H)^{-1}, \tag{2.20}$$

where δ is an arbitrarily small positive quantity, the plus and minus signs indicates the standard retarded and advanced Green's functions, respectively, and H is the Hamiltonian in the presence of a disorder potential. Recalling that such Hamiltonian can be formally diagonalized by solving the eigenvalue problem $H\left|\alpha\right\rangle = \epsilon_\alpha \left|\alpha\right\rangle$, we use the completeness condition associated with the eigenvectors $\sum_\alpha \left|\alpha\right\rangle \left\langle\alpha\right|$ to write down the Green's function in a diagonal form

$$G^{\pm}(\epsilon) = \sum_\alpha \frac{\left|\alpha\right\rangle \left\langle\alpha\right|}{\epsilon \pm i\delta - \epsilon_\alpha} \tag{2.21}$$

and in real space representation it is given by the following expression

$$\langle \mathbf{r}|G^{\pm}(\epsilon)|\mathbf{r}'\rangle = \sum_\alpha \frac{\phi_\alpha(\mathbf{r})\phi_\alpha^*(\mathbf{r}')}{\epsilon \pm i\delta - \epsilon_\alpha}, \tag{2.22}$$

where we have defined the eigenfunctions as $\phi_\alpha(\mathbf{r}) = \langle \mathbf{r}|\alpha\rangle$. In a typical disordered system, the structure involved is complex enough such that one does not have access to the eigenfunctions or the eigenvalues of the Hamiltonian. Although we have obtained a formal description for our Green's function, it is not usually feasible to perform explicit calculation with it. Bearing this in mind, we turn our attention to the representation via functional integral, which does not require knowledge of these unknown quantities.

The basic principle to obtain this helpful representation involves writing down the Green's function in terms of a Gaussian integral

$$\frac{1}{\epsilon + i\delta - \epsilon_\alpha} = \int \frac{dzdz^*}{\pi} e^{-z^*(\epsilon + i\delta - \epsilon_\alpha)z}. \tag{2.23}$$

From this identity, we move forward to write a product over all eigenvalues of the Hamiltonian

$$\prod_\alpha \frac{1}{\epsilon + i\delta - \epsilon_\alpha} = \prod_\alpha \int \frac{dz_\alpha dz_\alpha^*}{\pi} e^{-z_\alpha^*(\epsilon + i\delta - \epsilon_\alpha)z_\alpha} = \int \frac{dz_1 dz_1^* \cdots dz_N dz_N^*}{\pi^N} e^{-\sum_\alpha z_\alpha^*(\epsilon + i\delta - \epsilon_\alpha)z_\alpha}, \tag{2.24}$$

which is the well known determinant of the operator $\det(\epsilon + i\delta - H)$. In the second equality, we performed a few algebraic manipulations in order to obtain a more convenient expression for the integrations and we omitted the fact that $N \to \infty$.

The summation over the dummy variables can be converted into an integration over the D-dimensional real space with the aid of the eigenfunctions: $\sum_\alpha z_\alpha^*(\epsilon + i\delta - \epsilon_\alpha)z_\alpha = \sum_{\alpha\beta}\int d^D x z_\alpha^* \phi_\alpha^*(\epsilon - H)_{\alpha\beta} z_\beta \phi_\beta = \int d^D x \varphi^\dagger(\epsilon + i\delta - H)\varphi$. Assembling together these results, we obtain the functional representation of the determinant

$$\frac{1}{\det(\epsilon + i\delta - H)} = \int \mathcal{D}(\varphi^\dagger, \varphi) e^{-\int d^D x \varphi^\dagger(\epsilon + i\delta - H)\varphi}. \tag{2.25}$$

In the result above, we introduced the measure $\mathcal{D}(\varphi^\dagger, \varphi)$. We remind that such measure can always be reduced back to the simpler product over dz_α allowing us to perform the integrations in a more familiar form, that is, $\varphi \to z_\alpha$. In addition to that, we employ the translational invariance of the integral and write down the Gaussian integral in the presence of source terms

$$\int \mathcal{D}(\varphi^\dagger, \varphi) e^{-\int d^D x \varphi^\dagger(\epsilon + i\delta - H)\varphi - \int d^D x \varphi^\dagger j - \int d^D x j^\dagger \varphi} = \frac{\exp\left[\int d^D x d^D y j^\dagger(x)(\epsilon + i\delta - H)^{-1}_{x,y} j(y)\right]}{\det(\epsilon + i\delta - H)}. \tag{2.26}$$

With the aid of this expression we can generate the Green's function and other correlation functions by simply taking the derivative with respect to the sources j and $j^\dagger$.

In this new language, the propagator can be written in the following form

$$\langle\varphi\varphi^\dagger\rangle = \mathcal{N}\int\prod_\gamma \frac{dz_\gamma dz_\gamma^*}{i\pi} e^{-\sum_\lambda z_\lambda^*(\epsilon+i\delta-\epsilon_\lambda)z_\lambda}\sum_{\alpha\beta} z_\beta\phi_\beta z_\alpha^*\bar{\phi}_\alpha, \tag{2.27}$$

where we have introduced a soon to be defined normalization factor $\mathcal{N}$. It is straightforward to show that the right-hand side vanishes unless $\alpha=\beta$, then

$$\langle\varphi\varphi^\dagger\rangle = \mathcal{N}\int\prod_\gamma \frac{dz_\gamma dz_\gamma^*}{\pi} e^{-\sum_\lambda z_\lambda^*(\epsilon-\epsilon_\lambda)z_\lambda}\sum_{\alpha} z_\alpha\phi_\alpha z_\alpha^*\phi_\alpha^* = \mathcal{N}\int\prod_{\gamma\neq\alpha} \frac{dz_\gamma dz_\gamma^*}{\pi} e^{-\sum_\lambda z_\lambda^*(\epsilon-\epsilon_\lambda)z_\lambda}\sum_{\alpha} \frac{\phi_\alpha\phi_\alpha^*}{(\epsilon+i\delta-\epsilon_\alpha)^2} \tag{2.28}$$

the remaining integrations yield

$$\langle\varphi\varphi^\dagger\rangle = \mathcal{N}\sum_\alpha \frac{\phi_\alpha\phi_\alpha^*}{\epsilon+i\delta-\epsilon_\alpha}\frac{1}{\epsilon+i\delta-\epsilon_\alpha}\prod_{\gamma\neq\alpha}\frac{1}{\epsilon+i\delta-\epsilon_\gamma} = \mathcal{N}\sum_\alpha \frac{\phi_\alpha\phi_\alpha^*}{\epsilon+i\delta-\epsilon_\alpha}\det(\epsilon+i\delta-H). \tag{2.29}$$

This result suggests that it is convenient to fix the normalization constant as $\mathcal{N}=[\det(\epsilon+i\delta-H)]^{-1}$. With these results, we can finally define the Green's function via a functional integral:

$$G_\epsilon^+(\mathbf{x},\mathbf{x}') = \langle\varphi(\mathbf{x})\varphi^\dagger(\mathbf{x}')\rangle = \frac{\int\mathcal{D}(\varphi^\dagger,\varphi)\varphi(\mathbf{x})\varphi^\dagger(\mathbf{x}')e^{-\int d^Dy\varphi^\dagger(\mathbf{y})(\epsilon+i\delta-H)\varphi(\mathbf{y})}}{\int\mathcal{D}(\varphi^\dagger,\varphi)e^{-\int d^Dy\varphi^\dagger(\mathbf{y})(\epsilon+i\delta-H)\varphi(\mathbf{y})}}. \tag{2.30}$$

Analogously, the same procedure can be applied to the advanced Green's function and the result reads

$$G_\epsilon^-(\mathbf{x},\mathbf{x}') = \langle\varphi(\mathbf{x})\varphi^\dagger(\mathbf{x}')\rangle = \frac{\int\mathcal{D}(\varphi^\dagger,\varphi)\varphi(\mathbf{x})\varphi^\dagger(\mathbf{x}')e^{-\int d^Dy\bar{\varphi}(\mathbf{y})(\epsilon-i\delta-H)\varphi(\mathbf{y})}}{\int\mathcal{D}(\varphi^\dagger,\varphi)e^{-\int d^Dy\varphi^\dagger(\mathbf{y})(\epsilon-i\delta-H)\varphi(\mathbf{y})}}. \tag{2.31}$$

Hence, we write down the Green's function using a notation that contemplates both cases, retarded and advanced:

$$G_\epsilon^\pm(\mathbf{x},\mathbf{x}') = \frac{\int\mathcal{D}(\varphi^\dagger,\varphi)\varphi(\mathbf{x})\varphi^\dagger(\mathbf{x}')e^{-\int d^Dy\varphi^\dagger(\mathbf{y})(\epsilon\pm i\delta-H)\varphi(\mathbf{y})}}{\int\mathcal{D}(\varphi^\dagger,\varphi)e^{-\int d^Dy\varphi^\dagger(\mathbf{y})(\epsilon\pm i\delta-H)\varphi(\mathbf{y})}}. \tag{2.32}$$

2.4.1.2. Fermionic Integrals

Even though the integrations over the Fermionic variables share many similarities with its corresponding counterpart, the Bosonic variables, we shall see that its construction relies on a purely algebraic and combinatorial scheme. To clarify the language, in here sometimes we shall refer to complex variables as commuting variables and Grassmann variables as anti-commuting variables. We first briefly recall the basic properties of anti-commuting variables (Grassmann variables). The Grassmann numbers can be constructed in two forms, we can consider a set of m anti-commuting elements ψ_i, usually called real fermions, as generators of the Grassmann space. In the special case, where m is an even number, $m=2n$, we can split them into two independent classes and construct a set with two types of anti-commuting quantities: ψ_j and ψ_j^*, which are commonly known as complex fermions. For an even number of generators, there exists a one-to-one mapping between ψ_i and ψ_i^*. It is convenient to define the complex conjugation as follows

$$\chi_i^*\chi_j^* = -\chi_j^*\chi_i^*, \quad \chi_i^*\chi_j = -\chi_j\chi_i^*. \tag{2.33}$$

In here we will consider the special case with an even number of Grassmann variables and introduce a set of generators χ and $\chi^\dagger$, where these generators satisfy the following fundamental relations

$$\chi_i\chi_j + \chi_j\chi_i = 0, \quad \chi_i^2 = 0. \tag{2.34}$$

The first relation does not necessarily imply the second as an immediate consequence of fixing $j = i$. In this special case, we would obtain $2\chi_i^2 = 0$ as a result. So, just to be on the safe side, we added the second rule independently of the first. In terms of integrations, however strange these properties may be, they lead to a set of fundamental rules of integration, which are much simpler in comparison to classical numbers. We start out by defining the form of a derivative acting on Grassmann variables:

$$\partial_i \chi_{i_1}\chi_{i_2}\cdots\chi_{i_p} = \begin{cases} (-1)^{\alpha-1}\chi_{i_1}\chi_{i_2}\cdots\chi_{\alpha-1}\chi_{\alpha+1}\chi_{i_p}, & \text{if } i = i_\alpha \\ 0, & \text{if } i \neq i_\alpha. \end{cases} \tag{2.35}$$

It acts as a regular derivative, but we need to consider the anti-commutative nature of the quantum variables when operating the derivative. In constrast with the integration over commuting variables, in which the integrand may be excessively complicated, turning the task of integrating it unfeasible, Grassmannian integrations are defined uniquely by the following rules

$$\int d\chi\chi = \int d\chi^*\chi^* = 1 \tag{2.36}$$

and

$$\int d\chi = 0. \tag{2.37}$$

Notice that despite the nature of integrand, as long as we are able to represent it in terms of a power series in the Grassmann variables, it is very likely that we can perform the integration over a given function. Throughout all calculations we shall always write the infinitesimal element and the integral operator to the left of the integrand. Suppose we have a collection of m Grassmann variables and a function f. Within this framework, such function would invariably be described via a summation of powers of these variables

$$f(\chi) = \sum_i c_i\chi_i + \sum_{ij} c_{ij}\chi_i\chi_j + \sum_{ij} c'_{ij}\chi_i\chi_j^* + \sum_{ij} c''_{ij}\chi_i^*\chi_j^* + \cdots. \tag{2.38}$$

The anti-commutative nature of these variables implies that such power series is terminated after a finite quantity of terms. For instance, consider the case where there is a function f linear in the quantum variables, then f affords a representation in the form: $f(\eta) = f(0) + f'(0)\eta$, any additional contribution vanishes, since $\eta^2 = 0$. The iterated integral is defined as

$$I = \int \prod_{i=1}^{n} d\chi_i d\chi_i^* f(\chi, \chi^\dagger) \tag{2.39}$$

and according to the definition of Grassmann integration, the result of integrating over these anti-commuting variables is simply given by the coefficient of the top monomial contribution.

Building on this, we must also introduce how we can perform a change of variables in the integration. To

do so, we start with the following integral

$$I = \int d\chi f(a\chi). \tag{2.40}$$

Next, we fix $\psi = a\chi$, then

$$\int d\chi f(a\chi) = \int d(a^{-1}\psi) f(\psi). \tag{2.41}$$

Representing the function f in powers of Grassmann variables on both sides, we obtain

$$\int d\chi (1 + a\chi + \cdots) = \int d(a^{-1}\psi)(1 + \psi + \cdots). \tag{2.42}$$

Using the rules for Grassmann integration, we see that on the left-hand side the integration simply yields a factor a. To construct a consistent rule to perform change of variables in the integrations, we are required to let $d(a^{-1}\psi)$ transform in an opposite manner as we would do for a commuting variable: $d(a^{-1}\psi) = a d\psi$. To generalize this expression, we consider the special case with a set of $m = 2n$ generators $\{\chi_i\}_{i=1}^{m}$ and separate them out into two sets $\{\psi_j\}_{j=1}^{n}$ and $\{\psi_j^*\}_{j=1}^{n}$, for every ψ_k there exists a corresponding ψ_k^*. Then, the integration measure contains pairs $d\psi_k d\psi_k^*$ which are Grassmann-even allowing us to write the measure in the following convenient manner

$$\mathcal{D}(\psi, \psi^\dagger) = \prod_{i=1}^{n} d\psi_i d\psi_i^*. \tag{2.43}$$

Next, introducing the linear transformation for both quantum variables: $\psi = S\chi$ and $\psi^\dagger = \chi^\dagger S'$, the measure becomes

$$d\psi_1 d\psi_1^* \cdots d\psi_m d\psi_m^* = d\left(\sum_i S_{1i}^{-1}\chi_i\right) d\left(\sum_i \chi_i^* S_{1i}'^{-1}\right) \cdots d\left(\sum_i S_{mi}^{-1}\chi_i\right) d\left(\sum_i \chi_i^* S_{mi}'^{-1}\right). \tag{2.44}$$

To be consistent with our definition of measure, we order the elements such that they satisfy the form displayed in Eq. (2.43):

$$\prod_{i=1}^{m} d\psi_i d\psi_i^* = \left(\sum_\sigma \mathrm{sgn}(\sigma) \prod_{i=1}^{m} S_{i\sigma(i)}\right) \left(\sum_{\sigma'} \mathrm{sgn}(\sigma') \prod_{j=1}^{m} S'_{j\sigma'(j)}\right) \prod_{l=1}^{m} d\chi_l d\chi_l^*. \tag{2.45}$$

The two terms between parenthesis are, by definition, the determinant of the matrices S and S', thus

$$\prod_{i=1}^{m} d\psi_i d\psi_i^* = \det(SS') \prod_{l=1}^{m} d\chi_l d\chi_l^*. \tag{2.46}$$

A straightforward application of this transformation is the calculation of a Gaussian integral for a system with only two generators

$$I_2 = \int d\psi d\psi^* e^{\psi^* a \psi} = \int d\psi d\psi^* (1 + a\psi^*\psi) = a, \tag{2.47}$$

where only the top monomial is required to evaluate the integral. The same result can also be quickly obtained, if we perform a change of variables of the form $\psi \to \psi/\sqrt{a}$, then it immediately follows the displayed result. The situation becomes a bit more involved when we upgrade our system to four generators

$$I_4 = \int d\psi_1 d\psi_1^* d\psi_2 d\psi_2^* e^{\sum_{i,j=1}^{2} \psi_i^* A_{ij} \psi_j}. \tag{2.48}$$

Now there is a summation over a matrix structure which introduces some additional calculations. As in the previous case, we start the evaluation of the integral with a Taylor expansion of the exponential function

$$I_4 = \int d\psi_1 d\psi_1^* d\psi_2 d\psi_2^* \left(1 + \sum_{i_1,j_1=1}^{2} \psi_{i_1}^* A_{i_1 j_1} \psi_{j_1} + \frac{1}{2!} \sum_{i_1,j_1=1}^{2} \psi_{i_1}^* A_{i_1 j_1} \psi_{j_1} \sum_{i_2,j_2=1}^{2} \psi_{i_2}^* A_{i_2 j_2} \psi_{j_2} + \cdots \right). \quad (2.49)$$

By definition, the zeroth and first-orders of the expansion vanish and only a few contributions from the second-order term provide a non-zero result, as we display below:

$$I_4 = \int d\psi_1 d\psi_1^* d\psi_2 d\psi_2^* (A_{11}A_{22} - A_{12}A_{21}) \psi_2^* \psi_2 \psi_1^* \psi_1. \quad (2.50)$$

Thus, recognizing that $\det A = A_{11}A_{22} - A_{12}A_{21}$, the integration over the generators yields

$$I_4 = \det A, \quad (2.51)$$

a result which is upside down in comparison to what we obtained for classical numbers. The generalization of these results for integrals containing an arbitrary number of generators reads

$$I_n = \det A. \quad (2.52)$$

The proof of this identity can be found in many references [Efe99], [AS10]. In addition to that, translational invariance is a fundamental property of Grassmann integrals which allows us to obtain helpful identities, for any function of Grassmann variables, we have

$$\int d\psi f(\psi + \eta) = \int d\psi f(\psi). \quad (2.53)$$

Building on this discussion, we write down the following Fermionic Gaussian integral

$$I_n(\nu) = \int \mathcal{D}(\psi, \psi^\dagger) e^{\int d^D y [\psi^\dagger (\epsilon + i\delta - H)\psi + \nu^\dagger \psi + \psi^\dagger \nu]}, \quad (2.54)$$

where ν and $\nu^\dagger$ are sources whose purpose is to help us generate correlation functions. Next we use the translational invariance to performing a shift in ψ and evaluating the integral it yields

$$I_n(\nu) = \det(\epsilon + i\delta - H) e^{\int d^D y d^D x \nu^\dagger(y)(\epsilon + i\delta - H)^{-1}\nu(x)}. \quad (2.55)$$

With the aid of these expressions, we can define the Green's function for Fermionic fields:

$$G_\epsilon^\pm(\mathbf{x}, \mathbf{x}') = \frac{\int \mathcal{D}(\psi, \psi^\dagger)\psi(\mathbf{x})\psi^\dagger(\mathbf{x}') e^{\int d^D y \psi^\dagger(\mathbf{y})(\epsilon \pm i\delta - H)\psi(\mathbf{y})}}{\int \mathcal{D}(\psi, \psi^\dagger) e^{\int d^D y \psi^\dagger(\mathbf{y})(\epsilon \pm i\delta - H)\psi(\mathbf{y})}}. \quad (2.56)$$

2.4.1.3. Supermathematics

In order to develop some intuition about the nature of the supersymmetric formalism, we perform some manipulations with the bosonic and fermionic partition functions and demonstrate how the supersymmetry can appear naturally in the calculations. First, consider the following partition functions in the presence of

an external source, j and ν, bosonic and fermionic, respectively, whose role is to generate observables

$$\mathcal{Z}_B(j) = \det A \int \prod_{a=1}^{m} \frac{dz_a dz_a^*}{\pi} e^{-z_i^* A_{ij} z_j + j_i z_i^* + z_i j_i^*} = e^{j^\dagger A^{-1} j} \tag{2.57}$$

and

$$\mathcal{Z}_F(\nu) = \frac{1}{\det A} \int \prod_{a=1}^{m} d\chi_a d\chi_a^* e^{\chi_i^* A_{ij} \chi_j + \nu_i \chi_i^* + \chi_i \nu_i^*} = e^{\bar{\nu} A^{-1} \nu}. \tag{2.58}$$

This representation is often more convenient, because we can generate arbitrary correlators, instead of representing them individually. In a typical calculation, the matrix A is substituted by a Green's function. As a consequence of our construction, it yields the following results:

$$\frac{\partial^2 \mathcal{Z}_B(j)}{\partial j_i \partial j_m^*} = A_{mi}^{-1}, \tag{2.59}$$

$$\frac{\partial^2 \mathcal{Z}_F(\nu)}{\partial \nu_i \partial \nu_m^*} = A_{mi}^{-1}. \tag{2.60}$$

However powerful this method have proved itself to be, it lacks a simple approach when we have to average over the disorder configurations. In such case, one has to resort to a different representation scheme in order to circumvent this shortcoming. The problematic part of the previous results is the presence of a determinant in the denominator, it makes incredibly difficult to calculate averages over the quantities under scrutiny. Fortunately, it is possible to remove it from there by writing the matrix entry A_{mi}^{-1} in a form which contemplates both types of variables, bosonic (commuting variables) and fermionic (anti-commuting variables):

$$A_{mi}^{-1} = \frac{1}{2} \frac{\partial^2}{\partial j_i \partial j_m^*} \int \prod_{a=1}^{m} d\chi_a d\chi_a^* e^{\chi_i^* A_{ij} \chi_j} \mathcal{Z}_B(j) + \frac{1}{2} \frac{\partial^2}{\partial \nu_i \partial \nu_m^*} \int \prod_{a=1}^{m} \frac{dz_a dz_a^*}{\pi} e^{-z_i^* A_{ij} z_j} \mathcal{Z}_F(\nu). \tag{2.61}$$

Substituting the partition functions and operating the derivatives over the sources, we obtain this intermediate expression

$$A_{mi}^{-1} = \frac{1}{2} \int \prod_{a=1}^{m} d\chi_a d\chi_a^* \frac{dz_a dz_a^*}{\pi} e^{-z_i^* A_{ij} z_j} e^{\chi_i^* A_{ij} \chi_j} z_m z_i^* + \frac{1}{2} \int \prod_{a=1}^{m} d\chi_a d\chi_a^* \frac{dz_a dz_a^*}{\pi} e^{-z_i^* A_{ij} z_j} e^{\chi_i^* A_{ij} \chi_j} \chi_m \chi_i^*, \tag{2.62}$$

which can be simplified to

$$A_{mi}^{-1} = \frac{1}{2} \int \prod_{a=1}^{m} d\chi_a d\chi_a^* \frac{dz_a dz_a^*}{\pi} e^{-z_i^* A_{ij} z_j} e^{\chi_i^* A_{ij} \chi_j} (z_m z_i^* + \chi_m \chi_i^*). \tag{2.63}$$

Introducing the supervector $\Phi_i = (z_i \quad \chi_i)^T$, we can write down the matrix entry in a much more compact form:

$$A_{mi}^{-1} = \frac{1}{2} \int \prod_{a=1}^{m} \prod_{\zeta=1}^{2} d\Phi_a^\lambda d(\Phi_a^\zeta)^* e^{-(\Phi_i^\lambda)^* (\sigma_3)_{\lambda\lambda} A_{ij}^{\lambda\rho} \Phi_j^\rho} \Phi_m^\alpha (\Phi_i^\alpha)^*. \tag{2.64}$$

Notice that with this particular definition, the expressions are no longer plagued by the presence of the inconvenient determinant. Furthermore, if we define the Fermionic Gaussian integral with a minus sign, then the presence of the Pauli matrix in the exponential is no longer required, because both sectors follow

the same signature

$$A_{mi}^{-1} = \frac{1}{2}\int \prod_{a=1}^{m}\prod_{\zeta=1}^{2} d\Phi_a^{\zeta} d(\Phi_a^{\zeta})^* e^{-(\Phi_i^{\lambda})^* A_{ij}^{\lambda\rho}\Phi_j^{\rho}} \Phi_m^{\alpha}(\Phi_i^{\alpha})^*. \tag{2.65}$$

Combining the two formalisms presented above, we construct a $(n+m)$-component object which is usually called a supervector

$$\Phi = \begin{pmatrix} z_1 \\ \vdots \\ z_n \\ \chi_1 \\ \vdots \\ \chi_m \end{pmatrix}, \tag{2.66}$$

where z_i represents the commuting variables, while χ_i the anti-commuting. In addition to that, we also define the adjoint of the supervector

$$\Phi^{\dagger} = \begin{pmatrix} z_1^* & \cdots & z_n^* & \chi_1^* & \cdots & \chi_m^* \end{pmatrix}. \tag{2.67}$$

In order to satisfy the conventional rules of vector transposition, the transpose operation for the supervector and its adjoint is a bit different from the usual transposition operation:

$$\Phi^{\mathrm{st}} = \begin{pmatrix} z^T & -\chi^T \end{pmatrix}, \qquad (\Phi^{\dagger})^{\mathrm{st}} = \begin{pmatrix} (z^{\dagger})^T \\ (\chi^{\dagger})^T \end{pmatrix} \tag{2.68}$$

Using this hybrid structure, we introduce also the supermatrix and its supertranspose

$$F = \begin{pmatrix} a & \sigma \\ \rho & b \end{pmatrix}, \qquad F^{\mathrm{st}} = \begin{pmatrix} a^T & \rho^T \\ -\sigma^T & b^T \end{pmatrix}, \tag{2.69}$$

where a and b are $n \times n$ and $m \times m$ matrices, respectively, containing commuting variables and the off-diagonal entries σ and ρ are $n \times m$ and $m \times n$ matrices and the entries of these matrices consists of anti-commuting variables. In terms of indices, these blocks are usually called in the literature as Bose-Bose, Fermi-Fermi, Bose-Fermi and Fermi-Bose, respectively. Furthermore, the different structure displayed by the supertranspose in comparison to the conventional transpose is required in order to satisfy the property $(F_1F_2)^T = F_2^T F_1^T$). In the theory of conventional matrices, the operations of taking the trace and the determinant are of utmost importance. Having introduced the supermatrix, it is also necessary to define what do we mean by trace and determinant in this new framework. Starting with the former, we define:

$$\mathrm{str}(F) = \sum_{\nu=\mathrm{b,f}} \mathrm{tr}(F^{\nu\nu}) = \mathrm{tr}(a) - \mathrm{tr}(b), \tag{2.70}$$

where the minus sign is required to preserve the trace invariance under cyclic permutations and the symbol tr stands for the conventional trace. The determinant is promoted to a superdeterminant and its form is very unusual

$$\mathrm{sdet}(F) = \det(a - \sigma b^{-1}\rho)\det{}^{-1} b. \tag{2.71}$$

To conclude the discussion about supermathematics (graded algebra), we introduce the integrals over supermatrices. In particular, we state the results for a Gaussian integral with supermatrices

$$\int d\Phi d\bar{\Phi} e^{-\bar{\Phi}K\Phi} = \mathrm{sdet}(K) \tag{2.72}$$

and also the average of the product $\Phi_\alpha \bar{\Phi}_\beta$:

$$\left\langle \Phi_\alpha \bar{\Phi}_\beta \right\rangle = \int d\Phi d\bar{\Phi} \Phi_\alpha \bar{\Phi}_\beta e^{-\bar{\Phi}K\Phi} = (K)^{-1}_{\alpha\beta} \mathrm{sdet} K. \tag{2.73}$$

As far as the integration concerns, the blocks involving Fermionic variables do not have any issues associated with convergence. However, in terms of the Bosonic variables, in order to ensure the existence of this integration, the real part of the sector K_{bb} of the supermatrix K must be positive definite, that is, $\mathrm{Re}(z^\dagger K_{\mathrm{bb}} z) > 0$.

2.4.2. Non-Linear Sigma Model

Since the disorder configuration is much likely to vary from sample to sample, in order to properly understand the transport properties in a disordered system, a statistical approach is required. In such approach, we aim to describe the properties of the system in terms of a few universal characteristics of the scattering landscape, for instance, the strength of the impurity potential, the usual range of potential fluctuations. To implement the impurity potential in terms of a statistical approach, we introduce a disorder potential V whose statistical properties are descibred by a probability distribution $P[V]$. The averaged quantities are calculated via the functional integral

$$\langle \mathcal{O} \rangle_{\mathrm{dis}} = \int \mathcal{D}V \mathcal{O} P[V]. \tag{2.74}$$

In this work, without any loss of generality, we will consider applications of this approach by using a Gaussian distribution

$$P[V] = \mathcal{N} e^{-\pi\nu\tau \int d^D x \int d^D x' V(\mathbf{x}) K(\mathbf{x}-\mathbf{x}') V(\mathbf{x}')}, \tag{2.75}$$

where $\mathcal{N}$ is a normalization constant whose explicit form is irrelevant to our calculations, τ denotes the mean elastic scattering time, ν the density of states and the numerical pre-factor $\pi\nu\tau$ corresponds to the strength of the disorder potential. The function $K(\mathbf{x}-\mathbf{x}')$ represents the spatial correlation profile of the disorder potential. In most applications, considering a finite spatial correlation for V does not alter the physical properties [GMW01] and an advantageous choice of function to describe the spatial correlation profile is a Dirac delta $K(\mathbf{x}) = \delta(\mathbf{x})$. Then, the two-point correlation function for the disorder potential reads

$$\langle V(\mathbf{x}) V(\mathbf{x}') \rangle = \frac{1}{2\pi\nu\tau} \delta(\mathbf{x}-\mathbf{x}'). \tag{2.76}$$

As a result, the samples for the disorder potential are drawn from the following probability distribution:

$$P[V(\mathbf{x})] = \mathcal{N} e^{-\pi\nu\tau \int d^D x V^2(\mathbf{x})}. \tag{2.77}$$

We will use this framework to diagnosis how the disorder affects the properties of the systems under investigation. In principle, our next step could be the calculation of the average functional displayed in Eq. (2.74).

However, if we just had to average over the partition function $\mathcal{Z}$, the result would be a straightforward Gaussian integral again. Unfortunately, recalling the expressions we obtained for the Green's function (2.32) and (2.56), we immediate conclude that this is not the case. There is an additional complication in the average functional due to the presence of a denominator which also contains the disorder potential. To circumvent this problem, we will explore two options: the supersymmetric approach, as we explained above in Sec. 2.4.1.3, and the replica method.

The latter is more frequently employed in calculations involving perturbation theory, since its implementation is simpler than the former method. As in the case we will study later 5, the information about the average current and the Josephson fluctuations is encoded in the free energy, $F = -T \log \mathcal{Z}$. Although we take derivatives over the free energy in order to obtain the observables, there is still a partition function in the denominator

$$\langle \mathcal{O} \rangle = - \left\langle \frac{1}{\mathcal{Z}[V, J=0]} \frac{\delta \mathcal{Z}[V,J]}{\delta J} \right\rangle , \tag{2.78}$$

which depends on the disorder potential, turning the averaging usually unfeasible.

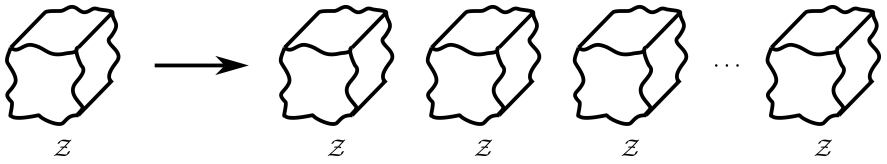

Figure 2.4.: Starting out from the original system, we make R replicas of it and this allows us to simplify the average functional.

In order to evaluate the average functional of the logarithm, it is advantageous to consider the R-th power of the partition function $\mathcal{Z}$. The power R is an integer number representing the quantity of replicated partition functions we have Fig. 2.4. With this construction, we explore a well known calculus identity

$$\langle \mathcal{O} \rangle = - \frac{\delta \log \mathcal{Z}[J]}{\delta J} = - \frac{\delta}{\delta J} \lim_{R \to 0} \frac{e^{R \log Z[J]} - 1}{R} = - \frac{\delta}{\delta J} \lim_{R \to 0} \frac{\mathcal{Z}^R}{R}, \tag{2.79}$$

where R denotes the number of replicated partition functions. In this sense, the average over the disorder is now linear in V, which is an incredible simplification in comparison to the previous representation. Hence, instead of performing the highly non-trivial task of averaging over the logarithm of the partition function, we artificially generate an arbitrary number of replicas of the original partition function and the final result is obtained by taking the limit of R to zero. More details about the replica formalism explored within the context of a nonlinear sigma model can be found in the appendix D.

Since the mentioned appendix already provides a solid derivation for the replica version of the non-linear sigma model, in here we will present the derivation within the framework of the supersymmetric variables. To compute the average over the disorder potential, we start out by defining the supervector ψ which belongs to the space composed of the retarded/advanced and Bose-Fermi spaces times the physical space, $\psi = \begin{pmatrix} \psi_{\mathrm{r}} & \psi_{\mathrm{a}} \end{pmatrix}^T$ and $\psi_\alpha = \begin{pmatrix} z_1 & \cdots & z_N & \chi_1 & \cdots & \chi_N \end{pmatrix}_\alpha^T$, and represent the partition function as

$$\mathcal{Z}[J] = \int \mathcal{D}(\psi,\psi^\dagger)\exp\left\{i\int d^Dx\bar{\psi}\left[E+\left(\frac{\omega}{2}+i\delta\right)\sigma_3^{\rm ra}-H_0-V\right]\psi\right\}, \tag{2.80}$$

where we have introduced $\bar{\psi}=\psi^\dagger(\sigma_3^{\rm ra}\otimes\Pi_{\rm bb}+\mathbb{1}_{\rm ra}\otimes\Pi_{\rm ff})$, $\Pi_{\rm aa}$ is a projector onto the Bosonic or Fermionic sectors, the Pauli matrix $\sigma_3^{\rm ra}$ acts on the retarded/advanced sector, H_0 is the free Hamiltonian containing only the kinetic contributions and V is the disorder potential. Envisioning the fact that the most interesting quantities, namely, density-density correlations, conductance and mesoscopic fluctuations, involve the product between Green's functions of distinct nature, i.e. $G^r_{\epsilon+\omega/2}G^a_{\epsilon-\omega/2}$, we introduced the partition function equipped with the additional retarded/advanced sectors. It is helpful to understand the disorder average process over the partition function, because from it we can generate arbitrary correlators by adding external sources J and taking derivatives with respect to them. Furthermore, starting from a symmetric Hamiltonian, $H^{\rm st}=H^T=H$, in order to accommodate the time-reversal symmetry into the action

$$S[\psi,\bar{\psi}] = \int d^Dx\bar{\psi}\left[E+\left(\frac{\omega}{2}+i\delta\right)\sigma_3^{\rm ra}-H_0-V\right]\psi, \tag{2.81}$$

we use that $S=S^{\rm st}$ to derive a version of the original action symmetrized under time-reversal operations

$$S[\psi,\bar{\psi}] = \int d^Dx\bar{\Psi}\left[E+\left(\frac{\omega}{2}+i\delta\right)\sigma_3^{\rm ra}-H\right]\Psi. \tag{2.82}$$

In the last equality we defined the symmetrized supervector and its adjoint

$$\Psi=\begin{pmatrix}\psi\\ \bar{\psi}^{\rm st}\end{pmatrix}, \qquad \bar{\Psi}=\begin{pmatrix}\bar{\psi} & \psi^{\rm st}\end{pmatrix}, \tag{2.83}$$

respectively. Notice that these recently defined supervectors are not independent quantities, they related to each other via the time-reversal supermatrix τ:

$$\Psi^{\rm st}=\bar{\Psi}\tau, \tag{2.84}$$

where

$$\tau=\begin{pmatrix}0 & \sigma_3^{\rm bf}\\ 1 & 0\end{pmatrix}. \tag{2.85}$$

Thus, the partition function including the external sources reads

$$\mathcal{Z}[J] = \int \mathcal{D}(\Psi,\bar{\Psi})\exp\left\{i\int d^Dx\bar{\Psi}\left[E+\left(\frac{\omega}{2}+i\delta\right)\sigma_3^{\rm ra}-H\right]\Psi+i\int d^Dx(\bar{\Psi}J+J\bar{\Psi})\right\}. \tag{2.86}$$

Next we set the external sources to zero again, since their presence is irrelevant to our computations, we average over the disorder potential V and it yields

$$\langle\mathcal{Z}[0]\rangle = \int \mathcal{D}(\Psi,\bar{\Psi})\exp\left\{i\int d^Dx\bar{\Psi}\left[E+\left(\frac{\omega}{2}+i\delta\right)\sigma_3^{\rm ra}-H_0\right]\Psi\right\}\left\langle\exp\left(-i\int d^Dx\bar{\Psi}V\Psi\right)\right\rangle. \tag{2.87}$$

In analogy with a simple one-dimensional Gaussian integral, we calculate the integration over the disorder potential and it generates a term with a quartic interaction

$$\left\langle \exp\left(-i\int d^D x\bar{\Psi}V\Psi\right)\right\rangle = \exp\left[-\frac{1}{4\pi\nu\tau}\int d^D x(\bar{\Psi}\Psi)^2\right]. \tag{2.88}$$

Substituting it back into Eq. (2.87) yields the following result

$$\langle\mathcal{Z}[0]\rangle = \int\mathcal{D}(\Psi,\bar{\Psi})\exp\left\{i\int d^D x\bar{\Psi}\left[E+\left(\frac{\omega}{2}+i\delta\right)\sigma_3^{\mathrm{ra}}-H_0\right]\Psi-\frac{1}{4\pi\nu\tau}\int d^D x(\bar{\Psi}\Psi)^2\right\}. \tag{2.89}$$

In this quartic interaction, it behoove us to apply a decoupling scheme to reduce the complexity of the computations. Within the weak disorder limit, not all decoupling channels lead to contributions that are relevant to the calculations of the spectral or transport properties and this greatly simplifies the action. A good strategy in here is to decompose the four-vertex interaction into its low lying energy excitations, which corresponds to energy excitations that are close to the Fermi surface, $|\epsilon(\mathbf{k})-\epsilon_F|\ll 1$. The isolation of this excitations also known as soft modes is conveniently performed in the Fourier space:

$$\int d^D\mathbf{x}[\bar{\Psi}(\mathbf{x})\Psi(\mathbf{x})]^2 = \int\prod_{i=1}^{4}d^D\mathbf{p}_i\delta(\mathbf{p}_1+\mathbf{p}_2+\mathbf{p}_3+\mathbf{p}_4)\bar{\Psi}_{\mathbf{p}_1}\Psi_{\mathbf{p}_2}\bar{\Psi}_{\mathbf{p}_3}\Psi_{\mathbf{p}_4}. \tag{2.90}$$

The Fourier transform of the quartic term, generates its representation in momentum space and the presence of the Dirac delta dictates the relevance of the momentum combinations. Next, we separate out the momenta into two components $\mathbf{k}=\mathbf{p}+\mathbf{q}$, where $\mathbf{p}$ lies on the Fermi surface and $\mathbf{q}$ is a momentum perpendicular to the Fermi surface, Fig. 2.5. This situation is analogous to what one encounters in the heavy quark effective theory, where the four-momentum is decomposed into $k_\mu = mv_\mu + q_\mu$ with q_μ begin a variable that measures the off-shellness of the heavy quark.

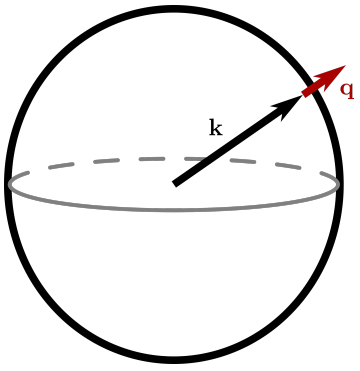

Figure 2.5.: Decomposition of the momentum $\mathbf{k}$ into two parts: $\mathbf{p}$ lying on top of the Fermi surface and $\mathbf{q}$ a small momentum displacement perpendicular to the Fermi surface.

Applying this to the interaction term, we are able to single out two relevant contributions:

$$\int d^D\mathbf{x}[\bar{\Psi}(\mathbf{x})\Psi(\mathbf{x})]^2 = \sum_{|\mathbf{p}_1|,|\mathbf{p}_2|,|\mathbf{q}|<\ell^{-1}}(\bar{\Psi}_{\mathbf{p}_1}\Psi_{\mathbf{p}_2}\bar{\Psi}_{-\mathbf{p}_2-\mathbf{q}}\Psi_{-\mathbf{p}_1+\mathbf{q}}+\bar{\Psi}_{\mathbf{p}_1}\Psi_{\mathbf{p}_2}\bar{\Psi}_{-\mathbf{p}_1+\mathbf{q}}\Psi_{-\mathbf{p}_2-\mathbf{q}}), \tag{2.91}$$

where ℓ is the mean free path and notice that the summation is now restricted to channels undergoing multiple scattering with the exchange of momentum smaller than the mean free path. The first contribution represents the diffuson channel, panel (a) in Fig. 2.6. This type of diagram is associated with pairs of trajectories experiencing the same set of scattering events and, in this sense, this contribution is a classical quantity and can only lead to localization via higher-order diagrams.

Figure 2.6.: In momentum space we display the two fundamental diffusion modes. In panel (a) the diffuson channel corresponding to a ladder diagram. In panel (b) the Cooperon channel with a maximally crossed diagram.

Contrary to the first contribution, which could be interpreted in terms of classical trajectories, the second contribution has a purely quantum mechanical origin and is named the Cooperon channel, see panel (b) in Fig. 2.6. In this type of diagram, the quantum diffusive effects emerge. Because, in terms of trajectories, such diagrams depicts pairs of coherent trajectories counter-propagating along the same set of multiple scattering events, which leads to the electron's amplitude constructively interfering at the origin of a closed loop. This causes a phase accumulation which is responsible for a reduction of the magnitude of the diffusion parameter and, depending on the dimensionality, can ultimately get the electron stuck or localized. In momentum space, the Cooperon modes are represented by the so-called maximally crossed diagrams.

In principle, in order to decouple the quartic interaction, we should introduce a different auxiliary matrix field for each channel individually. However, anticipating this issue, we doubled the field space to accommodate these two distinct low-lying excitations into a single auxiliary field. Using the time-reversal relation between the supervectors displayed in Eq. (2.84), it can be shown that the two channels exhibited above are identical and the effective action associated with the quartic interaction reads

$$S_{\text{quartic}}[\Psi,\bar{\Psi}] = -\frac{1}{2\pi\nu\tau}\int \sum_{|\mathbf{p}_1|,|\mathbf{p}_2|,|\mathbf{q}|<\ell^{-1}} \bar{\Psi}_{\mathbf{p}_1}\Psi_{\mathbf{p}_2}\bar{\Psi}_{-\mathbf{p}_2-\mathbf{q}}\Psi_{-\mathbf{p}_1+\mathbf{q}}. \tag{2.92}$$

In order to decouple these quartic contributions, we employ the famous Hubbard-Stratonovich transformation [Hub59], which consists of making use of the following idea: let x be a real variable, λ be a coupling setting the strength of the quartic interaction and suppose we exponentiated it $e^{\lambda x^4}$. Such term can be conveniently transformed into a Gaussian integral with the aid of an auxiliary variable α:

$$\exp\left(\lambda x^4\right) = \frac{1}{\sqrt{2\lambda}}\int d\alpha \exp\left(-\alpha^2/\lambda + 2\alpha x\right). \tag{2.93}$$

Applying this same principle to our case yields our decoupled action

$$\exp\left[-\frac{1}{2\pi\nu\tau}\int d^Dx(\bar{\Psi}\Psi)^2\right] = \int \mathcal{D}Q \exp\left[\frac{\pi\nu}{8\tau}\int d^Dx \text{str}(Q^2) - \frac{1}{2\tau}\int d^Dx\bar{\Psi}Q\Psi\right], \tag{2.94}$$

where Q is our auxiliary Hermitian supermatrix field with entries in the time-reversal, Bose-Fermi and retarded-advanced spaces. By construction, such supermatrix have the same rank and symmetry constraints as the dyadic product $\Psi \otimes \bar{\Psi}$ and it plays the role of our fundamental degree of freedom. The Hubbard-Stratonovich decoupling allowed us to return to an action which is quadratic in the Fermionic fields, at the cost of introducing a functional integration over a supermatrix field Q. Moreover, by fully exploring the configurational space defined by the Fermionic superfields, such calculation scheme made it possible for us to remove the irrelevant fast degrees of freedom. For more technical details about the calculations we performed to arrive at such result please check the appendix D. Assembling the previous result with Eq. (2.87), we obtain the unwound functional integral

$$\mathcal{Z}[0] = \int \mathcal{D}(\Psi, \bar{\Psi}) \mathcal{D}Q \exp\left\{ \frac{\pi\nu}{8\tau} \int d^D x \mathrm{str}(Q^2) + i \int d^D x \bar{\Psi} \left[E + \left(\frac{\omega}{2} + i\delta \right) \sigma_3^{\mathrm{ra}} - H_0 + \frac{iQ}{2\tau} \right] \Psi \right\}. \tag{2.95}$$

It is finally possible for us to integrate out the Fermionic degrees of freedom associated with the supervectors, yielding then a theory whose form only depends on the slow varying supermatrix Q. Calculating the Gaussian integral and using the identity $\mathrm{sdet} A = e^{\mathrm{str}\log A}$ yield

$$\mathcal{Z}[0] = \int \mathcal{D}Q \exp\left\{ \frac{\pi\nu}{8\tau} \int d^D x \mathrm{str}(Q^2) - \frac{1}{2} \int d^D x \mathrm{str} \log \left[E + \left(\frac{\omega}{2} + i\delta \right) \sigma_3^{\mathrm{ra}} - H_0 + \frac{iQ}{2\tau} \right] \right\}. \tag{2.96}$$

In the functional integration over the Fermionic superfields, we have previously pointed out that such fields are not independent entities, the 1/2 logarithmic prefactor reflects this reduced quantity of degrees of freedom. Varying the action and putting the first variation to zero, we search for a solution which is stationary and infinitely-slow (homogeneous field configuration), satisfying the mean field equation below:

$$\frac{\delta S[Q]}{\delta Q_{\mathrm{p}}} = 0. \tag{2.97}$$

Taking the limit of vanishingly small symmetry breaking source ω, we implement the protocol described above. After performing a few algebraic manipulations in the mean field equation, we obtain an equation of the type $Q_0 = f(Q_0)$ typically called a self-consistency equation in the literature:

$$Q_0 = \frac{i}{\pi\nu} \sum_{\mathbf{p}} \left[E + \left(\frac{\omega}{2} + i\delta \right) \sigma_3^{\mathrm{ra}} - \frac{p^2}{2m} + \frac{iQ_0}{2\tau} \right]^{-1}. \tag{2.98}$$

To seek a solution for this mean field equation, we assume that the supermatrix field Q_0 is diagonal in the Bose-Fermi and retarded-advanced spaces. Furthermore, to evaluate the summation, we adopt that $\sum_{\mathbf{p}} = \nu \int d\epsilon_p$ and use the weak disorder inequality $E\tau \gg 1$ to extend the integration over the energy ϵ_p from zero to minus infinity, while considering a constant density of states ν. Among the possible solution to this mean field equation, we recall that the retarded Green's function is analytic in the entire upper half-plane, whereas the advanced Green's function analyticity is present in the entire lower half-plane. The observation that the disorder average must preserve causality immediately singles out the field configuration $Q_0 = \sigma_3^{\mathrm{ra}}$, this saddle-point is typically called the metallic saddle-point in the literature.

In the zero frequency limit, the metallic saddle-point is satisfied by any homogeneous supermatrix Q of adequate rank and symmetry, as long as it obeys the non-linear constraint $Q^2 = 1$. This feature of our construction indicates that it is convenient to parametrize the supermatrix field Q in terms of rotations around this particular saddle-point, that is, $Q = T\sigma_3^{\mathrm{ra}} T^{-1}$, where T is a unitary supermatrix belonging

to a symmetry group G. However, such a choice of parametrization comes with a cost. Suppose S is a supermatrix in the symmetry group H which commutes with the metallic saddle-point and we perform a linear transformation of the form $T \to ST$. It is straightforward to see that this class of supermatrix generates a redundancy in the description of the supermatrix field Q, because Q does not change under transformations of this type. In order to remove this, we factorise out the matrix S from our construction. As a consequence of this procedure, we end up with a symmetry group G/H consisting of elements that do not leave the saddle-point invariant and the matrices T and Q are now in a one-to-one correspondence. Moreover, from the viewpoint of the Lie theory, this resulting structure is by construction a symmetric space.

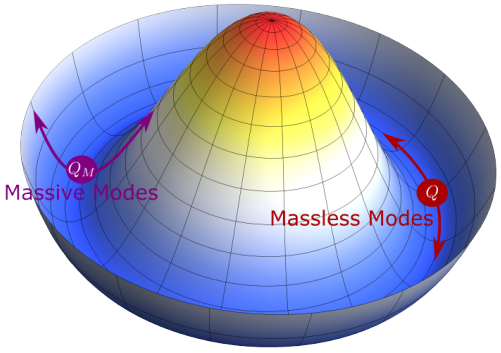

Figure 2.7.: Massive modes, with masses of the order ν/τ, correspond to oscillations along the radius of the potential. Massless modes, or Goldstone modes in the usual nomenclature, are associated with trajectories propagating perpendicularly to the radius, the flat region of the potential.

Next, we start our expansion scheme of the log-trace contribution. Recalling that to contemplate the entire manifold of saddle-point solutions, we made use of the rotation matrix T and conveniently parametrized the supermatrix field Q as $Q = T\sigma_3^{\mathrm{ra}}T^{-1}$. Using this construction of the supermatrix Q, we write down the logarithmic term such that it reproduces elements of the saddle-point equation

$$\log\left(E + \frac{\omega_+}{2}\sigma_3^{\mathrm{ra}} - H_0 + \frac{iT\sigma_3^{\mathrm{ra}}T^{-1}}{2\tau}\right) = \log\left[T^{-1}\left(E + \frac{\omega_+}{2}\sigma_3^{\mathrm{ra}} - H_0\right)T + \frac{i\sigma_3^{\mathrm{ra}}}{2\tau}\right], \tag{2.99}$$

where to simplify the notation we defined $\omega_+ = \omega + i\delta$. Note that, within this calculation scheme, the term involving Q^2 does not contribute to the effective action. Moreover, even if we relaxed a bit the non-linear constraint and separated the supermatrix Q into two parts $Q \to Q + Q_M$, where Q is associated with the massless modes and Q_M the massive modes. The massive modes would lead to contributions involving a gap of order ν/τ, which is much larger than the gap present in the contributions from the expansion of the trace-log term. This situation is closely analogous to what one encounters in the phenomenon of spontaneous symmetry breaking, Fig. 2.7. Returning to the main point, as a consequence of the non-linear constraint, the action reads

$$S[Q] = -\frac{1}{2}\int d^D x \mathrm{str}\log\left(-T^{-1}[H_0, T]E - H_0 + \frac{\omega_+}{2}T^{-1}\sigma_3^{\mathrm{ra}}T + \frac{i\sigma_3^{\mathrm{ra}}}{2\tau}\right) \tag{2.100}$$

In here, to simplify the notation, we define the impurity averaged Green's function:

$$\mathcal{G}_0^{-1} = E - H_0 + \frac{i\sigma_3^{\mathrm{ra}}}{2\tau}, \tag{2.101}$$

where $H_0 = p^2/(2m)$. Substituting it in the action above, the argument of the supertrace becomes

$$\log\left[1+\mathcal{G}_0\left(-T^{-1}[H_0,T]+\frac{1}{2}\omega_+T^{-1}\sigma_3^{\mathrm{ra}}T\right)\right], \tag{2.102}$$

where we neglected the term involving only the impurity averaged Green's function. To separate out the fast momenta from the slow momenta, we write the momenta as: $\mathbf{p} = \mathbf{k} + \hat{\mathbf{q}}$, where $\mathbf{k}$ denotes the fast momenta which we will integrate out in the next step and $\hat{\mathbf{q}}$ represents the slow momenta acting on the slowly fluctuating rotating matrices T. Recalling that the free Hamiltonian is given by a quadratic dispersion, we obtain the following result

$$H_0 = \frac{p^2}{2m} + \frac{k_i\hat{q}_i}{m} + \mathcal{O}(q^2). \tag{2.103}$$

Using this approximation leads to a commutator in the form

$$[H_0,T] = \frac{p_i}{m}[\hat{q}_i,T]. \tag{2.104}$$

We now expand the logarithm in gradients of the rotation matrices T up to linear order in ω and up to quadratic order in $\hat{\mathbf{q}}$, the linear order contribution in the momentum vanishes upon integration over the angular variables

$$\log\left[1+\mathcal{G}_0\left(-T^{-1}[H_0,T]+\frac{1}{2}\omega_+T^{-1}\sigma_3^{\mathrm{ra}}T\right)\right] \approx \frac{1}{2}\mathcal{G}_0\omega_+T^{-1}\sigma_3^{\mathrm{ra}}T - \frac{1}{2}\mathcal{G}_0T^{-1}[H_0,T]\mathcal{G}_0T^{-1}[H_0,T] \tag{2.105}$$

The first contribution stemming from the expansion is directly associated with the saddle-point equation and generates a term with no gradient

$$\mathrm{tr}(\mathcal{G}_0\omega_+T^{-1}\sigma_3^{\mathrm{ra}}T) = -i\pi\nu\mathrm{tr}(\sigma_3^{\mathrm{ra}}Q). \tag{2.106}$$

The second contribution requires some additional efforts to be properly evaluated. We first substitute the commutator Eq. (2.104) into the quadratic term and it yields

$$\mathrm{str}[\mathcal{G}_0(T^{-1}[H_0,T])\mathcal{G}_0(T^{-1}[H_0,T])] = \mathrm{str}\left[\frac{p_ip_j}{m^2}\mathcal{G}_0(T^{-1}q_iT)\mathcal{G}_0(T^{-1}q_jT)\right] = \mathrm{str}\left[\frac{p_ip_j}{m^2}\mathcal{G}_0\mathcal{A}_i\mathcal{G}_0\mathcal{A}_j\right], \tag{2.107}$$

where we have defined $\mathcal{A}_l = T^{-1}(q_lT)$. To evaluate these products, it is helpful to write down the Green's function in terms of projectors onto the retarded and advanced sectors

$$\mathcal{G}_0 = \frac{(1+\sigma_3^{\mathrm{ra}})}{2}\mathcal{G}_0^R + \frac{(1-\sigma_3^{\mathrm{ra}})}{2}\mathcal{G}_0^A, \tag{2.108}$$

with the retarded and advanced components given by

$$\mathcal{G}_0^R = \left(-\frac{p^2}{2m}+E+\frac{i}{2\tau}\right)^{-1}, \qquad \mathcal{G}_0^A = \left(-\frac{p^2}{2m}+E-\frac{i}{2\tau}\right)^{-1}. \tag{2.109}$$

In addition to that, a further simplification is found by noticing that if $i \neq j$ the integrations over the angular variables will vanish. This restricts our calculations to only terms concerning equal indices, thus

$$\mathrm{str}[\mathcal{G}_0(T^{-1}[H_0,T])\mathcal{G}_0(T^{-1}[H_0,T])] = \mathrm{str}\left(\frac{p_i^2}{m^2}\mathcal{G}_0\mathcal{A}_i\mathcal{G}_0\mathcal{A}_i\right). \tag{2.110}$$

To evaluate the integrations over the momentum, we observe that terms with both poles in the same region, namely the upper or lower-half plane, they vanish upon integration. This allows us to neglect contributions of the form $\mathcal{G}^{\alpha}\mathcal{G}^{\alpha}$ and focus our attention only on terms with different indices in the retarded-advanced sector:

$$\mathrm{str}[\mathcal{G}_0(T^{-1}[H_0,T])\mathcal{G}_0(T^{-1}[H_0,T])] = \mathrm{str}\left[\frac{p_i^2}{2m^2}(1+\sigma_3^{\mathrm{ra}})\mathcal{G}^R\mathcal{A}_i(1-\sigma_3^{\mathrm{ra}})\mathcal{G}^A\mathcal{A}_i\right]. \tag{2.111}$$

By this construction, we obtain the following result

$$\mathrm{str}[\mathcal{G}_0(T^{-1}[H_0,T])\mathcal{G}_0(T^{-1}[H_0,T])] = \frac{v^2}{2d}\mathrm{str}_{\mathbf{k}}[\mathcal{G}^R(\mathbf{k})\mathcal{G}^A(\mathbf{k})]\mathrm{str}[(1+\sigma_3^{\mathrm{ra}})\mathcal{A}_i(1-\sigma_3^{\mathrm{ra}})\mathcal{A}_i]. \tag{2.112}$$

Once again, with the help of complex analysis, we turn the calculation of the product between the two Green's function into a much simpler residue calculations, which yields the following result

$$\mathrm{str}[\mathcal{G}_0(T^{-1}[H_0,T])\mathcal{G}_0(T^{-1}[H_0,T])] = \pi\nu D\mathrm{str}(\mathcal{A}_i\mathcal{A}_i - \sigma_3^{\mathrm{ra}}\mathcal{A}_i\sigma_3^{\mathrm{ra}}\mathcal{A}_i), \tag{2.113}$$

where D is the diffusion parameter defined as $D = v^2\tau/d$, d is the spatial dimensionality, and we have written the term $(1+\sigma_3^{\mathrm{ra}})\mathcal{A}_i(1-\sigma_3^{\mathrm{ra}})\mathcal{A}_i$ in a more transparent form. To conclude the treatment of the gradient contribution, we write down Eq. (2.113) in real space. Recalling the parametrization we employed for the supermatrix field Q in terms of the rotation matrices T, $Q = T\sigma_3^{\mathrm{ra}}T^{-1}$ and the form of the momentum operator in real space: $q_j = -i\partial_j$, the Eq. (2.113) becomes

$$\mathrm{str}[\mathcal{G}_0(T^{-1}[H_0,T])\mathcal{G}_0(T^{-1}[H_0,T])] = \frac{\pi\nu D}{2}\mathrm{str}(\nabla Q)^2. \tag{2.114}$$

In this last step, we organized the gradient terms and identified the kinetic contribution of the supermatrix field $\mathrm{str}[-T^{-1}(\partial_j T)T^{-1}(\partial_j T) + \sigma_3^{\mathrm{ra}}T^{-1}(\partial_j T)\sigma_3^{\mathrm{ra}}T^{-1}(\partial_j T)] = (1/2)\mathrm{str}(\nabla Q)^2$. Assembling together the contributions from the gradient expansion, Eq. (2.106) and Eq. (2.114), we obtain our effective action to describe diffusive processes in terms of the supermatrix field

$$S[Q] = -\frac{\pi\nu}{8}\int d^D x\mathrm{str}[D(\nabla Q)^2 + 2i\omega_+\sigma_3^{\mathrm{ra}}Q], \qquad Q^2 = 1. \tag{2.115}$$

This concludes the derivation of the non-linear sigma model. The functional displayed above in Eq. (2.115) describes the physics of weakly disordered metals in terms of Goldstone modes and the interactions between these modes with the frequency ω playing the role of an external field. The Goldstone modes present in the effective action can be understood as the two diffusion modes we discussed, the diffusons and Cooperons.

The physical content present in this field theoretical functional for disordered conductors is analogous to the famous Heisenberg model, which is a model of classical magnetic moments with a ferromagnetic interaction in the presence of an external magnetic field

$$\mathcal{Z} = \int_{\mathbf{S}^2=1}\mathcal{D}\mathbf{S}\exp\left\{-\int d^D x\left[\frac{\kappa}{2}(\nabla\mathbf{S})^2 - \mathbf{B}\cdot\mathbf{S}\right]\right\}, \tag{2.116}$$

where κ sets the spin wave stiffness, $\mathbf{S}$ is vector proportional to the unit-length vector $\boldsymbol{\sigma}$, which represents a local spin allowed to rotate over the sphere $\boldsymbol{\sigma}\cdot\boldsymbol{\sigma} = 1$, and $\mathbf{B}$ represents an external magnetic field. To fully illustrate the comparison between the two models, we set $\mathbf{B}$ directed along the unit vector $\mathbf{e}_1$. In these types of system, the external magnetic field wants to align the classical spin configurations with itself, right panel in

Fig. 2.8, this same phenomenon appears in the non-linear sigma model, the frequency ω plays the role of the external magnetic field and wants to drive the supermatrix field configurations towards the metallic saddle-point. Furthering the argument, we observe that in the absence of an external magnetic field, the system displays invariance with respect to rotations along any direction. The presence of a non-zero $\mathbf{B}$ reduces the degree of symmetry enjoyed by the system and, as we considered for the non-linear sigma model, in order to capture the entire physical content of the theory, we must remove rotations that generates redundancies in the action. In here, we have a group G that generates rotations along any direction. However, among these rotations, there is a subgroup H consisting of rotations which do not affect the external magnetic field. For this reason, the theory free of redundancies is defined on the coset space G/H, the space of matrices which generates different vectors when acted upon the unit vector $\mathbf{e}_1$.

To summarize, we started out from a microscopic description of a disordered conductor via a single-particle Hamiltonian and derived the effective field theory for it in terms of diffusion modes. To start the derivation process, we anticipated the existence of two different diffusion processes and, to accommodate them, we observed that the Hamiltonian satisfies the equality $H^{\text{st}} = H^t = H$ and used it to perform a symmetry doubling of the action. In the next step, using a Gaussian white-noise disorder, we averaged over the disorder configurations and this procedure generated an effective quartic vertex. Then, to decouple this effective four-particle vertex, we introduced an auxiliary supermatrix field Q and carried out an integration over the supervectors. As a result of this, we removed the explicit dependence on the disorder potential, at the cost of giving rise to a dependence on the supermatrix field Q. Although it may appear that these steps do not strike as a good idea, we have moved from an action depending on a rapidly oscillating superfield and a δ-correlated disorder potential, to an action with a supermatrix field Q which is a slowly varying function representing the propagation of diffusion modes. Proceeding with the derivation, we sought stationary configurations of the action $S[Q]$ by taking the variation with respect to Q. This step led us to the saddle-point equation, whose solution, $Q_0 = \sigma_3^{\text{ra}}$, we obtained by identifying that the disorder must preserve the causality of the Green's function. Furthermore, we notice that there was an entire manifold $\mathcal{M}$ of solutions spanned by the saddle-point equation and to contemplate all of them we introduced the rotation matrix T and defined the supermatrix field as $Q = T\sigma_3^{\text{ra}}T^{-1}$. Within this framework, we wrote down the effective action in terms of a second-order gradient term and a symmetry breaking contribution linear in the frequency ω.

Finally, we identified the physical content of the non-linear sigma model defined on the manifold $\mathcal{M}$ in terms of long range diffuson and Cooperon modes, in Table 2.2 we display the tenfold universality classes and

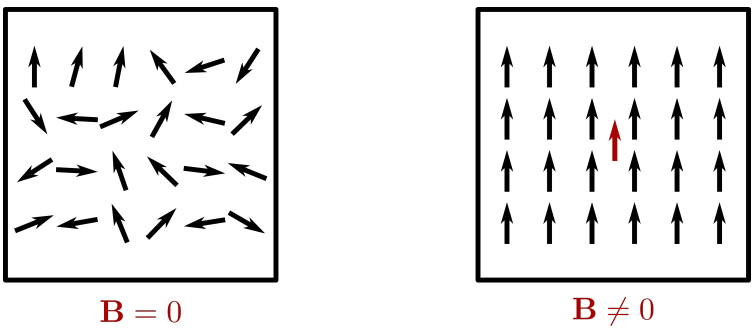

Figure 2.8.: Classical spins in a random lattice. Left panel, the system is in a disordered state. Right panel, there is an energetic preference of the spin configurations to align with the external magnetic field.

	Class	T^2	P^2	$(CT)^2$	Manifold ($\mathcal{M}_F \times \mathcal{M}_B$)
Wigner-Dyson	A	0	0	0	$\mathrm{Gl}(2m\|2n)/[\mathrm{Gl}(m\|n) \times \mathrm{Gl}(m\|n)]$
	AI	1	0	0	$\mathrm{Osp}(2n\|2n)/[\mathrm{Osp}(n\|n) \times \mathrm{Osp}(n\|n)]$
	AII	-1	0	0	$\mathrm{Osp}(2n\|2n)/[\mathrm{Osp}(n\|n) \times \mathrm{Osp}(n\|n)]$
Chiral	AIII	0	0	1	$\mathrm{Gl}(n\|n)$
	BDI	1	1	1	$\mathrm{Gl}(m\|n)/\mathrm{Osp}(m\|n)$
	CII	-1	-1	1	$\mathrm{Gl}(m\|n)/\mathrm{Osp}(m\|n)$
Bogoliubov-De Gennes	D	0	1	0	$\mathrm{Osp}(2m\|2n)/\mathrm{Gl}(m\|n)$
	C	0	-1	0	$\mathrm{Osp}(m\|n)$
	DIII	-1	1	1	$\mathrm{Osp}(2m\|2n)/\mathrm{Gl}(m\|n)$
	CI	1	-1	1	$\mathrm{Osp}(m\|n)$

Table 2.2.: Classification of universality classes in disordered systems. In the first column, we display the classes in terms of Cartan's symbols. In following columns we exhibit the symmetry requirements and the manifold where the field theory is defined. T denotes the time-reversal operator, P the charge conjugation operator and CT the chiral operator, which is a composition between the time-reversal and the charge conjugation operators [Zir96]. In the manifold column, $\mathrm{Gl}(m|n)$ stands for general linear supergroup with m components in the Fermionic sector and n components in the Bosonic sector. The notation $\mathrm{Osp}(m|n)$ represents the orthosymplectic supergroup.

their corresponding manifolds. The initial symmetry doubling we performed was an anticipation that these two modes are connected with each other via a time-reversal symmetry and, thus, would be convenient to construct our theory in terms of a symmetrized action. In the description of diffusive systems with the non-linear sigma model, depending on their symmetries, distinct soft modes will be present and this difference is reflected in the definition of the manifold $\mathcal{M}$ where the field lives. By taking all these steps and investing all this effort, we derived an effective action which provides a controllable environment to investigate the spectral and quantum transport properties of disordered conductors, in terms of a perturbative or non-perturbative framework.

As indicated above, to construct a field theory which is adequate to average over the disorder configurations, we can explore two distinct approaches: the replica trick or the supersymmetry (graded algebra). The former case is suitable to perform calculations that involve the perturbative regime. The latter approach works exceedingly well when the observables under scrutiny requires a more careful consideration in terms of non-perturbative contributions, for instance, limiting cases where there are no small parameters to provide a reliable platform to perform perturbation theory. In such cases, a calculation around a saddle-point is not enough, because quantum fluctuations fully restore the structure of the entire manifold, requiring us to go beyond a simple semiclassical approach and integrate over the entire manifold. In this sense, the well-defined finite quantity of degrees of freedom of the supersymmetric formalism provides a controllable environment to execute non-perturbative analytical calculations.

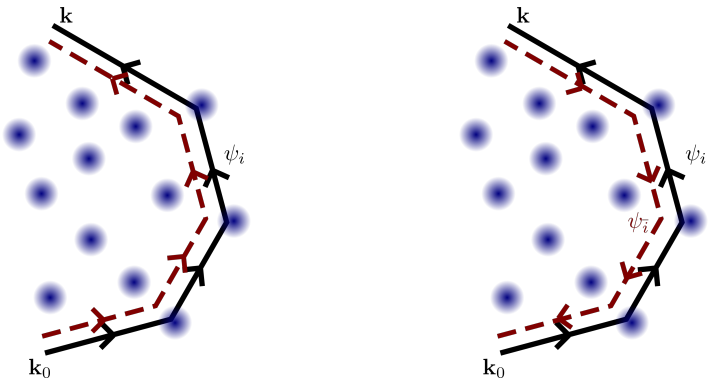

Figure 2.9.: Pair of trajectories experiencing the same set of multiple elastic scattering events. In (a) a classical contribution and (b) a coherent contribution characteristic of wave mechanics.

2.5. Coherent Multiple Scattering

2.5.1. Coherent Backscattering Peak

As we discussed in the previous sections, disorder can have dramatic consequences in the quantum transport properties of a given system. The effects of spatial randomness in cooperation with phase coherence can ultimately lead to a complete localization of a wave packet, resulting in the absence of diffusion, as demonstrated in the work of Anderson [And58]. Many observations of localization phenomenon have been reported in the literature for a variety of systems: light [St06], ultrasound [Hu+08] and microwave [CSG00]. In a typical experiment, one has to be able to distinguish interference-induced absence of diffusion from classical trapping or slow diffusion. Such distinction can be made clear by showing evidence of phase-coherent transport. The most prominent manner to do so involves the measurement of the well-known coherent backscattering peak, whose genesis is based on pairs of counter-propagating trajectories experiencing the same route of multiple elastic scattering events, resulting in a constructive interference in the backward region of the initial momentum. This interference is also intimately associated with the weak localization effect which reduces the strength of the diffusion parameter in comparison to its value in the presence of only phase-incoherent processes, suggesting that it can be interpreted as the precursor of Anderson localization in disordered systems. In addition to that, the formation of this peak in the backward region of the initial momentum is quintessentially a feature of systems displaying wavy behavior and has been observed in both classical and quantum matter.

Consider a short wave pulse of well-defined wave vector $\mathbf{k}_0$ launched at $t = 0$ into a disordered material. The wave field Ψ can be conveniently written as a superposition of elementary amplitudes ψ_i:

$$\Psi = \sum_i |\psi_i| e^{i\phi_i} \tag{2.117}$$

associated with multiple scattering paths i. The probability distribution $|\Psi|^2 = \sum_{ij} \psi_i \psi_j^* e^{i(\phi_i - \phi_j)}$ then composes to form a complicated interference pattern known as speckle. After performing the average over the disorder configurations in expressions of this form, it is expected that only the diagonal contributions survive, $i = j$, since for $i \neq j$ we would obtain a cancellation among the terms. The former type of expression defines the incoherent contributions and are displayed in panel (a) in Fig. 2.9, where the reflected signal is detected at a later time t with momentum in a direction $\mathbf{k}$ around $-\mathbf{k}_0$ and the averaged over disorder probability distribution reads $\langle |\Psi|^2 \rangle \sim \sum_i \langle |\psi_i|^2 \rangle$. For systems displaying time-reversal symmetry, there

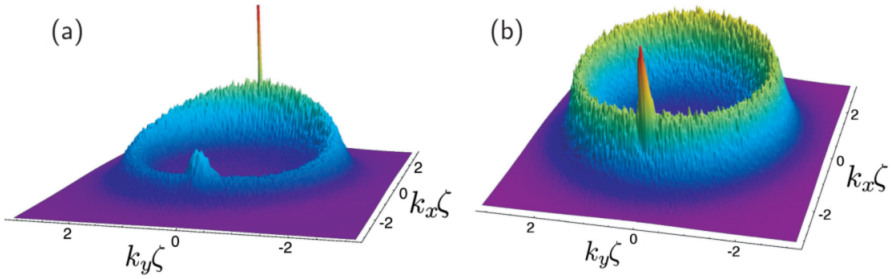

Figure 2.10.: Evolution of a momentum distribution of a matter wave packet launched with initial momentum $\mathbf{k}_0 = (k_0, 0)$ into a two-dimensional environment under the influence of random potential with correlation length ζ. In the panel (a), multiple elastic scatterings deplete the initial momentum followed by the formation of a smooth peak in the backward region of the initial momentum and an anisotropic ring associated with the broadening of the energy shell along the circle $|\mathbf{k}| = |\mathbf{k}_0|$ due to the presence of a disorder potential, energy conservation. [Che+12]

is an additional possible contribution, namely the coherent contribution which takes into account pairs of counter-propagating trajectories $i = \bar{i}$. This type of contribution is exhibited in panel (b) in Fig. 2.9. At the exact region of backscattering $\mathbf{k} = \mathbf{k}_0$, the phases of the pair of trajectories coincides $\phi_i = \phi_{\bar{i}}$ and we have an enhancement of the average probability distribution

$$\langle |\Psi|^2 \rangle = 2 \sum_i \langle |\psi_i|^2 \rangle \,. \tag{2.118}$$

The doubling of this return probability because of the interference between pairs of counter-propagating trajectories is the foundation of the coherent backscattering peak.

In Ref. [Che+12], using a approach involving analytical and numerical techniques, it was provided a complete description of the coherent backscattering peak. Assuming negligible interactions, it was prepared a cloud of atoms with mass m at a time $t = 0$ in the state $\Psi(\mathbf{k}, 0)$ with mean momentum $\mathbf{k}_0$ and a narrow momentum distribution width, $\Delta k \ll |\mathbf{k}_0|$. Consider that the initial distribution of this cloud of atoms has the form of an isotropic Gaussian:

$$\langle \mathbf{k}|\Psi(t=0)\rangle = n_0(\mathbf{k}) = \frac{1}{[2\pi(\Delta k)^2]^{d/2}} \exp\left[-\frac{(\mathbf{k}-\mathbf{k}_0)^2}{2\Delta k^2}\right]. \tag{2.119}$$

Starting at $t = 0$, the system's evolution is governed by the Schrödinger equation with single particle Hamiltonian given by $H = \mathbf{p}^2/(2m) + V(\mathbf{r})$. The potential $V(\mathbf{r})$ introduces the spatial randomness to the system satisfying the weak disorder condition $|\mathbf{k}_0|\ell \gg 1$, where ℓ is the mean scattering length. The disorder potential is characterized by a vanishing mean $\langle V(\mathbf{r})\rangle = 0$, a variance $\langle V(\mathbf{r})^2\rangle = V^2\delta(\mathbf{r})$ and a spatial correlation length ζ. In the panel (a) in Fig. 2.10, we display the evolution of the wave packet at short times, t approximately equal to the elastic scattering time $t \sim \tau_e$. The ring-shaped distribution exhibits two peaks, one reminiscent of the initial distribution which is being depleted as the energy is redistributed by multiple elastic scattering events along the circle of radius $|\mathbf{k}| = |\mathbf{k}_0|$ and the other reflects the presence of the time-reversal symmetry cooperating with these elastic scattering processes and the phase-coherent propagation of pairs of counter-propagating trajectories to the formation of constructive interferences in the backward region of the initial momentum.

At longer times, $t \gg \tau_e$, the initial momentum distribution is fully depleted and the diffusive background is entirely isotropic, the atoms scattered out of the initial cloud completely populate other energetically accessible modes in momentum space on the energy shell. At this point, the most memorable feature is the presence of the coherent backscattering peak. From this time onwards, it was observed a decay of the contrast, which is defined as the height of the peak measured from above the isotropic ring, and of the angular width of the peak.

On the experimental side, performing measurements in real condensed matter systems such as a crystal lattice have proven to be an incredibly hard task, since there many factors that ideal models fail to capture. In particular, for many years, the presence of interactions and finite temperature effects hampered experimental efforts to obtain a direct observation of the Anderson localization phenomenon. However, nowadays, ultra-cold atoms setup in the state-of-the-art provides a platform which allows one to access the mesoscopic physics in a considerably controllable environment. Using this setup, in Ref. [Jen+12] it was reported the first experimental findings of a direct observation of the coherent backscattering in ultra cold quantum matter.

In this experiment, a sample of non-interacting rubidium atoms was suspended against the gravity by an external magnetic field and launched with a well defined momentum distribution along the z-axis. To narrow the initial momentum distribution, the atomic gas was subjected to an harmonic pulse [AC97]. Such process also destroys the position-momentum correlation developed during the initial cloud's expansion, this additional effect results in a sharper characterization of coherent backscattering peak [CD13]. In the Fig. 2.11, the first plot represents the time frame $t = 0$ms corresponding to the initial momentum distribution. The spatial randomness is introduced in the system via an optical disordered potential. Under its influence, the atoms are allowed to scatter for a time t, then the potential is switched off and the evolution of the momentum distribution is monitored. As the system evolves, their findings display perfect agreement with the numerical simulation result described above.

2.5.2. Coherent Forward scattering Peak

For short times, we have demonstrated the existence of a coherent backscattering peak in a variety of different approaches. Such phenomenon is intimately connected to the weak localization, whose existence

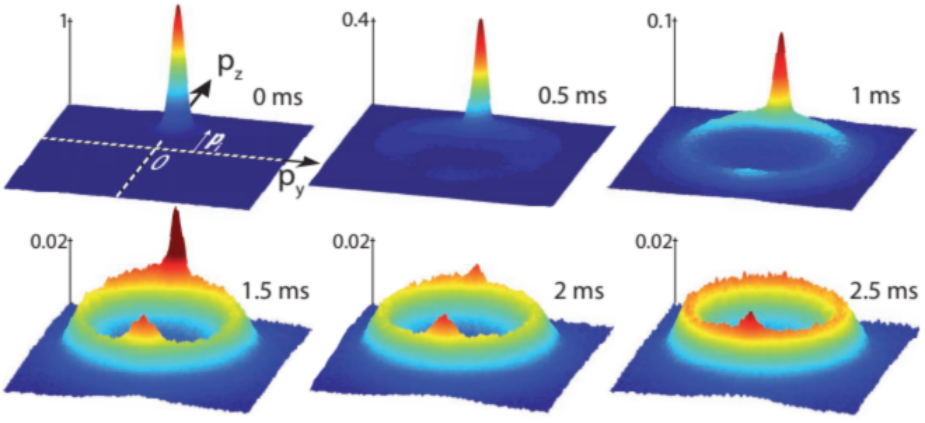

Figure 2.11.: Above we display the monitoring of the momentum distribution for a gas of non-interacting ultra cold atoms after different propagation times t in disorder. In the last we clearly observe the formation of the coherent backscattering peak above the isotropic ring.

hinges on the presence of the time-reversal symmetry and it can be thought of as a precursor for the Anderson localization, strong localization. To investigate further properties of this peculiar structure, in Ref. [Kar+12], it was launched a coherent matter wave with an initial narrow momentum distribution width, $|\mathbf{k}_0\rangle$, into a two-dimensional random potential.

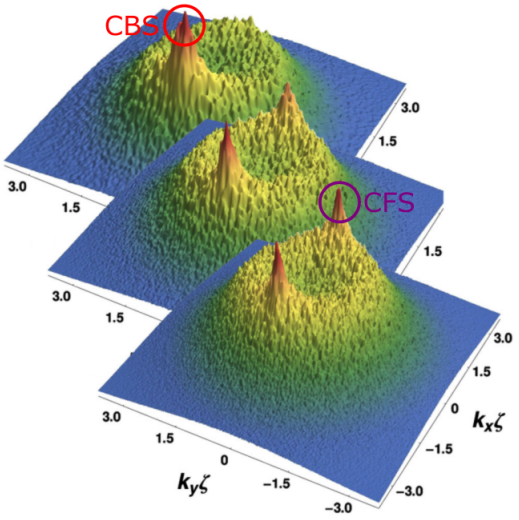

Figure 2.12.: Using a numerical approach [Kar+12], above we display the momentum distribution for different time frames of a wave packet propagating under the influence of a two-dimensional disorder potential with correlation length ζ

In Fig. 2.12, we display their numerical findings. The three different momentum distribution represents distinct time frames of the matter wave propagation. As expected, for a non-interacting system with time-reversal symmetry, for short times, there is a peak structure in the backward region of the initial momentum, top panel. In addition to that, in this numerical simulation, at the onset of Anderson localization, whose occurrence emerges in the vicinity of the localization time, which is much larger than the elastic scattering time, the coherent backscattering peak becomes a stationary phenomenon and, in the middle panel, there appears also a novel structure: a peak diametrically opposed to the backscattering peak, which progressively symmetrizes with the peak in the backward region. Such structure known as the coherent forward scattering peak is a smoking gun indicating the presence of Anderson localization. In the bottom panel, it is displayed the time frame under which the momentum distribution becomes symmetric with respect to transformations sending $\mathbf{k}_0$ to $-\mathbf{k}_0$.

In order to explain the formation of the ring structure plus the coherent backscattering peak, we considered two trajectories ψ_i and ψ_j propagating along the same scattering sequence and split it into two cases: when $i = j$, this configuration corresponds to the classical contribution, where the trajectories generate the isotropic ring, panel (a) in Fig. 2.13, and when $i = \bar{i}$ the trajectories experience the same sequence of scatterings, but in opposite directions leading to the formation of the coherent backscattering peak, panel (b) in Fig. 2.13. However, within this framework, the novel structure fails to be captured by it, indicating an insufficiency of this picture. In Ref. [Kar+12], along with the numerical simulation, an explanation of this phenomenon was offered in terms of maximally crossed diagrams of the form presented in panel (c) in Fig. 2.13, such diagram has a peak in the forward region of the momentum. This explanation is partially correct, because it turns out that there are diagrams of the form presented in panel (d), which are also peaked in the forward region of the momentum, this was proven rigorously in [MMA14], [Gho+14]. Diagrams of

the form exhibited in panel (d) have an striking characteristic, they do not depend on the time-reversal symmetry. This reveals that the formation of a coherent forward scattering peak is bound to occur even in systems where such symmetry is broken.

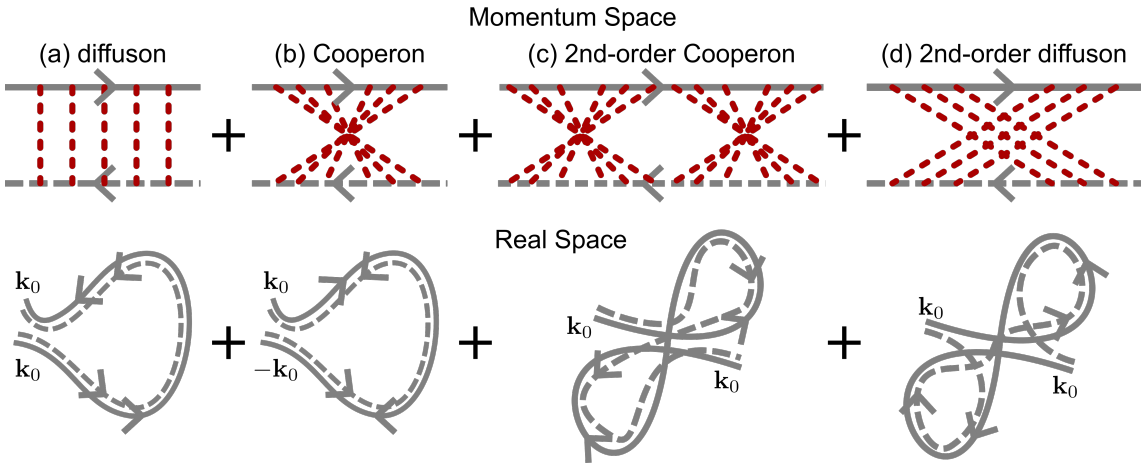

Figure 2.13.: The fundamental impurity diagrams which explains the formation of the twin peaks. In the first row the diagrams are represented in momentum space and in the second row in real space. Panel (a), the diffuson associated with classical diffusion. Panel (b), the Cooperon generates the peak at $-\mathbf{k}_0$. Panels (c) and (d) two concatenated Cooperons and diffusons generates the peak at $\mathbf{k}_0$.

Among these many interesting physics involved in the formation of the coherent forward scattering peak, a question of great relevance is: why does this remarkable feature only manifest itself at times close to the localization time? In order to give a proper response to this question, we will use an heuristic approach [LK82], [Efe99], [AM07], [Phi12]. Suppose a quantum particle propagates for a distance dl with Fermi velocity v_F, during a time interval dt. In contrast with the typical classical trajectory, the quantum description of the electron path should be considered as a flux tube of radius λ_F, where λ_F denotes the Fermi wavelength associated with the electron. Assembling together these elements, we suppose that this quantum mechanical particle travels in this tube through an infinitesimal volume given by the expression $dV = v_F \lambda_F^{d-1} dt$, left portion of Fig. 2.14, where v_F denotes the Fermi velocity. Furthermore, we suppose that the particle is allowed to wander over all space and as a result the maximum volume element spanned by the particle is given by $V = (Dt)^{d/2}$, for a diffusive regime, and $V = \xi^d$, for a localized regime. Then, to calculate the probability of that particle traversing a loop, we divide the infinitesimal volume by the maximum volume and integrate it over the time variable

$$P_{\text{cross}} = \int_{\tau_e}^{t} \frac{v_F \lambda_F^{d-1} dt'}{V}, \tag{2.120}$$

where the limits of integration are chosen such that it comprises the minimum time for a single collision, τ_e to an arbitrary time t, whose magnitude must be smaller than the shortest time at which phase coherence is lost.

Figure 2.14.: Volume element for a quantum particle propagating with velocity v_F, in a tube of radius λ_F, during a time interval dt.

Considering first the diffusive regime, the integration yields the following result for the probability:

$$P_{\text{cross}} = \left[\frac{1}{(k_F\ell)^{d-1}(1-d/2)}\right]\left[\left(\frac{t}{\tau_e}\right)^{1-d/2} - 1\right]. \tag{2.121}$$

For a weak disorder the product $k_F\ell$ is a small parameter, thus, in this regime, the peak is expected to be strongly suppressed and for $d = 3$ the probability even decays in time. In the localized regime, the result is significantly different from the diffusive regime:

$$P_{\text{cross}} = \frac{k_F\ell}{(k_F\xi)^d}\left(\frac{t}{\tau_e} - 1\right). \tag{2.122}$$

This expression indicates that at long times, the intersection probability increases linearly in time. However simple this approach is, it still manages to reproduce the qualitative physical behavior for both regimes, diffusive and localized [Kar+12].

Although the arguments presented above are enough to describe the existence of the coherent forward scattering peak, in order to construct a more solid picture, we also investigate its formation beyond the diagrammatic perturbative approach. The information about the effects of scattering particles in a disordered medium is contained in the time-dependent configuration averaged fidelity, (average momentum distribution):

$$n_{\mathbf{k}}(t) = \overline{\langle \mathbf{k}|e^{-iHt}|\mathbf{k}_0\rangle \langle \mathbf{k}_0|e^{iHt}|\mathbf{k}\rangle} \tag{2.123}$$

Expanding this observable in the basis of the disordered system's eigenstates $\{|\phi_n\rangle\}_{n=1}^{N}$ yields

$$n_{\mathbf{k}}(t) = \sum_{n,m} \overline{e^{-i(E_n - E_m)t}\phi_n(\mathbf{k})\phi_n^*(\mathbf{k}_0)\phi_m(\mathbf{k}_0)\phi_m^*(\mathbf{k})} \tag{2.124}$$

Considering the long time case, $t \gg t_{\text{loc}}$, the transport properties of the system are strongly affected by the Anderson localization and the atomic motion is confined to a volume ξ^d. In this limiting case, the typical separation between two energy levels satisfy the relation $|E_n - E_m| \sim 1/(\nu\xi^d)$, ν is the density of states and $1/(\nu\xi^d) = 2\pi\hbar/t_{\text{loc}}$ is the level spacing, which can be represented in terms of the localization time. Substituting this relation into Eq. (2.124), we obtain

$$n_{\mathbf{k}}(t) = \sum_{n,m} \overline{e^{-2\pi i\hbar(t/t_{\text{loc}})}\phi_n(\mathbf{k})\phi_n^*(\mathbf{k}_0)\phi_m(\mathbf{k}_0)\phi_m^*(\mathbf{k})}. \tag{2.125}$$

Since by definition $t \gg t_{\text{loc}}$, it is immediately clear that off-diagonal states oscillate very fast and, consequently, such states cannot possibly contribute to the observable as these terms will be washed out by the

disorder average. As a consequence of this observation, we are allowed to write down the configuration averaged fidelity in a simplified manner:

$$n_{\mathbf{k}}(t) \simeq \sum_{n} \overline{\phi_n(\mathbf{k})\phi_n^*(\mathbf{k}_0)\phi_n(\mathbf{k}_0)\phi_n^*(\mathbf{k})}. \tag{2.126}$$

Invoking the time-reversal invariance which provides a symmetry relation between time reversed eigenstates $\phi_a(\mathbf{k}) = \phi_a^*(-\mathbf{k})$. As a result of this, we can write $n_{\mathbf{k}_0}(t) = n_{-\mathbf{k}_0}(t)$ and see the existence of a symmetrical structure centered at $\mathbf{k}_0$, namely, the coherent backscattering and forward scattering peaks.

Performing a few manipulations in Eq. (2.124), we write down the averaged momentum distribution in a form analogous to a Fourier transform

$$n_{\mathbf{k}}(t) = \sum_{n,m} \int d\epsilon \int d\omega e^{-i\omega t} \overline{\delta\left(E_n - \epsilon - \frac{\omega}{2}\right)\delta\left(E_m - \epsilon + \frac{\omega}{2}\right)\phi_n(\mathbf{k})\phi_n^*(\mathbf{k}_0)\phi_m(\mathbf{k}_0)\phi_m^*(\mathbf{k})}. \tag{2.127}$$

As reported in the literature [LGM14], [Gho+14], the fluctuations of the eigenfunctions are decoupled from the fluctuations of the level spacing between two eigenenergies. Thus, assuming statistical independence of eigenfunctions and eigenenergies, we reveal a striking relation between the averaged momentum distribution and the level-level correlation:

$$n_{\mathbf{k}}(t) \sim \int e^{-i\omega t} K_\epsilon(\omega), \tag{2.128}$$

where

$$K_\epsilon(\omega) \sim \sum_{n,m} \overline{\delta\left(E_n - \epsilon - \frac{\omega}{2}\right)\delta\left(E_m - \epsilon + \frac{\omega}{2}\right)}. \tag{2.129}$$

Thus, by calculating the level-level correlation function, we can extract information about how the coherent forward scattering peak evolves in time. The calculation of this observable requires the usage of non-perturbative methods and we shall explore the versatility of the supersymmetric non-linear sigma model to approach the computation. In chapter 4, we will employ this framework to calculate the level-level correlation function for all three Wigner-Dyson ensembles [MM18].

2.6. Josephson Junctions

Suppose the existence of two superconductors separated from one another by a thin layer, typically of size around $10 - 15\text{Å}$, which we will refer to as the weak link. A naive approach to this setup would be to expect that, in the absence of an applied external voltage, no considerable amount of quantum transport of charge in the region between the superconductors could possibly develop, except for the famous single electron tunneling through the thin layer [BP82]. Around 1960, in a series of seminal articles [Jos62; Jos64; Jos65], Josephson demonstrated that indeed this way of thinking about the physics of such junctions was not correct. He showed that even in the absence of an external voltage, provided that the barrier is thin enough, Coopers pairs (a pair of electrons under the influence of an attraction strong enough to overcome the Coulomb repulsion) can coherently pass through the intermediate layer, leading to the appearance of a supercurrent flowing through the barrier, this phenomenon is what we will call as the DC Josephson effect. The behavior of such supercurrent would be governed by a sine function $\sin\phi$, where ϕ is defined as the

phase difference $\phi = \chi_1 - \chi_2$ between the phases of the superconductors order parameters $\Delta_1 = |\Delta_1|e^{i\chi_1}$ and $\Delta_2 = |\Delta_2|e^{i\chi_2}$. The supercurrent attains its maximum value at I_C, which depends on the properties of the material and the geometry of the system and in its simplest case can be written in the form

$$I(\phi) = I_C \sin\phi. \tag{2.130}$$

Complementary to the DC effect, there is also the AC Josephson effect. If we turn on an external voltage in the junction, according to Eq. (2.131) the phase difference will become time-dependent and, in addition to that, the supercurrent passing through the barrier will oscillate with a well-defined period. The theoretical foundation of both of these effect relies on the phase coherence associated with the involved superconducting states. The phase difference ϕ is related to the applied external voltage V via the relation

$$\frac{d\phi}{dt} = \frac{2e}{\hbar}V. \tag{2.131}$$

However, the latter will not be further discussed in this work, we will focus on the DC Josephson effect. Furthermore, it is important to mention that even though the equations Eq. (2.130) and Eq. (2.131) provide a quantitative description of the Josephson effect, there is a significant difference between them. The former is a result for a specific type of weak link, namely, an insulating barrier and the constant I_C depends on the geometrical and material properties of the system. Whereas, the latter is an equality derived from fundamental principles of quantum mechanics and in this sense is more robust against deviations.

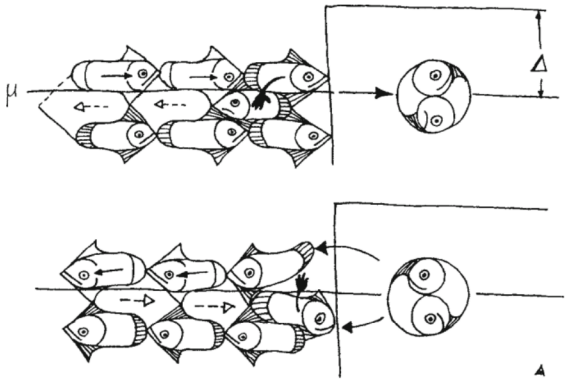

Figure 2.15.: The physical picture of the phenomenon of Andreev reflection [Zag14] in a Josephson junction. The electron e is reflected as a hole h leading to a transference of a pair of correlated electrons from the left to the right superconductor. As a consequence of this, the supercurrent flows across the junction.

Although in the original idea the Josephson effect was studied in SIS (superconductor-insulator-superconductor) tunneling junctions, the field blossomed into a wide variety of distinct weak links. It is well established that such effect is not limited to SIS junctions and it manifests itself as long as a supercurrent can flow into the weak link via coherent transport of Cooper pairs. For instance, we can construct a Josephson junction using a normal metal, a semi-conductor, a superconductor with a smaller critical temperature, a geometrical constriction, a point contact [GKI04]. The Josephson effect is an exquisite example of a macroscopic quantum phenomena, where the physics at the quantum scale cooperate to produce a measurable effect in the macroscopic scale. The underlying physics involved in such effect relies on the so called Andreev reflections, Fig. 2.15. The density of states of a superconductor displays an energy gap of size 2Δ. In this sense, the

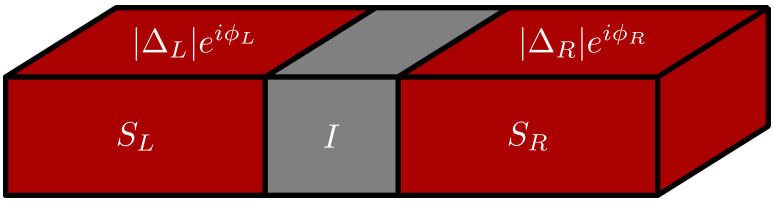

Figure 2.16.: The superconductor-insulator-superconductor Josephson junction.

quasiparticles living in the weak link are not allowed in the superconductor, unless their energies surpass this minimum energy. Nevertheless, there is still the formation of a supercurrent in the weak link.

This has to do with processes where an electron with momentum $\mathbf{k}$ impinging on one of the interfaces (weak link-superconductor) is reflected back as a hole with momentum $-\mathbf{k}$ and generates a Cooper pair inside the superconductor. An electron travelling in the weak link above the Fermi surface forms a Cooper pair with an electron below this surface, Fig. 2.15, and leaves the region to penetrate into the superconducting condensate. The reflected hole is a representation of the absent electron in the Fermi sea. Along with these processes, the appearance of this hole allows a Cooper pair to move into the weak-link. As a consequence of this cycle of Andreev reflections, the supercurrent flows across the junction into the weak link. A more detailed discussion on the fundamental aspects of the Josephson effect can be found in the literature [BP82; NB09; Zag14]. Following the demonstration discussed in reference [FLS71], below we shall present the mathematical framework of a simple Josephson junction consisting of two superconductors separated by a sufficiently thin layer of an insulating material, see Fig. 2.16 above. Each superconductor is represented via its pair wave function ψ_L and ψ_R, left and right superconductor, respectively. Throughout this derivation we will use the basis $\{|L\rangle, |R\rangle\}$. Within this framework, the density of Cooper pairs on each side of the junction reads

$$\langle X|\psi_X^*\psi_X|X\rangle = \rho_X. \tag{2.132}$$

This system composed of two superconductors connected via a thin layer of an insulating material can be described by the Hamiltonian

$$H = H_L + H_R + H_T, \tag{2.133}$$

where H_L and H_R are the Hamiltonians associated with the left and right superconductors, respectively, and H_T is tunneling Hamiltonian which allows transitions between the left and right states. Using the proposed basis, these building blocks can be written as

$$H_{L(R)} = E_{L(R)} |L(R)\rangle \langle L(R)|, \tag{2.134}$$

$$H_T = K(|L\rangle \langle R| + |R\rangle \langle L|), \tag{2.135}$$

where $E_{L(R)}$ denotes the ground state energies of the two superconductors, K is the parameter which sets the coupling strength between the superconductor and the weak link, it usually depends on the material and geometrical properties of the system. Such coupling has its physical origins in the finite overlap of the two pair wave functions ψ_L and ψ_R that occurs in the weak link region. In the basis introduced above, a general state vector representing an arbitrary Cooper pair in a Josephson junction is given by the following linear combination

$$|\psi\rangle = \psi_L |L\rangle + \psi_R |R\rangle, \tag{2.136}$$

a Cooper pair can be found in the left state with probability $|\psi_L|^2$, for the right state the probability obtains $|\psi_R|^2$. With this Hamiltonian, we may write the time-dependent Schrödinger equation

$$i\hbar\partial_t |\psi\rangle = H |\psi\rangle . \tag{2.137}$$

Substituting the general wave function $|\psi\rangle$, we introduced above, yields the set of coupled equations

$$i\hbar\partial_t\psi_L = E_L\psi_L + K\psi_R, \tag{2.138}$$
$$i\hbar\partial_t\psi_R = E_R\psi_R + K\psi_L. \tag{2.139}$$

These are standard equations describing two quantum mechanical systems coupled together via a parameter K. If $K = 0$, these equations would just describe the lowest energy state of each superconducting system, not an interesting scenario. On the other hand, if $K \neq 0$, then there exists leakage from one side to the other, the left states are allowed to transition to right states and vice-versa. If $E_L = E_R$, we could simply subtract away these energies. Instead, to turn the problem more appealing, we connect both sides to an external voltage supplier with a potential difference $E_L - E_R = 2qV$. For the sake of convenience, we fix the zero energy as $E_L = qV = -E_R$. At this point, it is convenient to represent the wave function in the polar form $\psi_X = |\psi_X|e^{i\phi_X}$. Using this parametrization, we obtain

$$i\hbar\partial_t|\psi_L| - \hbar|\psi_L|\partial_t\phi_L = qV|\psi_L| + K|\psi_R|e^{-i\phi}, \tag{2.140}$$
$$i\hbar\partial_t|\psi_R| - \hbar|\psi_R|\partial_t\phi_R = -qV|\psi_L| + K|\psi_L|e^{i\phi}, \tag{2.141}$$

where we have defined $\phi = \phi_L - \phi_R$. Next, we separate out the real from the imaginary part for each equation displayed above. In principle, this does not strike as a bright idea, since we end up with four equations instead of two. However, among these four equations, we can easily identify the relevant physical content. Performing this separation, the real part reads:

$$-\hbar|\psi_L|\partial_t\phi_L = qV|\psi_L| + K|\psi_R|\cos\phi, \tag{2.142}$$
$$-\hbar|\psi_R|\partial_t\phi_R = -qV|\psi_R| + K|\psi_L|\cos\phi. \tag{2.143}$$

Based on our construction, we may derive a differential equation in terms of ϕ by subtracting Eq. (2.142) from Eq. (2.143):

$$\partial_t\phi = -\frac{2qV}{\hbar} + \frac{K\cos\phi}{\hbar}\left(\left|\frac{\psi_L}{\psi_R}\right| - \left|\frac{\psi_R}{\psi_L}\right|\right). \tag{2.144}$$

We now treat the imaginary part of equations Eq. (2.140) and Eq. (2.141), namely,

$$\partial_t|\psi_L| = -\frac{K\sin\phi}{\hbar}|\psi_R|, \tag{2.145}$$
$$\partial_t|\psi_R| = \frac{K\sin\phi}{\hbar}|\psi_L|. \tag{2.146}$$

To clarify the underlying physical content in these equations, we make good use of the Born interpretation for the wave function and identify $|\psi_X| = \sqrt{\rho_X}$, the absolute value of the wave function is directly associated with the square root of the density of Cooper pairs. As a consequence of this observation, the set of coupled

equations displayed in Eq. (2.145) becomes

$$\partial_t \rho_L = -\frac{2K\sqrt{\rho_L \rho_R}}{\hbar} \sin\phi, \tag{2.147}$$

$$\partial_t \rho_R = \frac{2K\sqrt{\rho_L \rho_R}}{\hbar} \sin\phi. \tag{2.148}$$

From these two equations, we immediately identify the pair current density

$$J = \partial_t \rho_L = -\partial_t \rho_R. \tag{2.149}$$

Recalling that the two superconductors are of the same material, it is reasonable to assume that the density of Cooper pairs on both sides are almost identical $\rho = \rho_L = \rho_R$. In addition to that, as verified in reference [Oht77], without any loss of generality and causing no contradiction in our discussion, we may assume that ρ is constant. Such considerations, leads to the following expression for the Josephson current

$$J = J_C \sin\phi, \qquad J_C = \frac{2K\rho}{\hbar}, \tag{2.150}$$

the parameter J_C sets the maximum current density allowed in the junction and is a characteristic of the particular junction under investigation. Hence, we conclude that in a Josephson junction consisting of two superconductors connected via a thin insulating barrier under the influence of a constant external voltage, the pair current density displays a sinusoidal behavior and the phase difference can be defined to be a constant value.

An application of Josephson junctions is the famous superconducting quantum interference device, SQUID for short, see Fig. 2.17. The tunneling supercurrent developed in a Josephson junction is intimately associated with the phase differences between two superconductors and, in practice, the Josephson effect allows us to measure these phase differences. In addition to that, in the presence of an external magnetic flux, charged particles are affected by it in a manner that their quantum state acquires a phase factor that depends on the vector potential which describes the magnetic flux. Such principle allows us to explore Josephson junctions to perform precise measurements of magnetic fluxes.

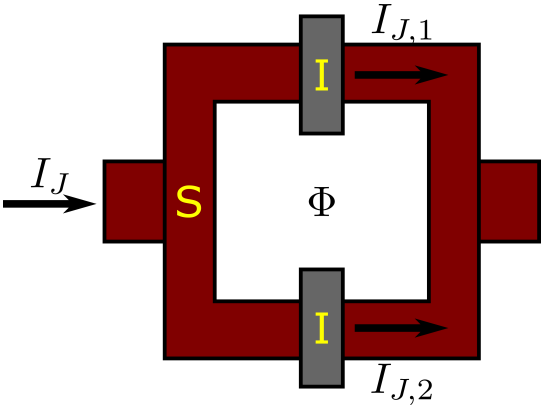

Figure 2.17.: Above we display two superconductors separated by a sufficiently thin insulating layer forming two parallel Josephson junctions. The supercurrent I_J enters the Josephson junction and splits into two $I_{J,1}$ and $I_{J,2}$. Φ denotes the external magnetic flux.

Such sensitivity to the presence of an external magnetic field flux enables these devices to be used as highly

precise magnetometer, for instance, it can be used to measure the magnetization of crystal samples or even the magnetic field in living organisms. The human heart has a magnetic field of the order of 10^{-10}T, a SQUID is capable of detecting a magnetic flux as small as 10^{-14}T, ten thousand times smaller than the human heart's magnetic field.

The game of science is, in principle, without end. He who decides one day that scientific statements do not call for any further test, and that they can be regarded as finally verified, retires from the game.

The Logic of Scientific Discovery, Karl R. Popper

3 Publications

Having introduced the fundamental mathematical machinery and the key physical concepts upon which we will extensively employ to investigate spectral and quantum transport properties of disordered systems, we will devote the next two chapters to present two successful applications of the non-linear sigma model.

Figure 3.1.: Exploration of an uncharted territory.

In the first publication [MM18], we discuss how the supersymmetric version of the non-linear sigma model is explored in order to calculate the level-level correlations in Anderson insulating wires for all Wigner-Dyson classes. Until then, the literature only contemplated the case with broken time-reversal symmetry (Gaussian Unitary Ensemble), but the most controllable and versatile setup to perform measurements of

this observable, namely, ultra cold atoms, does not have electrical charge and the typical way to break the time-reversal symmetry entails the usage of an external magnetic field. Hence, experimentally realizing such systems was quite challenging at the time. Bearing this in mind, we complemented the literature by deriving the level-level correlation functions for systems endowed with time-reversal, corresponding to the remaining Wigner-Dyson classes: Gaussian Orthogonal Ensemble and Gaussian Symplectic Ensemble. Later on, with the aid of some clever engineering, it was developed the artificial gauge field technique which operates exquisitely well in the platform of ultracold atoms, allowing, then, to quantum simulate existence of a time-reversal symmetry breaking process in a neutral system. Such technique consists of building a Hamiltonian that mimics a system where a gauge field is present. This construction made it possible to realize systems belonging to the Gaussian unitary and orthogonal classes. The experimental results displayed perfect agreement with our theoretical findings.

In the second publication [Mar+22], we will investigate the quantum transport properties of a set-up consisting of two superconductors on top of a topological insulator, typically called a topological insulator Josephson junction. Besides its enormous versatility and preciseness for measuring external magnetic fluxes, these Josephson junctions are also a potential candidate to help the construction of a quantum computer with logical circuits based on topological qubits. Superconducting systems are well known for their remarkable low dissipation transport of electrons. Such physical feature is of great importance, since it allows the possibility of working with coherence times exceeding one microsecond, much longer than the typical coherence time scale of the order of picoseconds. In any qubit implementation, the fundamental logical quantum states $\{|0\rangle, |1\rangle\}$ must be mapped to different physical states of the system and the energy level spacings are required to be non-degenerate. Being non-linear, the Josephson junctions provide a platform which ensures that the energy level spacings are not degenerate. Although linear circuit elements such as inductors and capacitors can also be constructed from superconducting system, these elements cannot be used to provide a usable qubit representation, because their energy level spacing is degenerate.

It is well reported in the literature that in such systems only a few quintuple layers close to the surface are responsible for the measured electrical transport, indicating that the electric charge is primarily transported via helical surface states and carriers in a charge accumulation region in the vicinity of the surface of the topological insulator, region indicated by L_1 in Fig. 3.2. The appearance of this region of charge-accumulation results in the formation of a two-dimensional electron gas, sometimes referred to as 2DEG, below the surface.

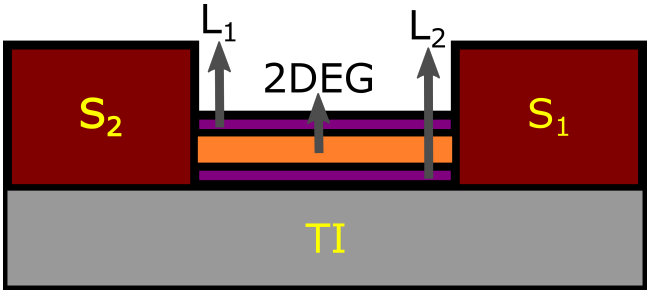

Figure 3.2.: L_1 represents the interface between the two-dimensional electron gas and the vacuum. L_2 is the boundary between the insulating bulk and the two-dimensional electron gas.

The wealth of experimental data indicates that a sizeable amount of supercurrent is carried by the helical surface states and the two-dimensional electron gas provides a protection mechanism against the disorder effects. In Fig. 3.3, the left panel displays the experimental data for the critical current in the regime of a

zero voltage bias compared to Usadel theory, dirty limit, and the Eilenberger theory, clean limit. The details of the experimental data is only fully captured by the latter theory for ballistic junctions. To determine in which band of the topological insulator the proximity effect is induced, we can compare the experimental data of the mean free path of the bulk and surface with the length of the junction, $L = 50$nm. The bulk mean free path of the junction, $\ell_b = 22$nm, is too small to support transport of ballistic nature in the junction. On the other hand, the surface conduction band has a much larger mean free path, $\ell_s = 105$nm, indicating that the supercurrent is carried primarily via the helical surface states.

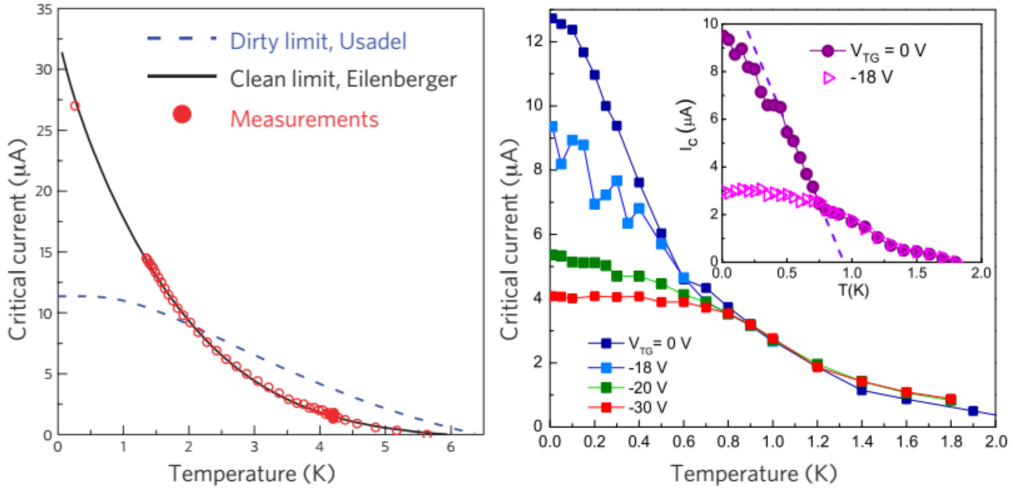

Figure 3.3.: On the left panel, the critical current when the bulk and surface states are coupled display a ballistic behavior. On the right panel, the negative voltage bias depletes the two-dimensional electron gas such that only surface states are present. In here the critical current exhibits a diffusive behavior.

On the right panel in Fig. 3.3, we display the experimental data for the critical current as a function of the temperature while the voltage bias is varied. In the zero voltage bias region, the critical current displays a ballistic behavior. As the voltage bias decreases, the two-dimensional electron gas states are gradually depleted in the topological insulator. At $V_G = -18$V, there is a striking difference from the other cases, there are more fluctuations in the measurements of the critical current and as the voltage bias is decreased the behavior transitions from ballistic to diffusive. This indicates that if we consider a topological insulator Josephson junction, whose helical surface states are present primarily in L_1, Fig. 3.2, and decoupled from the bulk, below L_1 we only have the insulating bulk, then the quantum transport is diffusive.

As part of a vigorous effort seeking a platform which hosts Majorana bound states that can be used to perform qubit operations, we employ the replica trick to derive the non-linear sigma model for the topological insulator Josephson junction in which the surface states are fully decoupled from the insulating bulk and use it to explore its quantum transport properties. Initially, we investigate the supercurrent and the supercurrent fluctuations of a topological insulator Josephson junction in the absence of an external magnetic field. Then, since the formation of the elusive Majorana bound states requires the presence of an external magnetic flux, we consider a second case, where the junction is threaded by an external magnetic field and study how its transport properties are modified by the presence of a non-zero magnetic flux.

4

Spectral Correlations in Anderson Insulating Wires

In this chapter, we use the supersymmetric non-linear sigma model to calculate the spectral level-level correlation function of Anderson insulating wires for all three Wigner-Dyson ensembles. Its Fourier transform is the spectral form factor, whose behavior have been recently measured with a state-of-the-art cold atom quantum quench experiment. We compare our theoretical result with the experimental findings reported in the literature. The derivation of our result is based on a representation of the level-level correlation in terms of a local generating function.

4.1. Introduction

The absence of diffusion in disordered media, namely, Anderson localization [And58; Abr+79], is quintessentially a wave phenomenon induced by the presence of constructive interferences and it forms one of the cornerstones of condensed matter physics with an extensive literature of recent advancements such as topological Anderson insulator [Gro+09; Li+09; DSV13; MS+14; ABK15] and many-body localization [BAA06; GMP05]. Nevertheless our theoretical and numerical strong development in understanding the rich physics involved in the single particle localization problem, experimental results demonstrating the validity of our knowledge on the dynamical correlation function within the Anderson insulating phase, which are amenable to direct experimental verification, are rare. The hindrances one faces on the experimental side are quite significant. For instance, the tight-binding model, which is a landmark of Anderson localization, is a single-particle approach; electron-electron interactions are fully neglected. In addition to that, the ions are supposed to be static and decoherence must be negligible, both factors are realizable only in experiments in the zero temperature limit. Finally, due to the large complexity of a typical condensed matter system, it is not a trivial to extract an unambiguous signature of Anderson localization in a crystal lattice, since, for instance, material absorption and other sources of dissipation also display an exponentially decaying profile in the observables. Hence, in order to access the physics in this phase, we need a set-up which provides a controlled investigation of strong localization by means of some tunable parameter. The Anderson metal-insulator transition has been observed in quantum chaotic systems, quasiperiodic kicked rotor with an amplitude modulated by two incommensurate frequencies [Cha+08]. It can be shown that this type of system affords a mapping onto the Anderson tight-binding Hamiltonian and, in this sense, such system is equivalent to a three-dimensional disordered system. With the help of ultra cold atoms, which in the following references consisted of a non-interacting Bose-Einstein condensate [Bil+08; Roa+08], it was observed an exponential spatial localization profile of matter-waves in strictly one-dimensional wave guides, a signal of the phenomenon of Anderson localization. On the theoretical side, since the onset of Anderson localization appears in the strong coupling limit, we do not have a small parameter to provide a reliable platform to perform perturbative calculations and one has to resort to tailored methods to deal with non-perturbative phenomena [EL83; Efe96].

Recently, a series of articles proposed the direct observation of spectral correlations in Anderson insulating wires within an ultra cold atom quantum quench experiment [Kar+12; LGM14; Gho+14; MMA14; Gar17]. Using the versatility of this type of set-ups to quantum simulate a kicked rotor, whose Hamiltonian can be mapped onto the Anderson Hamiltonian, it is expected that such observable is within the reach of current state-of-the art experiments [Lem+17]. In order to investigate disordered systems, the typical quantum quench protocol comprises the preparation of an eigenstate, $|\psi(0)\rangle = |\mathbf{k_0}\rangle$, of the free Hamiltonian, H_0, with a narrow width momentum distribution $\Delta k \ll \ell^{-1}$, this condition is required to obtain a well-contrasted signature of the coherent phenomena. Then, the cloud of ultra cold atoms is permitted to propagate under the influence of a disordered potential V for a time t and the system undergoes a unitary evolution for a fixed quench time $|\mathbf{k}\rangle = e^{-i(H_0+V)t}\,|\mathbf{k}_0\rangle$. After this time interval, the disorder is turned off and the evolution of the momentum distribution is monitored. Around a few elastic scattering times, it is expected the presence of a coherent backscattering peak at $\mathbf{k} = -\mathbf{k}_0$ and around the Heisenberg time, which is much later than the elastic scattering time, at the onset of Anderson localization, a new peak is predicted to appear in the forward direction at $\mathbf{k} = \mathbf{k}_0$ as a result of quantum coherence processes that leads to a phase accumulation. In a quantum quench set-up the time variable is the door knob providing us access to the physics of the forward scattering peak, which is described by the spectral form factor. As long as we assume that the eigenfunctions and eigenenergies are statistically independent, the spectral form factor is directly related to the connected level-level correlation function via a simple Fourier transform

$$K(\omega, L) = \nu_0^{-2} \left\langle \nu\left(\epsilon + \frac{\omega}{2}\right) \nu\left(\epsilon - \frac{\omega}{2}\right) \right\rangle_c , \tag{4.1}$$

where ν_0 is the density of states at the energy shell, $\langle \cdots \rangle_c$ denotes the connected contribution of the disorder average, ω measures distance between two energy levels and L is the system size.

Tremendous progress has been made throughout the long history of the theoretical study of level-level correlations functions Eq. (4.1) in disordered systems [G5; Efe82; Efe83; AS86; Al'+88; SI87; Izr90; Shk+93; EE92]. However, closed-form results are only known in certain specific limits. For low-dimensional systems ($d < 3$), the level-level correlation function Eq. (4.1) describes how, depending on the ratio between the system size L and the localization length ξ, Wigner-Dyson statistics at small systems $L < \xi$ transitions into Poisson statistics as the system size increases and becomes larger than the localization length, $L > \xi$. The former statistics is manifested in systems with non-integrable chaotic dynamics, whereas the latter signals the breaking of ergodicity due to localization effects [Por65; HGK19]. To describe a d-dimensional system in the Anderson insulating phase, $L > \xi$, an intuitive approach would be to consider that in this phase the system decouples into $(L/\xi)^d$ uncorrelated subsystems of volume ξ^d. As a result, the level-level correlation is governed by the following scaling law

$$K(\omega, L) \simeq \left(\frac{\xi}{L}\right)^d f\left(\frac{\omega}{\Delta_\xi}\right) \to 0, \quad \text{as } L \to \infty, \tag{4.2}$$

where Δ_ξ is the mean level spacing associated with a single localization volume and $f(\omega/\Delta_\xi) = K(\xi, \omega)$. Fully uncorrelated Poisson statistics is only possible in the thermodynamic limit of unbounded system sizes. The reality does not correspond to our overly simplified picture. In finite size systems, there are regions with overlapping tails of localized wave functions that induce correlations among neighboring localization volumes. It is particularly these types of correlations which are within the reach of ultra cold atom quench experiments. Insofar as concerns the literature, only asymptotic results have been obtained for the experimentally relevant

orthogonal and symplectic symmetry classes.

In this chapter, we will derive closed-form results for the spectral level-level correlation function for Anderson insulating wires belonging to the three Wigner-Dyson classes. The latter displays an intimate connection with the ground-state wave function of the transfer matrix Hamiltonian for the supersymmetric non-linear sigmal model reported in [KO17a]. The results obtained in this work are in perfect agreement with recent numerical simulations of the quench experiment [Lem+17]. The subsequent experimental verification of our results [Hai+18] marks an important benchmark for our understanding of Anderson localization.

4.2. Field Theory

Within the framework of the non-linear sigma model, we introduce the well known field theory description of the level-level correlation function for a d-dimensional disordered system [Efe99; Efe82; EL83]:

$$K(\omega) = \frac{1}{64}\mathrm{Re}\left\langle \left\{ \int (dx)\mathrm{str}[\sigma_3^{\mathrm{bf}}\sigma_3^{\mathrm{ra}}(Q-\sigma_3^{\mathrm{ra}})] \right\}^2 \right\rangle_S . \tag{4.3}$$

Bear in mind that in this representation, via a functional integral over a supermatrix Q, the average over the disorder has already been dealt with, so the nature of the brackets denoting an averaging process in here is different. Namely, the average in the expression above is with respect to the non-linear sigma model action, which is given by

$$S[Q] = -\frac{\pi\tilde{\nu}}{8}\int (dx)\mathrm{str}\left[D(\partial_{\mathbf{x}}Q)^2 + 2i\omega\sigma_3^{\mathrm{ra}}Q\right], \tag{4.4}$$

where D is the diffusion parameter, str represents the generalization of the trace of matrix to a trace over a superspace, or a graded space as sometimes appears in the literature, and the integration over x is normalized to unity, $\int(dx) = 1$. The specific structure of the supermatrix Q depends on which Wigner-Dyson class the system belongs to and the diagnosis tool used to detect its respective class is the squared time-reversal operator. In the absence of time-reversal symmetry, the unitary class, we have $\mathcal{T} = 0$. If the system displays time-reversal symmetry and spin-rotation symmetry, then it belongs to the orthogonal class and $\mathcal{T}^2 = 1$. Finally, if the system has time-reversal symmetry, but lacks spin-rotational symmetry, then $\mathcal{T}^2 = -1$ and the system is included in the symplectic class. Having said that, using the notation of Ref. [Efe99], we can now introduce the definition for $\tilde{\nu}_0$. For a system in the unitary and orthogonal classes, $\tilde{\nu}_0 = \nu_0$ and $\tilde{\nu}_0 = 2\nu_0$ in the symplectic class. The supermatrix Q represents the fundamental degree of freedom in our construction and it acts on an eight-dimensional super or graded space, whose composition consists of the product among two-dimensional subspaces referred to as bosonic-fermionic (bf), retarded-advanced (ra) and time-reversal (tr) sectors. The matrices σ_3^{bf} and σ_3^{ra} realizes the symmetry breaking in the bosonic-fermionic and retarded-advanced sectors, respectively. The field configuration $Q = \sigma_3^{\mathrm{ra}}$ describes the classical, diffusive fixed point and $Q_\Lambda = Q - \sigma_3^{\mathrm{ra}}$ measures deviations from the latter. We recall that the action exhibited in Eq. (4.4) is closely related to the famous Ginzburg-Landau theories for phase-transitions. At large level separations or short time scales, $t \sim \omega^{-1} \ll \Delta_\xi^{-1} = \xi^2/D$, the term $\mathrm{str}(\sigma_3^{\mathrm{ra}}Q)$ corresponds to a symmetry breaking which drives the supermatrix Q towards the metallic saddle point $Q = \sigma_3^{\mathrm{ra}}$. In this diffusive limit, this preferential field configuration provides us a controllable and reliable platform to perform perturbative calculations in terms of the Goldstone modes, which are understood as the diffusion modes of disordered single-particle systems. As the system evolves and the time scale becomes comparable to Δ_ξ^{-1}, the onset of strong Anderson localization occurs. In this limit, there are large quantum fluctuations that restore the

symmetry in the retarded-advanced sector, which demand us to integrate over the entire manifold and we have to explore non-perturbative methods. Fortunately, for quasi-one-dimensional geometries, $L \gg L_\perp$, such methods are within the reach of our theoretical grasp. For systems satisfying this inequality, the diffusive nonlinear sigma model action, Eq. (4.4), acquires the status of a Feynman path integral, where the coordinate variable x can be thought of as a fictitious time variable, Q is interpreted as a massive multi-dimensional quantum mechanical particle propagating in a manifold, whose nature depends on the squared time-reversal operator, with kinetic energy $K \sim 1/D^{-1}(\partial_x Q)^2$ under the influence of an imaginary potential of the form $V \sim \omega\sigma_3^{\mathrm{ra}}Q$. Drawing further the analogy with the Feynman path integral, we map the functional integration onto the corresponding Schrödinger equation and, in this sense, we circumvent the necessity of performing a functional integration over the entire manifold at the cost of having to solve a considerably difficulty differential equation.

4.3. Anderson Insulating Wires

Considering a system with a quasi-one-dimensional geometry, the typical approach reported in the literature to compute the spectral correlation function [AF95; Efe99] involves expressing it in terms of eigenfunctions of the Hamiltonian for the Schrödinger equation, known as the transfer matrix Hamiltonian. Recently, a more modern approach to derive the transfer matrix Hamiltonian has been presented in Ref. [KO17b], we included the details of the derivation in the appendix B. However, using this typical framework leads to rather cumbersome equations for the computation of the relevant function and closed-form solutions for all Wigner-Dyson ensemble are not known. Here in this work, we follow a different path, whose theoretical foundation lies on the graded symmetry of the action Eq. (4.4) with which we use to derive Eq. (4.1) from a local generating function. In comparison to the old-fashioned method, this novel approach depends only on the skeleton structure Q_0, see appendix C for details, of the supermatrix Q and the ground state wave function associated with the transfer matrix Hamiltonian. Such structure implies a dramatic simplification of the theoretical description of the problem and permits us to obtain the closed-form solution for the level-level correlation function Eq. (4.1). The technical details of the derivation are postponed for later sections and now we present the final expression for the generating function in the regime of Anderson insulating wires $L \gg \xi = \pi\tilde{\nu}_0 D/L$:

$$\begin{aligned} K(\omega) &= \frac{\xi}{2\beta L}\mathrm{Re}\left[\int (dx)\partial_\eta \mathcal{F}(\eta, x)|_{\eta=-\frac{i\omega}{\Delta_\xi}}\right], \\ \mathcal{F}(\eta) &= \frac{1}{2}\int dQ_0 \mathrm{str}(\sigma_3^{\mathrm{ra}}Q_0)Y_0^2(Q_0). \end{aligned} \tag{4.5}$$

Here Y_0 is the ground state wave function of the Schrödinger equation and β represents the symmetry dependent parameter, $\beta = 1(2)$ in the orthogonal and symplectic (unitary) class. We point out that in the expression above Eq. (4.5) some classical number and all Grassmann variables have already been integrated out. The only remaining dependences of Q_0 are on the complex number variables from the compact interval, usually referred to as fermionic radial variables, $|\lambda_{\mathrm{f}}| \leq 1$ and from the non-compact interval, correspondingly the bosonic radial variables, $1 \leq \lambda_{\mathrm{b}}$. Although these two domains of the variables in the supermatrix Q_0 are rather unusual, this structure has its origin explained in terms of physical effects. The fermionic radial variables are originated as an order parameter for a fermion gas with attraction which is well defined, whereas, the bosonic radial variables are associated with an order parameter for a Bose gas with an attraction. As expected, the precise parametrization of each supermatrix Q_0 depends on the Wigner-Dyson classification

of the system, or the symmetry class, that is, for a system in the unitary class $Q_0(\mathcal{R})$ is parametrized by only two variables $\mathcal{R} = \{\lambda_{\rm f}, \lambda_{\rm b}\}$. In the orthogonal class, we need three variables $\mathcal{R} = \{\lambda_{\rm f}, \lambda_{\rm b,1}, \lambda_{\rm b,2}\}$. The same number of variables is also present in the symplectic class, but the nature of the variables is different $\mathcal{R} = \{\lambda_{\rm f,1}, \lambda_{\rm f,2}, \lambda_{\rm b}\}$. For a more detailed discussion, the complete description of the parametrization scheme is presented in the appendix C. As a consequence of this parametrization, we obtain a rather complicated Jacobian, which once calculated can be explored in many other different physical quantities. The corresponding integration measure present in the definition of the local generating function may be written as a product between the flat measure $d\mathcal{R}$, whose form depends on the Wigner-Dyson ensemble, and the Jacobian $\sqrt{g}$. For the unitary, orthogonal and symplectic ensembles, we have $\sqrt{g} = (\lambda_{\rm b} - \lambda_{\rm f})^{-2}$, $\sqrt{g} = (1-\lambda_{\rm f}^2)(\lambda_{\rm b,1}^2 + \lambda_{\rm b,2}^2 + \lambda_{\rm f}^2 - 2\lambda_{\rm b,1}\lambda_{\rm b,2}\lambda_{\rm f} - 1)^{-2}$ and $\sqrt{g} = (\lambda_{\rm b}^2 - 1)(\lambda_{\rm f,1}^2 + \lambda_{\rm f,2}^2 + \lambda_{\rm b}^2 - 2\lambda_{\rm f,1}\lambda_{\rm f,2}\lambda_{\rm b} - 1)^{-2}$, respectively. Notice that none of the Jacobians associated with this parametrization dependen on anticommuting variables, which is a rather convenient feature in the construction of our observable. The ground state wave function Y_0 is a solution to the homogeneous Schrödinger equation:

$$\left[\Delta_Q + \frac{\eta}{2}\mathrm{str}(\sigma_3^{\rm ra} Q_0)\right] Y_0(Q_0) = 0, \tag{4.6}$$

which satisfies the boundary condition $Y_0(\sigma_3^{\rm ra}) = 1$ and it is important to recall that at the metallic saddle point all radial coordinates are unity, $\lambda_i = 1$ for all i. The symbol Δ_Q denotes the Laplace-Beltrami operator on the Q_0-field manifold, which is a generalization of the usual Laplace operator, given by the expression $\Delta_Q = (1/\sqrt{g})\partial_\lambda \sqrt{g} g^{\lambda\rho}\partial_\rho$, there is an implicit summation over the repeated indices $\lambda, \rho \in \mathcal{R}$, namely the radial variables, and the metric tensor reads $g^{\lambda\rho} = |\lambda^2 - 1|\delta^{\lambda\rho}$ for all symmetry classes, in here $\delta^{\lambda\rho}$ is the typical Kronecker-delta symbol.

4.4. Correlations from Zero-Mode

The Schrödinger equation plays a fundamental role in the derivation of our results, we explore it to obtain the following identities

$$\begin{aligned} \mathrm{str}(\sigma_3^{\rm ra} Q_0) Y_0(Q_0) &= -[2\Delta_Q + \eta\mathrm{str}(\sigma_3^{\rm ra} Q_0)] Y_0'(Q_0), \\ \eta\mathrm{str}(\sigma_3^{\rm ra} Q_0) Y_0(Q_0) &= -2\Delta_Q Y_0(Q_0), \end{aligned} \tag{4.7}$$

where for simplicity we have introduced the notation $\partial_\eta Y_0 = Y_0'$. With the aid of Eq. (4.7), we perform a few algebraic manipulations on the local generating function $\mathcal{F}$ and obtain the result:

$$\mathcal{F}(\eta) = \int dQ_0 (Y_0' \Delta_Q Y_0 - Y_0 \Delta_Q Y_0'). \tag{4.8}$$

Upon a partial integration, we arrive at a surprisingly simple result, which consists of just a boundary contribution

$$\mathcal{F}(\eta) = \int d\mathcal{R} \partial_\lambda \sqrt{g} g^{\lambda\rho} (Y_0' \partial_\rho Y_0 - Y_0 \partial_\rho Y_0'). \tag{4.9}$$

In particular, this boundary contribution Eq. (4.9) reflects the hybrid nature of the computation scheme employed, the boson-boson sector displays a non-compact parametrization, whereas the fermion-fermion is compact. This peculiar structure appears clearly in the metric elements $g^{\lambda\rho}$ whose entries vanish when evaluated at any boundary point. On the other hand, the Jacobian has a singular structure at $Q_0 = \sigma_3^{\rm ra}$. As a consequence of that, we have to deal with a product of the type $0 \times \infty$ and, to do so, we shift the

bound of integration via an arbitrarily small positive quantity ϵ, that is, $1^{\pm} = 1 \pm \epsilon$, where the positive (negative) sign holds for a bosonic (fermionic) variable. This simple scheme is already enough to regularize the integration Eq. (4.9) over the radial variables. In the limit of ϵ approaching zero from the right, which we denote as $\epsilon \searrow 0$, the boundary condition $(\sqrt{g}g^{\lambda\rho})_{\lambda=1^{\pm}}$ is reduced to a δ-function that depends solely on the radial coordinates multiplied by a numerical constant, this fixes the evaluation at the metallic saddle point $Q_0 = \sigma_3^{\mathrm{ra}}$. Furthering the calculations, we use the boundary condition $Y_0(\sigma_3^{\mathrm{ra}}) = 1$, which implies that $Y_0'(\sigma_3^{\mathrm{ra}}) = 0$, and this yields a memorably simple result

$$\mathcal{F}(\eta) = -2\partial_{\lambda_{\mathrm{f}}} Y_0'(Q_0 = \sigma_3^{\mathrm{ra}}), \tag{4.10}$$

where in the symplectic class, the computation is not sensitive whether it is $\lambda_{\mathrm{f},1}$ or $\lambda_{\mathrm{f},2}$. In addition to that, this expression affords a simple generalization which contemplates the bosonic variables. It can be shown that

$$\partial_{\lambda} Y_0'(Q_0 = \sigma_3^{\mathrm{ra}}) = s_{\lambda\rho}\partial_{\rho} Y_0'(Q_0 = \sigma_3^{\mathrm{ra}}), \tag{4.11}$$

where $s_{\lambda\rho}$ is 1 if both radial variables are bosonic or fermionic and -1 otherwise. The possibility of writing down the local generating function in this form ensures that our calculations will not depend on the particular regularization scheme explored, and, for instance, we may symmetrize the result in the radial variables. For a more detailed and comprehensive discussion regards this calculations, we refer the reader to the appendix C, where we present the specific form of the parametrization in polar coordinates and the zero modes for the three Wigner-Dyson classes. Furthermore, in this appendix we discuss the details about the calculations involving the local generating function and the computation of the forward scattering peak. A similar compact representation of the level-level correlation in terms of the ground state wave function and a local generating function for spectral correlations has been fairly recently reported in the literature [Mic16] for the unitary class. In this work, employing the non-perturbative theoretical framework introduced in Ref. [SO07] and based on a mapping of the localization problem in the unitary class onto the three-dimensional Coulomb-scattering problem, it was derived in closed-form solution the spectral statistics of a quasi-one-dimensional Anderson insulator. To conclude, it is interesting to point out that there is a confluence in the description of the spectral statistics of all Wigner-Dyson symmetries in terms of the expression Eq. (4.10), indicating that such a simple result is not just an accident. Recently, it has been reported in the literature the closed-form ground state wave function for the transfer matrix Hamiltonian problem for all three Wigner-Dyson classes [KO17a]. With the help of these results, we compute the local generating function for all symmetry classes:

$$\mathcal{F}^{\mathrm{U}}(\eta) = -8I_0(z_\eta)K_0(z_\eta), \tag{4.12}$$

$$\mathcal{F}^{\mathrm{O}}(\eta) = -4\left[I_0(z_\eta)K_0(z_\eta) + I_1(z_\eta)K_1(z_\eta)\right], \tag{4.13}$$

$$\mathcal{F}_{\pm}^{\mathrm{Sp}}(\eta) = -4\left\{\left[I_0(z_\eta) \pm 1\right]K_0(z_\eta) + I_1(z_\eta)K_1(z_\eta)\right\}, \tag{4.14}$$

where for simplicity we introduced the notation $z_\eta = 4\sqrt{\eta}$ and U, O and Sp represent the unitary, orthogonal and symplectic symmetry class, respectively, and within the symplectic class the plus (minus) sign indicates that the wire has an even (odd) number of channels.

4.5. Spectral Correlations

We substitute Eqs. (4.12)-(4.14) into the level-level correlation function Eq. (4.1) and a straightforward computation yields the spectral statistics in Anderson insulating wires for all Wigner-Dyson classes:

$$K(\omega) = \frac{32\xi}{\beta L}\mathrm{Re}[\mathcal{K}(z_\eta)], \tag{4.15}$$

where

$$\mathcal{K}^{\mathrm{U}}(z_\eta) = \left[K_1(z_\eta)I_0(z_\eta) - K_0(z_\eta)I_1(z_\eta)\right]/z_\eta, \tag{4.16}$$
$$\mathcal{K}^{\mathrm{O}}(z_\eta) = K_1(z_\eta)I_1(z_\eta)/z_\eta^2, \tag{4.17}$$
$$\mathcal{K}^{\mathrm{Sp}}_{\pm}(z_\eta) = K_1(z_\eta)\left[I_1(z_\eta) \pm z_\eta/2\right]/z_\eta^2. \tag{4.18}$$

This set of equations Eq. (4.15)-(4.18) corresponds to our main contribution to the literature of Anderson insulating wires and they provide a bridge connecting the two asymptotic limits $\omega > \Delta_\xi$ and $\omega < \Delta_\xi$. In the former limit, the potential term dominates the kinetic term confining the eigenvalues to stay close to the origin, causing the Laplace-Beltrami operator to collapse into the usual Laplace operator. This simplification in such regime permits us to obtain analytical solutions for the transfer matrix Hamiltonian problem. On the opposite limit, $\omega < \Delta_\xi$, we no longer have access to analytical solutions for the transfer matrix Hamiltonian problem. In Ref. [AF95], this problem was addressed by observing that in this large system regime $L/\xi \gg 1$ the physics is governed by a few low lying eigenvalues, which allows us to resort to a formal eigenfunction representation, with a finite number of functions, of the Hamiltonian. The Poisson statistics only holds for systems in the thermodynamic limit $\lim_{L\to\infty} K(L,\omega) = 0$ and, for finite size systems, there is an overlap among the exponentially localized eigenstates that induces correlations in the spectrum.

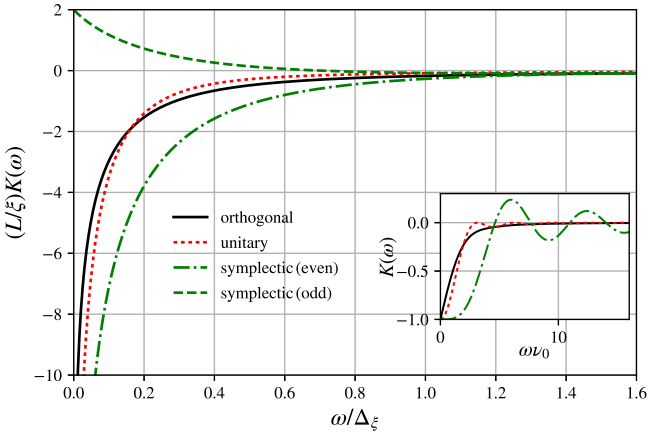

Figure 4.1.: Level-level correlations in Anderson insulating wires for the Wigner-Dyson classes. The residual level-attraction in the symplectic class with an odd number of channels reflects the presence of a topologically protected metallic channel. The inset shows for comparison Wigner-Dyson spectral correlations of fully chaotic systems.

At large level separation $\omega > \Delta_\xi$ these reflect the region of classical metallic diffusion which appears in short time scales, where quantum interference processes are not still developed. Drawing on the semiclassical analogy between spectral correlations and classical dynamics, we point out that we are probing the trajectories

of a particle on a time scale much smaller than Δ_ξ^{-1}, a time which is not long enough for the particle to explore the entire localization volume. In this sense, the localization effects are not yet felt. On the other hand, in the regime $\omega < \Delta_\xi$, small energies, the level-level correlation is mostly governed by the localization effects. In particular, in the deep quantum regime, the spectral statistics are dominated by pairwise repulsion among neighboring levels. In order to analyze the statistics within this regime, it is enough to consider a 2×2 Hamiltonian with non-zero off-diagonal terms [Mot70; SI87; Iva+12]. The crossover between these two limits is described by Eqs.(4.15)-(4.18) and in Fig. 4.1 we display the plot for these results. It is illustrative to compare this limit of a long wire with the fully chaotic short wire case which corresponds to the Wigner-Dyson correlations. We observe that at small level separations the latter limit displays the phenomenon of strong level repulsion, the spectral statistics completely vanishes at $\omega = 0$. Such result is in contrast with the former limit, where in the region of small level separations there is a residual logarithmic level repulsion among the localized states.

From the results above, it is straightforward to recover the asymptotic correlations of far-distant levels $\omega/\Delta_\xi = s \gg 1$ for all Wigner-Dyson classes [Zwi14],

$$\frac{L}{\xi}K(s) = -\frac{1}{4\sqrt{2}\beta}\left[\frac{1}{s^{3/2}} - \frac{3(-1)^\beta}{128 s^{5/2}}\right], \tag{4.19}$$

the leading order contribution reproduces the famous result by Altshuler-Shklovskii [AS86; AM07]. In the regime of small level separations $s \ll 1$, the asymptotic results for the unitary, orthogonal and symplectic, with an even number of channels, classes is given by

$$\frac{L}{\xi}K(s) = -a_\beta\left[\log\left(\frac{1}{4s}\right) - 2\gamma + b_\beta + \pi s c_\beta + \cdots\right], \tag{4.20}$$

with $\gamma \simeq 0.577$ being the Euler-Mascheroni constant, $a_{\mathrm{U,Sp+}} = 8$, $a_{\mathrm{O}} = 4$, $b_{\mathrm{U}} = 0$, $b_{\mathrm{O}} = 1/2$, $b_{\mathrm{Sp+}} = 3/4$ and $c_{\mathrm{U}} = 3$, $c_{\mathrm{Sp+}} = 3/2$. We single out the symplectic class with an odd number of channels, because its asymptotic correlations has a very distinct nature in comparison with the other ensembles

$$\frac{L}{\xi}K_-^{\mathrm{Sp}}(s) = 2 - 4\pi s - \left(\frac{8s}{\sqrt{3}}\right)^2 \log(s) + \cdots, \tag{4.21}$$

the frequency independent contribution signals the existence of a topologically protected metallic channel, which perfectly transmits through the system without backscattering. This phenomenon leads to the absence of Anderson localization and it was first reported in the literature in the study of carbon nanotubes [AN98; NA99; AS02].

4.6. Forward Peak

As long as we assume that the eigenenergies and eigenfunctions are statistically independent quantities, the spectral form factor is directly related to the level-level correlation function via the application of a Fourier transform. The former quantity provides the description of the genesis of the forward scattering peak in the quantum quench set-up. The explicit result for all three Wigner-Dyson classes is given by the following

expression:

$$\mathcal{C}_{\rm fs}^{\rm U}(t) = \theta(t) I_0\left(8/t\Delta_\xi\right) e^{-8/t\Delta_\xi}, \tag{4.22}$$

$$\mathcal{C}_{\rm fs}^{\rm O}(t) = \theta(t)\left[I_0\left(8/t\Delta_\xi\right) + I_1\left(8/t\Delta_\xi\right)\right] e^{-8/t\Delta_\xi}, \tag{4.23}$$

$$\mathcal{C}_{\rm fs}^{\rm Sp,\pm}(t) = \tfrac{1}{2}\left[\mathcal{C}_{\rm fs}^{\rm O}(t) \pm \theta(t) e^{-4/t\Delta_\xi}\right]. \tag{4.24}$$

These functions describing the temporal profile of the coherent forward scattering have been normalized with respect to its saturation value, $\lim_{t\to\infty}\mathcal{C}_{\rm fs}(t)$. Contrary to the orthogonal and symplectic classes, the time dependence of the coherent forward scattering peak in the unitary has already been reported in the literature [MMA14]. Recently, it has been reported in the literature the numerical simulations of the quantum quench experiment in the orthogonal class [Lem+17]. Using their results, we make a comparison with our theoretical predictions for the orthogonal class in Fig. 4.2.

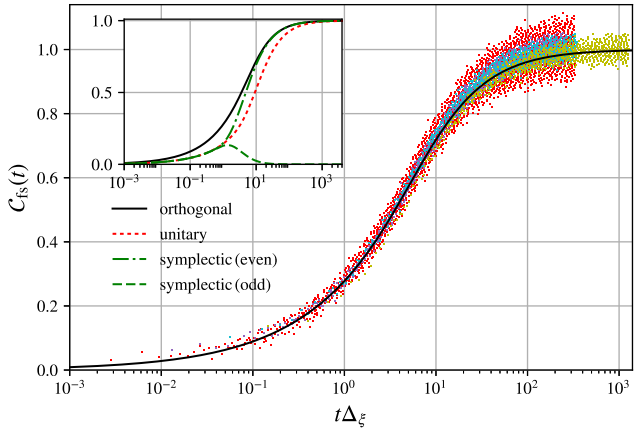

Figure 4.2.: Forward-scattering peak in the orthogonal class. Points are numerical data from a recent simulation of the quantum quench experiment in a kicked rotor set-up [Lem+17]. The universal curve is obtained after accounting for finite Ehrenfest-times and with Heisenberg-times $\sim 1/\Delta_\xi$ independently determined from the wave-packet dynamics (see Ref. [Lem+17] for further details). Different colors correspond to different sets of system parameters, and the solid line shows Eq. (4.23) without any fitting-parameter. Insets: Forward-scattering peak for all Wigner-Dyson classes, see main text for discussion.

In this plot, the dots represent the numerical data, each color corresponds to a different region of the parameter space and, for these distinct values, all the curves collapse to a universal curve, the solid black line denotes the theoretical prediction and it is clear that both results are in perfect agreement. However, such agreement, across all time scales in the temporal dynamics of the coherent forward scattering peak, is only reproducible accurately if we shift the onset by a certain delay time. This characteristic delay has its physical origin possibly related to the Ehrenfest time. Such line of reasoning has been introduced in Ref. [TKL04], where it was argued that dynamical localization should have its effects delayed by a time scale given by the Ehrenfest time of the system. In the inset of Fig. 4.2, we display again the forward peak for the orthogonal class along with the remaining temporal profile of the remaining classes, unitary and symplectic. In addition to that, although this phenomenon relies fundamentally on subtle quantum interference effects, the coherent forward scattering peak is completely insensitive to the time reversal symmetry, its origin is fully dependent on Anderson localization and, as a consequence of that, this peak provides a genuine marker

for the presence of Anderson localization. In the unitary class, the formation of the peaked structure can be understood as the sum of diagrams containing crossed ladders (Cooperon modes). For the orthogonal class, the diagrammatic construction involves a summation only over the ladder diagrams (diffuson modes). The symplectic class, in the short time region, $t\Delta_\xi \ll 1$, displays a behavior identical to the unitary class and is different from the orthogonal class by approximately a factor two. As the system evolves and reach times around $t\Delta_\xi \gtrsim 1$, the number of conducting channels becomes relevant. For systems possessing an odd number of channels, the signal smoothly decays to zero $\mathcal{C}_{\rm fs}^{\rm Sp,-} \sim (t\Delta_\xi)^{-2}$ indicating delocalization, which is associated with the presence of a single topologically protected channel. Fixing $\tau = t\Delta_\xi$, the asymptotic behavior of the remaining cases can be conveniently summarized as

$$\mathcal{C}_{\rm fs}(\tau) = \begin{cases} a_\alpha \tau^{1/2} + b_\alpha \tau^{3/2} + \cdots, & s \ll 1, \\ 1 - c_\alpha/\tau + d_\alpha/\tau^2 + \cdots, & s \gg 1, \end{cases} \tag{4.25}$$

where $a_{\rm O} = 2a_{\rm U,Sp+} = 1/(2\sqrt{\pi})$, $b_{\rm O} = -2b_{\rm U} = 2b_{\rm Sp+} = -1/(128\sqrt{\pi})$ $c_{\rm O,Sp+} = c_{\rm U}/2 = 4$, and $d_{\rm O} = d_{\rm U}/3 = 4d_{\rm Sp+}/3$.

4.7. Local Generating Function

With the aid of the supersymmetric framework of the action (4.4) and the polar parametrization $Q = UQ_0U^{-1}$ introduced in Ref. [Efe99], we established an important relation between the level-level correlation and the local generating function, Eqs. (4.28) and (4.29) upon which we derived our results. In here the supermatrix U has a diagonal structure in the retarded-advanced sector and it is the only source of anti-commuting variables, the matrix Q_0 is the skeleton of our fundamental degree of freedom Q and, contrary to U, this matrix has non-trivial entries in the off-diagonal retarded-advanced sector, $Q_0 = \cos\hat{\theta}\sigma_3^{\rm ra} - \sin\hat{\theta}\sigma_2^{\rm ra}$. The angle $\hat{\theta}$ is a 2×2 block diagonal matrix the Bose-Fermi sector, whose explicit form is given by $\hat{\theta} = {\rm diag}(i\hat{\theta}_{\rm b}, \hat{\theta}_{\rm f})_{\rm bf}$, where the matrices $\hat{\theta}_{\rm b(f)}$ have a structure whose form is dictated by the presence or absence of time-reversal symmetry. In addition to that, these matrices are parametrized by the non-compact and compact radial variables we already introduced above: $-1 \leq \lambda_{\rm f} = \cos\theta_{\theta_{\rm f}} \leq 1$ and $1 \leq \lambda_{\rm b} = \cosh\theta_{\rm b}$. Starting out with the following local generating function

$$\mathcal{F}(\eta, \mathbf{x}) = \left\langle \frac{\{{\rm str}[\sigma_3^{\rm bf}\sigma_3^{\rm ra}(Q(\mathbf{x}) - \sigma_3^{\rm ra})]\}^2}{{\rm str}[\sigma_3^{\rm ra}Q(\mathbf{x})]} \right\rangle_S , \tag{4.26}$$

which is straightforward to verify that indeed such an expression is connected to the level-level correlation function via a derivative with respect to the level spacing ω. For a general d-dimensional system, after we perform some algebraic manipulations to reduce the local generating function to a form containing only the terms with the highest possible number of Grassmann variables, we obtain the following expression

$$\mathcal{F}(\eta, \mathbf{x}) = \langle {\rm str}(\cos\hat{\theta}_{\mathbf{x}}) P_{\mathcal{G},\mathbf{x}} \rangle_S \, . \tag{4.27}$$

Recalling that the graded symmetry of the action is preserved by the symmetry-breaking term, we use this to perform constant rotations represented by the matrix $\bar{U}$ sharing the symmetries of U, namely, $U \to \bar{U}U$. This invariance permits us to linearly shift the Grassmann variables in the pre-exponential contribution of the correlation function. Since the finite contributions of the integration are all generated by terms involving the maximal order in the Grassmann variables, we consider only terms satisfying this requirement and as it was

demonstrated in Ref. [Zir86], it is convenient to introduce the maximal polynomial of Grassmann variables for the retarded and advanced sectors $P_{\mathcal{G}}^{\mathrm{r(a)}}$ with $P_{\mathcal{G}} = P_{\mathcal{G}}^{\mathrm{r}} P_{\mathcal{G}}^{\mathrm{a}}$ to perform this type of calculation. The same construction can be applied to the level-level correlation function yielding the following two equations:

$$\partial_{\eta}\mathcal{F}(\eta, \mathbf{x}) \sim \int (dy)\, \langle \mathcal{C}_{\mathbf{x},\mathbf{y}} P_{\mathcal{G},\mathbf{x}} \rangle_S \tag{4.28}$$

$$K(\omega) \sim \int (dx) \int (dy)\, \langle \mathcal{C}_{\mathbf{x},\mathbf{y}} P_{\mathcal{G},\mathbf{x}}^{\mathrm{a}} P_{\mathcal{G},\mathbf{y}}^{\mathrm{r}} \rangle_S \,, \tag{4.29}$$

where we defined $\mathcal{C}_{\mathbf{x},\mathbf{y}} = \mathrm{str}(\cos\hat{\theta}_{\mathbf{x}})\mathrm{str}(\cos\hat{\theta}_{\mathbf{y}})$. Once again, the graded symmetry permits us to explore the properties of the Grassmann variables, if we shift the maximal polynomial $P_{\mathcal{G},\mathbf{x}(\mathbf{y})}^{\mathrm{r}} \to P_{\mathcal{G},\mathbf{x}}^{\mathrm{r}} + P_{\mathcal{G},\mathbf{y}}^{\mathrm{r}}$, in the first(second) term, then it becomes immediately clear that the local generating function for a general d-dimensional system, Eq. (4.28), is fundamentally equivalent to the level-level correlation function, Eq. (4.29). Bringing back the numerical factors, we drop the proportionality and write down the explicit result

$$K(\omega) = -(16\pi\tilde{\nu}_0)^{-1}\mathrm{Im}\left[\int (dx)\partial_{\omega}\mathcal{F}(\omega, \mathbf{x})\right]. \tag{4.30}$$

For the local generating function, we introduce the normalized maximal polynomial $P_{\mathcal{G}}^{0}$ and it becomes

$$\mathcal{F}(\eta) = \frac{8}{\beta}\langle \mathrm{str}(\cos\hat{\theta}_{\mathbf{x}}) P_{\mathcal{G},\mathbf{x}} \rangle_S \,. \tag{4.31}$$

An integration over these remaining Grassmann variables yields the identity displayed in Eq. (4.5) for the Anderson insulating wires. It is important to point out that similar ideas have been previously explored in other contexts. For instance, in Ref. [SLA98], it was studied the spectral statistics of a disordered metal via a perturbative expansion. In their work, they demonstrated that such function affords a natural representation as the second derivative of the free energy of the given system. Another successful implementation of a similar idea was explored in Ref. [TSA96]. In this work, it was derived a general relation between the correlators of density of states fluctuations and the density response functions. In addition to that, it was shown that such a relation holds for quantum chaotic systems and also to the crossover region among the universality classes. Finally, this particular representation of the level-level correlation can possibly be helpful in other contexts, such as the one described in Ref. [TM16].

4.8. Conclusion

Within the framework of the supersymmetric non-linear sigma model, we have shown that by representing the level-level correlation function in terms of a local generating function, it is possible to fill the research

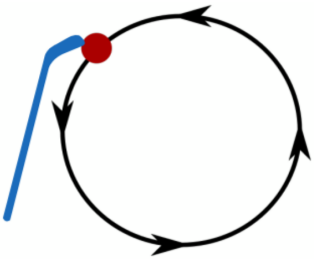

Figure 4.3.: The particle receives a periodic kick from an external force, a feature that helps to imitate the effects of the disorder in the system.

gap involving the physics between the asymptotic limits, $\omega \ll \Delta_\xi$ and $\omega \gg \Delta_\xi$, for all disordered quasi-one-dimensional long wires of pure symmetry, namely, the Wigner-Dyson classes (unitary, orthogonal and symplectic). In this particular case of Anderson insulating wires with pure symmetry, the theoretical approach we explored unveiled a simple relation between the spectral correlations and the ground state wave function associated with the transfer matrix Hamiltonian. With the help of the corresponding Schrödinger equation, we have shown that our calculations are reduced to a simple boundary contribution which depends only on the ground state wave function. Such observation provided us a reliable and simple platform to compute the spectral correlation function for the unitary, orthogonal and symplectic ensembles in a clear manner. Furthermore, by assuming statistical independence of eigenfunctions and eigenenergies, it is revealed that the level-level correlation function and the temporal profile of the coherent forward scattering peak are connected to each other via a Fourier transform. Building on these results, we have shown that the coherent forward scattering peak starts to grow around $t\Delta_\xi \approx 1$, the region where the non-perturbative quantum effects becomes fully manifested, and in the limit of $t\Delta_\xi \gg 1$ it saturates to unity. This intimate connection between these two quantities can be explored in an experimental set-up to extract information about the statistics of energy levels of a disordered system from measurements of the coherent forward scattering peak and vice-versa.

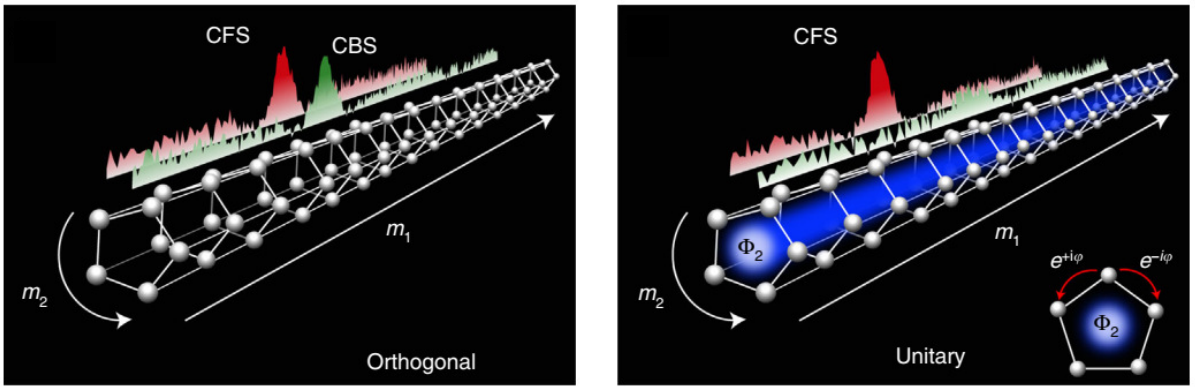

Figure 4.4.: Above we display two distinct disordered synthetic nanotubes in momentum space. In left panel, the time-reversal symmetry is preserved, whereas the right panel corresponds to a system with a non-zero external magnetic flux. We observe the manifestation of localization effects in both cases. In the former, the interference processes lead to the formation of a coherent forward scattering peak, which is a signature of the onset of Anderson localization. In the latter, the absence of the coherent backscattering peak is clear signal that indeed the time-reversal symmetry is broken.

Moreover, a comparison of our theoretical prediction with the numerical simulations reported in the literature displayed a perfect agreement between the two results in a parameter-free comparison. The experimental verification of the spectral form factor via cold atom quantum quench experiments reported in Ref. [Hai+18] was made possible thanks to the help of the artificial gauge field technology and quantum simulation. Both ideas hinges on the concept of using a model that is easier to build up and investigate to study the physical properties of a different system, as long as there is a mapping between the two distinct systems. The phenomenon of quantum dynamical localization has its origin in the quantum interference of trajectories that can lead to a complete absence of diffusion in momentum space. Such distinct localization phenomenon can be explored with the help of the quantum kicked rotor, which consists of a particle propagating in a closed orbit being periodically kicked by some external force, see Fig. 4.3. The typical Hamiltonian which

describes the physics of this type of system is given by

$$H = \frac{p^2}{2m} + K\cos(kx)\sum_n \delta(t-n), \tag{4.32}$$

where m is the mass of the particle, p its momentum, the parameter K sets the strength of the kicking and n the period. Such Hamiltonian can be mapped onto the Anderson Hamiltonian, we present the discussion involving the physics and the mathematical technicalities of the mapping in the appendix A. Therefore, the dynamical localization can be understood as a phenomenon that is analogous to the Anderson localization, the former occurs in the momentum space and the latter in the configuration space. With the aid quantum kicked rotor, as the fundamental building block of the experiment, a Hamiltonian mimicking a synthetic nanowire was built and by controlling its parameters generated a system in the presence or in the absence of an external magnetic field, see Fig. 4.4. In Fig. 4.5, we display the experimental data along with a comparison with our theoretical prediction for the coherent forward scattering peak contrast in the orthogonal class, both results seem to be in perfect agreement with each other. The contrast function is defined as

$$C_X(t) = \frac{n_0^X(t) - \widetilde{n}_0^X(t)}{\widetilde{n}_0^X(t)}, \tag{4.33}$$

where $\Pi_0^X(t)$ represents the total zero-momentum probability density distribution and in $\widetilde{n}_0^X(t)$ only the incoherent contributions are considered, the classical contributions. In addition to that, in the experiment, to take into account the stray decoherence present in the coherent backscattering peak, the contrast is multiplied by an exponentially decaying function, which gives us access to estimate the value of such time in the system.

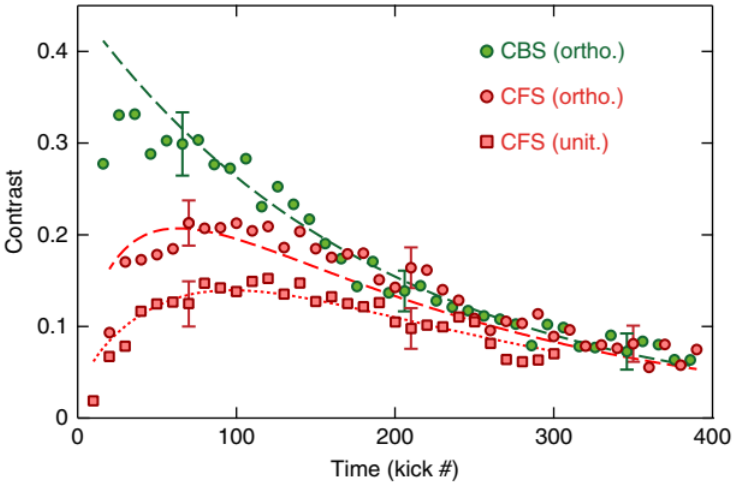

Figure 4.5.: The time evolution of the coherent backscattering and forward scattering peaks. In both cases, the contrast is multiplied by two exponentially decaying functions, one to take into account stray decoherence, $t_{\text{dec}} = 190$ and the other carrying only one fitting parameter, the localization time t_{loc}. In the absence of time-reversal symmetry (unitary class) $t_{\text{loc}} = 40$ and in the orthogonal class $t_{\text{loc}} = 37$.

For the coherent forward scattering, in both classes we multiply by an exponentially decaying function to model additional effects of the localization. For the unitary class, the localization time is $t_{\text{loc}} = 40$, whereas, for the orthogonal class we have $t_{\text{loc}} = 37$, as expected, since there are more possible processes contributing

to the phase accumulation.

5

Mesoscopic Fluctuations in Superconductor-Topological Insulator Josephson Junctions

In this chapter, we present the study for mesoscopic fluctuations in the supercurrent of a Josephson junction consisting of a topological insulator microbridge between two conventional superconductors. The model considered in here is investigated in the limit of a short Josephson junction. Within this regime, the strong proximity effect of the superconductors induces a gap in the spectrum of the surface states. The quantum transport properties of the junction are studied in the absence of an external magnetic field, as well as the with a non-zero external magnetic field piercing the junction area, which causes depairing and gap filling. The overall strength and functional expression of the Josephson current fluctuations are determined analytically. The results reported in here are found to sensitively depend on the coupling strength to surface states, Thouless energy, and pair-breaking energy scales in the problem. The density of states are also investigated, which are within the reach of experimental scanning probes. By construction, our field theoretical approach is capable of exploring the mesoscopic fluctuations on top of the mean field description of the proximity effect in the topological region, within the framework of the replica nonlinear σ-model in the class-D of the extended symmetry classification.

5.1. Introduction

Nanostructures incorporating topological insulator and superconducting elements form an interesting class of systems which may be explored to study mesoscopic quantum transport. In a conducting system, the mesoscopic physics is present when the phase coherence is preserved, a requirement which is satisfied as long as the junction length L, i.e., the separation of the two superconductor-weak link interfaces, is smaller than the dephasing length L_ϕ. The combination of these two types of structures introduces a new relation among the length scales, namely, the ratio between superconducting coherence length ξ and the junction length L. Depending on the magnitude of this ratio, qualitatively different regimes are revealed: the short junction limit $L \ll \xi$ and the long junction limit $L \gg \xi$. In addition to these two cases, we have the usual transport regimes which depends on the ratio between the junction length and the mean free path ℓ. When the junction length is largely exceeded by the mean free path $L \ll \ell$, the transport occurs in a ballistic manner, whereas, in the opposite regime, where the junction length dominates the mean free path $L \gg \ell$, the transport becomes diffusive. The characteristic fingerprint of mesoscopic quantum transport is the universality of conductance fluctuations, whose investigations have been vastly reported in the literature [Al'85; LS85; LSF87; Bee97] more reference therein. In order to understand more about the underlying physics of universality, we shall first consider a statistical ensemble of conducting systems in the diffusive regime, each characterized by

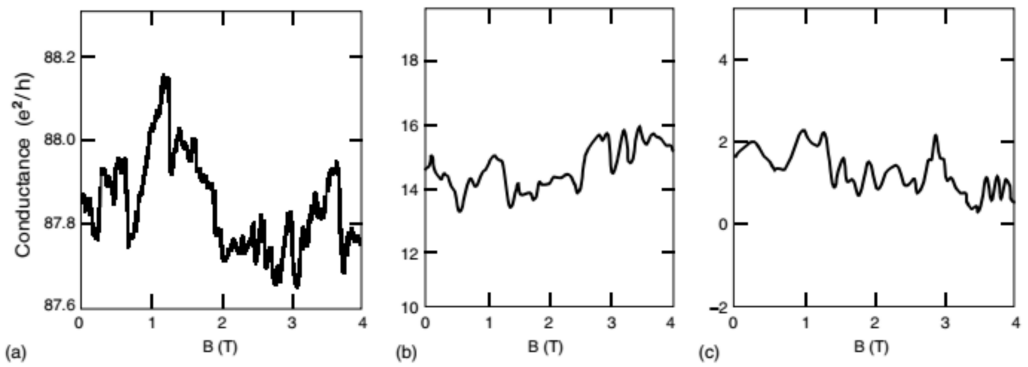

Figure 5.1.: Above we display the variations of the magnetoconductance for three different systems. In panel (a), we have a gold ring. In panel (b), a Si-MOSFET sample and in panel (c) the result of numerical simulations using the Anderson model. The most striking feature in these results is that for three distinct system, with a difference of several orders of magnitude magnetoconductances, the fluctuations are always within the order of e^2/h. [LSF87]

conductance a G. We define the average over the impurity configurations or the ensemble average in terms of the bracket notation $\langle \cdots \rangle$. The average conductance is given by $\langle G \rangle$ and we define the variance of the conductance as $\mathrm{var}(G) = \langle G^2 \rangle - \langle G \rangle^2$. Considering the scale of the mean free path, ℓ, we suppose that the conductance is determined by the microscopic configuration of impurities and that the conductor is formed by $N = (L/\ell)^d$ contiguous independent subsystems, where d is the dimension of the conductor. Hence, by the central limit theorem, we expect that the relative fluctuations of the conductance $\sqrt{\mathrm{var}(G)}/\langle G \rangle$ to vary as $\left(\frac{\ell}{L}\right)^{\frac{d}{2}}$. Considering this approach, the average conductance is given by the macroscopic transport $\langle G \rangle \sim L^{d-2}$, which leads us to the following expression for the variance of the conductance

$$\mathrm{var}(G) \sim L^{d-4}. \tag{5.1}$$

This result indicates that the fluctuations should depend on the degree of disorder manifested by ℓ and for any dimension smaller than four, it should vanish in the limit of an infinitely large system, $L \to \infty$. Contrary to this prediction, for systems where the phase coherence is preserved, the experiments and numerical simulations revealed a completely different behavior: the fluctuations around the average conductance are independent of the degree of disorder, the mean free path plays no role at all. In Fig. 5.1, we display the conductance measurement in units of the squared electron's charge over Planck's constant as a function of an external magnetic field. As the magnetic field is varied, we observe the development of aperiodic variations, whose origin stems from quantum interference processes which leads to reproducible sample-to-sample fluctuations at low temperatures. Furthermore, based on the ergodic hypothesis, the average conductance obtained by varying this physical parameter is equivalent to the average extracted from averaging over different disorder configurations.

Even though the conductance differ from each other by several orders of magnitude, the amplitude of the fluctuations is always of the order e^2/h, the conductance fluctuations are said to be universal. Typically the prefactor in the magnitude of the conductance fluctuations depends on the symmetries of the system and its dimensionality. For instance, considering a wire geometry, the variance is found as

$$\mathrm{var}(G) = \frac{2}{15\beta} G_0^2, \quad G_0^2 = \frac{2e^2}{h}, \quad \beta = 1, 2, 4, \tag{5.2}$$

with the values of the parameter β corresponding to the three Wigner-Dyson ensembles, orthogonal, unitary and symplectic respectively. Considering N to be the number of transverse modes (or conducting channels) and $N\ell$ the localization length. As long as the system satisfies the criteria for diffusive transport and short junction limit, $\ell \ll L \ll N\ell$ and $L \ll \xi$, respectively, the mesoscopic fluctuations are expected to be universal. The interactions have a direct influence on the typical scale of the dephasing length and its temperature dependence [AB02], nevertheless, universality remains robust against its effects provided that the inequality $L < L_\phi$ is not violated.

It is possible to heuristically justify the universality of conductance fluctuations in terms of three distinct explanations: the level statistics in disordered conductors [AS86], diagrammatic structure of the diffuson [AM07] and the distribution of transmission eigenvalues [Imr86]. In terms of level statistics, we start out by introducing the dimensionless average conductance of a finite system $g = \langle G \rangle / (e^2/h)$. Then, we express this quantity in terms of the ratio between the Thouless energy $E_{\rm Th}$ and the mean level spacing δ. This ratio works as a counting function which provides the number of energy levels in a window of width determined by the Thouless energy

$$g \sim \frac{E_T}{\delta} = \langle N(E_T) \rangle \,. \tag{5.3}$$

With the help of this relation, then, the conductance fluctuations $\langle g^2 \rangle$ becomes directly related to the fluctuations of the number of energy level in a window of width $E_{\rm Th}$, $\Sigma^2(E_T)$. For an uncorrelated statistics, the fluctuations in the number of levels would be of order $\sqrt{\langle N(E_{\rm Th}) \rangle}$. However, for a disordered conductor, the strong level repulsion, reveals a spectral rigidity which leads to extremely small fluctuations in the number of levels in a window of width set by the Thouless energy and thus $\sqrt{\mathrm{var}(g)}/g \simeq 1$. A second explanation concerns the general structure of the correlation function of two conductances, which involves two diffusons with two quantum crossing. The former involves the product of two average conductances g, whereas, each of the latter results in a $1/g$ weight. As a consequence of this, the fluctuations become of order unity. From the theory of localization, it is known that the transmission distribution in a diffusive structure is bimodal [Bee97; Dor84]:

$$\rho(\mathcal{T}) = \frac{N\ell}{2L} (\mathcal{T}\sqrt{1-\mathcal{T}})^{-1}, \tag{5.4}$$

with transport channels being closed at $\mathcal{T} = 0$ and open at $\mathcal{T} = 1$. Clearly this distribution function has a peak at unit transmission $\mathcal{T} \approx 1$ and a peak at exponentially small transmission $\mathcal{T} \approx 0$. In a disordered conductor, the manifestation of localization appears in the fact that most channels are closed, as the majority of transmission eigenvalues are exponentially small. There is only a small portion ℓ/L of the total number N of transmission eigenvalues whose magnitude is close to unity and provides a relevant contribution to the total conductance $\langle G \rangle = N_{\rm open} G_0$. In this sense, the conductance fluctuations can be understood as fluctuations in the number of open channels.

The situation becomes qualitatively different when superconductivity is introduced as a boundary effect, a normal metal attached at one end to a superconductor. In here, at the normal-superconductor interface the typical dissipative normal current is converted into a dissipationless supercurrent via the Andreev reflections, an electron impinges on the normal metal surface and is reflected as a hole followed by the addition of a Cooper pair to the superconducting condensate. As long as the interface resistance is negligibly small, such phenomenon does not affect the usual form of the average conductance and the conductance fluctuations

remain universal:

$$\mathrm{var}(G_{\mathrm{NS}}) = \frac{16}{15\beta}\left(1 - \frac{45}{\pi^4}\right) G_0^2, \quad \beta = 1, 4. \tag{5.5}$$

Such result deviates from Eq. (5.2) only by a dimensionless numerical prefactor. Although the conductance fluctuations for the case where the time-reversal symmetry is absent, $\beta = 2$, still displays a universal behavior, it has been shown that the fluctuations have an anomalous insensitivity to the presence of an external magnetic field, which was addressed in Ref. [BB95]. These result have been vastly verified and reported in the literature. Using a direct numerical approach [MBJ93; BHL94], a diagrammatic approach [TE91] and later on experimentally [Har+96; Hec+97].

Within this context it is, then, natural to ask if the phenomenon of universal conductance fluctuations have an analog in superconductivity. For instance, consider the supercurrent in a superconductor-normal-superconductor Josephson junctions, usually referred to as SNS junction, whose superconducting gap is given by Δ. For a short wire geometry with transparent normal-superconductor, the variance in the current-phase relation have been reported in Ref. [CM93; Bee91] and it displays a universal behavior in complete analogy with Eq. (5.2), as we exhibit below:

$$\mathrm{var}(I(\phi)) = \frac{2\pi^2}{15} I_0^2 \sin^2\phi \left[1 + \frac{62}{63}\sin^2\left(\frac{\phi}{2}\right) + \cdots\right], \quad I_0 = \frac{e\delta}{h}, \quad \beta = 1. \tag{5.6}$$

It is immediately clear that the mesoscopic fluctuations in this system is universal, since there is no dependence on the size of the junction or on the degree of disorder. This result holds as long as the criteria $\ell \ll L \ll N\ell$ and $L \ll \xi$ for the diffusive and short junction are satisfied. In the diffusive limit, the superconducting coherence length is given by the expression $\xi = \sqrt{v_F \ell/(\pi\Delta)}$, where v_F is the Fermi velocity. In this regime of a short disordered junction, the scale of supercurrent in this Josephson junction is set by the energy gap Δ in the superconductor. The root-mean-square value of the critical current,$I_c = \max(I(\phi))$, is given by [Bee91; CM93]

$$\mathrm{rms}(I_c) \approx 1.8 e\Delta/h. \tag{5.7}$$

Since the critical supercurrent is not a simple linear statistics of transmission eigenvalues, the phases for which the maximum supercurrent is attained has a dependence on all the transmission eigenvalues, the dimensionless numerical prefactor does not follow as an immediate consequence of the Eq. (5.6). The expression presented in Eq. (5.6), the critical supercurrent fluctuations is fully independent of the material properties of the junction and, in this sense, we say this result for the Josephson effect is analogous to the universal conductance fluctuations in metals.

The opposite limit of a long junction was considered in the theory introduced in Ref. [AS87]. In their work, it was studied the mesoscopic fluctuations in the supercurrent of a superconductor-normal metal-superconductor Josephson junction which is long compared to the mean free path and the superconducting coherence length, $L \gg \ell, \xi$. It was shown that critical supercurrent fluctuations are no longer universal and depend on both the junction length L and the mean free path ℓ via the presence of the Thouless energy, $\mathrm{var}(I_c) \simeq (eE_{\mathrm{Th}}/h)^2$. Contrary to the short junction limit, in the case of a long junction, the average critical supercurrent decays exponentially with the junction length $\langle I_c\rangle = (\Delta \langle G\rangle / e)\exp(-L/\xi)$. On the other hand, the mesoscopic contribution decays only algebraically. Thus, it is possible to reach a situation in which $\langle I_c^2\rangle \gg \langle I_c\rangle^2$ and, in this regime, the behavior of the critical supercurrent would be primarily

dictated by the mesoscopic contribution. Further investigations on the sensitivity of this type of junction with respect to the transparency of the normal metal-superconductor interfaces were reported in Ref. [Mic07]. Furthermore, based on the replica non-linear sigma model technique, in Ref. [HS08] it was reported results describing the mesoscopic fluctuations and weak localization corrections to the equilibrium supercurrent in Josephson junctions. In this study, two types of junctions were contemplated: a chaotic dot coupled to superconductors by tunnel barriers and a diffusive wire with transparent normal metal-superconductor interfaces, where the interface resistance is much smaller than the resistance of the wire. For the SNS junction the average supercurrent and the supercurrent fluctuations were calculated for various geometries. In Ref. [XL19], within the framework of scattering matrix, the mesoscopic fluctuations of supercurrents were studied in a single-channel multiterminal junction of topological superconductors.

Besides the development of a supercurrent through the junction, the normal metal when in contact with a superconductor may also develop a gap in the density of states, that is, a spectral gap. This additional equilibrium observable appears as a consequence of the proximity effect. In the non-universal regime of a long junction $L \gg \xi$, the scale of the spectral gap in the normal region is set by Thouless energy [BBS96; Ham+07]. As the junction size becomes increasingly smaller, the spectral gap grows. In the limit where the universality of mesoscopic fluctuations is restored $L \ll \xi$, it would be natural to expect the spectral gap becoming fully identical to the superconducting gap Δ. For a short junction the superconductive correlations are able to penetrate the entire volume of the normal metal, leading to a strong proximity effect. However, such result is only attainable in the limit of a point contact junction $L/\xi \to 0$ or equivalently in terms of the energy scale ratio $\Delta/E_{\mathrm{Th}} \to 0$. As it was demonstrated in Ref. [Lev08], for a large but finite Thouless energy, the spectral gap in the normal wire approaches the value of the superconducting gap with a finite size negative correction, $E_g = \Delta - \delta\Delta$, where $\delta\Delta = (\Delta/E_{\mathrm{Th}})^2\Delta$. Further investigations have shown that depending on the quality and properties of the interfaces, a secondary spectral gap may develop in the vicinity of the superconducting gap [Reu+14a; Reu+14b]. The mesoscopic fluctuations of the secondary spectral gap follows the Tracy-Widom distribution [Reu+21]. We notice that the same distribution was found in Ref. [Vav+01] for the opposite limit $E_{\mathrm{Th}}/\Delta \to 0$. As far as the literature concerns, the implications of these striking features on the supercurrent fluctuations has not been examined, only the average current-phase relation was computed [LKG06; WVL18]. Furthermore, when a Josephson junction is subjected to a perpendicular magnetic field B, a characteristic magnetic energy scale E_Φ, or magnetic depairing energy, is introduced into the problem. This scale quantifies the strength of the field-induced depairing effects, whose effects are manifested as the population of sub-gap states and depending on its intensity can ultimately lead to a complete gap closure. Having said that, it is then expected that such influence on the density of states may lead to a supercurrent and supercurrent fluctuation that depends sensitively on both the spectral gap E_g and the magnetic depairing energy E_Φ. In addition to that, it has been shown that when the junction width is smaller than the magnetic length $\xi_{\mathrm{H}} = \sqrt{\Phi_0/B}$, where $\Phi_0 = \pi/e$ is the flux quantum for paired superconductivity, the field acts as a pair breaking mechanism leading to a monotonic suppression of the superconductivity in the normal wire. In contrast with this result, in the opposite limit, there is an appearance of a vortex structure in the junction [BC08] such that it leads to the formation of the famous Fraunhofer pattern in the wide junction limit [Row63].

Despite the vigorous effort to describe the transport properties of topological insulator Josephson junctions, most of the recent theoretical work done on these devices has not involved the study of mesoscopic fluctuations. In our work, we shall explore these fluctuations in hybrid proximity circuits of topological insulator

thin films and conventional superconductors deposited on their surface. There is a wealth of experimental results involving the transport data of these junctions in various regimes [Sac+11; Vel+12; Qu+12; Wil+12; Cho+13; Kur+14; Fin+14; Kur+15; Soc+15; Ste+16]. Hence, it is an important issue to calculate the equilibrium quantities: density of states, supercurrent and supercurrent fluctuations, in order to be able to perform quantitative comparisons between theory and experiment. Our investigation is partially motivated by recent proposals that an architecture of topological insulator Josephson junctions holds the promise for realizing quantum computing hardware with topological states of matter [Heg+20]. In this sense, it is essential to have an adequate understanding of the mesoscopic effects to establish fundamental limits of their transport functionality. The rest of the paper is organized as follows. In the next section, Sec. 5.2, within the framework of a Hamiltonian description, we introduce the geometry of the junction, the relevant energy scales and the Hamiltonian for each component of the system, the two superconducting leads, the topological insulator and the topological insulator-superconductor tunneling interfaces. To study the equilibrium properties of our system, the Sec. 5.3 is devoted to a reformulation of the problem in the language of the effective field theory of the replica non-linear sigma model. This is a powerful method which allows us to conveniently perform the disorder averaging and, in addition to that, this formalism enables the computation of our observables and leaves room to further calculations of higher-order correlations functions. In Sec. 5.4, we derive the Usadel equation via a saddle-point analysis of the effective field theory. Considering only homogeneous field configurations, we solve it and apply the result to calculate and study the density of states in Sec. 5.5, we theoretically compare the limiting cases of zero and strong external magnetic field and present plots for the result across arbitrary magnetic field values. Also, we contrast our findings with results reported in the literature for similar geometries and settings. In Sec. 5.6, we introduce the theoretical framework with which we compute the observables, namely, the semiclassical partition function. We use this function to compute the main results of this work, the equilibrium observables, the Josephson current-phase relation and the variance of the Josephson current fluctuations. Although the action displays a spontaneous symmetry breaking, the presence of an external magnetic field leads to an absence, at least in the typical sense, of the famous massless diffusion modes, the diffuson and Cooperon. In particular, these modes are massive for a large portion of the parameter space. The foundation of our construction is such that there is no interaction between these modes. In the limiting case of a zero magnetic field, in Sec. 5.7, we discuss the average current, for the quantum dot geometry, and the sample-to-sample fluctuations, for both geometries, quantum dot and quasi-one-dimensional. In the subsequently section, Sec. 5.8, we study the modifications of these observables when a non-zero external magnetic field is applied on the Josephson junction. Finally, in Sec. 5.9, we conclude with a discussion of the results obtained and also summarize our result in a compact form in Table 5.1. The further technical details missing in the main text are accompanied in the several appendices.

5.2. Model

5.2.1. Setup

The fundamental structure of the junction investigated here is as shown in Fig. 5.2. It consists of a topological insulator (TI) in contact between two superconductors (SC) deposited on its upper surface and there is a phase difference ϕ between the superconducting islands. The system geometry we investigate is that of a line junction of width W along the y-direction. The topological insulator slab is assumed thicker enough so that the Josephson supercurrents are restricted to propagate only on the surface. In the x-direction we

assume rigid boundary conditions, that is, the superconducting gap vanishes in the topological insulator region $|x| < L/2$ and, at the superconducting side of the topological insulator-superconductor interface, it recovers its bulk value. Using this construction, the order parameter varies as a step-function:

$$\Delta(x) = \begin{cases} |\Delta| e^{i\phi(x)}, & |x| > L/2 \\ 0, & \text{otherwise}, \end{cases} \tag{5.8}$$

where $\phi(x) = \mathrm{sgn}(x)\phi/2$, with L being the length of the junction between the superconducting electrodes and Δ being the superconducting energy gap. We assume that the length of the junction is much smaller than the superconducting coherence length, the short junction limit. Furthermore, an external magnetic field $\mathbf{B}$ pierces through the junction, see Fig. 5.2 for an illustration. The width of the junction is supposed to be narrow enough such that the presence of the external magnetic flux does not lead to a position dependent superconducting phase along the junction. In addition to that, the short junction limit ensures that the magnetic field produced by the supercurrent is negligible in comparison with the external magnetic field.

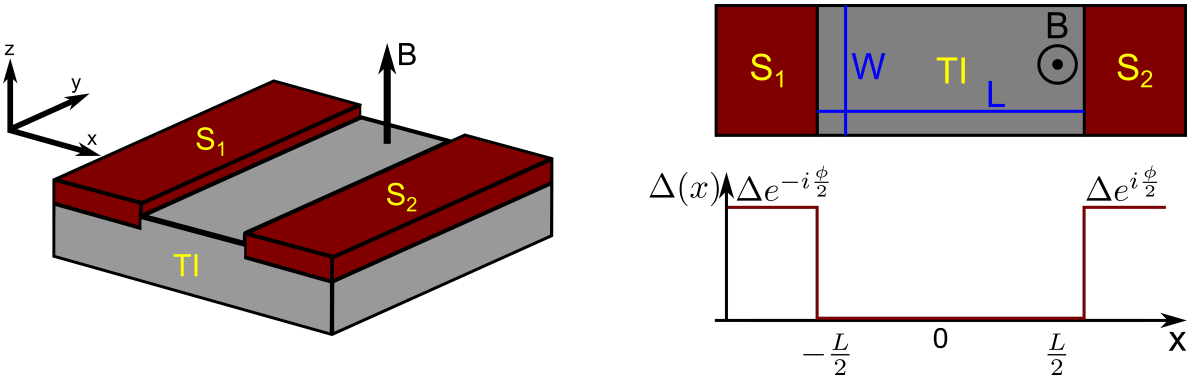

Figure 5.2.: A schematic of the planar STIS Josephson junction. Two superconductors, S_1 and S_2, are deposited onto the top surface of the topological insulator (TI) thin film marked by a gray slab. We chose TI surface as xy-plane of the coordinate system with magnetic field $\mathbf{B}$ pointing in z-direction. The length of the junction along x-direction is L, whereas its width along y-direction is W.

The magnitude of the coupling strength of electrons between the topological insulator and the superconductor lead is set by the squared coupling parameter w. The interface coupling is realized via tunneling contacts, which leads to the Fermi golden rule level broadening $E_t = \pi\nu w^2$ of surface states, where ν is the density of states. Any realistic topological insulator surface has some degree of disorder present. In here, we characterize the presence of disorder in the topological insulator surface via the elastic mean scattering time τ. We focus on the most relevant case of a strong proximity effect, whose appearance is a natural consequence of the short junction limit, and weak disorder, in which the Thouless energy is given by the expression $E_{\mathrm{Th}} = D/L^2$, where D is the diffusion coefficient, and the inverse elastic scattering time τ^{-1} sets the largest energy scale. Moreover, the weak disorder condition is defined by the inequality $E_F\tau \gg 1$ with E_F being the Fermi energy.

The external magnetic field provides a mechanism which creates a gateway for us to access the physics of the gapless surface states in the topological insulator. We shall explore this technology as a tuning parameter to manipulate the induced minigap of the topological surface states and investigate under which conditions the gap becomes fully closed. Hence, in this work we shall focus our attention on the following hierarchy of

energy scales:

$$\delta \ll \{E_t, E_\Phi, \Delta\} \ll \{E_{\rm Th}, 1/\tau\} \tag{5.9}$$

where $\delta = 1/\nu$ is the level spacing (recall that ν is the density of states) and the characteristic magnetic energy is defined as $E_\Phi = \frac{\pi^2 n_\Phi^2}{3\tau_{\rm tr}}$. For convenience we introduced the number of superconducting flux quanta $n_\Phi = \Phi/\Phi_0$, where we have defined $\Phi_0 = \pi/e$, the superconducting magnetic flux quantum. The intensity of the magnetic flux is set by the strength of the magnetic field piercing an area defined by the transport mean free path times the longitudinal length of the line junction, that is, $\Phi = L l_{\rm tr} B$ is the flux through an area $L l_{\rm tr}$ with $l_{\rm tr} = v\tau_{\rm tr}$, where the transport mean free time $\tau_{\rm tr}$ is related to the elastic mean scattering via the simple equality $\tau_{\rm tr} = 2\tau$.

5.2.2. Hamiltonian

The Hamiltonian with which we start out our description of the topological insulator Josephson junction has four distinct contributions

$$H = H_S + H_{S_1} + H_{S_2} + H_T, \tag{5.10}$$

$$H_S = \int_S d^2x \left[\psi^\dagger_{\mathbf{x}} \sigma_3^{\rm ph} \otimes (-i\boldsymbol{\sigma}\cdot\partial_{\mathbf{A}} + V_{\mathbf{x}})\,\psi_{\mathbf{x}}\right], \tag{5.11}$$

$$H_{S_i} = \int_{S_i} d^3x \left[\Psi^\dagger_{\mathbf{x}} \sigma_3^{\rm ph} \otimes \left(\epsilon_{\hat{\mathbf{p}}-e\mathbf{A}} + i\Delta\sigma_2^{\rm ph} e^{\frac{i}{2}\phi_i \sigma_3^{\rm ph}}\right)\Psi_{\mathbf{x}}\right], \tag{5.12}$$

$$H_T = \sum_{i=1,2} \int d^3x \left[\bar{w}_i(y)\Psi^\dagger_{\mathbf{x}} \sigma_3^{\rm ph} \psi_{\mathbf{x}} \delta_{x-x_i}\delta_{z-z_0} + \text{h.c.}\right], \tag{5.13}$$

where $\sigma_i^{\rm ph}$ represents the i-th Pauli matrix in the particle-hole space. To represent the fields, we find convenient to use Nambu spinors, since it comprises particle and hole degrees of freedom into a single object: $\psi^\dagger = \frac{1}{\sqrt{2}}(c^\dagger_\uparrow, c^\dagger_\downarrow, -c_\downarrow, c_\uparrow)$ and ψ for the central region and their counterparts $\Psi^\dagger$ and Ψ for the surfaces $S_{1,2}$ below the superconductors. In here, S and $S_{1(2)}$ are indices corresponding to the topological insulator surface in the central region and the bulk superconductors 1 and 2, respectively. The local coupling between the topological insulator surface and the superconducting lead is described by the Hamiltonian H_T. To describe the tunneling barrier, we suppose that such barriers between the superconducting lead and the topological insulator surface varies in thickness along the transverse y direction. This allows to model these barriers in terms of a collection of randomly distributed tunneling centers with short range correlations. We assume that the tunneling barrier between the superconductor and the topological insulator varies in thickness along the y direction, so that it can be effectively modelled as a collection of randomly distributed tunneling centers with short range correlations. This construction can be represented in terms of the ensemble average of the tunneling amplitudes $\langle \bar{w}_i(y)\bar{w}_j(y')\rangle \sim \delta_{ij} w^2 \delta(y-y')$. The dispersion relation in both superconductors is given by $\epsilon_{\mathbf{p}}$, whose form is proportional to the squared canonical momentum $\mathbf{p}$. The spatial coordinates x and y are defined along and perpendicular to the junction (where an infinitesimal shift to left and right of the interfaces is implicit), and z_0 is the z-coordinate of the topological insulator surface. The applied magnetic field is given by the divergenceless vector field $\mathbf{B} = \text{rot}\mathbf{A}$. Its presence promotes the spatial gradient term in the Hamiltonian $\hat{H}_S$ to a long covariant derivative $\partial_{\mathbf{A}}$. Making use of gauge invariance, we choose for the vector potential an expression such that the applied magnetic field becomes a constant, that is, $\mathbf{A} = Bx\mathbf{e}_y$. Besides providing a simple and efficient way to represent the magnetic field, this form also preserves the translational invariance in the y-direction parallel to the interfaces. Finally, since the material imperfections

of each disordered system reflects a necessarily random disorder realization, it is convenient to represent the disorder potential $V(\mathbf{x})$ in terms of a Gaussian white noise distribution disorder with vanishing mean and second moment:

$$\begin{aligned} \langle V(\mathbf{x})\rangle &= 0, \\ \langle V(\mathbf{x})V(\mathbf{x}')\rangle &= \frac{1}{\pi\nu\tau}\delta(\mathbf{x}-\mathbf{x}'). \end{aligned} \tag{5.14}$$

The reason for this construction is twofold. First, it provides an advantageous framework to apply a functional-based approach. Second, we are allowed to consider an ensemble of different samples displaying identical impurity concentration and average over it. It is important to distinguish between the different characteristic times: the single particle scattering time τ, which appears in this formula, from the transport scattering time $\tau_{\mathrm{tr}} = 2\tau$, which is the relevant time scale entering the diffusion coefficient $D = v\tau_{\mathrm{tr}}/2$.

5.2.3. Effective channel Hamiltonian

To avoid the additional complication of the inverse proximity effect, as well as the depairing effects associated with the development of a finite current density or the magnetic field in the leads [SL21], we suppose that the superconducting leads are sufficiently larger than the topological insulator thin film and integrate out the former degrees of freedom. This generates the following effective model for the tunneling junction $|x| \leq L/2$:

$$H_\Gamma = -\frac{E_t L}{\sqrt{\epsilon_n^2+\Delta^2}} \sum_{k=1,2} \begin{pmatrix} i\epsilon_n & -\Delta_k \\ -\Delta_k^* & i\epsilon_n \end{pmatrix} \delta(x-x_k). \tag{5.15}$$

In the short junction limit, the tunneling contribution H_Γ imposes the so-called rigid boundary conditions [GKI04].

5.2.4. Symmetries

The effective channel Hamiltonian satisfies the particle-hole symmetry,

$$\mathcal{H}(\mathbf{k}) = -(i\sigma_2)\otimes(i\sigma_2^{\mathrm{ph}})\mathcal{H}^t(-\mathbf{k})(-i\sigma_2)\otimes(-i\sigma_2^{\mathrm{ph}}), \tag{5.16}$$

where σ_2^{ph} and σ_2 are the standard Pauli matrices, the former operates in Nambu and the latter in the spin space. Noting that the particle-hole symmetry is given by the following operator $\Xi = (i\sigma_2)\otimes(i\sigma_2^{\mathrm{ph}})K$ with K the complex conjugation and $\Xi^2 = \mathbb{1}_4$, we conclude that this system fits in the class-D in the Altland-Zirnbauer symmetry classification [AZ97].

5.2.5. Josephson current and fluctuations

The Josephson current is an equilibrium phenomenon, as long as we know a thermodynamic potential of the system, the free energy F, for instance, as a function of the phase-difference ϕ between the superconductor pair potentials Δ_1, Δ_2, we can calculate the induced supercurrent that passes across the junction via the following identity

$$I(\phi) = 2e\partial_\phi\langle F\rangle, \tag{5.17}$$

where e is the charge of the electron, the functional form of the free energy in a given disorder configuration reads $F = -T\ln Z$ and $\langle\cdots\rangle$ refers to the disorder average. The maximum value attained by this supercurrent

is known as the critical supercurrent, $I(\phi_c) = I_c = \max[I(\phi)]$. In addition to that, in the limiting case of a diffusive junction, whose superconducting gap is independent of the momentum, is also known as the dirty limit. Such regime allows the supercurrent to be readily obtained from the Usadel equation [Usa70], which is based on Green's functions dressed with disorder. The fluctuations of the supercurrent requires us to compute higher-order correlators, $\langle I(\phi_1)I(\phi_2)\rangle$. Hence, for the calculation of the fluctuations of the Josephson supercurrent, it is convenient to introduce two sample copies subject to the same realization of the disorder potential. Building on the relation for the supercurrent, we introduce the correlator

$$K(\phi_1, \phi_2) = 4e^2\partial^2_{\phi_1\phi_2} \langle F(\phi_1)F(\phi_2)\rangle_c \,, \tag{5.18}$$

where $\langle\cdots\rangle_c$ is the connected disorder average and indices in $\phi_{1,2}$ refer to the sample. Then, the variance of the current fluctuations is given as

$$\mathrm{var}[I(\phi)] = K(\phi, \phi). \tag{5.19}$$

To apply these relations Eq. (5.17) and (5.19), we need to find a way to compute the free energy F. In contrast with the supercurrent, the fluctuations are beyond the scope of the Usadel equation and to calculate it we have to resort to taylored methods to deal with higher-order correlator for system in the dirty limit. The following section will be dedicated to introduce the fundamental framework we use to perform our calculations, namely, the replica non-linear sigma model.

5.3. Effective action

Following the standard approach to disordered systems, we employ the replica trick to express the disorder averaged free energy in terms of a replicated partition function [Weg79; EKL80]. We model our topological insulator Josephson junction as a two-dimensional system and derive an effective field theory representation for the replicated partition function $\mathcal{Z} = \int DQe^{-S[Q]}$, the corresponding non-linear sigma model action is

$$S[Q] = \frac{\pi\nu}{8}\int d^2x \ \mathrm{tr}\left[D(\partial_{\mathbf{A}}Q_{\mathbf{x}})(\partial_{\mathbf{A}}Q_{\mathbf{x}}) - 4(\epsilon + iH_\Gamma)\sigma_3^{\mathrm{ph}}Q_{\mathbf{x}}\right], \tag{5.20}$$

where we have defined the density of states of the topological insulator surface at the Fermi level $\nu(\mu = E_F) = E_F/(2\pi v^2)$. In our application, the situation involves the presence of an external magnetic field, which promotes the typical derivative to the status of a covariant derivative $\partial_{\mathbf{A}}O = \partial_{\mathbf{x}}O + ie[\mathbf{A}\sigma_3^{\mathrm{ph}}, O]$, with the standard notation for the commutator of two matrices $[A, B]$. The notation ϵ in here denotes a diagonal matrix of Fermionic Matsubara frequencies with diagonal elements $(\epsilon)_n = \epsilon_n$. In these conventions, $Q_{\mathbf{x}}$ is a matrix in Nambu, sample and replica space satisfying $Q^2 = 1$. The space where Q is defined is formed by the tensor product among the Nambu space with two degrees of freedom. The two-dimensional sample degree of freedom, introduced to accommodate the calculation of sample-to-sample fluctuations in Sec. 5.2.5. The replica space is constituted of R entries and in the Matsubara space only $M \sim (\tau T)^{-1}$ Matsubara frequencies are kept in the low energy description. This simple counting exercise shows that the final space, the tensor product of all the mentioned spaces, has $2 \times 2 \times M \times R$ dimensional structure. The symmetry doubling of the junction Hamiltonian

$$\mathcal{H}(\phi) \mapsto \mathrm{diag}[\mathcal{H}(\phi_1), \mathcal{H}(\phi_2)], \tag{5.21}$$

provides a convenient platform that allows us to simultaneously account for the Josephson currents in the same disorder realizations of the system at different superconductor phase differences ϕ_1, ϕ_2, and their

correlations. The Pauli matrices operating in the Nambu space are indicated by the index ph. We have to impose an additional constraint on the matrix degree of freedom:

$$Q(\mathbf{x};\tau,\tau') = \sigma_1^{\mathrm{ph}} Q^t(\mathbf{x};\tau',\tau)\sigma_1^{\mathrm{ph}}, \tag{5.22}$$

which is inherited from the particle-hole symmetry of the junction Hamiltonian described in Eq. (5.16). In the above τ, τ' are the imaginary time arguments related to Matsubara frequencies by the Fourier transformation

$$Q_{\epsilon\epsilon'} = \int d\tau d\tau' Q_{\tau\tau'} e^{i\epsilon\tau - i\epsilon'\tau'}. \tag{5.23}$$

A general derivation of the effective action can be found in the Ch. 2 and also in Ref. [AS10]. In a typical system, the kinetic energy is usually described in terms of a squared momentum. However, for a topological insulator surface, we have seen that the Hamiltonian displays a linear relation with the momentum. Nevertheless, it is still possible to perform the derivation of the non-linear sigma model within the usual protocol. We provide the technical details of the required adaptation in the derivation of the effective action for a topological insulator surface in the App. D. Below we shall sketch the main steps.

Starting out from the replicated partition function for the junction Hamiltonian, which we doubled to account for two realizations of the same sample, as discussed above, the disorder average induces an effective quartic interaction between fermions in different replicas, Nambu and sample sectors. However, some contributions stemming from this interaction are negligible. Bearing this in mind, we decouple the quartic interaction via a Hubbard-Stratonovich transformation in terms of a Hermitian matrix field Q and keep only the low energy contributions. The matrix field Q by construction must also satisfy the symmetry constraint displayed in the particle-hole sector of the junction Hamiltonian. This simplification allows us to integrate over the fermionic field leading to a representation of the averaged partition function entirely in terms of the matrix degree of freedom Q. Then, we perform a saddle point analysis of this action containing a trace log contribution. In here, the saddle point analysis is stabilized by the characteristic energy τ^{-1}, whose magnitude is the largest among all the energy scales in the problem, $\{\Delta, E_t, E_\Phi\} \ll \tau^{-1}$. We make good use of the ansatz $Q_0 = q\sigma_3^{\mathrm{ph}} \otimes \Lambda$ describing a homogeneous saddle point with the matrix structure in the Nambu and Matsubara spaces governed by causality, the matrix Λ is a diagonal matrix in the Matsubara space with its entries defined as $\Lambda_n = \mathrm{sgn}(\epsilon_n)$. For such ansatz, the saddle point equation reads

$$q = -\frac{2i}{\pi\mu}\int_0^\rho d\varepsilon\varepsilon \frac{\mu + \frac{i}{2\tau}q}{\varepsilon^2 - (\mu + \frac{i}{2\tau}q)^2}, \tag{5.24}$$

where we used that the ratio between the density of states evaluated at μ and at ϵ satisfies the equality $\nu(\mu)/\nu(\epsilon) = \mu/\epsilon$, which from the expression for the density of state is an immediately obvious statement $\nu(\epsilon) = \epsilon/(2\pi v^2)$. In addition to that, this integration has a logarithmic ultraviolet divergence and the upper cuttof $\rho \gg \mu$ has been introduced to regularize it. The contributions from low energy scales ϵ and H_Γ have been neglected. As usual, the saddle point equation is directly related to the self-consistent Born approximation (SCBA), which upon integration becomes

$$q = -\frac{i\alpha}{\pi\mu}\ln\frac{\alpha^2 - \rho^2}{\alpha^2} \approx -\frac{i\alpha}{\pi\mu}\ln\left(-\frac{\rho^2}{\alpha^2}\right), \tag{5.25}$$

where we fixed $\alpha = \mu + \frac{i}{2\tau}q$. Decomposing q into the real and imaginary parts, $q = q_1 + iq_2$, and using $q_1/\mu\tau$,

and $q_2/\mu\tau$ as small parameters, the equation can be quickly solved iteratively, with the leading solution $q_1 = 1$ and $q_2 = -(2/\pi)\ln\rho/\mu$ in the limit $(\mu\tau)^{-1} \to \infty$. In systems with quadratic dispersion, one usually absorbs the logarithmic divergence in q_2 into a redefinition of μ. However, the case of a linear dispersion is different and including subleading terms in $(\mu\tau)^{-1}$, one finds

$$q_1 \approx 1 + \frac{2}{\pi\mu\tau}\ln\frac{\rho}{\mu} \tag{5.26}$$

and

$$q_2 \approx -\frac{2}{\pi}\ln\frac{\rho}{\mu} - \frac{2}{\pi^2\mu\tau}\ln^2\frac{\rho}{\mu}. \tag{5.27}$$

The key point here is that the real part q_1 also acquires logarithmic corrections, $\ln(\rho/\mu) \ll \mu\tau$ is implied. Although such problem is visible in the self-consistent Born approximation, the latter is not sufficient to account for the logarithmic corrections systematically. Indeed, it has been reported in the literature of the closely related problem of disordered graphene that the term of the same order appear from contributions to the self-energy, which are not included in the self-consistent Born approximation scheme [AE06; OGM06]. In their findings via a renormalization group procedure on the level of the fermionic action [AE06], it was found that by summing the logarithmic divergencies, these renormalizations may be absorbed into effective parameters of the non-linear sigma model. As we argued above, it is clear that in order for the renormalizations remain weak, the inequality $(\mu\tau)^{-1}\ln(\rho/\mu) \ll 1$ must be satisfied by the system. We interpret the ultraviolet cutoff ρ as the scale at which the dispersion deviates from the linear approximation. The next step of our derivation consists in the inclusion of soft mode fluctuations around the saddle point. In here, we follow the typical structure usually explored to include these fluctuations. We assume that the fluctuations can be parametrized as slowly varying rotations of the saddle point solution, $Q_{\mathbf{x}} = T_{\mathbf{x}}Q_0T_{\mathbf{x}}^{-1}$, where $T_{\mathbf{x}}$ generates rotations in the replica, Matsubara, Nambu and sample spaces. We consider that the fluctuations in the spin sector are suppressed by the spin orbit interaction and their contribution to the underlying physics of the non-linear sigma model action in the spin singlet sector is a renormalization of the charge diffusion coefficient. A more detailed discussion on the role played by the surface soft modes and the renormalization issue can be found in the Refs. [GG12; Vel+18]. This construction amounts to a projection onto the spin singlet sector of the particle-hole degrees of freedom, which is stabilized by the mass of the order $\nu\tau^{-1}$ of the triplet modes. To conclude this derivation, we insert the soft mode ansatz into the action, a gradient expansion then yields the effective soft mode action displayed in Eq. (5.20). For more details on the mathematical machinery of this calculation, please check the App. D. Finally, with the replica field theory at hand, we formulate the average Josephson current and its sample-to-sample fluctuations as a functional integral

$$I(\phi) = \lim_{R\to 0}\frac{2eT}{R}\partial_{\phi_1}\,\mathcal{Z}|_{\phi_1=\phi}\,, \qquad K(\phi_1,\phi_2) = \lim_{R\to 0}\frac{4e^2T^2}{R^2}\partial^2_{\phi_1\phi_2}\mathcal{Z}. \tag{5.28}$$

5.4. Usadel equation

Henceforth, we shall focus our efforts on the particular case of the short junction limit, which is characterized by the inequality $L \ll \xi$ or, in terms of the energy scales, $E_{\mathrm{Th}} \gg \Delta$. The corresponding geometry of this limiting case allows us to assume that the matrix Q is almost constant as a function of the x-coordinate, perpendicular to the interfaces, and we simplify the action by integrating over this coordinate. In order to determine how the superconducting gap affects the low-lying structure of the effective action, Eq. (5.20), we

subject the non-linear sigma model action to a further saddle point analysis. The first saddle point analysis was used for the derivation of the nonlinear sigma model and did not account for the presence of $\hat{H}_\Gamma$ nor for the magnetic field. This first saddle point was stabilized by the inequality $E_F \gg \tau^{-1}, \Delta$. However, for systems in the regime satisfying the inequality $\tau^{-1}, \Delta \gg \delta$, the additional presence of the order parameter Δ leads to the formation of a more complex low energy structure than the first analysis is able to capture. We apply this second saddle point analysis to identify the low-lying substructure on the bottom of the large scale saddle point manifold. Since the second saddle point analysis occurs within the manifold of the first saddle point $Q^2 = 1$, we shall look for matrices Q for which the condition

$$d_\alpha S[\exp(-\alpha W) Q \exp(-\alpha W)] = 0 \tag{5.29}$$

holds for arbitrary generators W. Furthering our analysis, we explore the property of translational invariance parallel to the interfaces and restrict our matrix field configuration to be independent of the y coordinate. This procedure leads directly to the low energy saddle point equation and we identify it as the homogeneous Usadel equation [Usa70]:

$$\left[-E_\Phi Q_\perp + v_i \sigma_i^{\mathrm{ph}}, Q\right] = 0, \tag{5.30}$$

where $Q_\perp = \frac{1}{2}(Q - \sigma_3^{\mathrm{ph}} Q \sigma_3^{\mathrm{ph}})$. Furthermore, considering the limiting case of homogeneous field configurations. This equation is similar to equations that describe the effects of spin-flip processes or pair-breaking mechanisms, See Refs. [Ham+07; BC08].

We find it convenient to write down the potential contribution in terms of Pauli matrices in the particle-hole space: $\int dx(\epsilon + iH_\Gamma) = L v_i \sigma_i^{\mathrm{ph}}$ with the vector components v_i being represented as

$$v_1(i) = 0, \quad v_2(i) = \frac{2E_t \Delta \cos(\phi_i/2)}{\sqrt{\Delta^2 + \epsilon_i^2}}, \quad v_3(i) = \epsilon_i + \frac{2E_t \epsilon_i}{\sqrt{\Delta^2 + \epsilon_i^2}}. \tag{5.31}$$

In addition to that, we have used the short junction limit to justify the integration over the x coordinate and $(i) = (\epsilon_i, \phi_i)$ is a convenient multi-index notation. In order to a seek a solution for this homogeneous Usadel equation, we follow the typical practice reported in the literature [HS08; ASTS98] and propose inserting the ansatz

$$Q_\Delta = m_i \sigma_i^{\mathrm{ph}}, \tag{5.32}$$

with the unit vector $\mathbf{m}$, into Eq. (5.30). Then, we can express the saddle point condition as a geometric constraint

$$(\mathbf{v} + E_\Phi \mathbf{m}_3) \times \mathbf{m} = 0. \tag{5.33}$$

Due to the nonlinear normalization condition $\mathbf{m}^2 = 1$ inherited from the Q matrix, this simple equation becomes a fourth-order polynomial with non-zero coefficient at all orders. In this sense, the general solution of this equation is too cumbersome to extract any meaningful information. Nevertheless, in the case of general external magnetic field, we will use explore its numerical solutions to obtain the behavior of our observables across a wide range of values for E_Φ. For analytical calculations, we will therefore mainly

concentrate on the limiting cases of strong and vanishing magnetic fields, where analytical solutions can be constructed straightforwardly.

5.4.1. Zero magnetic field

In the absence of a magnetic field, $E_\Phi = 0$, we arrive at the Usadel equation for a chaotic dot $[v_i\sigma_i^{\mathrm{ph}}, Q_\Delta] = 0$, which can be conveniently written as

$$v_i m_j(\sigma_i^{\mathrm{ph}}\sigma_j^{\mathrm{ph}} - \sigma_j^{\mathrm{ph}}\sigma_i^{\mathrm{ph}}) = 2i(\mathbf{v}\times\mathbf{m})\cdot\boldsymbol{\sigma} = 0. \tag{5.34}$$

In this limit, it is clear that the solution is given by a mean field configuration Q_Δ whose vector component $\mathbf{m}$ is parallel to $\mathbf{v}$, that is, $\mathbf{m} = \mathbf{n} \parallel \mathbf{v}$, where $\mathbf{n}$ is given by

$$\mathbf{n} = \frac{1}{v}\begin{pmatrix} 0 \\ v_2 \\ v_3 \end{pmatrix}, \tag{5.35}$$

where $v = \sqrt{v_2^2 + v_3^2}$ provides the normalization, ensuring that indeed $Q_\Delta^2 = 1$.

5.4.2. Finite magnetic fields

In the presence of an external magnetic field, to reduce the number of variables involved in the Usadel equation, we use the geometric constraint to write m_3 as a function of m_2, namely $m_3(v_2 - E_\Phi m_2) = v_3 m_2$. Assuming that the solution of interest has $m_2 \neq 0$, then we may write down the mean field vector as

$$\mathbf{m} = \begin{pmatrix} 0 \\ m_2 \\ \frac{v_3 m_2}{v_2 - E_\Phi m_2} \end{pmatrix}, \tag{5.36}$$

where m_2 is to be fixed by the normalization condition $\mathbf{m}^2 = 1$. Substituting the components of the mean field yields

$$(s - m_2)^2(m_2^2 - 1) + s^2\beta^2 m_2^2 = 0, \tag{5.37}$$

where to obtain a more compact equation, we have defined $s = v_2/E_\Phi$ and $\beta = v_3/v_2$.

Since this equation is a fourth-order polynomial, there exists a general solution to it in closed form. However, the solutions are long and complex. To obtain from the mathematical expressions any form of underlying physics is not a feasible task. Fortunately, progress can be made in the limit of large magnetic fields where the solution can be constructed in terms of a power series in the small parameter s,

$$m_2(s) = \sum_{l=0}^{\infty} m_{2,l} s^l. \tag{5.38}$$

The leading contributions to the components of m read as

$$m_2(s) = \frac{s}{1 + |\beta| s}, \qquad m_3(s) = \sqrt{1 - m_2^2(s)}. \tag{5.39}$$

In constructing this solution, we considered the product $s\beta$ in Eq. (5.37) as an independent parameter. The strong magnetic field limit imposes that s is small. However, for the calculation of the current fluctuations we will need to work with the solution for a wide range of frequencies ϵ. Under these circumstances, the product $s\beta$ is not necessarily small, since β scales with the frequency. We confirmed numerically that the solution stated above provides an excellent approximation for a broad interval of β values as long as $s < 0.5$. Below in Fig. 5.3, we display the plots with the comparison between the theoretical and numerical results, at a zero phase difference.

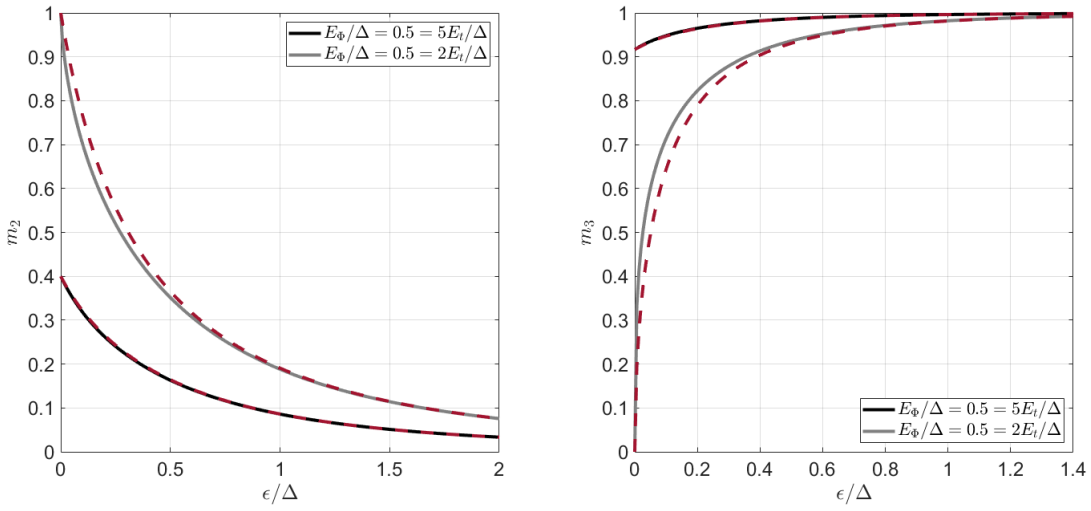

Figure 5.3.: The solid lines represent the theoretical expression and the dashed lines the numerical result. At zero phase difference, $\phi = 0$, we compare these two results for values close to the limit of validity of our perturbative computation.

In the limiting case of a strong magnetic, the results are in perfect agreement. We start to observe some small deviations from the theoretical prediction in the region where the E_Φ/Δ becomes similar to E_t/Δ.

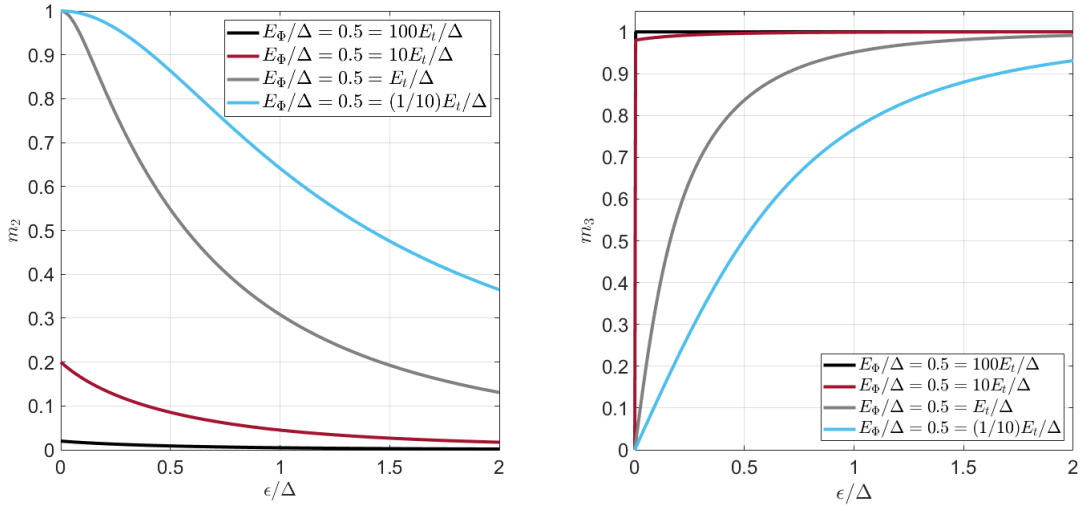

Figure 5.4.: The numerical results for various values of the ratio of dwell energy to superconducting gap, for a fixed applied magnetic flux. As we display above, the magnitude of m_2 is considerably sensitive to the dwell energy and, in the limit of a large ϵ, the mean field solution becomes purely metallic.

Note that for $v_2 = 0$ (i.e. no superconductor, $\Delta = 0$ or $E_t = 0$), the normalizable solution has $m_2 = 0$ and, as a consequence of this result, the solution for the third component of the mean field must necessarily collapse to $|m_3| = 1$. Within this condition, the correct solution is chosen by further demanding $\mathrm{sgn}(m_3) = \mathrm{sgn}(\epsilon)$, whose form is consistent with the conventional structure for a normal conductor. With the aid of the numerical results, the plots for the components of $\mathbf{m}$, as a function of ϵ, for various values of the applied magnetic flux and the dwell energy, are displayed below in Fig. 5.4. In these plots, we observe that as we increase the magnitude of the dwell energy, the mean field m_2 responds with an increase. For certain values of the dwell energy, $E_t/\Delta \lesssim 0.05$, the component m_3 dominates the contribution from the mean field m_2.

5.4.3. Rotation of the Q-field

The solution of the second saddle point equation, the homogeneous Usadel equation (5.30), is sufficient for finding the average Josephson current in the short junction limit. The calculation of the current fluctuations, in turn, requires us to go beyond the saddle point approximation and to include fluctuations. The typical protocol involving these calculations would be to decompose the Q matrix in terms of rotations around the ansatz Q_Δ performed by a rotation matrix $\tilde{T}$, that is, $Q = \tilde{T} Q_\Delta \tilde{T}^{-1}$. The rotation matrices may be conveniently parametrized as $\tilde{T} = e^{\tilde{W}}$ with $\tilde{W}$ being the generators, satisfying the constraint $\{Q_\Delta, \tilde{W}\} = 0$, where $\{A, B\}$ represents the anticommutator of two matrices. In the next step, we would perform an expansion in powers of $\tilde{W}$.

However, the rather non-trivial structure of the saddle point solution introduces unwelcome complications in the constraints for $\tilde{W}$. Instead of following the canonical path, we take an alternative route as was done in Ref. [Mic07]. We explore a different rotation scheme of the matrix Q, whose form will greatly simplifies the perturbative expansion in the generators. Bearing this in mind, we first define the rotation matrix T_Δ and use it to perform rotations around the first saddle point configuration leading to the relation

$$Q_\Delta = T_\Delta Q_0 T_\Delta^{-1}. \tag{5.40}$$

The underlying idea behind this construction is the possibility of expressing the matrix Q in terms of rotations around the first saddle point $Q = \hat{T} Q_0 \hat{T}^{-1}$, where $\hat{T} = T_\Delta^{-1} \tilde{T} T_\Delta$. We still use an exponential parametrization with generators $\hat{W}$ to represent the rotation matrix $\hat{T}$. However, the constraint for it becomes much simpler in comparison to the previous case with $\tilde{W}$. The generator $\hat{W} = T_\Delta^{-1} \tilde{W} T_\Delta$ immediately satisfies the anti-commutator relation $\{\hat{W}, Q_0\} = 0$. Next, we use that the trace is invariant under cyclic permutations to perform a change of variables from Q to $\hat{Q}$. We express the matrix field Q in terms of the rotated version $\hat{Q} = T_\Delta^{-1} Q T_\Delta$.

Unfortunately, these rotations are not cost free, the price we pay for them is a different representation of the Pauli matrices, whose new form is given by the relation

$$\hat{\sigma}_i^{\mathrm{ph}} = T_\Delta^{-1} \sigma_i^{\mathrm{ph}} T_\Delta. \tag{5.41}$$

After these steps, we finally arrive at the final form of the effective action in the presence of a vector potential for a short junction

$$S = \frac{\pi\nu}{8} \int d^2x \mathrm{tr} \left[D(\partial_{\mathbf{A}} \hat{Q})^2 - 4 v_i \hat{\sigma}_i^{\mathrm{ph}} \hat{Q} \right], \tag{5.42}$$

where the y coordinate is implicit $\hat{Q} = \hat{Q}_y$. To perform manipulations with the effective action, we must have access to the explicit knowledge of the rotated Pauli matrices $\hat{\sigma}_i^{\rm ph}$. In order to determine their specific form, we insert the ansatz $T_\Delta = \exp(i\theta\Lambda\sigma_1^{\rm ph}/2)$ into Eq. (5.40) and further use relation (5.32) to fix the rotation angle θ, where $\Lambda_n = \mathrm{sgn}(\epsilon_{\rm n})$. As a consequence of this computation, we end up with two conditions $\cos\theta\Lambda = m_3$ and $\sin\theta = m_2$. A direct application of this result into the rotated matrices yields:

$$\hat{\sigma}_2^{\rm ph} = (m_3\sigma_2^{\rm ph} + m_2\sigma_3^{\rm ph})\Lambda, \tag{5.43}$$

$$\hat{\sigma}_3^{\rm ph} = (-m_2\sigma_2^{\rm ph} + m_3\sigma_3^{\rm ph})\Lambda. \tag{5.44}$$

The effective action in the form given in Eq. (5.42) provides the foundation upon which we construct our observables: the average Josephson current and the current fluctuations. In order to simplify the notation, in the following discussions we shall drop the notation $\hat{Q}$ in favor of the simpler representation Q.

5.5. Density of states

In equilibrium, the global density of states is the simplest observable that reflects the proximity induced effects in the topological insulator and it can be computed from the matrix field Q_0 as

$$\frac{\nu(\epsilon)}{\nu} = \frac{1}{4}\mathrm{Re}\left\{\mathrm{tr}\left[Q_0(\epsilon \to -i\epsilon_+)\sigma_3^{\rm ph}\right]\right\}, \tag{5.45}$$

with Q_0 being the solution of the Usadel equation analytically continued from the discrete set of Matsubara frequencies to the axis of real energies, $\epsilon_+ = \epsilon + i\eta$ includes a positive small imaginary part and ν denotes the density of states at energy $\epsilon = \mu$ in absence of superconducting leads. Since we have already obtained the physical solution for the Usadel equation, we have all the necessary means to explore the features of the density of states of our topological insulator Josephson junction. In particular, we shall investigate the influence of the applied magnetic field on the proximity induced minigap in the topological insulator film. Building on the discussion of the previous section, we employ the mean field solution to derive the density of states for our system:

$$\nu(\epsilon) = \nu\mathrm{Re}\left[m_3(-i\epsilon_+)\right], \tag{5.46}$$

with m_3 specified through Eqs. (5.36) and (5.37).

First, we consider the density of states in absence of a magnetic field, $B = 0$. In this limit, the density of states depends on three energy scales: the dwell energy, E_t, the superconducting gap, Δ, and the energy ϵ. As shown in Fig. 5.5(a), the most prominent feature displayed is the appearance of the proximity induced minigap E_g, which is a function of the ratio E_t/Δ. As we can see in Fig. 5.5, for the weak coupling limit, $E_t \ll \Delta$, it displays the typical superconductor square-root singularity above the edge of the minigap $E_g = 2E_t\cos\phi$, $\nu(\epsilon) \sim \theta(\epsilon - E_g)(|\epsilon - E_g|)^{1/2}$, and a weaker singularity $\nu(\epsilon) \sim 1/(|\epsilon - \Delta|)^{1/4}$ around the superconducting gap. The induced minigap progressively increases as we increase the ratio E_t/Δ, until we reach strong-coupling limit, $\Delta \ll E_t$ and the first singularity is completely washed out and only the singularity above the superconducting gap remains with $E_g \sim \Delta$. In the intermediate case $E_t \approx \Delta$, the density of states displays two singularities, as for $E_t \ll \Delta$. Notice that, in this case, the induced minigap becomes considerably large $E_g \lesssim \Delta$, almost identical to the limiting case of a strong coupling, $E_t \gg \Delta$.

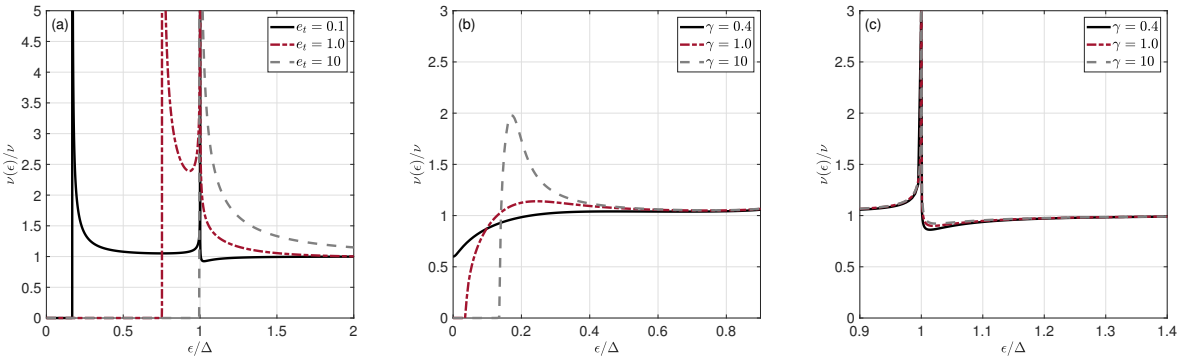

Figure 5.5.: (a) Density of states $\nu(\epsilon)$ for the vanishing magnetic field normalized to the density of states $\nu = \nu(\mu)$ in the absence of superconducting leads for different values of $e_t = E_t/\Delta = 0.1, 1, 10$. Panels (b) and (c) show density of states of the microbridge at a finite magnetic field as a function of frequency ϵ for different values of $\gamma = E_t/E_\Phi = (0.1/0.01, 0.1/0.1, 0.1/0.25)$ and fixed phase $\phi = 0$, where $e_\Phi = E_\Phi/\Delta$.

Now, we turn to the analysis of the influence of an external magnetic field on the density of states. It has been reported in the literature [BBS96] that the induced minigap is reduced in the presence of an external magnetic field or spin-flip mechanisms and, for sufficiently strong fields, the minigap can be fully closed. In here, we shall focus on the limiting case $E_t \ll E_\Phi \ll \Delta$. In this limit, we can explore the sensitivity of the minigap E_g to the external magnetic field without the additional complications associated with pair-breaking effect on the superconducting leads. In Fig. 5.5(b) we display the density of states for $E_t \ll \Delta$ and various values of E_Φ. Increasing the magnetic field from $B = 0$, we can see that the minigap is continuously reduced, until it ultimately closes once $E_\Phi \gtrsim E_g$. At the same time, the square root singularity at E_g is smoothed out and turns into a monotonic function, whose behavior qualitatively similar to that reported in the Abrikosov-Gor'kov theory of gapless superconductivity [AG61]. Once the gap closes, the density of states quickly evolves into the nearly constant function $\nu(\epsilon)$ with a clear metallic behavior. The singularity displayed at $\epsilon \sim \Delta$ remains robust against the effects of small magnetic fields $E_\Phi \ll \Delta$, see the right panel of Fig 5.5(c). In addition to that, we observe the formation of a small dip immediately above the singularity $\epsilon \gtrsim \Delta$ that develops and becomes more pronounced for smaller values of γ. It should be stressed that the sub- and above the gap features in the density of states are extremely sensitive to the boundary action used in the saddle point analysis of Usadel equation. For instance, in the model of transparent interfaces, that can be captured by the full circuit-theory action [Naz99], the density of states in the sub-gap region may display secondary gaps [Reu+14b; Reu+14a; WVL18], while a singularity at Δ may be turned into a vanishing DoS and an unusual structure of the crossover to higher energies arises [Lev08].

The results displayed above were derived using the exact solution of Eq. (5.37). The obtained homogeneous Usadel equation is a fourth-order polynomial whose coefficients are all non-vanishing, which leads to a rather cumbersome expression and, therefore, we do not state it in here. Although the mean field solution obtained via power series provides an exceedingly good approximation for the full-fledged solution, in both limiting cases, strong and weak magnetic field, it fails to fully capture the structure of the minigap. In the weak magnetic field limit, $E_\Phi < E_t$, it overestimates the size of the minigap and there is the appearance of a singularity in the region $\epsilon < \Delta$. In the opposite limit, $E_\Phi > E_t$, there exists a threshold value E_Φ^* beyond which the minigap closes. The approximated mean field solution fails to reproduce this behavior and always results in a gapless density of states. These striking features are all associated with the non-analyticity of

the mean field solution, which is a characteristic that our polynomial ansatz is not able to reproduce.

It is also worth stating that the mean field analysis of the density of states presented in this section does not contemplate sub-gap tails [Fra+96; MS01; LS00; BNA00; OSF01; FS12] and zero-bias peaks. The latter include disorder-induced class D peak [BA12] and Majorana peak [IOF12]. The onset of these features in the density of states is around energies closer to the mean level spacing. Hence, it is only possible to capture them within the framework of a non-perturbative analysis of Q-matrix manifold. Unfortunately, this parameter regime is beyond the domain of our assumptions specified earlier by Eq. (5.9). The results of this section are amenable to scanning-tunneling probes in hybrid S-TI proximity circuits and heterostructures, see e.g. Refs. [Gu96; Xu+14; Day+16; Sed+20; Rac+19; Yan+20].

5.6. Semiclassical partition function

In Sec. 5.4, we derived the saddle point equation of the nonlinear sigma model and identified that it was equivalent to the Usadel equation. Next, considering only homogeneous field configurations, we studied its solutions for various limits in different regions of the parameter space. The solution of this equation provides the fundamental building block upon which we perform the calculations of the average current through the Josephson junction.

In order to obtain the Josephson current fluctuations, we take full advantage of the versatility and generality of our field theoretical machinery and go one step further to find the semiclassical partition function from the sigma model action (5.42). We choose to represent the generators of the fluctuations in the neighborhood of the saddle point via the exponential parametrization

$$T = e^{W}, \tag{5.47}$$

where the generators W inherits the constraint: $[W, Q_0]_+ = 0$. The symmetry (5.22) of the Q field can be accounted for by imposing the constraint $W = \sigma_1^{\mathrm{ph}} W^t \sigma_1^{\mathrm{ph}}$ on the generators W. The condition $W^\dagger = -W$ is introduced to ensure the convergence of integrals in W. It is convenient to represent the generators of fluctuations W as the sum of two terms, $W = W_d + W_c$, where we define Diffusons (d) and Cooperons (c) by the conditions:

$$[W_d, \Lambda]_+ = 0, \quad [W_d, \sigma_3^{\mathrm{ph}}] = 0, \quad [W_c, \Lambda] = 0, \quad [W_c, \sigma_3^{\mathrm{ph}}]_+ = 0. \tag{5.48}$$

As we can see, to satisfy the constraint involving the anticommutator, we must impose that the Diffusons W_d are diagonal in particle-hole space and off-diagonal in Matsubara space. Whereas, the Cooperon is diagonal in Matsubara space, but displays an off-diagonal structure in the particle-hole space.

Relying on the quadratic expansion, the integration over generators leads to the semiclassical partition function

$$\mathcal{Z}(\phi_1, \phi_2) = (\det \mathcal{D})^{R^2} \, (\det \mathcal{C})^{R^2} \, e^{-RS_0}. \tag{5.49}$$

The action evaluated at the saddle point is given by

$$S_0 = \frac{\pi \nu V}{2} \sum_{\epsilon} \sum_{j=1,2} [E_\Phi m_2^2(\phi_j) - 2 v_i(\phi_j) m_i(\phi_j)]. \tag{5.50}$$

The fluctuation determinants are defined through

$$\det \mathcal{D}^{-1} = \prod_q \prod_{\epsilon_1>0} \prod_{\epsilon_2>0} \left(\lambda^{D,+}_{\epsilon_1,-\epsilon_2}\lambda^{D,-}_{\epsilon_1,-\epsilon_2}\right), \quad \det \mathcal{C}^{-1} = \prod_q \prod_{\epsilon_1>0} \prod_{\epsilon_2>0} \left(\lambda^{C,+}_{\epsilon_1\epsilon_2}\lambda^{C,-}_{\epsilon_1\epsilon_2}\right), \tag{5.51}$$

with the eigenvalues

$$\lambda^{\pm}_{\epsilon_1,\epsilon_2} = Dq^2 + \mathbf{m}(1)\cdot\mathbf{v}(1) + \mathbf{m}(2)\cdot\mathbf{v}(2) + M^{\pm}_{\Phi}(1,2), \tag{5.52}$$

$$M^{\pm}_{\Phi}(1,2) = \frac{E_\Phi}{8}\left(\left[m_3(1)+m_3(2)\right]^2 - 4\left[m_2(1)\mp m_2(2)\right]^2\right), \tag{5.53}$$

where we have introduced the multi-index notation $(i) = (\epsilon_i, \phi_i)$ and a mass term, $M^{\pm}_{\Phi}$, generated by the presence of an external magnetic field. Despite their identical functional form, these eigenvalues are defined on different regions of the Matsubara space. The Diffusons are only non-zero for $\epsilon_1 > 0$ and $-\epsilon_2 > 0$, whereas the Cooperon modes have positive frequencies only, $\epsilon_1, \epsilon_2 > 0$. The details of the derivation of Eq. (5.49) is documented in the App. D.9. The result exhibited in Eq. (5.49) does not contain all the contributions generated by the computation of the functional integral, we removed the terms that are diagonal in sample space and also discarded ϕ-independent constants, both types of contributions would not survive the process of taking the twofold derivative over the phase angles ϕ_1 and ϕ_2. Furthermore, these so called Diffusons and Cooperons do not possess the typical structure reported in the literature [AS10] and this has to do with the presence of the topological insulator-superconductor interface. In the absence of the component intimately connected with the superconductor properties, namely, $m_2(i)$, the Diffuson mass completely vanishes as this type of fluctuation is not sensitive to an applied magnetic field. On the other hand, the Cooperon still displays a mass term proportional to the intensity of the applied magnetic flux.

In the short junction limit and recalling that at the mean field level the matrix field Q is homogeneous, we substitute the partition function we calculated into Eq. (5.28), take the derivative with respect to the phase angle and compute the limit of $R \to 0$. Then, we arrive at the general expression for the average Josephson current

$$I(\phi) = 2eT\partial_\phi S_0 = -\pi\nu eTV \sum_\epsilon \left[\partial_\phi\left(2v_i m_i - E_\Phi m_2^2\right)\right]. \tag{5.54}$$

To compute the sample-to-sample current fluctuations Eq. (5.28), we proceed in an analogous manner. The crucial difference is that now there is an spatial structure involved, which manifests itself via a momentum dependence of the eigenvalues. Taking the twofold derivative over the phase angles and calculating the replica limit yield the following expression for the sample-to-sample current fluctuations

$$K(\phi_1,\phi_2) = (2eT)^2 \sum_{s=\pm}\left[F_2^s(\phi_1,\phi_2) - F_1^s(\phi_1,\phi_2)\right], \tag{5.55}$$

with

$$F_1^s(\phi_1,\phi_2) = \sum_q \sum_{\epsilon_1>0}\sum_{\epsilon_2} \frac{\partial^2_{12}\lambda^s_{\epsilon_1,\epsilon_2}}{\lambda^s_{\epsilon_1,\epsilon_2}}, \quad F_2^s(\phi_1,\phi_2) = \sum_q \sum_{\epsilon_1>0}\sum_{\epsilon_2} \frac{\partial_1\lambda^s_{\epsilon_1,\epsilon_2}\partial_2\lambda^s_{\epsilon_1,\epsilon_2}}{\left(\lambda^s_{\epsilon_1,\epsilon_2}\right)^2}, \tag{5.56}$$

where positive and negative frequencies ϵ_2 account for the Cooperon and Diffuson contribution, respectively, and $\partial_{1,2}$ denotes derivatives with respect to the two phase differences ϕ_1 and ϕ_2.

5.7. Average current and sample-to-sample fluctuations at zero magnetic field

Next, we discuss the average Josephson current and its fluctuations in the absence of an applied magnetic field. We focus on the set-up displayed in Fig. 5.2 in the short junction limit ($L \ll \xi$), for which $E_{\rm Th} = D/L^2$ is the largest energy scale. We further distinguish the regime of a quantum dot geometry with confined transverse direction, which satisfies the energy inequality $E_{\rm Th}^{\perp} \gg \{\Delta, E_t\}$, where $E_{\rm Th}^{\perp} = D/W^2$ is the Thouless energy related to the transverse direction. In this limit, the observables are insensitive to the geometric properties of the system. Conversely, in the opposite limit, the quasi-one dimensional geometry with extended transverse direction $E_{\rm Th}^{\perp} \ll \{\Delta, E_t\}$, the system is sensitive to spatial coordinates.

5.7.1. Average current

Building on our discussion in Sec. 5.4, the solution of the saddle point equation in the absence of a magnetic field is given by $Q_\Delta = m_i \sigma_i^{\rm ph}$. Therefore, the average current $I(\phi)$ can be found from Eq. (5.54) by setting $E_\Phi = 0$ and $m_i = v_i/\sqrt{v_1^2 + v_2^2}$, that is, the solution to the homogeneous Usadel equation is given by a mean field vector which is parallel to $\mathbf{v}$, leading to

$$I(\phi) = \frac{GE_t}{2e} J(\phi), \qquad J(\phi) = 4\pi \sin(\phi) T \sum_{\epsilon>0} \frac{\Delta^2}{\omega(\Delta,\epsilon) v(\epsilon,\phi)}, \tag{5.57}$$

where for the sake of clarity we indicated the dependence of the scalar $v(\epsilon,\phi) = |\mathbf{v}|$ on the phase difference ϕ and the Fermionic Matsubara frequency ϵ and we defined $\omega(\Delta,\epsilon) = \Delta^2 + \epsilon^2$. Here, we used the relation $E_t = \delta G/2e^2$ to connect the dwell energy with the normal-state conductance of the junction and δ represents the mean level spacing. Equation (5.57) is valid for arbitrary ratios $e_t \equiv E_t/\Delta$. We notice that the average Josephson current does not depend on the width of the junction. The result displayed in Eq. (5.57) is consistent with previously reported results [ALO68; KL88; BB97]. We will now address the parameter dependence of the average current in the limiting cases of long and short dwell times, $E_t \ll \Delta$ and $E_t \gg \Delta$, respectively. For these cases, simple analytical solutions can be obtained. In Sec. 5.7.1.3, we will then discuss arbitrary dwell times based on a fully numerical evaluation of Eq. (5.57).

5.7.1.1. Long dwell time: $E_t \ll \Delta$

Specializing on the limit $E_t \ll \Delta$, we may approximate

$$v_3(i) = \epsilon_i \left[1 + \frac{2(E_t/\Delta)}{\sqrt{1 + \epsilon_i^2/\Delta^2}} \right] \approx \epsilon_i. \tag{5.58}$$

The scale for the average current is then set by $GE_t/2e$, and J becomes a function of the dimensionless variables $t = T/\Delta$ and $e_t = E_t/\Delta$ only. In this approximation and at low temperatures, $T \ll \Delta$, the dimensionless $J(\phi)$ assumes the following asymptotic form

$$J(\phi) = 2\sin(\phi) \ln \left[\frac{1}{\max(t, e_t \cos(\phi/2))} \right]. \tag{5.59}$$

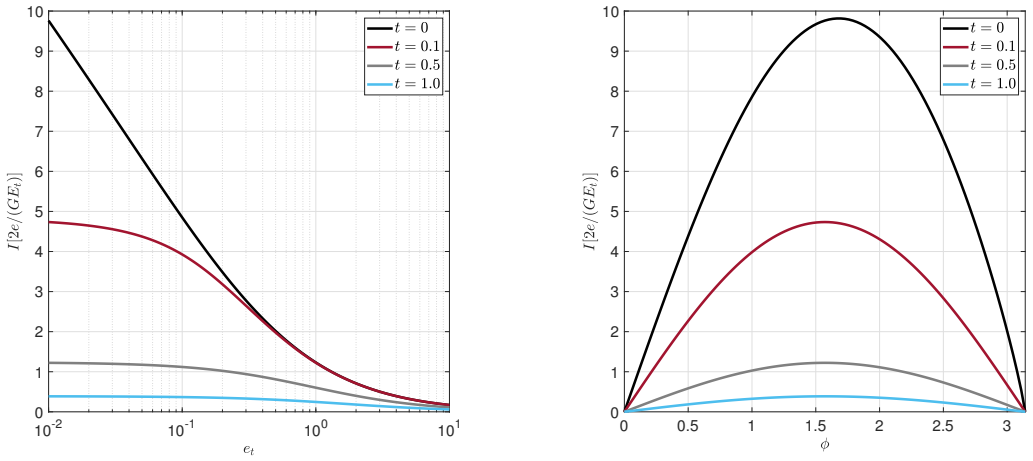

Figure 5.6.: The average current $I(\phi)$ at zero magnetic field. On the left hand side, as a function of the dwell energy $e_t = E_t/\Delta$ for various values of $t = T/\Delta$ and $\phi = \pi/2$. On the right hand side, as a function of ϕ for various t and $e_t = 0.01$.

5.7.1.2. Short dwell time: $E_t \gg \Delta$

In the short dwell time limit, and for zero temperature, the dimensionless function J is proportional to the complete elliptic integral of the first kind $\mathbf{K}$,

$$J(\phi) = \frac{1}{e_t}\sin(\phi)\mathbf{K}\left(\sin^2\frac{\phi}{2}\right) = \frac{1}{e_t}\sin(\phi)\int_0^\infty dy \frac{1}{\sqrt{\cos^2(\phi/2)+\sinh^2 y}}. \tag{5.60}$$

It is worth noting that, in contrast with the long dwell time limit, whose magnitude of the average current is set by the dwell energy. In this opposite limit, the scale of the average current is set by the order parameter Δ, compare Eqs. (5.57) and (5.60).

5.7.1.3. Arbitrary dwell time

For the general case of arbitrary dwell times, we employ Eq. (5.57) to perform numerical calculations. We display the dependence of the average current, I, on t and e_t in Fig. 5.6. As expected from Eq. (5.59), I grows monotonically as the temperature decreases, and the weak low-temperature singularity is cut-off for finite e_t. Likewise, I grows with decreasing e_t, but the growth is limited for finite T. The dependence of I on the phase difference ϕ is illustrated in Fig. 5.6 for fixed e_t. At the lowest temperatures, the average current attains its maximum around $\phi = \pi/2$. In the absence of a phase difference, $\phi = 0$, and at $\phi = \pi$ the average current vanishes. Overall, the ϕ-dependence of the average current I is completely dominated by the prefactor $\sin(\phi)$ in Eq. (5.57). The average Josephson current does not depend on width of the junction. This is different for the sample-to-sample fluctuations, as we discuss next.

5.7.2. Sample-to-sample fluctuations

The calculation of the current fluctuations requires the knowledge of the eigenvalues $\lambda^{\pm}_{\epsilon_1,\epsilon_2}$ of the fluctuation determinant stated in Eq. (5.52). For a vanishing magnetic field, the eigenvalues for Diffusons and Cooperons become identical and are given by

$$\lambda_{\epsilon_1,\epsilon_2} = Dq^2 + v(1) + v(2), \tag{5.61}$$

where $(i) = (\epsilon_i, \phi_i)$ is a convenient multi-index notation. At zero magnetic field, with the help of Eq. (5.55) and the two-fold derivatives with respect to the phases in Eq. (5.56), we obtain the general formula for the current fluctuations,

$$\mathrm{var}[I(\phi)] = (4eT)^2 \sum_{\epsilon_1,\epsilon_2>0} \sum_q \frac{\partial_{\phi_1} v(1) \partial_{\phi_2} v(2)}{[Dq^2 + v(1) + v(2)]^2}. \tag{5.62}$$

Compared to the results reported in Refs. [HS08; Mic07], the variance in Eq. (5.62) is four times smaller. This is due to the strong spin-orbit coupling in the topological insulator surface, which suppresses fluctuations in the spin triplet channel, while the singlet mode remains effective. We will discuss the current fluctuations in two limits, the quantum dot geometry, for which $E_{\mathrm{Th}}^{\perp} \gg E_t$, and the quasi-one-dimensional limit $E_{\mathrm{Th}}^{\perp} \ll E_t$.

Quantum dot limit, $E_{\mathrm{Th}}^{\perp} \gg E_t$:—In the quantum dot geometry, spatial fluctuations of the Diffuson modes in the transverse direction can be neglected and the current fluctuations are given by

$$\mathrm{var}[I_0(\phi)] = e^2 E_t^2 \mathcal{K}_0(\phi), \qquad \mathcal{K}_0(\phi) = \sin^2(\phi) T^2 \sum_{\epsilon_1,\epsilon_2>0} \frac{16 E_t^2 \Delta^4}{\omega(\Delta,\epsilon_1)\omega(\Delta,\epsilon_2) v(1) v(2) [v(1)+v(2)]^2}, \tag{5.63}$$

where the sub-index in the sample-to-sample fluctuations denotes the effective dimensionality of the system. In Fig. 5.7, the variance $\mathrm{var} I_0$ is displayed as a function of the ratio E_t/Δ.

Quasi-one-dimensional limit, $E_{\mathrm{Th}}^{\perp} \ll E_t$:— In the quasi-one-dimensional geometry spatial fluctuations of the Diffuson modes in the transverse direction have to be taken into account. Employing the same equations as in the previous limit, Eq. (5.55) and Eq. (5.56), and performing the sum over momenta q, we obtain the following expression for the variance of the Josephson current

$$\mathrm{var} I_1(\phi) = e^2 E_t^2 \sqrt{\frac{E_t}{E_{\mathrm{Th}}^{\perp}}} \mathcal{K}_1(\phi), \qquad \mathcal{K}_1(\phi) = 4 \sin^2(\phi) T^2 \sum_{\epsilon_1,\epsilon_2>0} \frac{\Delta^4 E_t^{3/2}}{\omega(\Delta,\epsilon_1)\omega(\Delta,\epsilon_2) v(1) v(2) [v(1)+v(2)]^{3/2}}. \tag{5.64}$$

The plot for the current fluctuations $\mathrm{var} I_1(\phi)$ is shown in Fig. 5.8. Next, we move on to discuss the current fluctuations specifically in the limit of long and short dwell times.

5.7.2.1. Long dwell time: $E_t \ll \Delta$

Quantum dot limit, $E_{\mathrm{Th}}^{\perp} \gg E_t$:—In the long dwell time limit and at zero temperature, the scale for the variance of the current is set by E_t^2, and we obtain an analytical expression

$$\mathrm{var} I_0(\phi) = e^2 E_t^2 \mathcal{K}_0(\phi), \qquad \mathcal{K}_0(\phi) = \frac{\sin^2(\phi)}{\pi^2} \iint_0^{\infty} \frac{dx_1 dx_2}{\sqrt{X_1(\phi) X_2(\phi)} \left(\sqrt{X_1(\phi)} + \sqrt{X_2(\phi)} \right)^2}, \tag{5.65}$$

where $X_i(\phi) = \cos^2(\phi/2) + x_i^2$ and $x_i = \epsilon_i/\Delta$. Investigating the behavior of the function $\mathcal{K}_0$, we observe that its dependence on the phase difference ϕ can be described by a simple power-law in $\cos(\phi/2)$, $\mathcal{K}_0 \approx \sin^2(\phi)[\cos(\phi/2)]^{-2}$. At $\phi = \pi$, we expect that both the average current and the current fluctuations vanish. However, it is clear that $\mathcal{K}_0$ does not reproduce this behavior as the phase ϕ approaches π. This peculiar feature is merely a shortcoming of the Gaussian approximation for the fluctuations. A more detailed analysis of the action reveals the correct result in this limit [Mic07]. As already suggested in Ref. [HS08], the vanishing

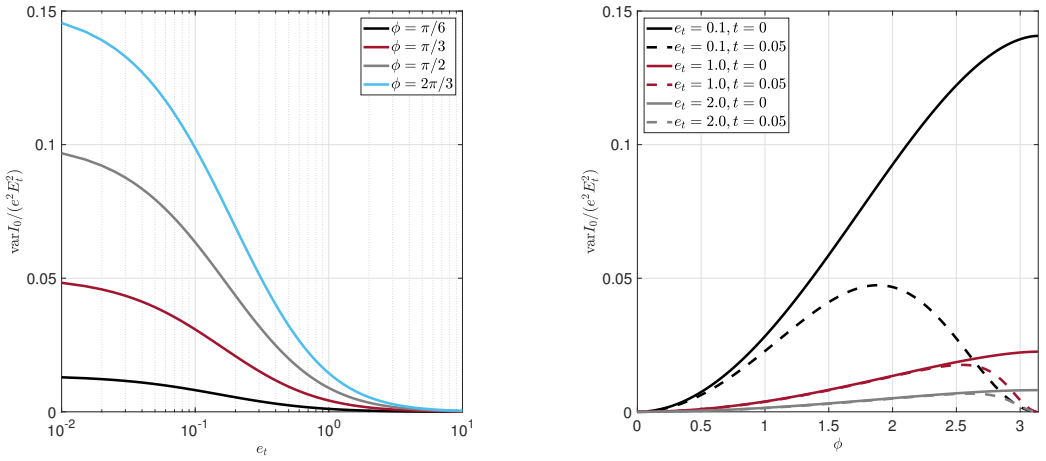

Figure 5.7.: On the right hand side, the variance of the Josephson current as a function of the phase difference ϕ in the quantum dot geometry. Solid lines represent the zero temperature limit, whereas dashed lines denote the finite temperature limit. On the left hand side, we display $\mathcal{K}_0$ as a function of $e_t = E_t/\Delta$ for various fixed phases, $\phi = \pi/6, \pi/3, \phi/2, 2\pi/3$.

of the average current and the current fluctuations for $\phi \to \pi$ is restored at finite temperatures even in the Gaussian approximation, as can be seen in Fig. 5.7.

Quasi-one-dimensional limit, $E_{\mathrm{Th}}^{\perp} \ll E_t$:—Focusing on the zero-temperature limit, we transform summations over Matsubara frequencies into integrations again, and express the latter in terms of dimensionless quantities to find

$$\mathrm{var}I_1(\phi) = e^2E_t^2\sqrt{\frac{E_t}{E_{\mathrm{Th}}^{\perp}}}\mathcal{K}_1(\phi), \qquad \mathcal{K}_1(\phi) = \frac{\sqrt{2}\sin^2(\phi)}{4\pi^2}\iint_0^{\infty}\frac{dx_1dx_2}{\sqrt{X_1(\phi)X_2(\phi)}\left(\sqrt{X_1(\phi)}+\sqrt{X_2(\phi)}\right)^{\frac{3}{2}}}. \quad (5.66)$$

The scale of the fluctuations is now set not only by the squared dwell energy but also by the parameter $\sqrt{E_t/E_{\mathrm{Th}}^{\perp}}$. The result of the integrations in x_1 and x_2 can be approximated by a power law in $\cos(\phi/2)$ and, as a consequence, the phase dependence of $\mathcal{K}_1(\phi)$ is governed by the function $\sin^2(\phi)[\cos(\phi/2)]^{-3/2}$, which monotonically vanishes as ϕ approaches π. This is a significant difference compared to the quantum dot geometry, for which finite temperatures had to be invoked in order to reproduce this behavior in the Gaussian approximation.

5.7.2.2. Short dwell time: $E_t \gg \Delta$

Quantum dot limit, $E_{\mathrm{Th}}^{\perp} \gg E_t$:—At zero temperature, the current fluctuations can be expressed in the form

$$\mathrm{var}I_0(\phi) = e^2E_t^2\mathcal{K}_0(\phi), \quad \mathcal{K}_0(\phi) = \frac{\Delta^2}{E_t^2}\mathcal{K}_0^S(\phi), \quad (5.67)$$

$$\mathcal{K}_0^S(\phi) = \frac{\sin^2(\phi)}{4\pi^2}\iint_0^{\infty}\frac{\sqrt{X_1(0)}\sqrt{X_2(0)}dx_1dx_2}{\sqrt{X_1(\phi)}\sqrt{X_2(\phi)}\left[\sqrt{X_2(0)}\sqrt{X_1(\phi)}+\sqrt{X_1(0)}\sqrt{X_2(\phi)}\right]^2}. \quad (5.68)$$

A quick inspection of this expression reveals that in this regime the scale is now set by Δ^2. In this limit, when ϕ approaches π the product between $\sin^2(\phi)$ and the dimensionless function $\mathcal{K}_0^S$ yields a non-zero

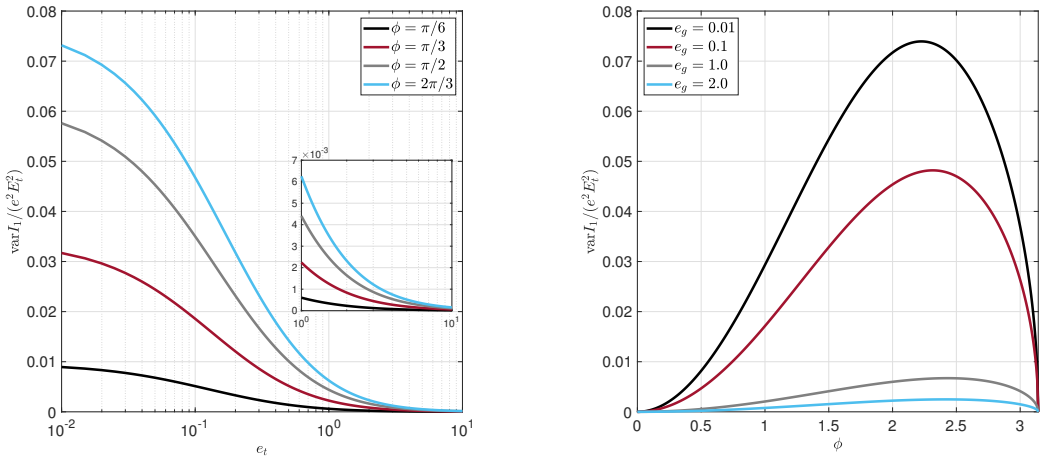

Figure 5.8.: On the right hand side, the variance of the Josephson current as a function of the phase difference ϕ in the quasi-one-dimensional geometry. On the left hand side, we display $\mathcal{K}_1$ as a function of $e_t = E_t/\Delta$ for various fixed phases, $\phi = \pi/6, \pi/3, \phi/2, 2\pi/3$.

result, which clearly violates the condition $\mathrm{var}I_0(\pi) = 0$. As already found in the long dwell time limit, finite temperatures restore the correct behavior in our formalism, see Fig. 5.7.

Quasi-one-dimensional limit, $E_{\mathrm{Th}}^{\perp} \ll E_t$:—Considering the zero temperature limit, the current fluctuations yield

$$\mathrm{var}I_1(\phi) = e^2E_t^2\sqrt{\frac{E_t}{E_{\mathrm{Th}}^{\perp}}}\mathcal{K}_1(\phi), \quad \mathcal{K}_1(\phi) = \frac{\Delta^2}{E_t^2}\mathcal{K}_1^S(\phi), \tag{5.69}$$

$$\mathcal{K}_1^S(\phi) = \frac{\sqrt{2}\sin^2(\phi)}{16\pi^2}\iint_0^{\infty}\frac{[X_1(0)]^{1/4}[X_2(0)]^{1/4}dx_1dx_2}{\sqrt{X_1(\phi)}\sqrt{X_2(\phi)}\left(\sqrt{X_2(0)}\sqrt{X_1(\phi)}+\sqrt{X_1(0)}\sqrt{X_2(\phi)}\right)^{3/2}}. \tag{5.70}$$

In analogy to the the long dwell-time limit, in a quasi-one-dimensional geometry the scale is set by Δ^2, and also by the parameter $\sqrt{E_t/E_{\mathrm{Th}}^{\perp}}$. In addition to that, as in the previous cases, we find that the quasi-one-dimensional geometry restores the correct result for the fluctuations at $\phi = \pi$, $\mathrm{var}I_1(\pi) = 0$, see details in Fig. 5.8.

5.7.2.3. Arbitrary dwell time

We can now compare the magnitudes of fluctuations and the average current for the quantum dot and the quasi-one-dimensional geometry. For the quantum dot geometry, we find

$$\frac{[\mathrm{var}I_0(\phi)]^{1/2}}{I(\phi)} = \frac{G_Q}{G}\frac{[4\pi^2\mathcal{K}_0(\phi)]^{1/2}}{J(\phi)}. \tag{5.71}$$

In the quasi-one-dimensional geometry, we obtain the following expression

$$\frac{[\mathrm{var}I_1(\phi)]^{1/2}}{I(\phi)} = \frac{G_Q}{G}\left(\frac{E_t}{E_{\mathrm{Th}}^{\perp}}\right)^{1/4}\frac{[4\pi^2\mathcal{K}_1(\phi)]^{1/2}}{J(\phi)}. \tag{5.72}$$

With the help of Eqs. (5.59), (5.60), (5.65), (5.66), (5.67) and (5.69), we can estimate that the ratios in Eqs. (5.71) and (5.72) are of the order of G_Q/G, where $G_Q = e^2/\pi$ is the conductance quantum. Furthermore,

as a result of the hierarchy of energy scales, $\delta \ll E_t \ll \Delta \ll E_{\rm Th}$, for a quasi-one-dimensional system, the ratio is proportional to the parameter $E_t/E_{\rm Th}^{\perp}$. As we observe in Fig. (5.9), for both geometries the approximate analytical results obtained in this section are in good agreement with numerical results. In the long dwell time limit, the fluctuation-to-average current ratio behaves as $1/\log(1/e_t)$. In the short dwell time limit, the dwell energy dependence is completely absent, which implies that ratio $[{\rm var}I_i(\phi)]^{1/2}/I(\phi)$ must necessarily tends to a constant value. Next we discuss how these findings are changed in presence of a magnetic field.

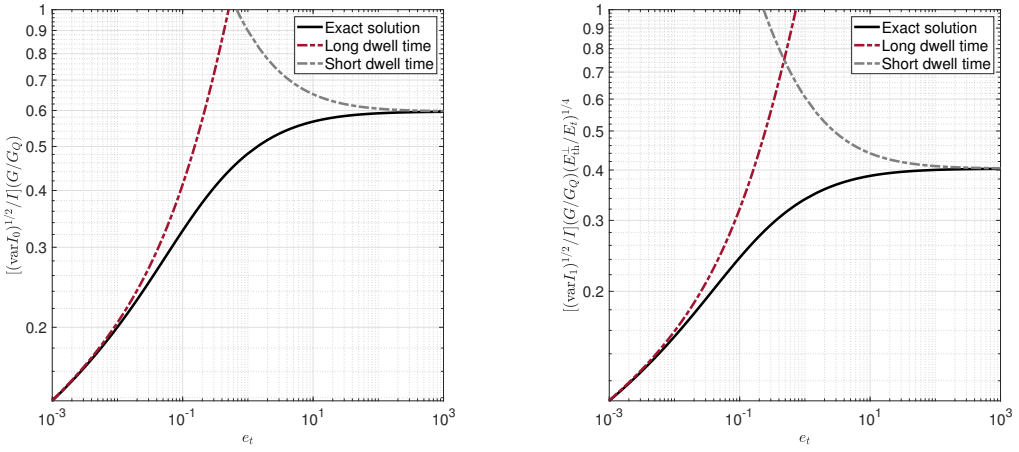

Figure 5.9.: The ratio between the current fluctuations and the average current as a function of e_t in the absence of a magnetic field and at zero temperature. On the left hand side, we show this ratio for the quantum dot geometry, on the right hand side for the quasi-one-dimensional case.

5.8. Average current and sample-to-sample fluctuations at finite magnetic field

As previously discussed, we continue to explore the average current and sample-to-sample fluctuations, but now in the presence of an external magnetic field and we shall restrict our analysis to the weak coupling regime $E_t \ll \Delta$, where the size of the induced mini gap is set by the dwell energy E_t. The presence of the external magnetic field allows us to tune the population of sub-gap states, with mini gap closure at $E_\Phi \sim E_t$, while pair-breaking effects on the superconducting leads can be neglected. We shall focus on the sensitivity of the average Josephson current and its fluctuations to the induced mini gap closure at strong magnetic fields, where an analytical solution of the mean field equation is available. Unfortunately, performing these calculations for the regime of weak magnetic field $E_t \gg E_\Phi$ has shown to be a hard task, which does not provide any new insights into the topological insulator Josephson junction. Nevertheless, building on the numerical solution of the mean field equation, we complement these analytical calculations and provide a complete description of the crossover into the weak magnetic field regime.

5.8.1. Average current

From the mean field solution $Q_\Delta = m_i\hat{\sigma}_i$, with m_i in the limit $E_\Phi \gg E_t$, and Eq. (5.54) we find the average Josephson current at strong magnetic fields

$$I_\Phi(\phi) = \frac{GE_t}{2e}J_\Phi, \qquad J_\Phi = 4\pi\sin(\phi)T\sum_{\epsilon>0}\frac{\Delta^2}{(\epsilon+E_\Phi)\Delta^2+\epsilon(\epsilon^2+2E_t\sqrt{\Delta^2+\epsilon^2}+\epsilon E_\Phi)}. \tag{5.73}$$

Using that $E_t \ll \Delta$, we can neglect terms involving the dwell energy in J_Φ, and perform the summation arriving at an expression for the average Josephson current in terms of polygamma functions, see D.7 for details. The result is shown in Fig. 5.10.

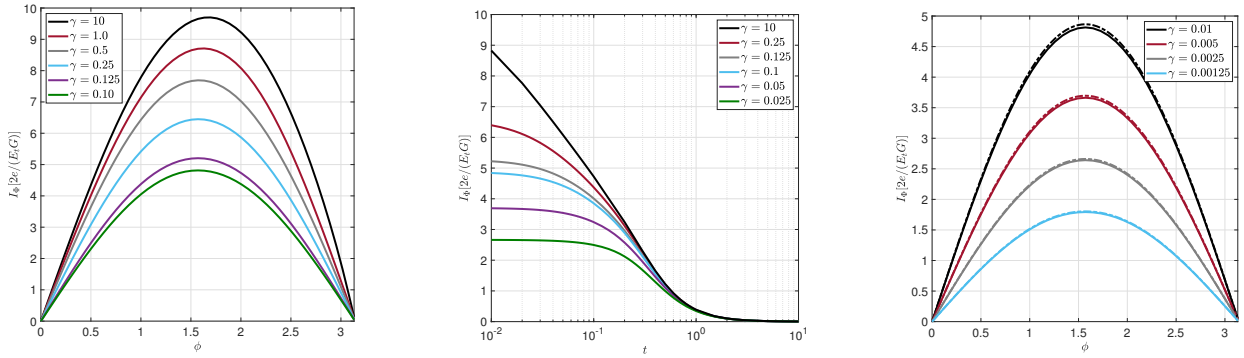

Figure 5.10.: Left panel: J_Φ at zero temperature as a function of ϕ and for various values of $\gamma = E_t/E_\Phi$. Middle panel: J_Φ as a function of temperature $t = T/\Delta$ for various values of γ, cf. Eq. (5.73). Here the dwell energy is chosen as $e_t = E_t/\Delta = 1/100$ and the phase difference as $\phi = \pi/2$. Right panel: The average current at zero temperature for various values of $\gamma = E_t/E_\Phi$, where we fixed $e_t = E_t/\Delta = 1/1000$. The solid lines represent the exact numerical solution and dash-dotted lines the analytical approximation.

The scale for the current is set by $GE_t/(2e)$, similar to the zero magnetic field case $B = 0$. However, in contrast with the latter, the phase dependence of J_Φ in the strong magnetic field limit is fully governed by the sine function, Eq. (5.73). Technically, corrections to the mean field solution Eq. (5.39) are suppressed in $E_t \ll E_\Phi$, leading to contributions whose magnitude is too small in comparison with the dominant terms. Thus, deviations from a sinusoidal behavior are expected to be strongly suppressed. It is evident from Eq. (5.73), that increasing the external magnetic field monotonically suppresses the average Josephson current. At low temperatures $T \ll \Delta$, the dimensionless function J_Φ shares the same logarithmic asymptotic form of the zero magnetic field expression

$$J_\Phi = 2\sin(\phi)\ln\left[\frac{1}{\max(t, e_\Phi)}\right], \tag{5.74}$$

where now $E_\Phi \gg E_t$ replaces the dwell energy E_t found at $B = 0$.

From the numerical solution of the mean field equation, we can calculate the average current for arbitrary ratios of E_t/E_Φ. The result is shown in Fig. 5.10. The average current as a function of the phase (left panel) shows a dominant sinusoidal behavior for all ratios E_t/E_Φ, attaining its maximum at $\pi/2$ in the strong magnetic field limit, which becomes slightly shifted to larger values when the ratio E_t/E_Φ is increased. The phase-dependence of the current does not show any signs of Fraunhofer patterns, in agreement with the discussions in references [Ham+07], [BC08] and [BP82]. The average current as a function of temperature is shown in the middle panel of Fig. 5.10. Since the weak logarithmic divergence of Eq. (5.74) is cut off by the largest value between T and E_Φ, the average current at low temperatures $T \ll \Delta$ decreases with an increase of the external magnetic field. In the opposite temperature limit $T \gg \Delta$, all curves for different values of the parameter $\gamma = E_t/E_\Phi$ display a tendency to collapse into a single curve.

Finally, we compare in right panel of Fig. 5.10 the average current from the analytical mean field solution at

strong magnetic fields to the exact current obtained from the numerical solution of the mean field equation, here at zero temperature and $e_t = E_t/\Delta = 1/1000$. As expected, the analytical solution describes the average current very well for these small values $E_t/E_\Phi \leq 0.01$.

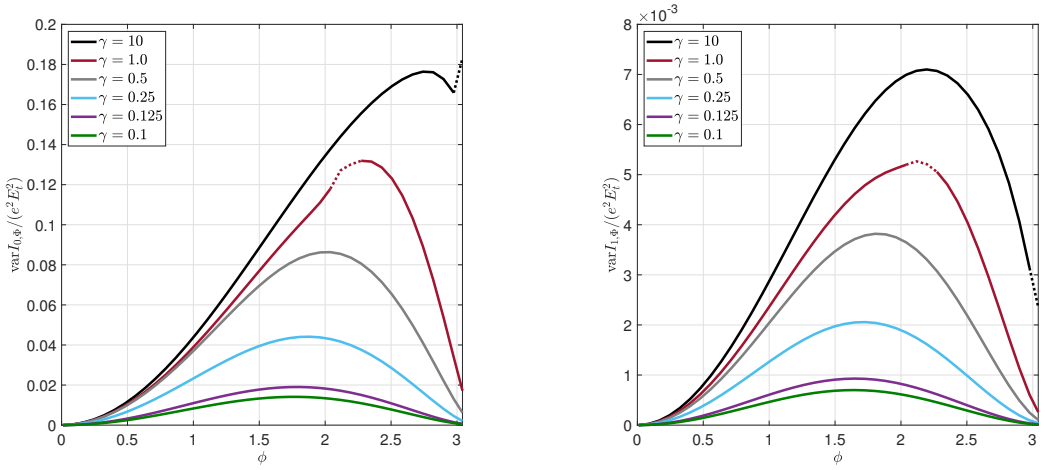

Figure 5.11.: Left panel: $\mathcal{K}_{0,\Phi}$ (quantum dot) as a function of phase angle ϕ for various values of $\gamma = E_t/E_\Phi$. Right panel: $\mathcal{K}_{1,\Phi}$ (quasi-one-dimensional geometry) as a function of phase difference ϕ for various values of $\gamma = E_t/E_\Phi$. The dashed lines indicate parameter region for which the semiclassical approximation becomes uncontrolled. In all figures we fixed $e_t = E_t/\Delta = 1/100$ and varied E_Φ.

5.8.2. Sample-to-sample fluctuations

To prepare the calculation of current fluctuations, we first notice that eigenvalues of Diffuson and Cooperon modes ($X = D, C$) at strong magnetic fields become

$$\lambda^{X,\pm}_{\epsilon_1,-\epsilon_2} = Dq^2 + \epsilon_1 + \epsilon_2 + M^\pm_X(\epsilon_1,\epsilon_2), \tag{5.75}$$

with Diffuson masses M^s_D

$$M^\pm_D(\epsilon_1,\epsilon_2) = 2E_t^2\Delta^2\cos^2\left(\frac{\phi}{2}\right)\left[\sum_{i=1}^{2}\frac{1}{(E_\Phi+\epsilon_i)\sqrt{\omega(\Delta,\epsilon_i)}} \mp \frac{2E_\Phi}{\sqrt{(E_\Phi+\epsilon_1)(E_\Phi+\epsilon_2)\omega(\Delta,\epsilon_1)\omega(\Delta,\epsilon_2)}}\right], \tag{5.76}$$

and Cooperon masses $M^\pm_C = M^\pm_D + E_\Phi/2$. Notice that the magnetic field lifts previous degeneracies at $B = 0$, and all four modes ($D/C, \pm$) now contribute differently to the current fluctuations. Then, starting out from the general expression for current fluctuations

$$\mathrm{var}I_\Phi(\phi) = (2eT)^2\sum_{s=\pm}\left[F^s_2(\phi) - F^s_1(\phi)\right], \tag{5.77}$$

we employ that in the limit of strong magnetic fields the functions F^s_1 and F^s_2 are given by

$$F^s_1(\phi) = \sum_{X=D,C}\sum_{\epsilon_1,\epsilon_2>0}\sum_q \frac{\partial_1[M^s_X(\epsilon_1,\epsilon_2)]\partial_2[M^s_X(\epsilon_1,\epsilon_2)]}{[Dq^2+\epsilon_1+\epsilon_2+M^s_X(\epsilon_1,\epsilon_2)]^2}, \tag{5.78}$$

$$F^s_2(\phi) = \sum_{X=D,C}\sum_{\epsilon_1,\epsilon_2>0}\sum_q \frac{\partial^2_{12}M^s_X(\epsilon_1,\epsilon_2)}{Dq^2+\epsilon_1+\epsilon_2+M^s_X(\epsilon_1,\epsilon_2)}. \tag{5.79}$$

We next explore these general expression for the two geometries of interest, that is, the quantum dot and quasi-one-dimensional structure, defined by $E_{\rm Th}^{\perp} \gg E_t$ and $E_{\rm Th}^{\perp} \ll E_t$, respectively.

5.8.2.1. Quantum dot limit: $E_{\rm Th}^{\perp} \gg E_t$

Current fluctuations for the quantum dot geometry in the zero temperature limit can be simplified to

$$\mathrm{var} I_{0,\Phi}(\phi) = e^2 E_t^2 \mathcal{K}_{0,\Phi}(\phi), \quad \mathcal{K}_{0,\Phi}(\phi) = \left(\frac{E_t}{E_\Phi}\right)^2 \mathcal{F}_{0,\Phi}(\phi), \tag{5.80}$$

$$\mathcal{F}_{0,\Phi}(\phi) = \frac{\sin^2(\phi)}{\pi^2} \sum_{X=C/D} \sum_{s=\pm 1} \left[f_{0,1}^{X,s}(\phi,\gamma) + f_{0,2}^{X,s}(\phi,\gamma) \right], \tag{5.81}$$

with functions $f_{0,1}$ and $f_{0,2}$ defined as

$$f_{0,1}^{X,1}(\phi,\gamma) + f_{0,1}^{X,-1}(\phi,\gamma) = 2 \iint_0^\infty dx dx' \frac{\omega(1,e_\Phi x)\omega(1,e_\Phi x')}{\Omega_X^+(x,x')\Omega_X^-(x,x')}, \tag{5.82}$$

$$f_{0,2}^{X,s}(\phi,\gamma) = \iint_0^\infty dx dx' \frac{\eta_X^s(x,x')}{[\Omega_X^s(x,x')]^2}. \tag{5.83}$$

To write the equations in a compact manner, we used $\omega(\Delta,\epsilon) = \Delta^2 + \epsilon^2$ and introduced

$$\eta_X^s(x_1,x_2) = \prod_{i\neq j,i,j=1}^{2} \left[\omega(1,e_\Phi x_i) - s b_X(x_i)(1+x_j)\sqrt{\omega(1,e_\Phi x_i)\omega(1,e_\Phi x_j)} \right]$$

$$\Omega_X^s(x_1,x_2) = (a_X + x_1 + x_2) \prod_{i=1}^{2} (1+x_i)\omega(1,e_\Phi x_i) + 2\gamma^2 \cos^2\left(\frac{\phi}{2}\right) \times$$
$$\times \left[\sum_{i=1}^{2} (1+x_i)\omega(1,e_\Phi x_i) - 2s\sqrt{\omega(1,e_\Phi x_1)\omega(1,e_\Phi x_2)} \right].$$

Here, the numerical constant a_X is zero for diffusons and 1/2 for Cooperons, and $b_D(\epsilon) = 1$ for diffusons, respectively, $b_C(\epsilon) = (1/2)[1 + \epsilon/(1+\epsilon)]$ for Cooperons.

While fluctuations in the absence of magnetic fields are set by the (squared) dwell energy, they are suppressed by the additional factor $(E_t/E_\Phi)^2$ in the strong magnetic field limit. The left panel of Fig. 5.11 shows the current fluctuations $\mathrm{var} I_{\Phi,0}$ as a function of ϕ for different values $\gamma = E_t/E_\Phi$. The increase of fluctuations with γ is clearly visible and we also observe a shift of the maximum from close to π at weak magnetic fields to smaller values as the magnetic field increases. We caution again that the semiclassical approximation loses its validity once the action takes values $\mathcal{O}(1)$. The corresponding regions are close to the maximum value of fluctuations and indicated by the dashed lines. For $E_t/E_\Phi \gtrsim 1$, the action becomes large enough to justify the semiclassical approximation for all values of ϕ.

In the left panel of Fig. 5.12, we compare the analytical solution based on the analytical mean field solution at large magnetic fields to the fluctuations calculated using the exact numerical solution of the mean field equation. Again we find very good agreement for all values $\gamma < 0.01$.

Finally, we show in the left panel of Fig. 5.13 the ratio between the square root of current fluctuations and

average current for the quantum dot geometry in the strong magnetic field regime,

$$\frac{\sqrt{\mathrm{var} I_{0,\Phi}(\phi)}}{I_\Phi(\phi)} = \left(\frac{G_Q}{G}\right)\left(\frac{E_t}{E_\Phi}\right)\frac{\sqrt{4\pi^2 \mathcal{F}_{0,\Phi}(\phi)}}{J_\Phi}. \tag{5.84}$$

As previously noted, large magnetic fields suppresses the relative size of fluctuations by an additional factor E_t/E_Φ compared to the zero magnetic field limit $B = 0$.

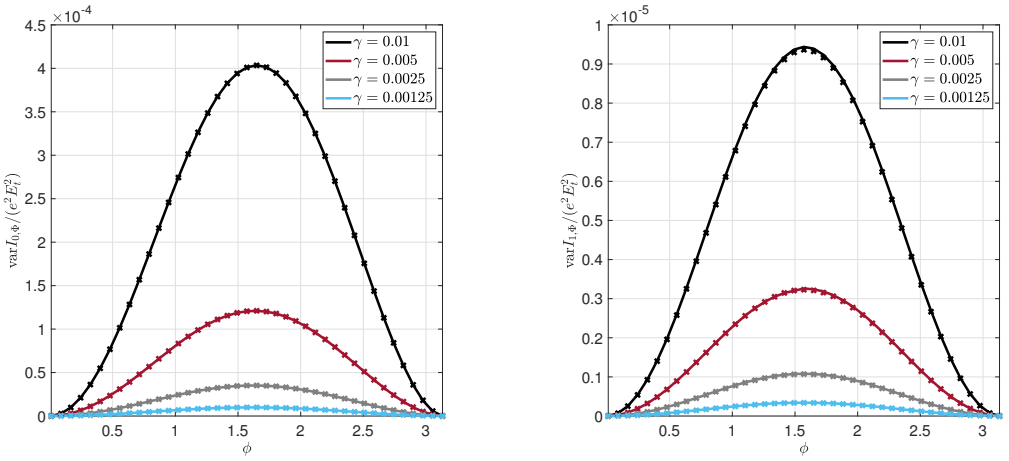

Figure 5.12.: Current fluctuations in the strong magnetic field limit as a function of phase for various values $\gamma = E_t/E_\Phi$ (we here fixed $e_t = E_t/\Delta = 1/1000$ and varied E_Φ). Solid lines and markers denote the analytical result employing the approximate solution of the mean field equation and the result building on the numerical solution of the mean field equation, respectively. Left panel: quantum dot geometry. Right panel: quasi-one-dimensional geometry.

5.8.2.2. Quasi-one-dimensional limit: $E_{\mathrm{Th}}^{\perp} \ll E_t$

For the quasi-one-dimensional geometry, at zero temperature, the current fluctuations read

$$\mathrm{var} I_{1,\Phi}(\phi) = e^2 E_t^2 \sqrt{\frac{E_t}{E_{\mathrm{Th}}^{\perp}}}\mathcal{K}_{1,\Phi}(\phi), \quad \mathcal{K}_{1,\Phi}(\phi) = \sqrt{\frac{E_t^3}{E_\Phi^3}}\mathcal{F}_{1,\Phi}(\phi), \tag{5.85}$$

$$\mathcal{F}_{1,\Phi}(\phi) = \frac{\sin^2(\phi)}{\pi^2}\sum_{s=\pm}\sum_{X=C,D}\left(f_{1,1}^{X,s} + f_{1,2}^{X,s}\right). \tag{5.86}$$

Here, the functions $f_{1,i}^{X,s}$ depend on the ratio $\gamma = E_t/E_\Phi$ and are defined as

$$\sum_{s=\pm} f_{1,1}^{X,s}(\gamma) = \iint_0^\infty dx dx' \frac{1}{\sqrt{(1+x)(1+x')\,\Omega_X^+(x,x')\Omega_X^-(x,x')}\left[\sqrt{\Omega_X^+(x,x')} + \sqrt{\Omega_X^-(x,x')}\right]}, \tag{5.87}$$

$$f_{1,2}^{X,s}(\gamma) = \frac{1}{4}\iint_0^\infty dx dx' \frac{\eta_X^s(x,x')}{\sqrt{(1+x)(1+x')[\Omega_X^s(x,x')]^3}}. \tag{5.88}$$

As compared to the zero magnetic field limit, fluctuations at strong magnetic fields in the quasi-one-dimensional geometry are suppressed by an additional factor $(E_t/E_\Phi)^{3/2}$. In terms of this small parameter, the one-dimensional integration over momenta leads to a mildly weaker suppression of fluctuations compared

to the quantum dot geometry. The relative scale of current fluctuations for the the quasi-one-dimensional geometry then reads

$$\frac{\sqrt{\mathrm{var} I_{1,\Phi}(\phi)}}{I_\Phi(\phi)} = \left(\frac{G_Q}{G}\right)\left(\frac{E_t}{E_\Phi}\right)^{3/4}\left(\frac{E_t}{E_{\mathrm{th}}^\perp}\right)^{1/4}\frac{\sqrt{4\pi^2\mathcal{F}_{1,\Phi}(\phi)}}{J_\Phi}, \tag{5.89}$$

with an additional suppression $(E_t/E_\Phi)^{3/4}$ compared to the corresponding zero magnetic field expression. The right panels of Figs. 5.11, 5.12, and 5.13 compare the corresponding results for the quantum dot and quasi-one-dimensional geometries. Specifically, we observe in Fig. (5.13) that in both geometries the relative size of current fluctuations monotonically increases as a function of E_t/E_Φ in a nearly power-law fashion.

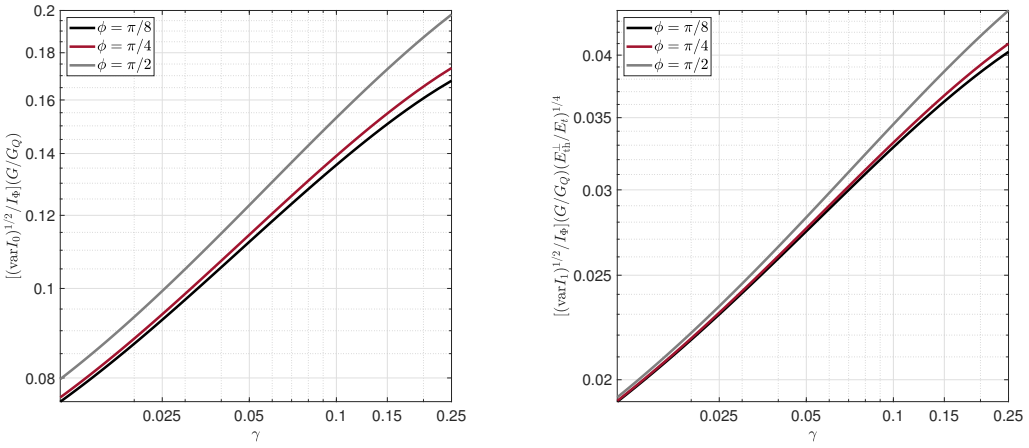

Figure 5.13.: Relative size of current fluctuations $\sqrt{\mathrm{var} I_\Phi}/I_\Phi$ in the strong magnetic field limit as a function of $\gamma = E_t/E_\Phi$ and various values of ϕ. Left panel: quantum dot geometry. Right panel: quasi-one-dimensional geometry.

5.9. Summary

In Table 5.1, we summarize the parametric dependence of the average current and current fluctuations on the four energy scales Δ, E_t, E_Φ and $E_{\mathrm{Th}}^\perp$ for a topological insulator contacted to identical superconducting leads, at zero temperature. The current-phase relation in the absence of an external magnetic field displays a typical Ambegaokar-Baratoff relation confirming previous findings already reported in the literature, where the scale of the current is set by $\min(E_t, \Delta)$. In the long dwell time limit, $E_t \ll \Delta$, the current-phase relation does not display a sinusoidal behavior and its scale is set by the dwell energy E_t [BB97]. In the opposite limit, short dwell time $E_t \gg \Delta$, the average current as a function of the phase only mildly deviates from a sinusoidal form and the scale is set by the superconducting gap Δ [KL88], [BB97]. In the limit of a strong magnetic field, $E_t \ll E_\Phi$, the scale of the average current is set by E_t, similarly to the long dwell time limit, but in here the current depends logarithmically on E_Φ.

In the limit of a zero magnetic field and in the quantum dot geometry, the current fluctuations are also separated into two groups: the long and short dwell times. In the former limit, the scale of the fluctuations is set by the squared dwell energy [HS08], similar to the average current. In the latter limit, the scale of the fluctuations is set by the squared superconducting gap, a result which is completely analogous to what we obtained for the corresponding average current and also in agreement with the finding reported in the

literature [HS08; Mic07]. Turning on the strong magnetic field, the scale of the fluctuations is still set by the dwell energy, in analogy to the long dwell time limit. However, the presence of a strong magnetic field generates an additional suppression of the fluctuations in terms of the small parameter E_t/E_Φ.

Finally, for a quasi-one-dimensional geometry, the energy scales setting the magnitude of the current fluctuations are identical to the quantum dot geometry. Notwithstanding, the integration over the momenta generates an additional energy dependence via the parameter $E_t/E_{\mathrm{Th}}^{\perp}$. In the absence of an external magnetic field, the qualitative discussion remains unchanged, but quantitatively the fluctuations are considerably smaller in comparison with the quantum dot geometry. In the presence of a strong magnetic field, the most striking difference between this present case and the quantum dot geometry is the magnitude of the current fluctuations. As a consequence of the integration over the momenta the fluctuations are smaller, though the suppression caused by the small parameter E_t/E_Φ in here is mildly weaker.

	$E_t \ll \Delta, E_\Phi = 0$	$E_t \gg \Delta, E_\Phi = 0$	$E_t \lesssim E_\Phi \ll \Delta$
$\frac{e}{G} I(\phi)$	$E_t \ln\left(\frac{\Delta}{E_t}\right) \sin(\phi)$	$\frac{1}{2}\Delta \mathbf{K}\left(\sin^2\frac{\phi}{2}\right)\sin(\phi)$	$E_t \ln\left(\frac{\Delta}{E_\Phi}\right)\sin(\phi)$
$\frac{1}{e^2}\mathrm{var} I_0(\phi)$	$E_t^2 \mathcal{K}_0(\phi)$	$\Delta^2 \mathcal{K}_0^S(\phi)$	$E_t^2 \frac{E_t^2}{E_\Phi^2}\mathcal{F}_{0,\Phi}(\phi)$
$\frac{1}{e^2}\mathrm{var} I_1(\phi)$	$E_t^2 \sqrt{\frac{E_t}{E_{\mathrm{Th}}^{\perp}}}\mathcal{K}_1(\phi)$	$\Delta^2 \sqrt{\frac{E_t}{E_{\mathrm{Th}}^{\perp}}}\mathcal{K}_1^S(\phi)$	$E_t^2 \sqrt{\frac{E_t}{E_{\mathrm{Th}}^{\perp}}}\sqrt{\frac{E_t^3}{E_\Phi^3}}\mathcal{F}_{1,\Phi}(\phi)$

Table 5.1.: At zero temperature, the average current, $I(\phi)$, and the current fluctuations in $d-$dimensions, $\mathrm{var} I_d(\phi)$.

The experimental measurement of sample-to-sample fluctuations of supercurrents is not easily accessible. The investigation of the fluctuations in a given sample as a function of the chemical potential offers a more approachable alternative to perform the experimental verification. Josephson junctions consisting of a topological insulator surface states in contact with superconducting leads allow the variation of the chemical potential μ via a gate voltage control. Moreover, with the help of split gates, narrow constrictions and point-contact junctions can be defined in the topological insulator surface states either lithographically or electrostatically.

In these types of systems, at low temperatures, it is expected that when the chemical potential is modified on the scale of the Thouless energy, the critical current will display a universal fluctuation by an amount of the order $\sim e\Delta/h$, a result insensitive to the properties of the junction. A recent experiment has reported the measurement of the critical current noise in topological insulator Josephson junctions [Kur+14]. However, thus far such result has been interpreted in terms of the charge noise and relocation of topological surface states induced by the gate control.

The frontier of science extends all along a long line from the newest and most modern intensive research, over the extensive research recently spawned by the intensive research of yesterday, to the broad and well developed web of extensive research activities based on intensive research of past decades.

More is Different, Philip W. Anderson

6

Conclusion

In this thesis, we aimed to construct an effective field theory to describe the spectral and quantum transport properties of low dimensional disordered systems. To achieve this goal, we started out with a microscopic description of our low dimensional systems, then, anticipating the necessity of performing a disorder average over a large collection of possible impurity configurations, we introduced two methods to calculate the disorder average: the supersymmetric method and the replica trick. In both cases, the averaging process generated an effective quartic vertex. In such quartic vertex, we singled out the slowly varying contributions, momenta smaller than the inverse mean free path, and noticed that this vertex has only two relevant modes, the diffuson and Cooperon. With the aid of the Hubbard-Stratonovich transformation, we introduced an auxiliary matrix field carrying the structure of these soft modes to decouple the effective vertex and turn the action into a Gaussian form.

Furthering the derivation, we performed the analysis of the saddle-point equation which allowed us to write this matrix field in terms of rotation matrices around the metallic saddle-point. Recalling the weak disorder limit, we expanded the action up to second-order in the gradient terms and kept only the linear order term of the symmetry breaking contribution. Then, we drew an analogy of the resulting non-linear sigma model with the famous Heisenberg ferromagnetic system, where in our case the role of the symmetry breaking contribution is played by the frequency, which initially wants to drive the system towards the metallic saddle-point region. Having obtained the formal expression for the non-linear sigma model, we then moved to applications.

In the first part, within the framework of the supersymmetric non-linear sigma model, we demonstrated that the spectral correlations for the three Wigner-Dyson classes can be calculated from a local generating function. Such relation when applied for Anderson insulating wires revealed a simple way to connect the level-level correlations with the ground state wave function of the transfermatrix Hamiltonian and this allowed us to derive spectral correlation functions for all Wigner-Dyson classes. This result complemented the literature, which previously had only been contemplated with non-perturbative results for the unitary class.

From the experimental viewpoint, such result was not immediately possible to be verified, because the most versatile platform to investigate spectral correlations is based on ultra cold atoms, which are neutral. In this

sense, a theoretical result for the spectral correlations of systems endowed with time-reversal symmetry are the most prominent candidates to experimental verification. In addition to that, this work highlights the importance of symmetries in the localization properties of a low dimensional disordered system and opens up the possibility to provide a theoretical guideline for the experimental realization of systems with spin-orbit coupling which belongs to the symplectic symmetry class. This class is particularly interesting because it displays the Anderson metal-insulator transition even for dimensions as low as two.

A further interesting development of this work would be to derive the Schrödinger equation for higher-dimensional non-linear sigma models, which seems to be a formidable task, and use the local generating function approach in order to simplify the calculations. Furthermore, an important application for this local generating function is found in the study of phenomenon near the metal-insulator transition. The difficulty in this potential study lies in demonstrating that indeed the level-level correlations function only depends on a boundary contribution of the local generating function, because in this regime we can no longer bypass the calculations with the help of manipulations involving the Schrödinger equation.

In the second part, using the replica method, we explored the quantum transport properties of a hybrid structure consisting of two superconductors spatially separated by a sufficiently thin layer of a topological insulator. The choice to employ this method over the supersymmetric formalism is of purely convenience. To perform perturbative calculations, the replica method is more advantageous, because we are not required to compute a functional integration over an entire manifold. Advancing towards the development of the effective action, to determine the influence of the superconductor structure on the low-lying structure of our action, on top of our first saddle-point analysis, we performed a second saddle-point analysis which led us to the well known Usadel equation. Focusing on the homogeneous field configurations, we obtained the second saddle-point solution, which allowed us to analytically compute the current-phase relation in the following two limiting cases, the zero external magnetic flux and the strong magnetic flux (strong in the sense that the characteristic energy associated with the external magnetic flux is larger than the dwell energy, but smaller than the superconducting gap).

The result for the current-phase relation indicated that as we turn on and increase the strength of the external magnetic flux, any type of non-sinusoidal behavior becomes strongly suppressed. In the next step, around this new saddle-point solution, we investigated the behavior of the current fluctuations in the same limiting cases we studied the current-phase relation and also for systems with zero and quasi-one-dimensional geometries. For this observable, we obtained that the fluctuations are stronger in the zero-dimensional than the quasi-one-dimensional limit and this has to do with the required additional momentum integration present in the latter. In addition to that, the same pattern observed in the current-phase relation also materializes in this observable, the fluctuations become strongly suppressed as we increase the external magnetic flux.

This work opens up a few research gaps that would be interesting to be addressed in future investigations. To further determine the influence of the order parameter on the low-lying structure of the non-linear sigma model action, we subjected the action to a second saddle-point analysis within the first saddle-point, but we restricted ourselves to consider only homogeneous field configurations and this led us to the Usadel equation which was possible to solve algebraically. An immediate and welcome improvement to this calculation would be to consider a more elaborated scheme involving non-homogeneous field configurations. However, instead of an algebraic equation, one will have to deal with the complete Usadel equation, which is a non-linear partial differential equation notoriously difficult to solve. Nevertheless, a numerical solution may still be

within the reach of our computational resources and perhaps it is even possible to obtain analytical solutions within certain limiting cases. In addition to that, we constructed a Hamiltonian in which the surface and bulk were fully decoupled from each other and, as the experimental data shows, there is an interesting interplay among the two-dimensional electron gas states with the helical surface states and the insulating bulk, whose consequences are manifested in the critical current, drastically changing it behavior. In this sense, a further improvement for our study would be the inclusion of a finite surface-bulk coupling. As it has already been reported in the literature of topological insulators, this can be done by assuming that the coupling between the surface and the bulk occurs randomly, the local tunneling operator can then be modeled as a random matrix belonging to the symplectic symmetry class. A further field of research that has attracted much attention recently is the Josephson diode. This technology relies on a Hamiltonian whose construction is quite similar to the one we explored in our study. It is possible that in the study of short junctions, the framework developed in here to investigate the quantum transport properties and fluctuations in these system may provide a platform to future studies of this recent technology.

Bibliography

[AB02] I. L. Aleiner and Ya. M. Blanter. "Inelastic scattering time for conductance fluctuations". In: *Phys. Rev. B* 65.11 (Feb. 28, 2002). Publisher: American Physical Society, p. 115317. DOI: 10.1103/PhysRevB.65.115317. URL: https://link.aps.org/doi/10.1103/PhysRevB.65.115317 (visited on 05/11/2022).

[ABK15] Alexander Altland, Dmitry Bagrets, and Alex Kamenev. "Topology versus Anderson localization: Nonperturbative solutions in one dimension". In: *Phys. Rev. B* 91.8 (Feb. 27, 2015). Publisher: American Physical Society, p. 085429. DOI: 10.1103/PhysRevB.91.085429. URL: https://link.aps.org/doi/10.1103/PhysRevB.91.085429 (visited on 05/02/2022).

[Abr+79] E. Abrahams et al. "Scaling Theory of Localization: Absence of Quantum Diffusion in Two Dimensions". In: *Phys. Rev. Lett.* 42.10 (Mar. 5, 1979). Publisher: American Physical Society, pp. 673–676. DOI: 10.1103/PhysRevLett.42.673. URL: https://link.aps.org/doi/10.1103/PhysRevLett.42.673 (visited on 05/02/2022).

[AC97] Hubert Ammann and Nelson Christensen. "Delta Kick Cooling: A New Method for Cooling Atoms". In: *Phys. Rev. Lett.* 78.11 (Mar. 17, 1997). Publisher: American Physical Society, pp. 2088–2091. DOI: 10.1103/PhysRevLett.78.2088. URL: https://link.aps.org/doi/10.1103/PhysRevLett.78.2088 (visited on 06/23/2022).

[AE06] I. L. Aleiner and K. B. Efetov. "Effect of Disorder on Transport in Graphene". In: *Phys. Rev. Lett.* 97.23 (Dec. 4, 2006). Publisher: American Physical Society, p. 236801. DOI: 10.1103/PhysRevLett.97.236801. URL: https://link.aps.org/doi/10.1103/PhysRevLett.97.236801 (visited on 05/19/2022).

[AF95] Alexander Altland and Dirk Fuchs. "Spectral Statistics of Mesoscopic Wires: Crossover from Wigner-Dyson to Poisson Regime". In: *Phys. Rev. Lett.* 74.21 (May 22, 1995). Publisher: American Physical Society, pp. 4269–4272. DOI: 10.1103/PhysRevLett.74.4269. URL: https://link.aps.org/doi/10.1103/PhysRevLett.74.4269 (visited on 05/17/2022).

[AG61] A. A. Abrikosov and L. P. Gor'kov. "On the Problem of the Knight Shift in Superconductors". In: 12 (1961), p. 3.

[AI77] A. Aharony and Y. Imry. "The mobility edge as a spin-glass problem". In: *J. Phys. C: Solid State Phys.* 10.17 (Sept. 1977). Publisher: IOP Publishing, pp. L487–L492. ISSN: 0022-3719. DOI: 10.1088/0022-3719/10/17/005. URL: https://doi.org/10.1088/0022-3719/10/17/005 (visited on 05/02/2022).

[Al'85] B. L. Al'tshuler. "Fluctuations in the extrinsic conductivity of disordered conductors". In: *Soviet Journal of Experimental and Theoretical Physics Letters* 41 (June 1, 1985). ADS Bibcode: 1985JETPL..41..648A, p. 648. ISSN: 0021-3640. URL: https://ui.adsabs.harvard.edu/abs/1985JETPL..41..648A (visited on 05/18/2022).

[Al'+88] B L Al'tshuler et al. "Repulsion between energy levels and the metal-insulator transition". In: 67 (1988), p. 7.

[ALO68] L. G. Aslamazov, A. I. Larkin, and Y. N. Ovchinnikov. "Josephson effect in superconductors separated by a normal metal". In: *Zh. Eksp. Teor. Fiz.* 55 (July 1, 1968). Institution: Inst. of Theoretical Physics, Moscow. URL: https://www.osti.gov/biblio/7368038 (visited on 05/19/2022).

[AM07] Eric Akkermans and Gilles Montambaux. *Mesoscopic Physics of Electrons and Photons*. Cambridge: Cambridge University Press, 2007. ISBN: 978-0-521-85512-9. DOI: 10.1017/CBO9780511618833. URL: https://www.cambridge.org/core/books/mesoscopic-physics-of-electrons-and-photons/49F9FB8AF5E5AFFA23FA6F309BA9A046 (visited on 05/16/2022).

[AMG18] Fangzhao Alex An, Eric J. Meier, and Bryce Gadway. "Engineering a Flux-Dependent Mobility Edge in Disordered Zigzag Chains". In: *Phys. Rev. X* 8.3 (Aug. 17, 2018). Publisher: American Physical Society, p. 031045. DOI: 10.1103/PhysRevX.8.031045. URL: https://link.aps.org/doi/10.1103/PhysRevX.8.031045 (visited on 07/28/2022).

[AN98] Tsuneya Ando and Takeshi Nakanishi. "Impurity Scattering in Carbon Nanotubes – Absence of Back Scattering –". In: *J. Phys. Soc. Jpn.* 67.5 (May 15, 1998). Publisher: The Physical Society of Japan, pp. 1704–1713. ISSN: 0031-9015. DOI: 10.1143/JPSJ.67.1704. URL: https://journals.jps.jp/doi/10.1143/JPSJ.67.1704 (visited on 11/06/2022).

[And58] P. W. Anderson. "Absence of Diffusion in Certain Random Lattices". In: *Phys. Rev.* 109.5 (Mar. 1, 1958). Publisher: American Physical Society, pp. 1492–1505. DOI: 10.1103/PhysRev.109.1492. URL: https://link.aps.org/doi/10.1103/PhysRev.109.1492 (visited on 05/15/2022).

[AS02] Tsuneya Ando and Hidekatsu Suzuura. "Presence of Perfectly Conducting Channel in Metallic Carbon Nanotubes". In: *J. Phys. Soc. Jpn.* 71.11 (Nov. 15, 2002). Publisher: The Physical Society of Japan, pp. 2753–2760. ISSN: 0031-9015. DOI: 10.1143/JPSJ.71.2753. URL: https://journals.jps.jp/doi/10.1143/JPSJ.71.2753 (visited on 11/06/2022).

[AS10] Alexander Altland and Ben D. Simons. *Condensed Matter Field Theory*. 2nd ed. Cambridge: Cambridge University Press, 2010. ISBN: 978-0-521-76975-4. DOI: 10.1017/CBO9780511789984. URL: https://www.cambridge.org/core/books/condensed-matter-field-theory/0A8DE6503ED868D96985D9E7847C63FF (visited on 05/16/2022).

[AS86] O. L. Al'tshuler and B. I. Shklovskii. "Repulsion of energy levels and conductivity of small metal samples". In: *Soviet Journal of Experimental and Theoretical Physics* 64 (July 1, 1986). ADS Bibcode: 1986JETP...64..127A, p. 127. ISSN: 1063-7761. URL: https://ui.adsabs.harvard.edu/abs/1986JETP...64..127A (visited on 05/18/2022).

[AS87] B. L. Al'tshuler and B. Z. Spivak. "Mesoscopic fluctuations in a superconductor-normal metal-superconductor junction". In: *Soviet Journal of Experimental and Theoretical Physics* 65 (Feb. 1, 1987). ADS Bibcode: 1987JETP...65..343A, p. 343. ISSN: 1063-7761. URL: https://ui.adsabs.harvard.edu/abs/1987JETP...65..343A (visited on 05/19/2022).

[ASTS98] A. Altland, B. D. Simons, and D. Taras-Semchuk. "Field theory of mesoscopic fluctuations in superconductor/normal-metal systems". In: *Jetp Lett.* 67.1 (Jan. 1, 1998), pp. 22–27. ISSN: 1090-6487. DOI: 10.1134/1.567622. URL: https://doi.org/10.1134/1.567622 (visited on 05/18/2022).

[AZ97] Alexander Altland and Martin R. Zirnbauer. "Nonstandard symmetry classes in mesoscopic normal-superconducting hybrid structures". In: *Phys. Rev. B* 55.2 (Jan. 1, 1997). Publisher: American Physical Society, pp. 1142–1161. DOI: 10.1103/PhysRevB.55.1142. URL: https://link.aps.org/doi/10.1103/PhysRevB.55.1142 (visited on 05/19/2022).

[BA12] Dmitry Bagrets and Alexander Altland. "Class D Spectral Peak in Majorana Quantum Wires". In: *Phys. Rev. Lett.* 109.22 (Nov. 29, 2012). Publisher: American Physical Society, p. 227005. DOI: 10.1103/PhysRevLett.109.227005. URL: https://link.aps.org/doi/10.1103/PhysRevLett.109.227005 (visited on 05/19/2022).

[BAA06] D. M. Basko, I. L. Aleiner, and B. L. Altshuler. "Metal–insulator transition in a weakly interacting many-electron system with localized single-particle states". In: *Annals of Physics* 321.5 (May 1, 2006), pp. 1126–1205. ISSN: 0003-4916. DOI: 10.1016/j.aop.2005.11.014. URL: https://www.sciencedirect.com/science/article/pii/S0003491605002630 (visited on 05/02/2022).

[BB95] P. W. Brouwer and C. W. J. Beenakker. "Insensitivity to time-reversal symmetry breaking of universal conductance fluctuations with Andreev reflection". In: *Phys. Rev. B* 52.23 (Dec. 15, 1995). Publisher: American Physical Society, pp. 16772–16775. DOI: 10.1103/PhysRevB.52.16772. URL: https://link.aps.org/doi/10.1103/PhysRevB.52.16772 (visited on 05/18/2022).

[BB97] P. W. Brouwer and C. W. J. Beenakker. "Anomalous temperature dependence of the supercurrent through a chaotic Josephson junction". In: *Chaos, Solitons & Fractals*. Chaos and Quantum Transport in Mesoscopic Cosmos 8.7 (July 1, 1997), pp. 1249–1260. ISSN: 0960-0779. DOI: 10.1016/S0960-0779(97)00018-0. URL: https://www.sciencedirect.com/science/article/pii/S0960077997000180 (visited on 05/19/2022).

[BBS96] W. Belzig, C. Bruder, and Gerd Schön. "Local density of states in a dirty normal metal connected to a superconductor". In: *Phys. Rev. B* 54.13 (Oct. 1, 1996). Publisher: American Physical Society, pp. 9443–9448. DOI: 10.1103/PhysRevB.54.9443. URL: https://link.aps.org/doi/10.1103/PhysRevB.54.9443 (visited on 05/18/2022).

[BC08] F. S. Bergeret and J. C. Cuevas. "The Vortex State and Josephson Critical Current of a Diffusive SNS Junction". In: *J Low Temp Phys* 153.5 (Dec. 1, 2008), pp. 304–324. ISSN: 1573-7357. DOI: 10.1007/s10909-008-9826-2. URL: https://doi.org/10.1007/s10909-008-9826-2 (visited on 05/19/2022).

[Bee91] C. W. J. Beenakker. "Universal limit of critical-current fluctuations in mesoscopic Josephson junctions". In: *Phys. Rev. Lett.* 67.27 (Dec. 30, 1991). Publisher: American Physical Society, pp. 3836–3839. DOI: 10.1103/PhysRevLett.67.3836. URL: https://link.aps.org/doi/10.1103/PhysRevLett.67.3836 (visited on 05/18/2022).

[Bee97] C. W. J. Beenakker. "Random-matrix theory of quantum transport". In: *Rev. Mod. Phys.* 69.3 (July 1, 1997). Publisher: American Physical Society, pp. 731–808. DOI: 10.1103/RevModPhys.69.731. URL: https://link.aps.org/doi/10.1103/RevModPhys.69.731 (visited on 05/18/2022).

[BHL94] J. Bruun, V. C. Hui, and C. J. Lambert. "Coherence-length dependence of fluctuations in the conductance of normal-superconducting interfaces". In: *Phys. Rev. B* 49.6 (Feb. 1, 1994). Publisher: American Physical Society, pp. 4010–4014. DOI: 10.1103/PhysRevB.49.4010. URL: https://link.aps.org/doi/10.1103/PhysRevB.49.4010 (visited on 05/18/2022).

[Bil+08] Juliette Billy et al. "Direct observation of Anderson localization of matter waves in a controlled disorder". In: *Nature* 453 (June 1, 2008). ADS Bibcode: 2008Natur.453..891B, pp. 891–894. ISSN: 0028-0836. DOI: 10.1038/nature07000. URL: https://ui.adsabs.harvard.edu/abs/2008Natur.453..891B (visited on 05/19/2022).

[BNA00] I. S. Beloborodov, B. N. Narozhny, and I. L. Aleiner. "Effect of Time Reversal Symmetry Breaking on the Density of States in Small Superconducting Grains". In: *Phys. Rev. Lett.* 85.4 (July 24, 2000). Publisher: American Physical Society, pp. 816–819. DOI: 10.1103/PhysRevLett.85.816. URL: https://link.aps.org/doi/10.1103/PhysRevLett.85.816 (visited on 05/19/2022).

[Boh91] Oriol Bohigas. *Random Matrix Theories and Chaotic Dynamics*. Elsevier Science Publishers, 1991. 116 pp. URL: https://inis.iaea.org/collection/NCLCollectionStore/_Public/23/079/23079901.pdf.

[BP82] Antonio Barone and Gianfranco Paterno. *Physics and Applications of the Josephson Effect*. 1st edition. New York: Wiley-VCH, May 14, 1982. 529 pp. ISBN: 978-0-471-01469-0.

[Cap+13] Thibaut Capron et al. "Ergodic versus diffusive decoherence in mesoscopic devices". In: *Phys. Rev. B* 87.4 (Jan. 29, 2013). Publisher: American Physical Society, p. 041307. DOI: 10.1103/PhysRevB.87.041307. URL: https://link.aps.org/doi/10.1103/PhysRevB.87.041307 (visited on 05/11/2022).

[CD13] Nicolas Cherroret and Dominique Delande. "Backscattering echo of correlated wave packets". In: *Phys. Rev. A* 88.3 (Sept. 12, 2013). Publisher: American Physical Society, p. 035602. DOI: 10.1103/PhysRevA.88.035602. URL: https://link.aps.org/doi/10.1103/PhysRevA.88.035602 (visited on 06/23/2022).

[CGS89] Giulio Casati, Italo Guarneri, and D. L. Shepelyansky. "Anderson Transition in a One-Dimensional System with Three Incommensurate Frequencies". In: *Phys. Rev. Lett.* 62.4 (Jan. 23, 1989), pp. 345–348. ISSN: 0031-9007. DOI: 10.1103/PhysRevLett.62.345. URL: https://link.aps.org/doi/10.1103/PhysRevLett.62.345 (visited on 04/30/2022).

[Cha+08] Julien Chabé et al. "Experimental Observation of the Anderson Metal-Insulator Transition with Atomic Matter Waves". In: *Physical Review Letters* 101 (Dec. 1, 2008). ADS Bibcode: 2008PhRvL.101y5702C, p. 255702. ISSN: 0031-9007. DOI: 10.1103/PhysRevLett.101.255702. URL: https://ui.adsabs.harvard.edu/abs/2008PhRvL.101y5702C (visited on 05/19/2022).

[Che+12] Nicolas Cherroret et al. "Coherent backscattering of ultracold matter waves: Momentum space signatures". In: *Phys. Rev. A* 85.1 (Jan. 10, 2012). Publisher: American Physical Society, p. 011604. DOI: 10.1103/PhysRevA.85.011604. URL: https://link.aps.org/doi/10.1103/PhysRevA.85.011604 (visited on 06/22/2022).

[Cho+13] Sungjae Cho et al. "Symmetry protected Josephson supercurrents in three-dimensional topological insulators". In: *Nat Commun* 4.1 (Apr. 9, 2013). Number: 1 Publisher: Nature Publishing Group, p. 1689. ISSN: 2041-1723. DOI: 10.1038/ncomms2701. URL: https://www.nature.com/articles/ncomms2701 (visited on 05/18/2022).

[CM93] J. T. Chalker and A. M. S. Macêdo. "Complete characterization of universal fluctuations in quasi-one-dimensional mesoscopic conductors". In: *Phys. Rev. Lett.* 71.22 (Nov. 29, 1993). Publisher: American Physical Society, pp. 3693–3696. DOI: 10.1103/PhysRevLett.71.3693. URL: https://link.aps.org/doi/10.1103/PhysRevLett.71.3693 (visited on 05/18/2022).

[Col15] Piers Coleman. *Introduction to Many-Body Physics*. New York, NY: Cambridge University Press, Nov. 26, 2015. ISBN: 978-0-521-86488-6.

[CSG00] A. A. Chabanov, M. Stoytchev, and A. Z. Genack. "Statistical signatures of photon localization". In: *Nature* 404.6780 (Apr. 2000). Number: 6780 Publisher: Nature Publishing Group, pp. 850–853. ISSN: 1476-4687. DOI: 10.1038/35009055. URL: https://www.nature.com/articles/35009055 (visited on 06/22/2022).

[Day+16] Ian M. Dayton et al. "Scanning tunneling microscopy of superconducting topological surface states in Bi_2Se_3". In: *Phys. Rev. B* 93.22 (June 20, 2016). Publisher: American Physical Society, p. 220506. DOI: 10.1103/PhysRevB.93.220506. URL: https://link.aps.org/doi/10.1103/PhysRevB.93.220506 (visited on 05/19/2022).

[Dor84] O. N. Dorokhov. "On the coexistence of localized and extended electronic states in the metallic phase". In: *Solid State Communications* 51.6 (Aug. 1, 1984), pp. 381–384. ISSN: 0038-1098. DOI: 10.1016/0038-1098(84)90117-0. URL: https://www.sciencedirect.com/science/article/pii/0038109884901170 (visited on 05/18/2022).

[DSV13] Wade DeGottardi, Diptiman Sen, and Smitha Vishveshwara. "Majorana Fermions in Superconducting 1D Systems Having Periodic, Quasiperiodic, and Disordered Potentials". In: *Physical Review Letters* 110 (Apr. 1, 2013). ADS Bibcode: 2013PhRvL.110n6404D, p. 146404. ISSN: 0031-9007. DOI: 10.1103/PhysRevLett.110.146404. URL: https://ui.adsabs.harvard.edu/abs/2013PhRvL.110n6404D (visited on 05/19/2022).

[Dys62] Freeman J. Dyson. "The Threefold Way. Algebraic Structure of Symmetry Groups and Ensembles in Quantum Mechanics". In: *J. Math. Phys.* 3.6 (Nov. 1962). Publisher: American Institute of Physics, pp. 1199–1215. ISSN: 0022-2488. DOI: 10.1063/1.1703863. URL: https://aip.scitation.org/doi/10.1063/1.1703863 (visited on 05/11/2022).

[EA75] S. F. Edwards and P. W. Anderson. "Theory of spin glasses". In: *J. Phys. F: Met. Phys.* 5.5 (May 1975). Publisher: IOP Publishing, pp. 965–974. ISSN: 0305-4608. DOI: 10.1088/0305-4608/5/5/017. URL: https://doi.org/10.1088/0305-4608/5/5/017 (visited on 05/02/2022).

[EE92] S. N. Evangelou and E. N. Economou. "Spectral density singularities, level statistics, and localization in a sparse random matrix ensemble". In: *Phys. Rev. Lett.* 68.3 (Jan. 20, 1992). Publisher: American Physical Society, pp. 361–364. DOI: 10.1103/PhysRevLett.68.361. URL: https://link.aps.org/doi/10.1103/PhysRevLett.68.361 (visited on 05/02/2022).

[Efe82] K. B. Efetov. "Statistics of the levels in small metallic particles". In: *Soviet Journal of Experimental and Theoretical Physics* 56 (Aug. 1, 1982). ADS Bibcode: 1982JETP...56..467E, p. 467. ISSN: 1063-7761. URL: https://ui.adsabs.harvard.edu/abs/1982JETP...56..467E (visited on 05/19/2022).

[Efe83] K. B. Efetov. "Supersymmetry and theory of disordered metals". In: *Advances in Physics* 32 (Nov. 1, 1983). ADS Bibcode: 1983AdPhy..32...53E, pp. 53–127. ISSN: 0001-8732. DOI: 10.1080/00018738300101531. URL: https://ui.adsabs.harvard.edu/abs/1983AdPhy..32...53E (visited on 05/19/2022).

[Efe96] K. B. Efetov. *Supersymmetry method in localization theory*. Pages: 194-201 Publication Title: 30 Years of the Landau Institute - Selected Papers. Edited by KHALATNIKOV ISAAK M ET AL. Published by World Scientific Publishing Co. Pte. Ltd ADS Bibcode: 1996tyli.book..194E. Jan. 1, 1996. DOI: 10.1142/9789814317344_0027. URL: https://ui.adsabs.harvard.edu/abs/1996tyli.book..194E (visited on 05/18/2022).

[Efe99] K. B. Efetov. *Supersymmetry in Disorder and Chaos*. Publication Title: Supersymmetry in Disorder and Chaos ADS Bibcode: 1999sdc..book.....E. Dec. 1, 1999. 457 pp. URL: https://ui.adsabs.harvard.edu/abs/1999sdc..book.....E (visited on 05/19/2022).

[EKL80] K. B. Efetov, D. E. Khernl'nitskil, and A. I. Larkin. "Interaction of diffusion modes in the theory of localization". In: (1980), p. 7.

[EL83] K. B. Efetov and A. I. Larkin. "Kinetics of a quantum particle In a long metallic wire". In: *Soviet Journal of Experimental and Theoretical Physics* 58 (Aug. 1, 1983). ADS Bibcode: 1983JETP...58..444E, p. 444. ISSN: 1063-7761. URL: https://ui.adsabs.harvard.edu/abs/1983JETP...58..444E (visited on 05/19/2022).

[Eme75] V. J. Emery. "Critical properties of many-component systems". In: *Phys. Rev. B* 11.1 (Jan. 1, 1975). Publisher: American Physical Society, pp. 239–247. DOI: 10.1103/PhysRevB.11.239. URL: https://link.aps.org/doi/10.1103/PhysRevB.11.239 (visited on 05/10/2022).

[Fin+14] A.D.K. Finck et al. "Phase Coherence and Andreev Reflection in Topological Insulator Devices". In: *Phys. Rev. X* 4.4 (Nov. 4, 2014). Publisher: American Physical Society, p. 041022. DOI: 10.1103/PhysRevX.4.041022. URL: https://link.aps.org/doi/10.1103/PhysRevX.4.041022 (visited on 05/18/2022).

[FLS71] Richard P. Feynman, Robert B. Leighton, and Matthew Sands. *The Feynman Lectures on Physics, Vol. 3*. Later Printing edition. Reading/Mass.: Addison Wesley, Jan. 11, 1971. 379 pp. ISBN: 978-0-201-02118-9.

[FM91] Yan V. Fyodorov and Alexander D. Mirlin. "Scaling properties of localization in random band matrices: A σ-model approach". In: *Phys. Rev. Lett.* 67.18 (Oct. 28, 1991). Publisher: American Physical Society, pp. 2405–2409. DOI: 10.1103/PhysRevLett.67.2405. URL: https://link.aps.org/doi/10.1103/PhysRevLett.67.2405 (visited on 09/02/2022).

[Fra+96] K. M. Frahm et al. "Effect of the Coupling to a Superconductor on the Level Statistics of a Metal Grain in a Magnetic Field". In: *Phys. Rev. Lett.* 76.16 (Apr. 15, 1996). Publisher: American Physical Society, pp. 2981–2984. DOI: 10.1103/PhysRevLett.76.2981. URL: https://link.aps.org/doi/10.1103/PhysRevLett.76.2981 (visited on 05/19/2022).

[FS12] M. V. Feigel'man and M. A. Skvortsov. "Universal Broadening of the Bardeen-Cooper-Schrieffer Coherence Peak of Disordered Superconducting Films". In: *Phys. Rev. Lett.* 109.14 (Oct. 3, 2012). Publisher: American Physical Society, p. 147002. DOI: 10.1103/PhysRevLett.109.147002. URL: https://link.aps.org/doi/10.1103/PhysRevLett.109.147002 (visited on 05/19/2022).

[Gar17] Jean-Claude Garreau. "Quantum simulation of disordered systems with cold atoms". In: *Comptes Rendus Physique*. Prizes of the French Academy of Sciences 2015 / Prix de l'Académie des sciences 2015 18.1 (Jan. 1, 2017), pp. 31–46. ISSN: 1631-0705. DOI: 10.1016/j.crhy.2016.09.002. URL: https://www.sciencedirect.com/science/article/pii/S1631070516301426 (visited on 05/02/2022).

[GG12] Ion Garate and Leonid Glazman. "Weak localization and antilocalization in topological insulator thin films with coherent bulk-surface coupling". In: *Phys. Rev. B* 86.3 (July 16, 2012). Publisher: American Physical Society, p. 035422. DOI: 10.1103/PhysRevB.86.035422. URL: https://link.aps.org/doi/10.1103/PhysRevB.86.035422 (visited on 05/19/2022).

[Gho+14] S. Ghosh et al. "Coherent forward scattering in two-dimensional disordered systems". In: *Physical Review A* 90 (Dec. 1, 2014). ADS Bibcode: 2014PhRvA..90f3602G, p. 063602. ISSN: 1050-29470556-2791. DOI: 10.1103/PhysRevA.90.063602. URL: https://ui.adsabs.harvard.edu/abs/2014PhRvA..90f3602G (visited on 05/19/2022).

[GKI04] A. A. Golubov, M. Yu. Kupriyanov, and E. Il'ichev. "The current-phase relation in Josephson junctions". In: *Rev. Mod. Phys.* 76.2 (Apr. 26, 2004). Publisher: American Physical Society, pp. 411–469. DOI: 10.1103/RevModPhys.76.411. URL: https://link.aps.org/doi/10.1103/RevModPhys.76.411 (visited on 05/19/2022).

[GMP05] I. V. Gornyi, A. D. Mirlin, and D. G. Polyakov. "Interacting Electrons in Disordered Wires: Anderson Localization and Low-T Transport". In: *Phys. Rev. Lett.* 95.20 (Nov. 8, 2005). Publisher: American Physical Society, p. 206603. DOI: 10.1103/PhysRevLett.95.206603. URL: https://link.aps.org/doi/10.1103/PhysRevLett.95.206603 (visited on 05/02/2022).

[GMW01] I. V. Gornyi, A. D. Mirlin, and P. Wölfle. "Current correlations and quantum localization in two-dimensional disordered systems with broken time-reversal invariance". In: *Phys. Rev. B* 64.11 (Aug. 16, 2001). Publisher: American Physical Society, p. 115403. DOI: 10.1103/PhysRevB.64.115403. URL: https://link.aps.org/doi/10.1103/PhysRevB.64.115403 (visited on 07/12/2022).

[Gro+09] C. W. Groth et al. "Theory of the Topological Anderson Insulator". In: *Phys. Rev. Lett.* 103.19 (Nov. 6, 2009). Publisher: American Physical Society, p. 196805. DOI: 10.1103/PhysRevLett.103.196805. URL: https://link.aps.org/doi/10.1103/PhysRevLett.103.196805 (visited on 05/02/2022).

[Gu96] S. Guéron et al. "Superconducting Proximity Effect Probed on a Mesoscopic Length Scale". In: *Phys. Rev. Lett.* 77.14 (Sept. 30, 1996). Publisher: American Physical Society, pp. 3025–3028. DOI: 10.1103/PhysRevLett.77.3025. URL: https://link.aps.org/doi/10.1103/PhysRevLett.77.3025 (visited on 12/02/2022).

[G5] L. P. Gor'kov and G. M. Éliashberg. "Minute Metallic Particles in an Electromagnetic Field". In: *Soviet Journal of Experimental and Theoretical Physics* 21 (Nov. 1, 1965). ADS Bibcode: 1965JETP...21..940G, p. 940. ISSN: 1063-7761. URL: https://ui.adsabs.harvard.edu/abs/1965JETP...21..940G (visited on 05/19/2022).

[Hai+18] Clément Hainaut et al. "Controlling symmetry and localization with an artificial gauge field in a disordered quantum system". In: *Nat Commun* 9.1 (Apr. 11, 2018). Number: 1 Publisher: Nature Publishing Group, p. 1382. ISSN: 2041-1723. DOI: 10.1038/s41467-018-03481-9. URL: https://www.nature.com/articles/s41467-018-03481-9 (visited on 05/07/2022).

[Ham+07] J. C. Hammer et al. "Density of states and supercurrent in diffusive SNS junctions: Roles of nonideal interfaces and spin-flip scattering". In: *Phys. Rev. B* 76.6 (Aug. 14, 2007). Publisher: American Physical Society, p. 064514. DOI: 10.1103/PhysRevB.76.064514. URL: https://link.aps.org/doi/10.1103/PhysRevB.76.064514 (visited on 05/18/2022).

[Har+96] S. G. den Hartog et al. "Sample-Specific Conductance Fluctuations Modulated by the Superconducting Phase". In: *Phys. Rev. Lett.* 76.24 (June 10, 1996). Publisher: American Physical Society, pp. 4592–4595. DOI: 10.1103/PhysRevLett.76.4592. URL: https://link.aps.org/doi/10.1103/PhysRevLett.76.4592 (visited on 05/18/2022).

[Hec+97] Klaus Hecker et al. "Conductance Fluctuations in Mesoscopic Normal-Metal/Superconductor Samples". In: *Phys. Rev. Lett.* 79.8 (Aug. 25, 1997). Publisher: American Physical Society, pp. 1547–1550. DOI: 10.1103/PhysRevLett.79.1547. URL: https://link.aps.org/doi/10.1103/PhysRevLett.79.1547 (visited on 05/18/2022).

[Heg+20] Suraj S. Hegde et al. "A topological Josephson junction platform for creating, manipulating, and braiding Majorana bound states". In: *Annals of Physics* 423 (Dec. 1, 2020), p. 168326. ISSN: 0003-4916. DOI: 10.1016/j.aop.2020.168326. URL: https://www.sciencedirect.com/science/article/pii/S0003491620302608 (visited on 05/18/2022).

[HGK19] Fritz Haake, Sven Gnutzmann, and Marek Kuś. *Quantum Signatures of Chaos*. 4th ed. 2018 edition. New York, NY: Springer, Feb. 28, 2019. 685 pp. ISBN: 978-3-319-97579-5.

[Hik81] Shinobu Hikami. "Anderson localization in a nonlinear-σ-model representation". In: *Phys. Rev. B* 24.5 (Sept. 1, 1981). Publisher: American Physical Society, pp. 2671–2679. DOI: 10.1103/PhysRevB.24.2671. URL: https://link.aps.org/doi/10.1103/PhysRevB.24.2671 (visited on 05/05/2022).

[HS08] Manuel Houzet and Mikhail A. Skvortsov. "Mesoscopic fluctuations of the supercurrent in diffusive Josephson junctions". In: *Phys. Rev. B* 77.2 (Jan. 28, 2008). Publisher: American Physical Society, p. 024525. DOI: 10.1103/PhysRevB.77.024525. URL: https://link.aps.org/doi/10.1103/PhysRevB.77.024525 (visited on 05/18/2022).

[Hu+08] Hefei Hu et al. "Localization of ultrasound in a three-dimensional elastic network". In: *Nature Phys* 4.12 (Dec. 2008). Number: 12 Publisher: Nature Publishing Group, pp. 945–948. ISSN: 1745-2481. DOI: 10.1038/nphys1101. URL: https://www.nature.com/articles/nphys1101 (visited on 06/22/2022).

[Hub59] J. Hubbard. "Calculation of Partition Functions". In: *Phys. Rev. Lett.* 3.2 (July 15, 1959). Publisher: American Physical Society, pp. 77–78. DOI: 10.1103/PhysRevLett.3.77. URL: https://link.aps.org/doi/10.1103/PhysRevLett.3.77 (visited on 09/05/2022).

[Imr08] Yoseph Imry. *Introduction to Mesoscopic Physics*. 2nd edition. Oxford: Oxford University Press, Dec. 15, 2008. 254 pp. ISBN: 978-0-19-955269-6.

[Imr86] Y. Imry. "Active Transmission Channels and Universal Conductance Fluctuations". In: *EPL* 1.5 (Mar. 1986). Publisher: IOP Publishing, pp. 249–256. ISSN: 0295-5075. DOI: 10.1209/0295-5075/1/5/008. URL: https://doi.org/10.1209/0295-5075/1/5/008 (visited on 05/18/2022).

[IOF12] P. A. Ioselevich, P. M. Ostrovsky, and M. V. Feigel'man. "Majorana state on the surface of a disordered three-dimensional topological insulator". In: *Phys. Rev. B* 86.3 (July 26, 2012). Publisher: American Physical Society, p. 035441. DOI: 10.1103/PhysRevB.86.035441. URL: https://link.aps.org/doi/10.1103/PhysRevB.86.035441 (visited on 05/19/2022).

[Iva+12] D. A. Ivanov et al. "Hybridization of wave functions in one-dimensional localization". In: *Physical Review B* 85 (Jan. 1, 2012). ADS Bibcode: 2012PhRvB..85c5109I, p. 035109. ISSN: 0163-18291098-0121. DOI: 10.1103/PhysRevB.85.035109. URL: https://ui.adsabs.harvard.edu/abs/2012PhRvB..85c5109I (visited on 05/19/2022).

[Izr90] Felix M. Izrailev. "Simple models of quantum chaos: Spectrum and eigenfunctions". In: *Physics Reports* 196.5 (Nov. 1, 1990), pp. 299–392. ISSN: 0370-1573. DOI: 10.1016/0370-1573(90)90067-C. URL: https://www.sciencedirect.com/science/article/pii/037015739090067C (visited on 05/02/2022).

[Jen+12] F. Jendrzejewski et al. "Coherent Backscattering of Ultracold Atoms". In: *Physical Review Letters* 109 (Nov. 1, 2012). ADS Bibcode: 2012PhRvL.109s5302J, p. 195302. ISSN: 0031-9007. DOI: 10.1103/PhysRevLett.109.195302. URL: https://ui.adsabs.harvard.edu/abs/2012PhRvL.109s5302J (visited on 05/19/2022).

[Jos62] B. D. Josephson. "Possible new effects in superconductive tunnelling". In: *Physics Letters* 1.7 (July 1, 1962), pp. 251–253. ISSN: 0031-9163. DOI: 10.1016/0031-9163(62)91369-0. URL: https://www.sciencedirect.com/science/article/pii/0031916362913690 (visited on 07/26/2022).

[Jos64] B. D. Josephson. "Coupled Superconductors". In: *Rev. Mod. Phys.* 36.1 (Jan. 1, 1964). Publisher: American Physical Society, pp. 216–220. DOI: 10.1103/RevModPhys.36.216. URL: https://link.aps.org/doi/10.1103/RevModPhys.36.216 (visited on 07/26/2022).

[Jos65] B.D. Josephson. "Supercurrents through barriers". In: *Advances in Physics* 14.56 (Oct. 1, 1965). Publisher: Taylor & Francis _eprint: https://doi.org/10.1080/00018736500101091, pp. 419–451. ISSN: 0001-8732. DOI: 10.1080/00018736500101091. URL: https://doi.org/10.1080/00018736500101091 (visited on 07/26/2022).

[Kar+12] T. Karpiuk et al. "Coherent Forward Scattering Peak Induced by Anderson Localization". In: *Physical Review Letters* 109 (Nov. 1, 2012). ADS Bibcode: 2012PhRvL.109s0601K, p. 190601. ISSN: 0031-9007. DOI: 10.1103/PhysRevLett.109.190601. URL: https://ui.adsabs.harvard.edu/abs/2012PhRvL.109s0601K (visited on 05/19/2022).

[KL88] M.Yu. Kurpianov and V.F. Lukichev. "Influence of boundary transparency on the critical current of dirty SS'S structures". In: *Soviet Physics - JETP (English Translation)* 67.6 (1988). Place: United States INIS Reference Number: 22024754, pp. 1163–1168. ISSN: 0038-5646.

[KO17a] E. Khalaf and P. M. Ostrovsky. "Dynamics of Anderson localization in disordered wires". In: *Physical Review B* 96 (Nov. 1, 2017). ADS Bibcode: 2017PhRvB..96t1105K, p. 201105. ISSN: 0163-18291098-0121. DOI: 10.1103/PhysRevB.96.201105. URL: https://ui.adsabs.harvard.edu/abs/2017PhRvB..96t1105K (visited on 05/19/2022).

[KO17b] E. Khalaf and P.M. Ostrovsky. "Localization Effects on Magnetotransport of a Disordered Weyl Semimetal". In: *Phys. Rev. Lett.* 119.10 (Sept. 8, 2017). Publisher: American Physical Society, p. 106601. DOI: 10.1103/PhysRevLett.119.106601. URL: https://link.aps.org/doi/10.1103/PhysRevLett.119.106601 (visited on 07/27/2022).

[KS98] Hervé Kunz and Boris Shapiro. "Transition from Poisson to Gaussian unitary statistics: The two-point correlation function". In: *Phys. Rev. E* 58.1 (July 1, 1998). Publisher: American Physical Society, pp. 400–406. DOI: 10.1103/PhysRevE.58.400. URL: https://link.aps.org/doi/10.1103/PhysRevE.58.400 (visited on 09/02/2022).

[Kur+14] C. Kurter et al. "Dynamical gate-tunable supercurrents in topological Josephson junctions". In: *Phys. Rev. B* 90.1 (July 3, 2014). Publisher: American Physical Society, p. 014501. DOI: 10.1103/PhysRevB.90.014501. URL: https://link.aps.org/doi/10.1103/PhysRevB.90.014501 (visited on 05/18/2022).

[Kur+15] C. Kurter et al. "Evidence for an anomalous current–phase relation in topological insulator Josephson junctions". In: *Nat Commun* 6.1 (June 1, 2015). Number: 1 Publisher: Nature Publishing Group, p. 7130. ISSN: 2041-1723. DOI: 10.1038/ncomms8130. URL: https://www.nature.com/articles/ncomms8130 (visited on 05/18/2022).

[Lem+09] Gabriel Lemarié et al. "Observation of the Anderson metal-insulator transition with atomic matter waves: Theory and experiment". In: *Phys. Rev. A* 80.4 (Oct. 28, 2009). Publisher: American Physical Society, p. 043626. DOI: 10.1103/PhysRevA.80.043626. URL: https://link.aps.org/doi/10.1103/PhysRevA.80.043626 (visited on 08/01/2022).

[Lem+17] G. Lemarié et al. "Coherent backscattering and forward-scattering peaks in the quantum kicked rotor". In: *Physical Review A* 95 (Apr. 1, 2017). ADS Bibcode: 2017PhRvA..95d3626L, p. 043626. ISSN: 1050-29470556-2791. DOI: 10.1103/PhysRevA.95.043626. URL: https://ui.adsabs.harvard.edu/abs/2017PhRvA..95d3626L (visited on 05/19/2022).

[Lev08] Alex Levchenko. "Crossover in the local density of states of mesoscopic superconductor/normal-metal/superconductor junctions". In: *Phys. Rev. B* 77.18 (May 12, 2008). Publisher: American Physical Society, p. 180503. DOI: 10.1103/PhysRevB.77.180503. URL: https://link.aps.org/doi/10.1103/PhysRevB.77.180503 (visited on 05/18/2022).

[LGM14] Kean Loon Lee, Benoît Grémaud, and Christian Miniatura. "Dynamics of localized waves in one-dimensional random potentials: Statistical theory of the coherent forward scattering peak". In: *Physical Review A* 90 (Oct. 1, 2014). ADS Bibcode: 2014PhRvA..90d3605L, p. 043605. ISSN: 1050-29470556-2791. DOI: 10.1103/PhysRevA.90.043605. URL: https://ui.adsabs.harvard.edu/abs/2014PhRvA..90d3605L (visited on 05/19/2022).

[Li+09] Jian Li et al. "Topological Anderson Insulator". In: *Phys. Rev. Lett.* 102.13 (Apr. 1, 2009). Publisher: American Physical Society, p. 136806. DOI: 10.1103/PhysRevLett.102.136806. URL: https://link.aps.org/doi/10.1103/PhysRevLett.102.136806 (visited on 05/02/2022).

[LK82] A. I. Larkin and D. E. Khmel'nitskii. "Anderson localization and anomalous magnetoresistance at low temperatures". In: *Physics-Uspekhi* 25.3 (Mar. 1, 1982), pp. 185–187. ISSN: 1063-7869. URL: https://ufn.ru/en/articles/1982/3/h/ (visited on 06/29/2022).

[LKG06] Alex Levchenko, Alex Kamenev, and Leonid Glazman. "Singular length dependence of critical current in superconductor/normal-metal/superconductor bridges". In: *Phys. Rev. B* 74.21 (Dec. 29, 2006). Publisher: American Physical Society, p. 212509. DOI: 10.1103/PhysRevB.74.212509. URL: https://link.aps.org/doi/10.1103/PhysRevB.74.212509 (visited on 05/18/2022).

[LS00] A. Lamacraft and B. D. Simons. "Tail States in a Superconductor with Magnetic Impurities". In: *Phys. Rev. Lett.* 85.22 (Nov. 27, 2000). Publisher: American Physical Society, pp. 4783–4786. DOI: 10.1103/PhysRevLett.85.4783. URL: https://link.aps.org/doi/10.1103/PhysRevLett.85.4783 (visited on 05/19/2022).

[LS85] P. A. Lee and A. Douglas Stone. "Universal Conductance Fluctuations in Metals". In: *Phys. Rev. Lett.* 55.15 (Oct. 7, 1985). Publisher: American Physical Society, pp. 1622–1625. DOI: 10.1103/PhysRevLett.55.1622. URL: https://link.aps.org/doi/10.1103/PhysRevLett.55.1622 (visited on 05/19/2022).

[LSF87] P. A. Lee, A. Douglas Stone, and H. Fukuyama. "Universal conductance fluctuations in metals: Effects of finite temperature, interactions, and magnetic field". In: *Phys. Rev. B* 35.3 (Jan. 15, 1987). Publisher: American Physical Society, pp. 1039–1070. DOI: 10.1103/PhysRevB.35.1039. URL: https://link.aps.org/doi/10.1103/PhysRevB.35.1039 (visited on 05/18/2022).

[LTW09] Ad Lagendijk, Bart van Tiggelen, and Diederik S. Wiersma. "Fifty years of Anderson localization". In: *Physics Today* 62.8 (Aug. 2009). Publisher: American Institute of Physics, pp. 24–29. ISSN: 0031-9228. DOI: 10.1063/1.3206091. URL: https://physicstoday.scitation.org/doi/10.1063/1.3206091 (visited on 06/21/2022).

[Mar+22] Marcus Marinho et al. "Mesoscopic fluctuations in superconductor-topological insulator Josephson junctions". In: *Annals of Physics* (June 22, 2022), p. 168978. ISSN: 0003-4916. DOI: 10.1016/j.aop.2022.168978. URL: https://www.sciencedirect.com/science/article/pii/S0003491622001373 (visited on 10/10/2022).

[MBJ93] I. K. Marmorkos, C. W. J. Beenakker, and R. A. Jalabert. "Three signatures of phase-coherent Andreev reflection". In: *Phys. Rev. B* 48.4 (July 15, 1993). Publisher: American Physical Society, pp. 2811–2814. DOI: 10.1103/PhysRevB.48.2811. URL: https://link.aps.org/doi/10.1103/PhysRevB.48.2811 (visited on 05/18/2022).

[Meh04] Madan Lal Mehta. *Random Matrices, Volume 142, Third Edition*. 3rd edition. Academic Press, Nov. 29, 2004. 706 pp. ISBN: 978-1-4832-9989-1.

[Mic07] T. Micklitz. "Interface dependence of the Josephson-current fluctuations in short mesoscopic superconductor/normal-conductor/superconductor junctions". In: *Phys. Rev. B* 75.14 (Apr. 20, 2007). Publisher: American Physical Society, p. 144509. DOI: 10.1103/PhysRevB.75.144509. URL: https://link.aps.org/doi/10.1103/PhysRevB.75.144509 (visited on 05/18/2022).

[Mic16] T. Micklitz. "Spectral correlations in finite-size Anderson insulators". In: *Physical Review B* 93 (Mar. 1, 2016). ADS Bibcode: 2016PhRvB..93i4201M, p. 094201. ISSN: 0163-18291098-0121. DOI: 10.1103/PhysRevB.93.094201. URL: https://ui.adsabs.harvard.edu/abs/2016PhRvB..93i4201M (visited on 05/19/2022).

[Mir00] Alexander D. Mirlin. "Statistics of energy levels and eigenfunctions in disordered systems". In: *Physics Reports* 326.5 (Mar. 1, 2000), pp. 259–382. ISSN: 0370-1573. DOI: 10.1016/S0370-1573(99)00091-5. URL: https://www.sciencedirect.com/science/article/pii/S0370157399000915 (visited on 05/13/2022).

[MM18] M. Marinho and T. Micklitz. "Spectral correlations in Anderson insulating wires". In: *Phys. Rev. B* 97.4 (Jan. 11, 2018). Publisher: American Physical Society, p. 041406. DOI: 10.1103/PhysRevB.97.041406. URL: https://link.aps.org/doi/10.1103/PhysRevB.97.041406 (visited on 05/13/2022).

[MMA14] T. Micklitz, C. A. Müller, and A. Altland. "Strong Anderson Localization in Cold Atom Quantum Quenches". In: *Physical Review Letters* 112 (Mar. 1, 2014). ADS Bibcode: 2014PhRvL.112k0602M, p. 110602. ISSN: 0031-9007. DOI: 10.1103/PhysRevLett.112.110602. URL: https://ui.adsabs.harvard.edu/abs/2014PhRvL.112k0602M (visited on 05/19/2022).

[Mot70] N. F. Mott. "Conduction in non-Crystalline systems". In: *Philosophical Magazine* 22 (July 1, 1970). ADS Bibcode: 1970PMag...22....7M, pp. 7–29. ISSN: 0141-8610. DOI: 10.1080/14786437008228147 URL: https://ui.adsabs.harvard.edu/abs/1970PMag...22....7M (visited on 05/19/2022).

[MS01] J. S. Meyer and B. D. Simons. "Gap fluctuations in inhomogeneous superconductors". In: *Phys. Rev. B* 64.13 (Sept. 12, 2001). Publisher: American Physical Society, p. 134516. DOI: 10.1103/PhysRevB.64.134516. URL: https://link.aps.org/doi/10.1103/PhysRevB.64.134516 (visited on 05/19/2022).

[MS+14] Ian Mondragon-Shem et al. "Topological Criticality in the Chiral-Symmetric AIII Class at Strong Disorder". In: *Phys. Rev. Lett.* 113.4 (July 23, 2014). Publisher: American Physical Society, p. 046802. DOI: 10.1103/PhysRevLett.113.046802. URL: https://link.aps.org/doi/10.1103/PhysRevLett.113.046802 (visited on 05/02/2022).

[NA99] Takeshi Nakanishi and Tsuneya Ando. "Numerical Study of Impurity Scattering in Carbon Nanotubes". In: *J. Phys. Soc. Jpn.* 68.2 (Feb. 15, 1999). Publisher: The Physical Society of Japan, pp. 561–566. ISSN: 0031-9015. DOI: 10.1143/JPSJ.68.561. URL: https://journals.jps.jp/doi/10.1143/JPSJ.68.561 (visited on 11/06/2022).

[Naz99] Yuli V. Nazarov. "Novel circuit theory of Andreev reflection". In: *Superlattices and Microstructures* 25.5 (May 1, 1999), pp. 1221–1231. ISSN: 0749-6036. DOI: 10.1006/spmi.1999.0738. URL: https://www.sciencedirect.com/science/article/pii/S0749603699907383 (visited on 05/19/2022).

[NB09] Yuli V. Nazarov and Yaroslav M. Blanter. *Quantum Transport: Introduction to Nanoscience*. Illustrated edition. Cambridge University Press, May 28, 2009. 590 pp.

[OGM06] P. M. Ostrovsky, I. V. Gornyi, and A. D. Mirlin. "Electron transport in disordered graphene". In: *Phys. Rev. B* 74.23 (Dec. 28, 2006). Publisher: American Physical Society, p. 235443. DOI: 10.1103/PhysRevB.74.235443. URL: https://link.aps.org/doi/10.1103/PhysRevB.74.235443 (visited on 05/19/2022).

[Oht77] Hiroshi Ohta. "A self-consistent model of the Josephson junction". In: *A self-consistent model of the Josephson junction*. De Gruyter, 1977, pp. 35–50. ISBN: 978-3-11-088749-5. DOI: 10.1515/9783110887495-005. URL: https://doi.org/10.1515/9783110887495-005 (visited on 08/03/2022).

[OSF01] P. M. Ostrovsky, M. A. Skvortsov, and M. V. Feigel'man. "Density of States below the Thouless Gap in a Mesoscopic SNS Junction". In: *Phys. Rev. Lett.* 87.2 (June 22, 2001). Publisher: American Physical Society, p. 027002. DOI: 10.1103/PhysRevLett.87.027002. URL: https://link.aps.org/doi/10.1103/PhysRevLett.87.027002 (visited on 05/19/2022).

[Phi12] Philip Phillips. *Advanced Solid State Physics*. 2nd edition. Cambridge ; New York: Cambridge University Press, Apr. 9, 2012. 413 pp. ISBN: 978-0-521-19490-7.

[Por65] Charles E. Porter. *Statistical theories of spectra: fluctuations; a collection of reprints and original papers, with an introductory review*. Perspectives in physics. New York: Academic Press, 1965. 576 pp.

[Pri+94] V. N. Prigodin et al. "Mesoscopic dynamical echo in quantum dots". In: *Phys. Rev. Lett.* 72.4 (Jan. 24, 1994). Publisher: American Physical Society, pp. 546–549. DOI: 10.1103/PhysRevLett.72.546. URL: https://link.aps.org/doi/10.1103/PhysRevLett.72.546 (visited on 05/16/2022).

[PS79] G. Parisi and N. Sourlas. "Random Magnetic Fields, Supersymmetry, and Negative Dimensions". In: *Phys. Rev. Lett.* 43.11 (Sept. 10, 1979). Publisher: American Physical Society, pp. 744–745. DOI: 10.1103/PhysRevLett.43.744. URL: https://link.aps.org/doi/10.1103/PhysRevLett.43.744 (visited on 05/02/2022).

[Qu+12] Fanming Qu et al. "Strong Superconducting Proximity Effect in Pb−Bi_2Te_3 Hybrid Structures". In: *Sci Rep* 2.1 (Mar. 28, 2012). Number: 1 Publisher: Nature Publishing Group, p. 339. ISSN: 2045-2322. DOI: 10.1038/srep00339. URL: https://www.nature.com/articles/srep00339 (visited on 05/18/2022).

[Rac+19] Bryan Rachmilowitz et al. "Proximity-induced superconductivity in a topological crystalline insulator". In: *Phys. Rev. B* 100.24 (Dec. 4, 2019). Publisher: American Physical Society, p. 241402. DOI: 10.1103/PhysRevB.100.241402. URL: https://link.aps.org/doi/10.1103/PhysRevB.100.241402 (visited on 05/19/2022).

[Reu+14a] J. Reutlinger et al. "Secondary "smile"-gap in the density of states of a diffusive Josephson junction for a wide range of contact types". In: *Phys. Rev. B* 90.1 (July 31, 2014). Publisher: American Physical Society, p. 014521. DOI: 10.1103/PhysRevB.90.014521. URL: https://link.aps.org/doi/10.1103/PhysRevB.90.014521 (visited on 05/18/2022).

[Reu+14b] J. Reutlinger et al. ""Smile" Gap in the Density of States of a Cavity between Superconductors". In: *Phys. Rev. Lett.* 112.6 (Feb. 11, 2014). Publisher: American Physical Society, p. 067001. DOI: 10.1103/PhysRevLett.112.067001. URL: https://link.aps.org/doi/10.1103/PhysRevLett.112.067001 (visited on 05/18/2022).

[Reu+21] Johannes Reutlinger et al. *Universal Properties of Mesoscopic Fluctuations of the Secondary "Smile" Gap*. arXiv:2109.03055. type: article. arXiv, Sept. 7, 2021. DOI: 10.48550/arXiv.2109.03055. arXiv: 2109.03055[cond-mat]. URL: http://arxiv.org/abs/2109.03055 (visited on 05/18/2022).

[Roa+08] Giacomo Roati et al. "Anderson localization of a non-interacting Bose-Einstein condensate". In: *Nature* 453 (June 1, 2008). ADS Bibcode: 2008Natur.453..895R, pp. 895–898. ISSN: 0028-0836. DOI: 10.1038/nature07071. URL: https://ui.adsabs.harvard.edu/abs/2008Natur.453..895R (visited on 05/19/2022).

[Row63] J. M. Rowell. "Magnetic Field Dependence of the Josephson Tunnel Current". In: *Phys. Rev. Lett.* 11.5 (Sept. 1, 1963). Publisher: American Physical Society, pp. 200–202. DOI: 10.1103/PhysRevLett.11.200. URL: https://link.aps.org/doi/10.1103/PhysRevLett.11.200 (visited on 11/22/2022).

[RP60] Norbert Rosenzweig and Charles E. Porter. ""Repulsion of Energy Levels" in Complex Atomic Spectra". In: *Phys. Rev.* 120.5 (Dec. 1, 1960). Publisher: American Physical Society, pp. 1698–1714. DOI: 10.1103/PhysRev.120.1698. URL: https://link.aps.org/doi/10.1103/PhysRev.120.1698 (visited on 09/02/2022).

[Sac+11] Benjamin Sacépé et al. "Gate-tuned normal and superconducting transport at the surface of a topological insulator". In: *Nat Commun* 2.1 (Dec. 6, 2011). Number: 1 Publisher: Nature Publishing Group, p. 575. ISSN: 2041-1723. DOI: 10.1038/ncomms1586. URL: https://www.nature.com/articles/ncomms1586 (visited on 05/18/2022).

[Sch+08] Andreas P. Schnyder et al. "Classification of topological insulators and superconductors in three spatial dimensions". In: *Phys. Rev. B* 78.19 (Nov. 26, 2008). Publisher: American Physical Society, p. 195125. DOI: 10.1103/PhysRevB.78.195125. URL: https://link.aps.org/doi/10.1103/PhysRevB.78.195125 (visited on 07/25/2022).

[Sed+20] Nicholas Sedlmayr et al. *Dirac surface states in superconductors: a dual topological proximity effect*. arXiv:1805.12330. type: article. arXiv, Apr. 9, 2020. DOI: 10.48550/arXiv.1805.12330. arXiv: 1805.12330[cond-mat]. URL: http://arxiv.org/abs/1805.12330 (visited on 05/19/2022).

[Shk+93] B. I. Shklovskii et al. "Statistics of spectra of disordered systems near the metal-insulator transition". In: *Phys. Rev. B* 47.17 (May 1, 1993). Publisher: American Physical Society, pp. 11487–11490. DOI: 10.1103/PhysRevB.47.11487. URL: https://link.aps.org/doi/10.1103/PhysRevB.47.11487 (visited on 05/02/2022).

[SI87] U. Sivan and Y. Imry. "Energy-level correlation function and ac conductivity of a finite disordered system". In: *Physical Review B* 35 (Apr. 1, 1987). ADS Bibcode: 1987PhRvB..35.6074S, pp. 6074–6083. ISSN: 0163-18291098-0121. DOI: 10.1103/PhysRevB.35.6074. URL: https://ui.adsabs.harvard.edu/abs/1987PhRvB..35.6074S (visited on 05/19/2022).

[SL21] Nicholas Sedlmayr and Alex Levchenko. "Hybridization mechanism of the dual proximity effect in superconductor–topological insulator interfaces". In: *Solid State Communications* 327 (Mar. 1, 2021), p. 114221. ISSN: 0038-1098. DOI: 10.1016/j.ssc.2021.114221. URL: https://www.sciencedirect.com/science/article/pii/S003810982100034X (visited on 05/19/2022).

[SLA98] R. A. Smith, I. V. Lerner, and B. L. Altshuler. "Spectral statistics in disordered metals: A trajectories approach". In: *Physical Review B* 58 (Oct. 1, 1998). ADS Bibcode: 1998PhRvB..5810343S, pp. 10343–10350. ISSN: 0163-18291098-0121. DOI: 10.1103/PhysRevB.58.10343. URL: https://ui.adsabs.harvard.edu/abs/1998PhRvB..5810343S (visited on 05/19/2022).

[SO07] M. A. Skvortsov and P. M. Ostrovsky. "Local correlations of different eigenfunctions in a disordered wire". In: *Soviet Journal of Experimental and Theoretical Physics Letters* 85 (Mar. 1, 2007). ADS Bibcode: 2007JETPL..85...72S, pp. 72–76. ISSN: 0021-3640. DOI: 10.1134/S0021364007010015 URL: https://ui.adsabs.harvard.edu/abs/2007JETPL..85...72S (visited on 05/19/2022).

[Soc+15] Ilya Sochnikov et al. "Nonsinusoidal Current-Phase Relationship in Josephson Junctions from the 3D Topological Insulator HgTe". In: *Phys. Rev. Lett.* 114.6 (Feb. 9, 2015). Publisher: American Physical Society, p. 066801. DOI: 10.1103/PhysRevLett.114.066801. URL: https://link.aps.org/doi/10.1103/PhysRevLett.114.066801 (visited on 05/18/2022).

[Sou85] Nicolas Sourlas. "Introduction to supersymmetry in condensed matter physics". In: *Physica D: Nonlinear Phenomena* 15.1 (Feb. 1, 1985), pp. 115–122. ISSN: 0167-2789. DOI: 10.1016/0167-2789(85)90153-8. URL: https://www.sciencedirect.com/science/article/pii/0167278985901538 (visited on 05/02/2022).

[Ste+16] M. P. Stehno et al. "Signature of a topological phase transition in the Josephson supercurrent through a topological insulator". In: *Phys. Rev. B* 93.3 (Jan. 19, 2016). Publisher: American Physical Society, p. 035307. DOI: 10.1103/PhysRevB.93.035307. URL: https://link.aps.org/doi/10.1103/PhysRevB.93.035307 (visited on 05/18/2022).

[St06] Martin Störzer et al. "Observation of the Critical Regime Near Anderson Localization of Light". In: *Phys. Rev. Lett.* 96.6 (Feb. 15, 2006). Publisher: American Physical Society, p. 063904. DOI: 10.1103/PhysRevLett.96.063904. URL: https://link.aps.org/doi/10.1103/PhysRevLett.96.063904 (visited on 05/02/2022).

[SW80] Lothar Schäfer and Franz Wegner. "Disordered system withn orbitals per site: Lagrange formulation, hyperbolic symmetry, and goldstone modes". In: *Z. Physik B - Condensed Matter* 38.2 (June 1, 1980), pp. 113–126. ISSN: 1431-584X. DOI: 10.1007/BF01598751. URL: https://doi.org/10.1007/BF01598751 (visited on 05/02/2022).

[TE91] Yositake Takane and Hiromichi Ebisawa. "Conductance Fluctuations in Small Normaland Superconductor Composite Wire Systems". In: *J. Phys. Soc. Jpn.* 60.9 (Sept. 15, 1991). Publisher: The Physical Society of Japan, pp. 3130–3138. ISSN: 0031-9015. DOI: 10.1143/JPSJ.60.3130. URL: https://journals.jps.jp/doi/10.1143/JPSJ.60.3130 (visited on 05/18/2022).

[TKL04] C. Tian, A. Kamenev, and A. Larkin. "Weak Dynamical Localization in Periodically Kicked Cold Atomic Gases". In: *Phys. Rev. Lett.* 93.12 (Sept. 17, 2004). Publisher: American Physical Society, p. 124101. DOI: 10.1103/PhysRevLett.93.124101. URL: https://link.aps.org/doi/10.1103/PhysRevLett.93.124101 (visited on 11/07/2022).

[TM16] K. S. Tikhonov and A. D. Mirlin. "Fractality of wave functions on a Cayley tree: Difference between tree and locally treelike graph without boundary". In: *Physical Review B* 94 (Nov. 1, 2016). ADS Bibcode: 2016PhRvB..94r4203T, p. 184203. ISSN: 0163-18291098-0121. DOI: 10.1103/PhysRevB.94.184203. URL: https://ui.adsabs.harvard.edu/abs/2016PhRvB..94r4203T (visited on 05/19/2022).

[TSA96] N. Taniguchi, B. D. Simons, and B. L. Altshuler. "Spectral correlation and response functions in quantum dots". In: *Physical Review B* 53 (Mar. 1, 1996). ADS Bibcode: 1996PhRvB..53.7618T, R7618–R7621. ISSN: 0163-18291098-0121. DOI: 10.1103/PhysRevB.53.R7618. URL: https://ui.adsabs.harvard.edu/abs/1996PhRvB..53.7618T (visited on 05/19/2022).

[Usa70] Klaus D. Usadel. "Generalized Diffusion Equation for Superconducting Alloys". In: *Phys. Rev. Lett.* 25.8 (Aug. 24, 1970). Publisher: American Physical Society, pp. 507–509. DOI: 10.1103/PhysRevLett.25.507. URL: https://link.aps.org/doi/10.1103/PhysRevLett.25.507 (visited on 05/19/2022).

[Vav+01] M. G. Vavilov et al. "Universal Gap Fluctuations in the Superconductor Proximity Effect". In: *Phys. Rev. Lett.* 86.5 (Jan. 29, 2001). Publisher: American Physical Society, pp. 874–877. DOI: 10.1103/PhysRevLett.86.874. URL: https://link.aps.org/doi/10.1103/PhysRevLett.86.874 (visited on 05/18/2022).

[Vel+12] M. Veldhorst et al. "Josephson supercurrent through a topological insulator surface state". In: *Nature Mater* 11.5 (May 2012). Number: 5 Publisher: Nature Publishing Group, pp. 417–421. ISSN: 1476-4660. DOI: 10.1038/nmat3255. URL: https://www.nature.com/articles/nmat3255 (visited on 05/18/2022).

[Vel+18] H. Velkov et al. "Transport in topological insulators with bulk-surface coupling: Interference corrections and conductance fluctuations". In: *Phys. Rev. B* 98.16 (Oct. 5, 2018). Publisher: American Physical Society, p. 165408. DOI: 10.1103/PhysRevB.98.165408. URL: https://link.aps.org/doi/10.1103/PhysRevB.98.165408 (visited on 05/19/2022).

[VWZ85] J. J. M. Verbaarschot, H. A. Weidenmüller, and M. R. Zirnbauer. "Grassmann integration in stochastic quantum physics: The case of compound-nucleus scattering". In: *Physics Reports* 129.6 (Dec. 1, 1985), pp. 367–438. ISSN: 0370-1573. DOI: 10.1016/0370-1573(85)90070-5. URL: https://www.sciencedirect.com/science/article/pii/0370157385900705 (visited on 05/02/2022).

[VZ85] J. J. M. Verbaarschot and M. R. Zirnbauer. "Critique of the replica trick". In: *J. Phys. A: Math. Gen.* 18.7 (May 1985). Publisher: IOP Publishing, pp. 1093–1109. ISSN: 0305-4470. DOI: 10.1088/0305-4470/18/7/018. URL: https://doi.org/10.1088/0305-4470/18/7/018 (visited on 05/03/2022).

[Weg16] Franz Wegner. *Supermathematics and Its Applications in Statistical Physics: Grassmann Variables and the Method of Supersymmetry: 920*. 2016ª edição. New York, NY: Springer, Mar. 26, 2016. ISBN: 978-3-662-49168-3.

[Weg79] Franz Wegner. "The mobility edge problem: Continuous symmetry and a conjecture". In: *Z Physik B* 35.3 (Sept. 1, 1979), pp. 207–210. ISSN: 1431-584X. DOI: 10.1007/BF01319839. URL: https://doi.org/10.1007/BF01319839 (visited on 05/19/2022).

[Wig51] Eugene P. Wigner. "On the statistical distribution of the widths and spacings of nuclear resonance levels". In: *Mathematical Proceedings of the Cambridge Philosophical Society* 47.4 (Oct. 1951). Publisher: Cambridge University Press, pp. 790–798. ISSN: 1469-8064, 0305-0041. DOI: 10.1017/S0305004100027237. URL: https://www.cambridge.org/core/journals/mathematical-proceedings-of-the-cambridge-philosophical-society/article/abs/on-the-statistical-distribution-of-the-widths-and-spacings-of-nuclear-resonance-levels/97EAA86F8F11C09D67D47CD700107D34 (visited on 05/17/2022).

[Wil+12] J. R. Williams et al. "Unconventional Josephson Effect in Hybrid Superconductor-Topological Insulator Devices". In: *Phys. Rev. Lett.* 109.5 (July 30, 2012). Publisher: American Physical Society, p. 056803. DOI: 10.1103/PhysRevLett.109.056803. URL: https://link.aps.org/doi/10.1103/PhysRevLett.109.056803 (visited on 05/18/2022).

[WVL18] Colin M. Whisler, Maxim G. Vavilov, and Alex Levchenko. "Josephson currents in chaotic quantum dots". In: *Phys. Rev. B* 97.22 (June 18, 2018). Publisher: American Physical Society, p. 224515. DOI: 10.1103/PhysRevB.97.224515. URL: https://link.aps.org/doi/10.1103/PhysRevB.97.224515 (visited on 05/18/2022).

[XL19] Hong-Yi Xie and Alex Levchenko. "Topological supercurrents interaction and fluctuations in the multiterminal Josephson effect". In: *Phys. Rev. B* 99.9 (Mar. 26, 2019). Publisher: American Physical Society, p. 094519. DOI: 10.1103/PhysRevB.99.094519. URL: https://link.aps.org/doi/10.1103/PhysRevB.99.094519 (visited on 05/18/2022).

[Xu+14] Jin-Peng Xu et al. "Artificial Topological Superconductor by the Proximity Effect". In: *Phys. Rev. Lett.* 112.21 (May 30, 2014). Publisher: American Physical Society, p. 217001. DOI: 10.1103/PhysRevLett.112.217001. URL: https://link.aps.org/doi/10.1103/PhysRevLett.112.217001 (visited on 05/19/2022).

[Yan+20] Hao Yang et al. "Multiple In-Gap States Induced by Topological Surface States in the Superconducting Topological Crystalline Insulator Heterostructure $Sn_{1-x}Pb_xTe - Pb$". In: *Phys. Rev. Lett.* 125.13 (Sept. 21, 2020). Publisher: American Physical Society, p. 136802. DOI: 10.1103/PhysRevLett.125.136802. URL: https://link.aps.org/doi/10.1103/PhysRevLett.125.136802 (visited on 05/19/2022).

[Zag14] Alexandre Zagoskin. *Quantum Theory of Many-Body Systems: Techniques and Applications*. 2nd edition. Springer, June 26, 2014. 511 pp.

[Zir86] Martin R. Zirnbauer. "Anderson localization and non-linear sigma model with graded symmetry". In: *Nuclear Physics B* 265 (Feb. 1, 1986). ADS Bibcode: 1986NuPhB.265..375Z, pp. 375–408. ISSN: 0550-3213. DOI: 10.1016/0550-3213(86)90316-0. URL: https://ui.adsabs.harvard.edu/abs/1986NuPhB.265..375Z (visited on 05/19/2022).

[Zir96] Martin R. Zirnbauer. "Riemannian symmetric superspaces and their origin in random-matrix theory". In: *J. Math. Phys.* 37.10 (Oct. 1996). Publisher: American Institute of Physics, pp. 4986–5018. ISSN: 0022-2488. DOI: 10.1063/1.531675. URL: https://aip.scitation.org/doi/abs/10.1063/1.531675 (visited on 07/25/2022).

[Zwi14] Daniel Zwillinger, ed. *Table of Integrals, Series, and Products*. 8th edition. Amsterdam ; Boston: Academic Press, Oct. 2, 2014. 1200 pp. ISBN: 978-0-12-384933-5.

Appendix

A. Quantum Simulation

Magnetic phenomena is a fundamental tool to investigate charged systems. Notions as diverse as gauge invariance, quantum Hall, Aharonov–Bohm effect and topological insulators are just a few among many other types of systems stemming their particular behaviour from the coupling between the electromagnetic fields and particles carrying an electric charge. Consider a single particle with mass M and charge Q travelling with velocity $\mathbf{v}$, it is well known that such type of motion generates the so-called Lorentz force, $\mathbf{F} = q(\mathbf{v} \times \mathbf{B})$, or, in a similar manner, we can use the Hamiltonian

$$\hat{H} = \frac{[\hat{p} - q\mathbf{A}(\hat{x})]^2}{2M} \tag{1}$$

where $\mathbf{A}$ is the vector potential associated with the field $\mathbf{B}$, $\hat{p}$ and $\hat{x}$ are the momentum and position operators of the particle, respectively. Such interaction can be exploited in many different ways to perform quantum simulations with these systems and explore a large variety of quantum phenomena, as long as it existence does not hinge on the time-reversal symmetry. However powerful this method have shown to be, when the system is neutral the magnetic interaction is inoperative and the approach becomes irrelevant, at least in the conventional way. This observation becomes particularly problematic in the context of the very versatile platform of ultra cold atoms, which we provides an unprecedented environment to perform controllable condensed matter experiments. Therefore, it is crucial that we manage to circumvent this inability to perform time-reversal symmetry breaking. The way found to overcome this roadblock is finding a Hamiltonian which mimics the present of an artificial gauge field and in this sense provides substitute to the real magnetism, for instance, light beams with some particular choice of frequency and direction [AMG18; Hai+18].

To perform such quantum simulations, the most noteworthy candidate is the atomic kicked rotor. In its most basic version, it is defined by a pair of phase-space variables: an angular variable x and an angular momentum p. Being quantum variables, this pair of variables satisfies the canonical commutation relation $[\hat{x}, \hat{p}] = i\hbar$. The dynamics of the system is generated by the Hamiltonian:

$$H = \frac{\hat{p}^2}{2} + KV(\hat{x}) \sum_n \delta(t - n), \tag{2}$$

where K is the oscillation amplitude, V is periodic potential given by $V(\hat{x}) = \cos(\hat{x})$ and n is the kicking period. This model can be understood in terms of a particle constrained to move on a circular orbit under the influence of a periodic kick of constant force.

Among the many striking features that this model exhibits, we shall demonstrate its unexpected connection with the phenomenon of Anderson localization [CGS89]. It is important to bear in mind that localization via the quantum kicked rotor is a phenomenon that occurs in the momentum space, thus it is more adequate to name it a dynamical localization. Supposing that the dimensionless potential is 2π periodic, a stroboscopic description of the system is made possible via the Floquet operator F:

$$F \left|\omega\right\rangle = U_p U_V \left|\omega\right\rangle = e^{-i\omega} \left|\omega\right\rangle, \tag{3}$$

where the $|\omega\rangle$ is the Floquet "quasi-eigenstate" and $\omega \in [0, 2\pi)$ represent its "quasi-energy" and we defined the operators U_p and U_V as

$$U_p = \exp\left(-\frac{i\hat{p}^2}{2}\right), \qquad U_V = \exp\left(-iK\cos\hat{x}\right). \tag{4}$$

We may use Heisenberg's equation to represent the time evolution of the above Hamiltonian: $H_{t+1} = F^\dagger H_t F$. As a consequence of the commutation relation between the angle and the momentum variable, we obtain the following set of coupled equations known as the standard map

$$\theta_{t+1} = \theta_t + p_t, \tag{5}$$

$$p_{t+1} = p_t + K\sin(\theta_{t+1}). \tag{6}$$

It is incredible that with such simple set of equations, we can observe a full transition from regular behavior, $K \ll 1$, to mixed, $1 \leq K \leq 5$, in this intermediate case the phase space in composed of a mixture of chaotic and regular orbits. For $K > 5$, the dynamics develops to become fully ergodic, in this sense the entire phase has been completely explored. In Fig. A.1, using MATLAB R2021b, we exhibit the resulting phase space for various values of K. This wealth of dynamical behavior can be understood as follows, at each kick the momentum is modified by a quantity $|K\sin x|$, if the parameter K is large enough, then the kicks are so strong such that a given sequence of kicks can be taken as statistically uncorrelated. Within this framework, at each step, the momentum is modified by kick with a random amplitude which leads to random walk in momentum.

We now return to our original discussion, which is establishing a connection between the kicked rotor and the Anderson localization phenomenon. Since we are searching for a connection of this model with the dynamical Anderson localization, it is natural to seek a representation of the Floquet operator in the momentum space. The most unfortunate downside of this endeavor is that this operator is not diagonal in momentum space. To surpass this barrier, we represent the exponential via the following exponential identity

$$e^{ix} = \frac{1 + i\tan(x/2)}{1 - i\tan(x/2)}. \tag{7}$$

Using this representation, we transform the Floquet operator in Eq. (3) into the expression

$$\left(\frac{1 + i\tan\hat{v}}{1 - i\tan\hat{v}}\right)(1 - i\tan\hat{t})\left(\frac{1}{1 + i\tan\hat{t}}\right)|\omega\rangle = |\omega\rangle\,, \tag{8}$$

where we defined $\hat{v} = \omega/2 - \hat{p}^2/4$ and $\hat{t} = K\cos(\hat{x}/2)$. Based on the form of the previous equations, we find it helpful to expand the term

$$(1 + i\tan\hat{t})\,|\omega\rangle = \sum_s u_s\,|s\rangle \tag{9}$$

on the momentum eigenbasis $|s\rangle$.

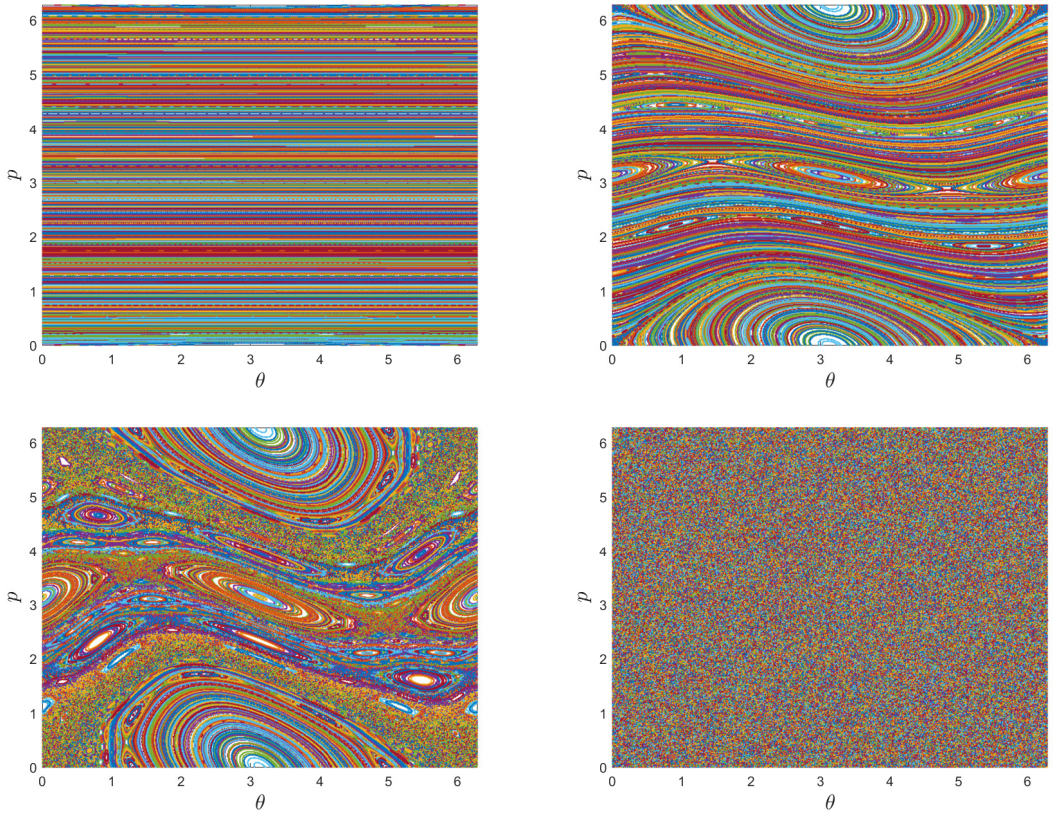

Figure A.1.: The phase space of the kicked rotor represented via the standard map for various values of the kicking strength. In the top left and top right panels, we fixed $K = 1/100$ and $K = 1/2$, respectively. In the bottom left and bottom right panels, we fixed $K = 1$ and $K = 10$, respectively. We observe above that as we increase the kicking strength the dynamics transitions from classical to ergodic behavior.

At last, we project the equation in a momentum eigenstate $\langle m|$ and substitute the identity shown in Eq. (9) into the expression Eq. (8). After a few algebraic manipulations, we arrive at the equation that establishes that connection between the quantum kicked rotor and the Anderson's hopping model

$$\tan v_m u_m + \sum_{s\neq 0} u_{m+s} t_{m,s} = -u_m t_{m,0}, \tag{10}$$

where we defined $t_{m,n} = -\langle m|\tan\hat{t}|m+n\rangle$. To employ the quantum simulation technique to investigate the Anderson model for system with higher-dimensions we need to adopt a slightly different construction in the kicked rotor. The most advantageous form to successfully simulate such systems is obtained via the usage of a modulation function f to play the role of a time-dependent amplitude

$$H = \frac{p^2}{2} + K\cos(x)[1+\epsilon f(t)]\sum_n \delta(t-n), \tag{11}$$

where, supposing that d denotes the dimensionality of the given system, then the modulation function has the form

$$f(t) = \prod_{j=2}^{d} \cos(\omega_j t + \phi_j), \tag{12}$$

the frequencies ω_j are all incommensurate with respect to each other. In references [CGS89; Lem+09; Gar17] it is shown that the time evolution operator of the real degree of freedom is identical in both cases, the incommensurate frequencies are thought of as virtual degrees of freedom. As a consequence of this mathematical result, we are allowed to explore the easier to experimentally implement quasi-periodic kicked rotor as a substitute for the d-dimensional periodic kicked rotor.

In addition to the fabrication of synthetic dimensions, the time dependent modulation also allows us to manipulate the fundamental symmetries of the system. Among them, we are particularly interested in the time-reversal symmetry, since such symmetry is of utmost relevance to the observation of weak localization effects. To perform quantum simulation in systems whose time-reversal symmetry is broken one has to resort to an artificial gauge field. Such task would be essentially impossible without it, since cold atoms are neutral and hence a magnetic field would be inoperative in such set-up. The artificial gauge field hinges on the modulation period of the time-dependent function f. For instance, if the modulation period is at most two, then the system necessarily belongs to the orthogonal class. In Fig. A.2, we display two different modulation periods, where it is clear that the time-reversal symmetry is preserved.

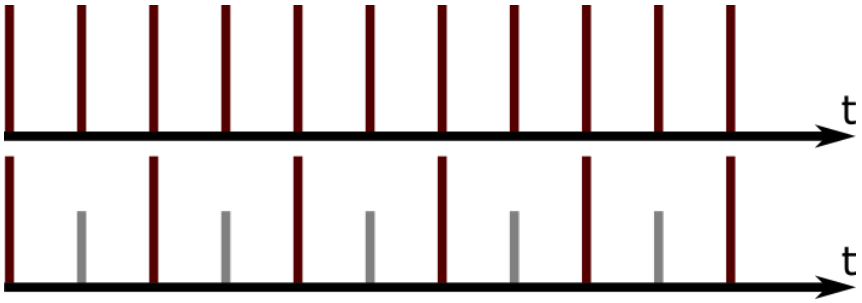

Figure A.2.: For a kicking modulation with at most two periods, it is straightforward to notice that the system belongs to the orthogonal class.

Below in Fig. A.3, we display a kicking pattern where modulation period is three, which clearly breaks the time-reversal symmetry as we expected.

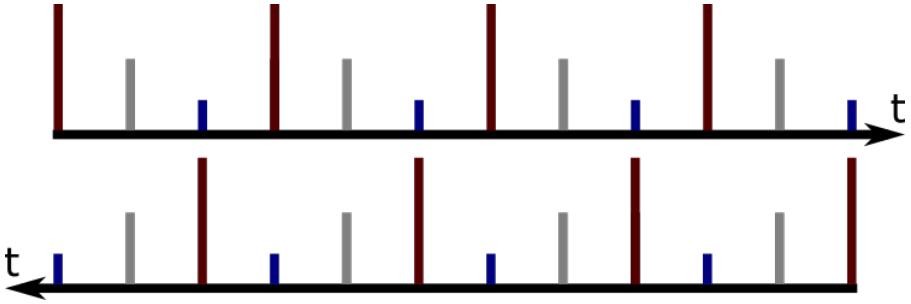

Figure A.3.: When the kicking modulation has more than two periods, then it is possible to construct a Hamiltonian with no time-reversal symmetry.

B. Transfer Matrix Method

There exists a long standing connection between the path integral formalism and the Schrödinger equation, whose foundations are originated in the works of Feynman. Within the path integral framework, instead of dealing with the Schrödinger equation, we have to perform a functional integration. In statistical physics,

our calculations usually concerns a similar structure. We have a partition function that is either constructed from a lattice or a continuous model. In the particular case of a one-dimensional classical model, there is only one space coordinate and, if we identity this space coordinate as a fictitious time variable, this immediately leads to an action with a structure similar to those in the Feynman representation. We can, then, draw an analogy with such representation and reduce the computation of the functional integral for the partition function to solving the corresponding Schrödinger equation, which is typically a more feasible task. The underlying mathematical justification for the transfer matrix method relies on the observation that, in a path integral, it is possible to relate its value at a given time t to an arbitrarily close time t', for instance, $t' = t - \epsilon$, where ϵ is a positive quantity, and this construction permits us to derive a differential equation. In here we shall present a modern derivation of the transfer matrix method, which was introduced in Ref. [KO17b]. Let $\mathcal{M}$ be a manifold endowed with a metric tensor g where the field theory is defined, A be a vector potential, y be a vector field and t the time. We start out with the generic action

$$S[y] = \int_0^{L/\xi} dt \left(\dot{y}^\alpha \dot{y}^\beta g_{\beta\alpha} + \dot{y}^\alpha A_\alpha \right). \tag{13}$$

It is not necessary to define the specify the nature of the vector field y, if it is a bosonic or fermionic field. To contemplate such generality, we must introduce the identity $y^\alpha y^\beta = y^\beta y^\alpha s_{\beta\alpha}$, where the tensor field $s_{\alpha\beta}$ is -1 if both indices are associated with Grassmann variables and is 1 otherwise. With the help of this definition, we notice that the metric tensor must satisfy the following equality $g_{\alpha\beta} = s_{\alpha\beta} g_{\beta\alpha}$. Using the Feynman construction, we write down the wave function associated with such action

$$\psi(y,t) = \int dy' \int_{(y',t')}^{(y,t)} \mathcal{D}y e^{-S[y]} \psi(y',t'), \tag{14}$$

where $t' = t - \epsilon$, ϵ is an arbitrarily small positive quantity and $y' = y(t') = y(t - \epsilon)$. In order to derive the Schrödinger equation for this system, we find it useful to first obtain the equation of motion corresponding to our action. To do so, we employ that the first variation of the action must vanish

$$\delta S = \int_0^{L/\xi} dt \left[(\delta \dot{y}^\alpha) \dot{y}^\beta g_{\beta\alpha} + \dot{y}^\alpha (\delta \dot{y}^\beta) g_{\beta\alpha} + \dot{y}^\alpha \dot{y}^\beta (\delta g_{\beta\alpha}) + (\delta \dot{y}^\alpha) A_\alpha + \dot{y}^\alpha \delta A_\alpha \right]. \tag{15}$$

Integrating it by parts, we obtain

$$\delta S = \int_0^{L/\xi} dt \left[-\delta y^\alpha \partial_t (\dot{y}^\beta g_{\beta\alpha}) - \delta y^\alpha s_{\nu\alpha} \partial_t (\dot{y}^\nu g_{\alpha\nu}) + \dot{y}^\alpha \dot{y}^\beta \delta y^\lambda \partial_\lambda g_{\beta\alpha} - \delta y^\alpha \partial_t A_\alpha + \dot{y}^\alpha \delta A_\alpha \right], \tag{16}$$

where $\partial_\lambda = \partial / \partial y^\lambda$. Evaluating the time derivatives and the infinitesimal variations yield the following result

$$\begin{aligned} \delta S = \int_0^{L/\xi} dt (&-\delta y^\alpha \ddot{y}^\beta g_{\beta\alpha} - \delta y^\alpha \dot{y}^\beta \dot{y}^\lambda \partial_\lambda g_{\beta\alpha} - \delta y^\alpha s_{\nu\alpha} \ddot{y}^\nu g_{\alpha\nu} - \delta y^\alpha s_{\nu\alpha} \dot{y}^\nu \dot{y}^\lambda \partial_\lambda g_{\alpha\nu} \\ &+ \dot{y}^\alpha \dot{y}^\beta \delta y^\lambda \partial_\lambda g_{\beta\alpha} - \delta y^\alpha \dot{y}^\lambda \partial_\lambda A_\alpha + \dot{y}^\alpha \delta y^\lambda \partial_\lambda A_\alpha). \end{aligned} \tag{17}$$

After a few algebraic manipulations, we have our intermediate result

$$\begin{aligned} \delta S = \int_0^{L/\xi} dt (&-2\delta y^\alpha \ddot{y}^\beta g_{\beta\alpha} - 2\delta y^\alpha \dot{y}^\beta \dot{y}^\lambda \partial_\lambda g_{\beta\alpha} \\ &+ s_{\beta\alpha} s_{\nu\alpha} \delta y^\alpha \dot{y}^\nu \dot{y}^\beta \partial_\alpha g_{\beta\nu} - \delta y^\alpha \dot{y}^\lambda \partial_\lambda A_\alpha + s_{\nu\alpha} \delta y^\alpha \dot{y}^\nu \partial_\alpha A_\nu). \end{aligned} \tag{18}$$

With this equation, it is pretty straightforward now to isolate the variation δy^{α}:

$$\delta S = \int_0^{L/\xi} dt \delta y^{\alpha} (-2\ddot{y}^{\beta} g_{\beta\alpha} - 2\dot{y}^{\beta}\dot{y}^{\lambda}\partial_{\lambda} g_{\beta\alpha} + s_{\beta\alpha}s_{\nu\alpha}\dot{y}^{\nu}\dot{y}^{\beta}\partial_{\alpha} g_{\beta\nu} - \dot{y}^{\lambda}\partial_{\lambda} A_{\alpha} + s_{\nu\alpha}\dot{y}^{\nu}\partial_{\alpha} A_{\nu}). \tag{19}$$

Imposing the condition that the first functional derivative must vanish at its extreme, we obtain

$$\delta S[y] = \int_0^{L/\xi} dt \delta y^{\alpha} [-2\ddot{y}^{\beta} g_{\beta\alpha} + \dot{y}^{\beta}\dot{y}^{\lambda}(s_{\beta\alpha}s_{\lambda\alpha}\partial_{\alpha} g_{\lambda\beta} - 2\partial_{\lambda} g_{\beta\alpha}) + \dot{y}^{\lambda}(s_{\lambda\alpha}\partial_{\alpha} A_{\lambda} - \partial_{\lambda} A_{\alpha})] = 0. \tag{20}$$

Then, the first variation of the action only vanishes if the field y^{ν} satisfies the following equation of motion

$$\ddot{y}^{\beta} g_{\beta\alpha} = \dot{y}^{\beta}\dot{y}^{\lambda}\left(\frac{s_{\beta\alpha}s_{\lambda\alpha}\partial_{\alpha} g_{\lambda\beta}}{2} - \partial_{\lambda} g_{\beta\alpha}\right) + \frac{\dot{y}^{\lambda}}{2}(s_{\lambda\alpha}\partial_{\alpha} A_{\lambda} - \partial_{\lambda} A_{\alpha}). \tag{21}$$

In a next step, we expand the action around an infinitesimally small time interval $(t-\epsilon, t)$ up to the second order in the arbitrarily small positive ϵ and express the result in terms of the coordinates and its derivatives at the given time t:

$$S[y] = \epsilon(\dot{y}^{\alpha}\dot{y}^{\beta} g_{\beta\alpha} + \dot{y}^{\alpha} A_{\alpha}) - \frac{\epsilon^2}{2}(2\dot{y}^{\alpha}\ddot{y}^{\beta} g_{\beta\alpha} + \dot{y}^{\alpha}\dot{y}^{\beta}\dot{y}^{\lambda}\partial_{\lambda} g_{\beta\alpha}) - \frac{\epsilon^2}{2}(\ddot{y}^{\alpha} A_{\alpha} + \dot{y}^{\alpha}\dot{y}^{\lambda}\partial_{\lambda} A_{\alpha}) + \mathcal{O}(\epsilon^3). \tag{22}$$

Substituting the equation of motion into the second contribution, we see that this term vanishes. As a consequence of that, the action evaluated at infinitesimally close trajectories reads

$$S[y] = \epsilon\dot{y}^{\alpha}\dot{y}^{\beta} g_{\beta\alpha} + \epsilon\dot{y}^{\alpha} A_{\alpha} - \frac{\epsilon^2}{2}(\ddot{y}^{\alpha} A_{\alpha} + \dot{y}^{\alpha}\dot{y}^{\lambda}\partial_{\lambda} A_{\alpha}). \tag{23}$$

Considering that in Eq. (23) the leading order contribution is represented by terms of zeroth-order in the small parameter ϵ. Within this approximation, it is possible to keep only the kinetic term in Eq. (23), the first term, and we replace the wave function $\psi(y', t')$ by $\psi(y, t)$. Then, we arrive at the conclusion that the proper integration measure is given by the relation $dy' = \sqrt{|g|}d\dot{y}$, which ensures that the Gaussian integration over the velocity coordinates yield unity

$$\int \sqrt{|g|}d\dot{y} \exp\left(-\epsilon\dot{y}^{\alpha}\dot{y}^{\beta} g_{\beta\alpha}\right) = 1. \tag{24}$$

This normalization condition indicates that the typical values of the derivative over the vector field y^{ν} must have a scaling given by $\dot{y} \sim \epsilon^{-1/2}$. Analyzing the equation of motion, we obtain that $\ddot{y} \sim (\dot{y})^2 \sim \epsilon^{-1}$. This categorization, then, permits us to single out and organize each contribution in Eq. (23) in powers of ϵ. The first term is of zeroth-order in ϵ, the second contribution is of order $\sqrt{\epsilon}$ and the last contribution is linear in ϵ.

The next step in our derivation requires us to expand the wave function, Eq. (14), in terms of the arbitrarily small positive ϵ, which yields the following result

$$\psi(y', t') = \psi\left(y - \epsilon\dot{y} + \frac{\epsilon^2}{2}\ddot{y}, t - \epsilon\right) = \left[1 - \epsilon(\partial_t + \dot{y}^{\alpha}\partial_{\alpha}) + \frac{\epsilon^2}{2}(\ddot{y}^{\alpha}\partial_{\alpha} + \dot{y}^{\alpha}\dot{y}^{\beta}\partial_{\beta}\partial_{\alpha})\right]\psi(y, t), \tag{25}$$

with the aid of the estimates we made above, it is possible to conclude that such expansion is valid up to the linear order in ϵ. Substituting the equations Eq. (23) and Eq. (25) displayed above into the initial path

integral Eq. (14), we obtain

$$\psi(y,t) = \int dy' e^{-\epsilon(\dot{y}^\alpha \dot{y}^\beta g_{\beta\alpha} + \dot{y}^\alpha A_\alpha) + \frac{\epsilon^2}{2}(\ddot{y}^\alpha A_\alpha + \dot{y}^\alpha \dot{y}^\lambda \partial_\lambda A_\alpha)} \times \left[1 - \epsilon(\partial_t + \dot{y}^\alpha \partial_\alpha) + \frac{\epsilon^2}{2}(\ddot{y}^\alpha \partial_\alpha + \dot{y}^\alpha \dot{y}^\beta \partial_\beta \partial_\alpha)\right] \psi(y,t). \tag{26}$$

As we discussed, the accuracy of the equation of motion is at most linear. So in the expression below, we must restrict ourselves contributions that are within the range of this accuracy in here:

$$0 = -\epsilon \partial_t \psi(y,t) + \frac{\epsilon^2}{2}\left[\langle \ddot{y}^\alpha \rangle (\partial_\alpha + A_\alpha)\psi(y,t) + \langle \dot{y}^\alpha \dot{y}^\beta \rangle (\partial_\alpha + A_\alpha)(\partial_\beta + A_\beta)\right]\psi(y,t), \tag{27}$$

where we have used the normalization condition and the fact that we have conveniently parametrized the trajectories in terms of the velocity $\dot{y}$ at a time t in place of the point y'. It is now straightforward to arrive at the following expression:

$$\partial_t \psi(y,t) = \frac{\epsilon}{2}[\langle \ddot{y}^\alpha \rangle (\partial_\alpha + A_\alpha) + \langle \dot{y}^\alpha \dot{y}^\lambda \rangle (\partial_\alpha + A_\alpha)(\partial_\lambda + A_\lambda)]\psi(y,t), \tag{28}$$

with the average being taken with respect to the kinetic action $S = \epsilon \dot{y}^\alpha \dot{y}^\beta g_{\beta\alpha}$. The average $\langle \dot{y}^\mu \dot{y}^\nu \rangle$ is readily obtained from the action

$$\langle \dot{y}^\mu \dot{y}^\nu \rangle = \frac{1}{\epsilon} s_{\mu\mu} g^{\mu\nu}, \tag{29}$$

the metric tensor $g^{\mu\nu}$ satisfies the identity $g_{\alpha\mu} g^{\mu\nu} = \delta^\nu_\alpha$. To compute the remaining average $\langle \ddot{y}^\mu \rangle$, we use the equation of motion and the tensor identity above to reduce the calculation to the previous case. In doing so, we obtain the final evolution equation for the wave function ψ in terms of an imaginary time Schrödinger equation

$$\partial_t \psi(y,t) = \mathcal{H}\psi(y,t), \tag{30}$$

whose Hamiltonian is given by the Laplace-Beltrami operator on a supermanifold

$$\mathcal{H} = \frac{1}{\sqrt{|g|}}(\partial_\alpha + A_\alpha)\sqrt{|g|} g^{\alpha\beta}(\partial_\beta + A_\beta). \tag{31}$$

C. Supersymmetric field theory

In this appendix, we provide additional details about the polar coordinates for Q-matrices and zero-modes of the transfer matrix Hamiltonian in the three Wigner-Dyson classes. We perform explicit computations of the local generating function, the evaluation of the boundary integrals and the calculation of the forward scattering peak.

C.1. Polar coordinates and zero modes

Below we discuss the polar coordinates and ground state wave function, or zero modes, for the three Wigner-Dyson classes. The underlying mathematical principle that permits us to explore the polar coordinates, in this context, lies in the observation that an arbitrary non-Hermitian supermatrix can be diagonalized with the aid of two unitary supermatrices.

Polar coordinates:—The building block of this representation is the skeleton supermatrix Q_0, which affords the following decomposition $Q = UQ_0U^{-1}$, as we employed in the main text. Notice that this representation

immediately satisfies the non-linear constraint $Q^2 = Q_0^2 = 1$. It is convenient to represent the skeleton supermatrix as

$$Q_0 = \cos\hat{\theta}\sigma_3^{\rm ra} - \sin\hat{\theta}\sigma_2^{\rm ra} = \begin{pmatrix} \cos\hat{\theta} & i\sin\hat{\theta} \\ -i\sin\hat{\theta} & -\cos\hat{\theta} \end{pmatrix}_{\rm ra}, \quad U = u\left(\frac{1+\sigma_3^{\rm ra}}{2}\right) + v\left(\frac{1-\sigma_3^{\rm ra}}{2}\right) = \begin{pmatrix} u & 0 \\ 0 & v \end{pmatrix}_{\rm ra}, \quad (32)$$

with $\hat{\theta} = \mathrm{diag}(i\hat{\theta}_{\rm bb}, \hat{\theta}_{\rm ff})_{\rm bf}$, and matrices $\hat{\theta}_{\rm bb,ff}$ in 'tr'-sector depending on the fundamental symmetries,

$$\hat{\theta}_{\rm bb} = \begin{pmatrix} \theta_{\rm b} & 0 \\ 0 & \theta_{\rm b} \end{pmatrix}_{\rm tr}, \quad \hat{\theta}_{\rm ff} = \begin{pmatrix} \theta_{\rm f} & 0 \\ 0 & \theta_{\rm f} \end{pmatrix}_{\rm tr}, \quad ({\rm U}) \quad (33)$$

$$\hat{\theta}_{\rm bb} = \begin{pmatrix} \theta_{\rm b,1} & \theta_{\rm b,2} \\ \theta_{\rm b,2} & \theta_{\rm b,1} \end{pmatrix}_{\rm tr}, \quad \hat{\theta}_{\rm ff} = \begin{pmatrix} \theta_{\rm f} & 0 \\ 0 & \theta_{\rm f} \end{pmatrix}_{\rm tr}, \quad ({\rm O}) \quad (34)$$

$$\hat{\theta}_{\rm bb} = \begin{pmatrix} \theta_{\rm b} & 0 \\ 0 & \theta_{\rm b} \end{pmatrix}_{\rm tr}, \quad \hat{\theta}_{\rm ff} = \begin{pmatrix} \theta_{\rm f,1} & \theta_{\rm f,2} \\ \theta_{\rm f,2} & \theta_{\rm f,1} \end{pmatrix}_{\rm tr}, \quad ({\rm Sp}), \quad (35)$$

where compact and non-compact parameters $0 < \theta_{\rm f} < \pi$ and $\theta_{\rm b} > 0$, respectively [Efe99]. These variables are conveniently expressed in terms of trigonometric and hyperbolic functions, $-1 \leq \lambda_{\rm f} \equiv \cos\theta_{\rm f} \leq 1$, $1 \leq \lambda_{\rm b} \equiv \cosh\theta_{\rm b}$, respectively. To perform the calculations, we parametrize the matrix U as a product of two diagonal matrices U_1 and U_2, namely, $U = U_1U_2$, with $U_i = \mathrm{diag}(u_i, v_i)_{\rm ra}$. All Grassmann variables are contained in the matrices u_1 and v_1. As a consequence of this construction, the matrices u_2 and v_2 carry the remaining commuting variables (c-numbers). Although the latter does not play a major role in our evaluation, for bookkeeping purposes we shall at least present their form

$$u_2 = \begin{pmatrix} \mathcal{F}_1 & 0 \\ 0 & \mathcal{F}_2 \end{pmatrix}, \quad v_2 = \begin{pmatrix} \Phi_1 & 0 \\ 0 & \Phi_2 \end{pmatrix}. \quad (36)$$

These matrices have the same structure for all Wigner-Dyson ensembles, their difference becomes apparent in the form of the matrices $\mathcal{F}_j$ and Φ_j, where $j = 1, 2$. For the orthogonal ensemble, we have

$$\mathcal{F}_1 = (1 - iM)(1 + iM)^{-1}, \quad \mathcal{F}_2 = \exp(i\phi\sigma_3^{\rm tr}) \quad (37)$$

$$\Phi_1 = 1, \quad \Phi_2 = \exp(i\chi\sigma_3^{\rm tr}), \quad (38)$$

in here and for the next ensembles, the angles ϕ and χ are defined on the finite interval $(0, 2\pi)$ and the matrix M reads

$$M = \begin{pmatrix} m & m_1^* \\ m_1 & -m \end{pmatrix}_{\rm tr}, \quad (39)$$

with m an arbitrary real and m_1 a complex number. The symplectic ensemble exhibits a similar parametrization

$$\mathcal{F}_1 = \exp(i\phi\sigma_3^{\rm tr}), \quad \mathcal{F}_2 = (1 - iM)(1 + iM)^{-1} \quad (40)$$

$$\Phi_1 = \exp(i\chi\sigma_3^{\rm tr}), \quad \Phi_2 = 1. \quad (41)$$

The unitary ensemble displays the simplest structure

$$\mathcal{F}_1 = \exp(i\phi\sigma_3^{\rm tr}), \quad \mathcal{F}_2 = \exp(i\chi\sigma_3^{\rm tr}) \tag{42}$$

$$\Phi_1 = 1, \quad \Phi_2 = 1. \tag{43}$$

In the fermion-fermion compact sector, we can see that this parametrization is analogous to a vector on the unit sphere, where the angles in the spherical coordinates of the vector are represented by the variables θ and ϕ. On the boson-boson non-compact sector, we can draw an analogy with a vector on a hyperboloid with χ the rotational coordinate and $\theta_{\rm b,1}$ the associated hyperbolic angle. With a fundamental role in our calculation we have the matrices u_1 and v_1, whose general form valid for all ensembles can be written as

$$u_1(\hat{\eta}) = 1 - 2\hat{\eta} + 2\hat{\eta}^2 - 4\hat{\eta}^3 + 6\hat{\eta}^4 \tag{44}$$

$$v_1(\hat{\kappa}) = 1 - 2\hat{\kappa} + 2\hat{\kappa}^2 - 4\hat{\kappa}^3 + 6\hat{\kappa}^4, \tag{45}$$

where $\hat{\eta}$ and $\hat{\kappa}$ still have a structure that is identical to all ensembles

$$\hat{\eta} = \begin{pmatrix} 0 & \eta^\dagger \\ -\eta & 0 \end{pmatrix}_{\rm bf}, \quad \hat{\kappa} = \begin{pmatrix} 0 & i\kappa^\dagger \\ -i\kappa & 0 \end{pmatrix}_{\rm bf}. \tag{46}$$

In contrast with $\hat{\eta}$ and $\hat{\kappa}$, the matrices η and κ depend on the ensemble and are given by the following expressions

$$\eta = \begin{pmatrix} \eta_1 & 0 \\ 0 & -\eta_1^* \end{pmatrix}_{\rm tr}, \quad \kappa = \begin{pmatrix} \kappa_1 & 0 \\ 0 & -\kappa_1^* \end{pmatrix}_{\rm tr}, \quad ({\rm U}) \tag{47}$$

$$\eta = \begin{pmatrix} \eta_1 & \eta_2 \\ -\eta_2^* & -\eta_1^* \end{pmatrix}_{\rm tr}, \quad \kappa = \begin{pmatrix} \kappa_1 & \kappa_2 \\ -\kappa_2^* & -\kappa_1^* \end{pmatrix}_{\rm tr}, \quad ({\rm O, Sp}). \tag{48}$$

It is important to recall the result of a twofold conjugation of a Grassmann variable $(\eta_i^*)^* = -\eta_i$ and similarly for κ_i, and notice that $[u_1(\hat{\eta})]^{-1} = u_1(-\hat{\eta})$, and $[v_1(\hat{\kappa})]^{-1} = v_1(-\hat{\kappa})$ [Efe99].

Zero-modes for Wigner-Dyson classes:—The zero mode for the transfer matrix Hamiltonian in the unitary, orthogonal and symplectic has been recently derived in Ref. [KO17a]. To describe the results, we find it convenient to set $p(\lambda_i) = p_i = \sqrt{(\lambda+1)/2}$. In the unitary ensemble, the ground state wave function, $Y_0^{\rm U}$, has a dependence on a single non-compact radial variable $1 \leq \lambda_{\rm b} = \cosh\theta_{\rm b}$, a single compact radial variable $-1 \leq \lambda_{\rm f} = \cos\theta_{\rm f} \leq 1$ and it reads

$$Y_0^{\rm U} = 4\sqrt{\eta}\left[p_{\rm f}K_0(4\sqrt{\eta}p_{\rm b})I_1(4\sqrt{\eta}p_{\rm f}) + p_{\rm b}K_1(4\sqrt{\eta}p_{\rm b})I_0(4\sqrt{\eta}p_{\rm f})\right]. \tag{49}$$

In the orthogonal ensemble the ground state wave function depends on three variables, two non-compact radial variables $\lambda_{\rm b,1} = \lambda_1$ and $\lambda_{\rm b,2} = \lambda_2$ and a compact radial variable $\lambda_{\rm f}$ and the wave function associated with the zero modes is given by

$$Y_0^{\rm O} = \sqrt{\eta}\left[4p_1p_2I_0(4\sqrt{\eta}p_{\rm f})K_1(4\sqrt{\eta}p_1p_2) + \left(\frac{1+\lambda_1+\lambda_2+\lambda_{\rm f}}{p_{\rm f}}\right)I_1(4\sqrt{\eta}p_{\rm f})K_0(4\sqrt{\eta}p_1p_2)\right]. \tag{50}$$

In the symplectic ensemble, there are two distinct ground state wave functions, which are associated with an

even and odd number of channels. The wave function in here has a dependence on one non-compact radial variable $\lambda_{\rm b}$ and two compact radial variables $\lambda_{{\rm f},1} = \lambda_1$ and $\lambda_{{\rm f},2} = \lambda_2$. To display the results, it is helpful to first define the following function

$$Y_0^{\rm Sp}(\lambda_{\rm b}, \lambda_1, \lambda_2) = \sqrt{\eta}\left[4p_1p_2 I_1(4\sqrt{\eta}p_1p_2)K_0(4\sqrt{\eta}p_{\rm b}) + \left(\frac{1+\lambda_1+\lambda_2+\lambda_{\rm f}}{p_{\rm f}}\right) I_0(4\sqrt{\eta}p_1p_2)K_1(4\sqrt{\eta}p_{\rm b})\right]. \quad (51)$$

With the help of the function introduce above, we display the ground state wave function for an even number of channels (+) and for an odd number of channels (−):

$$Y_\pm^{\rm Sp}(\lambda_{\rm b}, \lambda_1, \lambda_2) = Y_0^{\rm Sp}(\lambda_{\rm b}, \lambda_1, \lambda_2) \pm Y_0^{\rm Sp}(\lambda_{\rm b}, -\lambda_1, -\lambda_2). \quad (52)$$

C.2. Generating function

Starting out from the generating function, introduced in the main text,

$$\mathcal{F}(\eta, \mathbf{x}) = \left\langle \frac{\{{\rm str}[\sigma_3^{\rm bf}\sigma_3^{\rm ra}(Q(\mathbf{x}) - \sigma_3^{\rm ra})]\}^2}{{\rm str}[\sigma_3^{\rm ra}Q(\mathbf{x})]} \right\rangle_S . \quad (53)$$

Using the polar parametrization introduced above, it is straightforward to verify that

$$\begin{aligned}
&{\rm str}(\sigma_3^{\rm ra}Q) = 2{\rm str}(\cos\hat{\theta}) && (54)\\
&{\rm str}[\sigma_3^{\rm bf}(1+\sigma_3^{\rm ra})Q] = 2{\rm str}(u^{-1}\sigma_3^{\rm bf}u\cos\hat{\theta}) && (55)\\
&{\rm str}[\sigma_3^{\rm bf}(1-\sigma_3^{\rm ra})Q] = -2{\rm str}(v^{-1}\sigma_3^{\rm bf}v\cos\hat{\theta}) && (56)\\
&{\rm str}(\sigma_3^{\rm bf}\sigma_3^{\rm ra}Q) = {\rm str}(\sigma_3^{\rm bf}\sigma_3^{\rm ra}U_2^{-1}U_1^2U_2Q_0), && (57)
\end{aligned}$$

where we have used the invariance of the trace under cyclic permutation and the anti-commutation of $\hat{\eta}$ and $\sigma_3^{\rm bf}$. The result of the matrix product $\sigma_3^{\rm bf}U_2^{-1}U_1^2U_2$ is a diagonal matrix in the retarded-advanced sector, the projection onto the retarded-retarded block yields

$$\sigma_3^{\rm bf}U_2^{-1}U_1^2U_2 = u_2^{-1}\left[\sigma_3^{\rm bf} + 8\begin{pmatrix} -\eta^\dagger\eta + 4(\eta^\dagger\eta)^2 & 0 \\ 0 & -\eta\eta^\dagger + 4(\eta\eta^\dagger)^2 \end{pmatrix}_{\rm bf}\right]u_2. \quad (58)$$

There are additional contributions, but we omitted them since such terms are off-diagonal in the boson-fermion sector and would vanish under the trace over this sector. An analogous expression involving $\hat{\kappa}$ is obtained if project the very same matrix onto the advanced-advanced block. In the unitary ensemble, as expected, the matrix η has a diagonal structure in the time-reversal sector, that is, it satisfies the following equalities $\eta^\dagger\eta = -\eta\eta^\dagger = \eta_1^*\eta_1$ and the squared terms vanish, $(\eta^\dagger\eta)^2 = 0$ and $(\eta\eta^\dagger)^2 = 0$. In the remaining two ensembles, the matrix η has an off-diagonal structure in the time-reversal sector which leads to the equalities $(\eta\eta^\dagger)^2 = -(\eta\eta^\dagger)^2 = 2\eta_1^*\eta_2^*\eta_1\eta_2$. As we discussed in the main text, within this framework we only need to take into account the polynomials of highest order in the Grassmann variables [Zir86]. Bearing this in mind, we further simply the matrix entry in Eq. (58) to the following form

$$\sigma_3^{\rm bf}U_2^{-1}U_1^2U_2 = \sigma_3^{\rm bf} + P_{\mathcal{G}}^{\rm r} \quad (59)$$

with $P^{\mathrm{r}}_{\mathcal{G}} \sim \eta^*_1\eta_1$ and $P^{\mathrm{r}}_{\mathcal{G}} \sim \eta^*_1\eta^*_2\eta_1\eta_2$ the unnormalized maximal polynomials of Grassmann variables in the retarded-retarded block for the unitary and orthogonal and symplectic ensembles, respectively. We perform the same computation for the advanced-advanced block and focusing only on the non-vanishing contributions, we assemble together the contributions from both blocks which yield the result

$$\mathrm{str}(\sigma_3^{\mathrm{bf}}\sigma_3^{\mathrm{ra}}Q) = \mathrm{str}[(2\sigma_3^{\mathrm{bf}} + P^{\mathrm{r}}_{\mathcal{G}} + P^{\mathrm{a}}_{\mathcal{G}})\cos\hat{\theta}]. \tag{60}$$

With these results, we can now write down a simplified version of the local generating function

$$\mathcal{F}(\eta, \mathbf{x}) = \left\langle \mathrm{str}(\cos\hat{\theta})P_{\mathcal{G}} \right\rangle_S, \tag{61}$$

where for convenience we defined $P_{\mathcal{G}} = P^{\mathrm{r}}_{\mathcal{G}}P^{\mathrm{a}}_{\mathcal{G}}$ and we used that

$$\{\mathrm{str}[\sigma_3^{\mathrm{bf}}\sigma_3^{\mathrm{ra}}(Q - \sigma_3^{\mathrm{ra}})]\}^2 = \{\mathrm{str}[2\sigma_3^{\mathrm{bf}}(\cos\hat{\theta} - 1)]\}^2 + 2[\mathrm{str}(\cos\hat{\theta})]^2 P_{\mathcal{G}}. \tag{62}$$

It is important to point out that in here the first contribution vanish. Finally, we explore this shifting freedom to demonstrate the equivalence between the local generating function and the level-level correlation function. The former reads

$$\int (dx)\int (dy)\,\langle \mathcal{F}(\eta,\mathbf{x})\mathrm{str}[\sigma_3^{\mathrm{ra}}Q(\mathbf{y})]\rangle_S = 2\int (dx)\int (dy)\,\langle \mathrm{str}[\cos\hat{\theta}(\mathbf{x})]\mathrm{str}[\cos\hat{\theta}(\mathbf{y})]P^{\mathrm{a}}_{\mathcal{G}}(\mathbf{x})P^{\mathrm{r}}_{\mathcal{G}}(\mathbf{x})\rangle_S, \tag{63}$$

whereas the latter displays a form that closely resembles our local generating function

$$\int (dx)\int (dy)\,\langle \mathrm{str}[\sigma_3^{\mathrm{bf}}\sigma_3^{\mathrm{ra}}Q(\mathbf{x})]\mathrm{str}[\sigma_3^{\mathrm{bf}}\sigma_3^{\mathrm{ra}}Q(\mathbf{y})]\rangle_S = 2\int (dx)\int (dy)\,\langle \mathrm{str}[\cos\hat{\theta}(\mathbf{x})]\mathrm{str}[\cos\hat{\theta}(\mathbf{y})]P^{\mathrm{a}}_{\mathcal{G}}(\mathbf{x})P^{\mathrm{r}}_{\mathcal{G}}(\mathbf{y})\rangle_S. \tag{64}$$

The equivalence between these two functions displayed in Eq. (58) and (64) is made complete with the help of a shifting in the maximal polynomial of Grassmann variables $P^{\mathrm{r}}_{\mathcal{G}}(\mathbf{x}) \to P^{\mathrm{r}}_{\mathcal{G}}(\mathbf{x}) + P^{\mathrm{r}}_{\mathcal{G}}(\mathbf{y})$. To conclude this discussion, we still have to fix the numerical factors. In order to do so, we take the quantum dot limit, where the supermatrix degree of freedom becomes homogeneous $Q(\mathbf{x}) = Q_0$, and we obtain

$$P_{\mathcal{G}} = \frac{8}{\beta}P^0_{\mathcal{G}}, \tag{65}$$

where the term $P^0_{\mathcal{G}}$ represents the normalized maximal polynomial of Grassmann variables.

C.3. Boundary terms

In Ch. 4, in order to obtain the level-level correlation function in a closed-form, we introduced the local generating function $\mathcal{F}$ and, with the help of the transfer matrix Hamiltonian, we simplified its form to a simple boundary term

$$\mathcal{F}(\eta) = \int d\mathcal{R}\partial_\lambda\sqrt{g}g^{\lambda\rho}(Y_0'\partial_\rho Y_0 - Y_0\partial_\rho Y_0'), \tag{66}$$

where $Y_0' = \partial_\eta Y_0$. However, this boundary term has a non-trivial structure which involves an undefined product $0\times\infty$, below we shall discuss a method to overcome this difficulty. We start where the calculations are simplest, namely, in the unitary ensemble. Substituting the ground state wave function and the metric

tensor in Eq. (66), the local generating function becomes

$$\mathcal{F}^{\mathrm{U}}(\eta) = \int_1^\infty d\lambda_{\mathrm{b}} \int_{-1}^1 d\lambda_{\mathrm{f}} \left[\partial_{\lambda_{\mathrm{f}}} \frac{(1-\lambda_{\mathrm{f}}^2) G_{\mathrm{f}}(\lambda_{\mathrm{b}}, \lambda_{\mathrm{f}})}{(\lambda_{\mathrm{b}} - \lambda_{\mathrm{f}})^2} + \partial_{\lambda_{\mathrm{b}}} \frac{(\lambda_{\mathrm{b}}^2 - 1) G_{\mathrm{b}}(\lambda_{\mathrm{b}}, \lambda_{\mathrm{f}})}{(\lambda_{\mathrm{b}} - \lambda_{\mathrm{f}})^2} \right] \tag{67}$$

with $G_{\mathrm{f,b}} = Y_0' \partial_{\mathrm{f,b}} Y_0 - Y_0 \partial_{\mathrm{f,b}} Y_0'$. Inspecting the numerator, it is immediately obvious that the first contribution should vanish when evaluated at the boundary $\lambda_{\mathrm{f}} = 1$, whereas the second contribution should vanish at $\lambda_{\mathrm{b}} = 1$. In the denominator we have a contributions which stems from the Jacobian (square root of the metric tensor) whose form in the unitary ensemble is given by the expression $\sqrt{g} = (\lambda_{\mathrm{b}} - \lambda_{\mathrm{f}})^{-2}$, which clearly diverges at the boundary $\lambda_{\mathrm{f}} = \lambda_{\mathrm{b}} = 1$. To overcome this troublesome feature of our construction, we regularize the radial variables by shifting the limit of integration $1 \to 1^{\pm} = 1 \pm \epsilon$, where the positive (negative) sign corresponds to bosonic (fermionic) variables. We employ this method first for the bosonic radial variable and it yields

$$\mathcal{F}^{\mathrm{U}}(\eta) = 2 \lim_{\epsilon \to 0} \int_0^\infty dx_{\mathrm{f}} \frac{\epsilon G_{\mathrm{f}}(1,1)}{(x_{\mathrm{f}} + \epsilon)^2} = 2 G_{\mathrm{f}}(1,1), \tag{68}$$

where $x_{\mathrm{f}} = \lambda_{\mathrm{f}} - 1$ and we only kept the leading order contributions in $x_{\mathrm{f}} \ll 1$, since these will be the only non-vanishing terms in the limit of ϵ approaching zero from the right. There is an analogous result for a regularization in the fermionic variable $\mathcal{F}^{\mathrm{U}}(\eta) = -2 G_{\mathrm{b}}(1,1)$. Notice that this result provides us a relation between G_{f} and G_{b}, that is, $G_{\mathrm{f}} = -G_{\mathrm{b}}$. It is also possible to perform the calculation using a symmetric regularization scheme contemplating both fermionic and bosonic radial variables

$$\mathcal{F}^{\mathrm{U}}(\eta) = 2 \lim_{\epsilon \to 0} \int_\epsilon^\infty dx_{\mathrm{f}} \frac{\epsilon G_{\mathrm{f}}(1,1)}{(x_{\mathrm{f}} + \epsilon)^2} - 2 \lim_{\epsilon \to 0} \int_\epsilon^\infty dx_{\mathrm{f}} \frac{\epsilon G_{\mathrm{b}}(1,1)}{(x_{\mathrm{f}} + \epsilon)^2} = G_{\mathrm{f}}(1,1) - G_{\mathrm{b}}(1,1), \tag{69}$$

a result which, upon using the identity between G_{b} and G_{f} obtained above, reproduces the previous expressions for the local generating function.

Analogous calculations can be performed for the remaining ensembles. The main difficulty in here is that the orthogonal and symplectic ensembles are parametrized by three radial variables, which leads to a twofold integration, in contrast with the unitary case where we only had to compute a integral over a single variable. As in the previous calculations, the integrand present in the boundary contribution is a function whose values are zero everywhere, except close to the origin where it displays a peak and, in this sense, such function can be reduced to a constant times a δ-function. For all symmetry classes the ground state wave functions share the same properties at the metallic saddle point, that is, $Y_0(\sigma_3^{\mathrm{ra}}) = 1$, $Y_0'(\sigma_3^{\mathrm{ra}}) = 0$ and $\partial_\lambda Y_0'(\sigma_3^{\mathrm{ra}}) = b_{\lambda\rho} \partial_\rho Y_0'(\sigma_3^{\mathrm{ra}})$. We define $b_\alpha \beta = 1$ if both indices are either associated with fermionic or bosonic radial variables and $b_\alpha \beta = -1$ otherwise. For the sake of completeness, we perform the calculation for the orthogonal class exploring the regularization scheme on the fermionic radial variable

$$\mathcal{F}^{\mathrm{O}}(\eta) = \lim_{\epsilon \to 0} \int_1^\infty d\lambda_1 \int_1^\infty d\lambda_2 \frac{4\epsilon^2 G_{\mathrm{f}}(1, \lambda_1, \lambda_2)}{[\epsilon^2 + \lambda_1^2 + \lambda_2^2 - 2\lambda_1\lambda_2 - 2\epsilon(1 - \lambda_1\lambda_2)]^2} = 2 G_{\mathrm{f}}(1,1,1). \tag{70}$$

A similar process using the regularization scheme over any of the bosonic radial variables, λ_1 or λ_2, yields the following result $\mathcal{F}^{\mathrm{O}}(\eta) = -2 G_{\mathrm{b}}(1,1,1)$. As we expected both variables, fermionic and bosonic, may provide an equally valid expression for the local generating function. Hence, to fully contemplate this hybrid

nature of our construction, we present the final result of our calculation in the symmetrized form

$$\mathcal{F}_0(\eta) = (\partial_{\lambda_\mathrm{b}} - \partial_{\lambda_\mathrm{f}}) Y_0'|_{\lambda_\mathrm{b}=\lambda_\mathrm{f}=1}, \tag{71}$$

with this expression being valid for all symmetry classes.

C.4. Forward peak

As we discussed in the main text, the temporal profile of the coherent forward scattering peak is related to the level-level correlation function via a Fourier transform. Below we will display the calculations in the unitary class

$$\mathcal{C}_\mathrm{fs}(t) \sim \frac{1}{\Delta_\xi^{-1}} \int_{-\infty}^{\infty} d\omega e^{-i\omega t} \partial_\eta K_0(4\sqrt{\eta}) I_0(4\sqrt{\eta}) \tag{72}$$

Recalling that $\eta = -i\omega/\Delta_\xi$, we perform a change of variables and obtain

$$\mathcal{C}_\mathrm{fs}(t) \sim i\Delta_\xi t\theta(t) \int_0^{\infty} dz [K_0(4i\sqrt{z}) I_0(4i\sqrt{z}) - K_0(-4i\sqrt{z}) I_0(-4i\sqrt{z})]. \tag{73}$$

Using the following identities in the expression above

$$K_n(-z) = (-1)^n K_n(z) + [\log(z) - \log(-z)] I_n(z), \tag{74}$$

$$I_n(-z) = (-1)^n I_n(z), \tag{75}$$

$$I_n(iz) = i^n J_n(z), \tag{76}$$

we obtain an integrand with a much simpler form

$$\mathcal{C}_\mathrm{fs}(t) \sim \Delta_\xi t\theta(t) \int_0^{\infty} dz e^{-zt\Delta_\xi} J_0(4\sqrt{z}) J_0(4\sqrt{z}) = \theta(t) I_0\left(\frac{8}{\Delta_\xi t}\right) e^{-8/(\Delta_\xi t)}. \tag{77}$$

The calculations for the remaining symmetry classes are performed in a similar manner.

D. Replica field theory

D.1. Replica trick

Employing the replica trick, we can write the free energy via the formal relation

$$F = T \lim_{R\to 0} \frac{1}{R}(Z^R - 1). \tag{78}$$

The replicated partition function $Z^R = \int \mathcal{D}[\bar{\psi}\psi]\, e^{-S[\bar{\psi},\psi,V]}$ is described by the action

$$S[\bar{\psi},\psi,V] = \sum_{r=1}^{R} \sum_n \int d^2x \bar{\psi}_n^r \left(-i\epsilon_n + \mathcal{H} - \mu\sigma_3^\mathrm{ph}\right) \psi_n^r, \tag{79}$$

with $\mathcal{H} = H_S + H_\Gamma$ being the effective junction Hamiltonian, introduced in Eqs. (5.11) and (5.15) in the main text. This Hamiltonian provides a description of the topological insulator surface states subjected to a particular realization V of the random disorder potential and takes into account the coupling to the

superconducting leads via the boundary Hamiltonian $\hat{H}_\Gamma$, which is generated by integrating out the superconducting leads. The spinors $\bar{\psi}_n$, ψ_n in Eq. (79) are $4 \times R$ dimensional fields, living in the direct product of spin, particle-hole (Nambu) and replica space and the sum is over fermionic Matsubara frequencies $\epsilon_n = (2n+1)\pi T$.

D.2. Sample-space

The calculation of sample-to-sample fluctuations is simplified by enlarging the auxiliary field space to introduce two copies of the system. That is, doubling once more spinor components, and introducing the (block) diagonal matrices

$$\mathcal{H} \mapsto \mathcal{H}(\phi_1, \phi_2) \equiv \mathrm{diag}[\mathcal{H}(\phi_1), \mathcal{H}(\phi_2)], \quad \epsilon \mapsto \epsilon \otimes \mathbb{1}_2, \quad \mu \mapsto \mu \otimes \mathbb{1}_2. \tag{80}$$

This two dimensional extension is referred to as 'fluctuation space' or 'sample space' in the following. We are thus working with the replicated partition function in enlarged space, $Z^R = \int \mathcal{D}[\bar{\psi}\psi]\, e^{-S[\bar{\psi},\psi,V]}$, with action

$$S[\bar{\psi}, \psi, V] = \int d^2x\, \bar{\psi} \left[-i\epsilon + \mathcal{H}(\phi_1, \phi_2) - \mu\sigma_3^{\mathrm{ph}} \right] \psi, \tag{81}$$

where $\bar{\psi}$, ψ are now $2 \times 2 \times 2 \times M \times R$ dimensional fields living in the direct product of spin, particle-hole (Nambu), sample, Matsubara and replica space, respectively. We did not write out explicitly scalar products in Matsubara and replica spaces, and to compactify notation also introduced the matrix of Matsubara frequencies ϵ_n operating in an M dimensional space of Matsubara frequencies, M in here is some irrelevant cut off for frequencies, e.g. set by the largest energy scale $(T\tau)^{-1}$. The partition function Z^R allows the calculation of the average Josephson current and its fluctuations as described in Eq. (5.28) in the main text. Finally, recalling the Nambu spinor structure, there is a symmetry relation for the fields

$$\sigma_2 \otimes \sigma_2^{\mathrm{ph}} \bar{\psi}^t(\mathbf{x}, \tau) = -\psi(\mathbf{x}, \tau), \tag{82}$$

where sigma matrices with no upper index, σ_i, operates on the spin space, sigma matrix with ph operates on the particle-hole space and notice that such relation renders a dependence between the field and its conjugated form.

D.3. Disorder average

The replica trick allows us to readily perform the average over the random disorder potential. The price we pay for the disorder average is the presence of a four fermion contribution

$$\ln \left\langle \exp \left[\int dx \bar{\psi} V(\mathbf{x}) \sigma_3^{\mathrm{ph}} \psi \right] \right\rangle = \frac{1}{2\pi\nu\tau} \int dx \left[\bar{\psi}\sigma_3^{\mathrm{ph}}\psi \bar{\psi}\sigma_3^{\mathrm{ph}}\psi \right], \tag{83}$$

which can be further organized by separating the two low-momentum channels that represent the slow diffusion modes in a disordered single-particle system with time-reversal symmetry, namely, the 'diffusons' and 'Cooperons'. Proceeding with the Hubbard-Stratonovich transformation, we introduce the $8RM$-dimensional matrix Q slowly fluctuating in space and with an identical structure in comparison to the dyadic product $\Psi\bar{\Psi}$, that is, the matrix field has entries in spin, Nambu, sample, Matsubara and replica space. Furthermore,

the matrix field Q satisfies the symmetry constraint

$$Q(\mathbf{x},\tau\tau') = \sigma_2 \otimes \sigma_1^{\rm ph} Q^t(\mathbf{x},\tau'\tau)\sigma_2 \otimes \sigma_1^{\rm ph}, \tag{84}$$

inherited from the Nambu spinors. It makes it possible to decouple both slow modes via the transformation

$$\exp\left[-\frac{1}{\pi\nu\tau}\int d^2x {\rm tr}(\sigma_3^{\rm ph}\psi\bar{\psi}\sigma_3^{\rm ph}\psi\bar{\psi})\right] = \int \mathcal{D}Q \exp\left[-\frac{\pi\nu}{16\tau}{\rm Tr}(Q^2) + \frac{i}{2\tau}\int d^2x \bar{\psi}(\mathbf{x})Q(\mathbf{x})\sigma_3^{\rm ph}\psi(\mathbf{x})\right]. \tag{85}$$

It makes system action to be quadratic in fermionic fields that can be explicitly integrated out leading to the determinant of the corresponding matrix Green's function operator. Using the celebrated formula for the determinant to the trace-log transformation, $\det O = \exp({\rm Tr}\ln O)$, we arrive at the disorder averaged generating functional, $\left\langle Z^R \right\rangle_V = \int \mathcal{D}Q\, e^{-S[Q]}$, with the action

$$S[Q] = \frac{\pi\nu}{16\tau}{\rm Tr}(Q^2) - \frac{1}{2}{\rm Tr}\ln(G_Q^{-1}). \tag{86}$$

Here, we defined the Greens' function

$$G_Q^{-1} = i\epsilon - (v\mathbf{k}\cdot\boldsymbol{\sigma} - \mu)\,\sigma_3^{\rm ph} - H_\Gamma + \frac{i}{2\tau}Q\sigma_3^{\rm ph}, \tag{87}$$

with ϵ and Δ and ϕ being diagonal matrices in sample space. The Eq. (86) is still an exact representation of the original replica partition function. It defines the starting point for a derivation of the low energy effective action. The latter describes the soft rotations around saddle points of Eq. (86), as discussed next.

D.4. Mean field equation

The variation of the action (86) leads to the saddle point equation

$$Q_0 = \frac{2i}{\pi\nu}\int \frac{d^2k}{(2\pi)^2}\frac{\mu + \frac{i}{2\tau}Q_0 + v\mathbf{k}\cdot\boldsymbol{\sigma}}{\left(\mu + \frac{i}{2\tau}Q_0\right)^2 - v^2\mathbf{k}^2}, \tag{88}$$

discussed in the main text. Referring to the latter for further details, we here only recall its solution

$$Q_0 = \sigma_3^{\rm ph} \otimes \Lambda, \tag{89}$$

in accordance with the causal structure of the model. Here, Λ is the diagonal matrix in Matsubara space with elements $(\Lambda)_n = {\rm sgn}(\epsilon_n)$. The parametrization $T(\mathbf{x})Q_0T^{-1}(\mathbf{x})$ includes soft fluctuations around the saddle point which leave the first term invariant, namely the high energy contribution to Eq. (86). The final soft mode action then is found from a low energy expansion of the remaining 'trace log'.

D.5. Trace-log expansion

We then organize the second contribution to Eq. (86) as follows

$$S_{\rm eff} = -\frac{1}{2}{\rm Tr}\ln(G_Q^{-1}) \equiv -\frac{1}{2}{\rm Tr}\ln\left(1 - G_0O_T\right), \tag{90}$$

where we dropped an inessential constant that vanishes in the replica limit and introduced

$$G_0^{-1} = -v\mathbf{k}\cdot\boldsymbol{\sigma} + \mu + \frac{i}{2\tau}Q_0, \tag{91}$$

$$O_T = T^{-1}\left(-i\hat{\epsilon}\sigma_3^{\rm ph} - T[v\mathbf{k}\cdot\boldsymbol{\sigma}, T^{-1}] + H_\Gamma\sigma_3^{\rm ph}\right)T. \tag{92}$$

Expanding in the small energies $\{\epsilon, E_t, \Delta\} \ll 1/\tau$ and gradients $\partial_{\mathbf{x}}T(\mathbf{x})$ of the slowly fluctuating field, we arrive at

$$S_{\rm eff} \simeq \frac{1}{2}{\rm Tr}\left(G_0 O_T\right) + \frac{1}{4}{\rm Tr}\left(G_0 O_T G_0 O_T\right) \equiv S_1 + S_2. \tag{93}$$

D.6. Spin singlet mode

We notice that only homogeneous modes $T(\mathbf{x}) \equiv T$ lacking any structure in spin-space have vanishing commutator $[v\mathbf{k}\cdot\boldsymbol{\sigma}, T^{-1}]$ in O_T. that is, only spin singlet matrices are soft modes. Indeed, a perturbative calculation shows that spin triplet modes have masses of the order $\sim \nu/\tau$, whose magnitude constitutes a large energy in our problem. We shall neglect these massive modes and simply project the action onto the spin singlet mode. Using this approximation, we find from the linear order trace log expansion the following action:

$$S_1 = -\frac{\pi\nu}{2}\int dx {\rm tr}\left(\epsilon\sigma_3^{\rm ph}Q + iH_\Gamma\sigma_3^{\rm ph}Q\right), \tag{94}$$

notice that the spin space is now traced out in the action above and we defined the matrix field $Q = TQ_0T^{-1}$. Similarly, we find from the second order trace log expansion

$$S_2 = -\frac{v^2}{4}\sum_{i,k=0}^{2}\sum_{j,l=1}^{2}{\rm Tr}\left(g_0^i\sigma_i A_j\sigma_j g_0^k\sigma_k A_l\sigma_l\right) = -\frac{v^2}{2}\sum_{i=0}^{2}{\rm tr}\left[\Xi(Q_0, A_i)\right], \tag{95}$$

where we have fixed $A_i = T\partial_i T^{-1}$, the trace tr excludes the trace over the spin-space, the function Ξ encodes the information obtained from integrating over the momentum space and it is given by the expression:

$$\Xi(Q_0, A_i) \equiv D_R A_i A_i - D_I A_i Q_0 A_i Q_0 + 2iD' A_i A_i Q_0, \tag{96}$$

we will define below the constants D_R, D_I and D'. In addition to that, to arrive at the result displayed in Eq. (95), we have decomposed the Green's functions in terms of a linear combination of Pauli matrices and the identity matrix

$$G_0 = \sum_{i=0}^{2} g_0^i\sigma_i = \frac{1}{2}\sum_{i=0}^{2}\sum_{j=\pm} g_0^{ij}(1 + jQ_0)\sigma_i. \tag{97}$$

Fixing $\alpha = \mu + i/(2\tau)$, we have defined the Green's functions above as

$$g_0^{0+} = \frac{\mu + \frac{i}{2\tau}}{\left(\mu + \frac{i}{2\tau}\right)^2 - v^2k^2} = \left(g_0^{0-}\right)^*, \quad g_0^{i+} = \frac{vk_i}{\left(\mu + \frac{i}{2\tau}\right)^2 - v^2k^2} = \left(g_0^{i-}\right)^* \tag{98}$$

and the constants

$$D_R \equiv \int \frac{d^2k}{(2\pi)^2}[\mathrm{Re}g_0^{0+}(\mathbf{k})][\mathrm{Re}g_0^{0+}(\mathbf{k})], D_I \equiv \int \frac{d^2k}{(2\pi)^2}[\mathrm{Im}g_0^{0+}(\mathbf{k})][\mathrm{Im}g_0^{0+}(\mathbf{k})]. \tag{99}$$

Converting the summations into integrations, we obtain

$$D_R = \frac{1}{2\pi v^2}\int d\epsilon\epsilon[\mathrm{Re}g_0^{0+}(\epsilon/v)][\mathrm{Re}g_0^{0+}(\epsilon/v)] = \frac{\pi\nu\tau}{4}, \tag{100}$$

$$D_I = \frac{1}{2\pi v^2}\int d\epsilon\epsilon[\mathrm{Im}g_0^{0+}(\epsilon/v)][\mathrm{Im}g_0^{0+}(\epsilon/v)] = \frac{\pi\nu\tau}{4}, \tag{101}$$

where we have performed a change of variables using $\epsilon = vk$. While these constants provide the dominant contributions in $(\mu\tau)^{-1}$, the contribution from the region we neglected, $D' \equiv \sum_{\mathbf{k}}[\mathrm{Re}g_0^{0+}(\mathbf{k})][\mathrm{Im}g_0^{0+}(\mathbf{k})]$ is only subleading in $1/\mu\tau$. Employing the identity $\mathrm{tr}(A_iA_i - Q_0A_iQ_0A_i) = -\mathrm{tr}(\frac{1}{2}(\partial_iQ_0)^2)$, the above action can be rewritten as $S_2 = \frac{1}{8}\pi\nu D_0\int d^2x\mathrm{tr}\,(\partial_iQ\partial_iQ)$, where $Q = TQ_0T^{-1}$, $D_0 = v^2\tau/2$ and the density of states per spin direction is defined as $\nu = \mu/(2\pi v^2)$. In the derivation presented so far, the massive spin fluctuations were neglected entirely. In fact, it is known that these modes can renormalize the diffusion coefficient for the singlet modes. Here, we will take a pragmatic approach and account for this effect by introducing the renormalized diffusion coefficient $D_0 \to D = v^2\tau_{\mathrm{tr}}/2$ into the action, so that finally

$$S_2 = \frac{\pi\nu D}{8}\int d^2x\mathrm{tr}\,(\partial_iQ\partial_iQ)\,. \tag{102}$$

Notice that after projection onto the spin singlet mode, the matrix field satisfies the symmetry constraint

$$Q = \sigma_1^{\mathrm{ph}}Q^t\sigma_1^{\mathrm{ph}}. \tag{103}$$

Finally, adding both contributions $S_1 + S_2$, we arrive at action Eq. (5.20) in the main text.

D.7. Average Current

Starting out from the general expression for the current phase relation

$$I(\phi) = -\pi\nu eTV\sum_{\epsilon}\left[\partial_\phi\left(2v_im_i - E_\Phi m_2^2\right)\right], \tag{104}$$

we find the average current in the strong magnetic field limit,

$$I_\Phi(\phi) = \left(\frac{GE_t}{e}\right)\mathrm{Re}\left[\sum_{\epsilon>0}\frac{2\pi t\sin\phi}{(e_\Phi + |\epsilon|)(1+i\epsilon)}\right]. \tag{105}$$

The summation is then readily done using the identity

$$\sum_{n=0}^{\infty}\frac{1}{(n+a)(n+b)} = \frac{\psi(a)-\psi(b)}{a-b}, \tag{106}$$

resulting in

$$I_\Phi(\phi) = \left(\frac{GE_t}{e}\right)\mathrm{Re}\left[\frac{(1+ie_\Phi)\psi\left(\frac{1}{2}-\frac{i}{2\pi t}\right) - (1+ie_\Phi)\psi\left(\frac{1}{2}+\frac{e_\Phi}{2\pi t}\right)}{1+e_\Phi^2}\right]\sin\phi, \tag{107}$$

where ψ is the polygamma function.

D.8. Fourier Transform in Matsubara Space

In here we shall present the Fourier transform conventions we used for our calculations of the fluctuations. Consider the matrix field P_c representing the Cooperons, its Fourier is given by the following relation

$$P_c(\epsilon_1,\epsilon_2)=\int dt_1\int dt_2 e^{i\epsilon_1 t_1-i\epsilon_2 t_2}P_c(t_1,t_2)=\begin{pmatrix}c_{1,\epsilon_1,\epsilon_2} & 0\\ 0 & c_{2,\epsilon_1,\epsilon_2}\end{pmatrix}. \tag{108}$$

If both energies are positive, then we identify the matrix entry as $P_c(\epsilon_1,\epsilon_2)=c_{1,\epsilon_1,\epsilon_2}$, whereas if both energies are negative the corresponding matrix entry reads $c_{2,\epsilon_1,\epsilon_2}$. Within this framework, the matrix transposition operation has a different behavior than the typical simple exchange of indices $A^T_{ab}=A_{ba}$. We employ the rules presented above to define how to compute the transposition of a matrix in Matsubara space:

$$\begin{aligned}P^t_c(\epsilon_1,\epsilon_2)&=\int dt_1\int dt_2 e^{i\epsilon_1 t_1-i\epsilon_2 t_2}P^t_c(t_1,t_2) &(109)\\ &=\int dt_1\int dt_2 e^{i\epsilon_1 t_1-i\epsilon_2 t_2}P^T_c(t_2,t_1) &(110)\\ &=P^T_c(-\epsilon_2,-\epsilon_1), &(111)\end{aligned}$$

not only we exchange the energy, but also its sign. Thus, the definition of Hermitian conjugate becomes

$$\begin{aligned}P^\dagger_c(\epsilon_1,\epsilon_2)&=\left(\int dt_1\int dt_2 e^{i\epsilon_1 t_1-i\epsilon_2 t_2}P_c(t_1,t_2)\right)^\dagger &(112)\\ &=\int dt_1\int dt_2 e^{-i\epsilon_1 t_1+i\epsilon_2 t_2}[P_c(t_1,t_2)]^\dagger &(113)\\ &=\int dt_1\int dt_2 e^{-i\epsilon_1 t_1+i\epsilon_2 t_2}[P_c(t_2,t_1)]^{*T} &(114)\\ &=P^{*T}_c(\epsilon_2,\epsilon_1). &(115)\end{aligned}$$

Hopefully, with the help of these definitions, the derivation of the fluctuations will not be a challenge to the reader.

D.9. Fluctuations

In here, we shall provide additional details on the derivation of the semiclassical partition function $\mathcal{Z}$, Eq. (5.49), with the non-linear sigma model action (5.42). We start out with an expansion of the matrix field Q in terms of generators of fluctuations W, c.f. (5.47), up to second order and find the fluctuation determinant. At zeroth order, we just have to replace Q by Q_0, this already yields the saddle point action $S^{(0)}=RS_0$, where

$$S_0=\frac{\pi\nu V}{2}\mathrm{tr}'(E_\Phi\hat{m}_2^2-2\hat{v}_i\hat{m}_i), \tag{116}$$

Here, we traced out the Nambu and replica spaces, so that the trace operation tr' only comprises summations over Matsubara frequencies and the sample space. Furthermore, in order to eliminate any source of possible confusion, we introduced a hat notation to indicate that there is a diagonal structure in the sample space of m_i and v_i. At linear order in the generators W, the action vanishes in the geometry we study. The saddle point equation eliminates terms containing no spatial derivatives. The remaining term in the action is an irrelevant boundary contribution. Fluctuations are determined by the second order expansion in W. For

this term, we obtain the expression

$$\begin{aligned} S^{(2)} =& \pi\nu \int d^2x De^2 \mathbf{A}^2 \mathrm{tr}[(\hat{m}_2 \sigma_1^{\mathrm{ph}} W_i)^2 + \hat{m}_2^2 W^2] \\ &+ \frac{\pi\nu}{2} \int d^2x \mathrm{tr}[D(Q_0 \partial_y W + ie\mathbf{A}[\hat{m}_3, W]_+)^2 - 2\hat{v}_i \hat{m}_i W^2] \end{aligned} \tag{117}$$

In order to perform the Gaussian integration over the generators W and find the fluctuation determinant, we need to impose the constraints discussed below Eq. (5.47). As a result of considering these constraints, we must parametrize the Diffuson and Cooperon contributions to W as

$$W_d = \begin{pmatrix} P_d & 0 \\ 0 & P_d^t \end{pmatrix}_{\mathrm{ph}}, \quad W_c = \begin{pmatrix} 0 & P_c \\ -P_c^* & 0 \end{pmatrix}_{\mathrm{ph}}, \tag{118}$$

where the Diffuson and Cooperon matrices P_d and P_c fulfill the additional constraints $W = \sigma_1^{\mathrm{ph}} W^t \sigma_1^{\mathrm{ph}}$, that is, the matrices P_d and P_c satisfy the equalities: $P_d^\dagger = -P_d$, $P_c^t = P_c$. All fields in these equation are functions of two imaginary time arguments. The fields P_c and P_d have a further constraint by the relations $[P_d, \Lambda]_+ = 0$, and $[P_c, \Lambda] = 0$. Since Λ takes a particularly simple form in Matsubara frequency space, $\Lambda_n = \mathrm{sgn}(\epsilon_n)$, the constraints are conveniently resolved in frequency space as well,

$$P_d(\epsilon_1, \epsilon_2) = d_{\epsilon_1,\epsilon_2} \theta_{\epsilon_1} \theta_{-\epsilon_2} - d^\dagger_{\epsilon_1,\epsilon_2} \theta_{-\epsilon_1} \theta_{\epsilon_2}, \quad P_c(\epsilon_1, \epsilon_2) = c_{\epsilon_1,\epsilon_2} \theta_{\epsilon_1} \theta_{\epsilon_2} + c^t_{-\epsilon_1,-\epsilon_2} \theta_{-\epsilon_1} \theta_{-\epsilon_2}, \tag{119}$$

where θ is the Heaviside step function.

Using the parametrization introduced above, we obtain the quadratic forms for Diffuson and Cooperon modes as

$$\begin{aligned} \frac{S_D^{(2)}}{2\pi\nu L} = \sum_{\epsilon_1>0,\epsilon_2<0} \sum_{ab,mn} \int dy \Big(& D\,|\mathcal{D}_y d_\alpha|^2 + \frac{1}{8} E_\Phi [m_3^a(\epsilon_1) + m_3^b(\epsilon_2)]^2 |d_\alpha|^2 + [m_i^a(\epsilon_1) v_i^a(\epsilon_1) + m_i^b(\epsilon_2) v_i^b(\epsilon_2)] |d_\alpha|^2 \\ & - \frac{1}{2} E_\Phi [m_2^a(\epsilon_1)^2 + m_2^b(\epsilon_2)] |d_\alpha|^2 - E_\Phi [m_2^a(\epsilon_1) m_2^b(\epsilon_2) \mathrm{Re}(d_\alpha^* d^t_{\bar{\alpha}})] \Big), \end{aligned} \tag{120}$$

where we integrated along the x-direction and introduced the long derivative

$$\mathcal{D}_y = \partial_y + ieBL[m_3^a(\epsilon_1) + m_3^b(\epsilon_2)]/2 \tag{121}$$

and used the convenient multi-index notation $\alpha = \epsilon_1\epsilon_2, ab, mn$, $\bar{\alpha} = (-\epsilon_1)(-\epsilon_2), ab, mn$, and

$$\begin{aligned} \frac{S_C^{(2)}}{2\pi\nu L} = \sum_{\epsilon_1>0,\epsilon_2>0} \sum_{ab,nm} \int dy \Big(& D|\mathcal{D}_y c_\alpha|^2 + \frac{1}{8} E_\Phi [m_3^a(\epsilon_1) + m_3^b(\epsilon_2)]^2 |c_\alpha|^2 + [m_i^a(\epsilon_1) v_i^a(\epsilon_1) + m_i^b(\epsilon_2) v_i^b(\epsilon_2)] |c_\alpha|^2 \\ & - \frac{1}{2} E_\Phi [m_2^a(\epsilon_1)^2 + m_2^b(\epsilon_2)^2] |c_\alpha|^2 + E_\Phi [m_2^a(\epsilon_1) m_2^b(\epsilon_2) \mathrm{Re}(c_\alpha c_\alpha^t)] \Big). \end{aligned} \tag{122}$$

The next step in our calculation will be to integrate out the d and c modes, in order to find the fluctuation determinant. Unfortunately, the presence of the derivative $\mathcal{D}_y$ and due the nontrivial structure present in the last line of Eqs. (120) and (122), it is not possible to immediately read off the eigenvalues and compute the functional determinant. Our first modification in the action for the calculation of the fluctuation determinant is to explore the translational invariance along the y-direction and effectively replace the long derivative by

the usual derivative, $\mathcal{D}_y \to \partial_y$. Since the action for both modes are almost identical, we shall focus our efforts on the diagonalization of the quadratic form for the case of the Cooperon. The Diffuson contribution can be treated by analogy. The form of the Cooperon action signals to us that it is convenient to split the Cooperon field in terms of a real and a imaginary component $c_\alpha = c'_\alpha + ic''_\alpha$, where c' and c'' are the real and imaginary parts of c, respectively. Hence, the Cooperon contribution to the quadratic action becomes

$$\frac{S_C^{(2)}}{2\pi\nu L} = \sum_{\epsilon_1>0,\epsilon_2>0}\sum_{ab,mn}\int\frac{dq}{2\pi}(c'_{\alpha,q}\mathcal{O}^{ab}_{\epsilon_1\epsilon_2}c'_{\alpha,-q} + c'_{\alpha,q}\mathcal{N}^{ab}_{\epsilon_1\epsilon_2}c'^{T}_{\alpha,-q} + c''_{\alpha,q}\mathcal{O}^{ab}_{\epsilon_1\epsilon_2}c''_{\alpha,-q} - c''_{\alpha,q}\mathcal{N}^{ab}_{\epsilon_1\epsilon_2}c''^{T}_{\alpha,-q}), \tag{123}$$

where we introduced the notation

$$\begin{aligned}\mathcal{O}^{ab}_{\epsilon_1\epsilon_2} =& Dq^2 + \frac{1}{8}E_\Phi[\hat{m}^a_3(\epsilon_1) + \hat{m}^b_3(\epsilon_2)]^2 + \hat{m}^a_i(\epsilon_1)v^a_i(\epsilon_1) + \hat{m}^b_i(\epsilon_2)v^b_i(\epsilon_2) - \frac{1}{2}E_\Phi[\hat{m}^a_2(\epsilon_1)^2 + \hat{m}^b_2(\epsilon_2)^2]\\ \mathcal{N}^{ab}_{\epsilon_1\epsilon_2} =& E_\Phi\hat{m}^a_2(\epsilon_1)\hat{m}^b_2(\epsilon_2).\end{aligned} \tag{124}$$

For the fully diagonal terms in the action, for which all entries are pairwise identical $\epsilon_1 = \epsilon_2$, $a = b$, $m = n$, we readily read off the two eigenvalues $\mathcal{O}^{aa}_{\epsilon_1\epsilon_1} \pm \mathcal{N}^{aa}_{\epsilon_1\epsilon_1}$. However, inspecting the expression for the sample-to-sample fluctuation, it is possible to immediately conclude that such terms cannot possibly provide a non-zero contribution to our observable. In order to find the remaining eigenvalues, we will first arrange the variables c' and c'' into vectors so that the quadratic form is represented by a block-diagonal matrix. For $(\epsilon_1\epsilon_2, ab, mn) \neq (\epsilon_2\epsilon_1, ba, mn)$, we introduce four-component vectors χ as

$$\chi = (c', [c']^t, c'', [c'']^t)^T, \tag{125}$$

where the transposition T indicates that we view this object as a column vector. For a given α, the contribution to the quadratic form can then be represented as

$$\chi^T_{\alpha,q}\begin{pmatrix}[\mathcal{M}^C]^{ab}_{\epsilon_1\epsilon_2} & 0\\ 0 & [\bar{\mathcal{M}}^C]^{ab}_{\epsilon_1\epsilon_2}\end{pmatrix}\chi_{\alpha,-q}, \tag{126}$$

where we introduced the block matrices

$$\mathcal{M}^C = \begin{pmatrix}\mathcal{O} & \mathcal{N}\\ \mathcal{N} & \mathcal{O}\end{pmatrix}, \quad \bar{\mathcal{M}}^C = \begin{pmatrix}\mathcal{O} & -\mathcal{N}\\ -\mathcal{N} & \mathcal{O}\end{pmatrix}. \tag{127}$$

To determine the form of these block matrices, we used the symmetries $\mathcal{O} = \mathcal{O}^t$ and $\mathcal{N} = \mathcal{N}^t$. Both matrices $\mathcal{M}$ and $\bar{\mathcal{M}}$ have the two eigenvalues

$$\tilde{\lambda}^{C,\pm} = \mathcal{O} \pm \mathcal{N}. \tag{128}$$

Having identified all eigenvalues of the fully diagonal and the off-diagonal parts of the quadratic form, what remains is to find their multiplicity. When grouping c', $[c']^t$ (and c'', $[c'']^t$) into vector χ, the summation in α needs to be constraint to cover only half of the degrees of freedom in order to avoid overcounting. This is compensated by the degeneracy of eigenvalues from the c' and c'' sectors. We can summarize the above discussion by stating that for each $\alpha = (\epsilon_1, \epsilon_2, ab, mn)$ we find two associated eigenvalues $(\tilde{\lambda}^{C,+})^{ab}_{\epsilon_1\epsilon_2}$ and $(\tilde{\lambda}^{C,-})^{ab}_{\epsilon_1\epsilon_2}$, whose form does not dependent on the replica indices m and n. Following the notation used in

the main text, we define

$$\lambda^{C,\pm}_{\epsilon_1\epsilon_2} = (\tilde{\lambda}^{C,\pm})^{12}_{\epsilon_1\epsilon_2} = (\tilde{\lambda}^{C,\pm})^{21}_{\epsilon_2\epsilon_1}. \tag{129}$$

Upon integrating over fields c' and c'', we obtain the corresponding Cooperon partition function

$$\mathcal{Z}^C(\phi_1,\phi_2) = \prod_q \prod_{\epsilon_1>0,\epsilon_2>0} [\det(\mathcal{M}^C_{\epsilon_1\epsilon_2,12})]^{-R^2/2}, \tag{130}$$

where we discarded the irrelevant ϕ-independent contributions and sample-space terms with identical indices, both types of contributions vanishing when we take the twofold derivative over the phase angles. In a completely analogous manner, we perform the same steps for the diffuson partition function and it yields the following result

$$\mathcal{Z}^D(\phi_1,\phi_2) = \prod_q \prod_{\epsilon_1>0,-\epsilon_2>0} [\det(\mathcal{M}^D_{\epsilon_1\epsilon_2,12})]^{-R^2/2}, \tag{131}$$

with the matrix $\mathcal{M}^D$ being defined identically to $\mathcal{M}^C$, except that the diffuson matrix must satisfy a different energy relation, namely, $\epsilon_1\epsilon_2 < 0$. Assembling together these contributions, along with the action evaluated at the saddle point (classical contribution), we finally arrive at the expression for $\mathcal{Z}$ stated in Eq. (5.49).